THE UNIVERSITY
of EDINBURGH

The Role of Cyclin-Dependent Kinase 9 in the Resolution of Innate Inflammation in a Zebrafish Tailfin Injury Model

Laura Jane Hoodless

Submitted for the degree of Doctor of Philosophy

The University of Edinburgh

2016

Declaration

I hereby declare that this thesis has been composed by myself, describes my own work and has not been submitted for any other degree or professional qualification.

Laura Jane Hoodless

April 2016

This thesis is dedicated to the Hoodless family - my mother and father, Lynn and Allan; my brothers Allan and Graeme; my late grandmother Jane and my grandmother Helen Barrass.

Acknowledgements

First and foremost I am very grateful to my project supervisors, Professor Adriano Rossi and Dr Carl Tucker, for giving me the opportunity to work on this project. Thank you for your time, patience and support over the last 4 years and teaching me to think about and criticise my data in different ways. Thank you to the Medical Research Council and my interview panel almost 5 years ago, who awarded me the scholarship to carry out this project.

Many thanks are due to the past and present members of the Rossi lab for technical advice and also for listening to and commenting on many lab meeting presentations which were an invaluable part of my training. Dr Leticia Alessandri, Dr Chris Lucas, Dr Rodger Duffin, Dr David Dorward and Dr John Marwick helped me to get set up in the lab in the beginning and have been excellent examples to follow. To my colleagues/office friends Dr Tiina Kipari, Ms Jennifer Felton, Dr Silke Currie, Dr Calum Robb, Dr Dip Datta and Dr Pallavi Bedi, thank you for your help and being such fun to share a lab with. I would also like to mention the Masters/PhD students Nicolette Mineo, Ana Rondelli and Maria Twardowska for helping to keep my brain sharp with lots of questions.

The staff of the Zebrafish facility (Charli Corcoran, John Arthur, Paul Wright, Angus Taylor, James Boott) have been generous with their help with husbandry over the last 4 years, and entertained me during tail-chopping and injection sessions. Fiona Rossi, Shonna Johnston and Will Ramsey were invaluable in helping with the confocal imaging, cell sorting and flow cytometry aspects of the project. The laboratory group of Dr Yi Feng have been very generous in giving advice and allowing me access to equipment.

I would like to also acknowledge the collaborators from outside the Centre for Inflammation Research who have given assistance along the way. Thank you to Dr Martin Denvir and his former students Dr Gianfranco Matrone and Dr Kat Wilson (BHF Centre for Cardiovascular Science, U of Edinburgh) for advice on protocols and allowing us to test their morpholinos. I am grateful to Dr Seb Rider (BHF Centre for Cardiovascular Science) for teaching me his methods for kidney dissection and flow sorting. Professor Stephen Renshaw (University of Sheffield) and his laboratory group provided transgenic lines, plasmids and advice with staining protocols, and kindly invited me to visit their laboratory for a lovely week during my PhD. Finally I would like to thank Dr Tim Czopka (Centre for Neuroregeneration, U of Edinburgh) for helping me to mend my broken PCRs, broken spirits (and broken bones).

Contents

List of Figures

List of tables

Abbreviations

The following abbreviations and units of measurement have been used throughout the text

- ALI - Acute lung injury
- AnnV – Annexin V
- Apaf-1 - Apoptotic protease activating factor-1
- ATG - Adenine-guanine-thymine
- ATP - Adenosine triphosphate
- Bak - Bcl-2 homologous antagonist killer
- BAL - Bronchoalveolar lavage fluid
- Bax - Bcl-2 associated X protein
- BCA - Bicinchoninic acid assay
- Bcl-2 - B cell lymphoma-2
- BID - BH3 interacting-domain death agonist
- c-FLIP - Cellular FLICE-like inhibitor protein
- *C. elegans* - *Caenorhabditis elegans*
- c5a - Complement component 5a
- Ca - Calcium (
- Cdc - cell division cycle
- CDK - Cyclin-dependent kinase
- CDKi - Cyclin dependent kinase inhibitor
- cmlc2 - Cardiac myosin light chain 2
- COX - Cyclooxygenase
- CRISPR/cas9 - Clustered regularly interspaced short palindromic repeats/caspase 9
- CTD - Carboxyl terminal domain
- CTP - Cytidine triphosphate
- CXCL8 - CXC ligand 8
- DC - Dendritic cell

- DIABLO - Direct IAP binding protein with low pI
- DISC - Death-inducing signalling complex
- DMOG - Dimethyloxalogylglycine
- DMSO - Dimethyl sulfoxide
- DNA - Deoxyribonucleic acid
- dpf -Days post-fertilisation
- E. coli - *Escherichia coli*
- ECL – Electrochemiluminescence
- EGFP Enhanced green fluorescent protein
- ENU - Ethyl nitrosourea
- EOL-1 - Eosinophilic leukaemia
- ERK - Extracellular signal-related kinase
- FACS - Fluorescent-activated cell sorting
- FasL - Fas ligand
- FBS – Foetal bovine serum
- FGF - Fibroblast growth factor
- FITC - fluorescein isothiocynate
- FLICE - FADD-like IL-1beta-converting enzyme
- fMLF - Formyl-methionyl-leucyl phenylalanine
- FPR1 - Formyl peptide receptor 1
- FVP - Flavopiridol
- G - Gauge
- gDNA - Genomic DNA
- GM-CSF - Granulocyte-macrophage colony stimulating factor
- GTP - Guanosine triphosphate
- h - Hours
- HIF1α - Hypoxia inducible factor 1α
- HL-60 - Human promyelocytic leukaemia cell-60
- hpf - Hours post-fertilisation
- hpi – Hours post-injury
- IAPs - Inhibitor of apoptosis proteins

- ICAM - Intracellular adhesion molecule
- IL – Interleukin
- IMDM -Iscove's Modified Dulbecco's Medium
- kDa - Kilodaltons
- LaRP7 - La-ribonucleoprotein family member 7
- LFA-1 - Lymphocyte function-associated antigen-1
- LPS - Lipopolysaccharide
- LTB_4 - Leukotriene B_4
- LXA4 - Lipoxin A4
- LysC - Lysozyme C
- Mcl-1 - Myeloid cell leukaemia 1
- MCP-1 - Monocyte chemoattractant protein-1
- min - Minutes
- MMP - Matrix metalloproteinases
- mpx - Myeloperoxidase
- mRNA - Messenger RNA
- Mtz - Metrodinazole
- N-TEF - Negative transcription elongation factor (N-TEF)
- NADPH oxidase - Nicotinamide adenine dinucleotide phosphate-oxidase
- NET - Neutrophil extracellular trap
- NF-κB - Nuclear factor κ-light-chain-enhancer of activated B cells
- NSAID - Non-steroidal anti-inflammatory drugs
- NTR - Nitroreductase enzyme
- OD - Optical Density
- P-TEFb - Positive transcription elongation factor b
- PAGE - Polyacrylamide gel electrophoresis
- PBS - Phosphate-Buffered Saline
- PBS-T, TBS-T - Phosphate/Tris-Buffered Saline with Tween
- PCR - Polymerase chain reaction
- PDGF - Platelet-derived growth factor
- PFA - Paraformaldehyde solution

- PI3K - Phosphoinositide 3-kinase
- PSGL-1 - P-selectin glycoprotein ligand-1
- PTU - Propylthiouracil
- PVDF - Polyvinylidene fluoride
- QVD-Oph - Quinoline-Val-Asp-Difluorophenoxymethylketone
- RNA - Ribonucleic acid
- ROS - Reactive oxygen species
- RPMI - Roswell Park Memorial Institute
- RT - Room temperature
- s – Seconds
- SDS - Sodium dodedcyl sulphate
- siRNA - Small interfering RNA
- SMAC- Second mitochondria-derived activator of caspases
- snRNP - 7SK small nuclear ribonucleoprotein
- STAT3 - Signal transducer and activator of transcription 3
- TAE - Tris base, acetic acid, EDTA
- TALEN - Transcription activator-like effector nuclease
- TAM - Tyro, axl and mer
- TBS - Tris-Buffered Saline
- TdT - Terminal deoxynucleotidyl transferase
- TE - Tris-EDTA
- TEM - Transendothelial migration
- TFIIH - Transcription factor II H
- TGFβ - Transforming growth factor β
- TLR - Toll-like receptors
- TNF -Tumor necrosis factor
- TRAIL - TNF-related apoptosis-inducing ligand
- TSA - Tyramide Signal Amplification
- TUNEL - Terminal deoxynucleotidyl transferase dUTP nick end labelling
- UTP - Uridine triphosphate
- VCAM - Vascular cell adhesion molecule

- VEGF - Vascular endothelial growth factor
- ZFN - Zinc finger nucleases
- zVAD-fmk – Carbobenzoxy-valyl-alanyl-aspartyl-[O-methyl]-fluoromethylketone

Abstract

Neutrophils are an important cell in host defence and migrate rapidly to sites of inflammation when the host is compromised (e.g., in infection or wounding). There, they produce and/or release inflammatory mediators (e.g., LTB4, TNF, IL-8) and ingest and degrade pathogens (e.g., by release of granule proteins and reactive oxygen species). Neutrophils then undergo apoptosis and are cleared by phagocytes such as macrophages, to allow efficient resolution of inflammation. Inducing neutrophil apoptosis by pharmacological means could be a therapeutic strategy to dampen inflammation in diseases where neutrophils are prevalent, e.g., acute respiratory distress syndrome (ARDS) and rheumatoid arthritis (RA). Inhibition of cyclin-dependent kinases (CDKs) using CDK inhibitor (CDKi) compounds induces mammalian neutrophil apoptosis *in vitro,* and can drive resolution of inflammation *in vivo* in mouse models. Evidence indicated that this is due to inhibition of CDK9 and CDK7-mediated transcription of the anti-apoptotic protein Mcl-1.

The hypothesis of this project was that CDK9, CDK7 and Mcl-1 are pivotal regulators of resolution of inflammation *in vivo*. The model selected to test this hypothesis was tailfin injury of embryonic zebrafish (*Danio rerio*). Zebrafish are optically transparent and reporter transgenic lines with neutrophils labelled by enhanced GFP (EGFP - Tg[mpx:EGFP]^{i114}) and macrophages (Tg[MPEG1:mCherry]) have been created, permitting the imaging of the behaviour of these cells *in vivo.* The model of tailfin transection was chosen to cause an inflammatory response in these animals, with neutrophil and macrophage recruitment to the tailfin.

This response was manipulated using CDKi compounds and specific gene knockdowns (using morpholino and CRISPR/cas9 technologies). It was shown that CDKi compounds could reduce neutrophil numbers at 24 h post-injury at the transected tailfin, but did not affect macrophage numbers. The CDKi AT7519 increased neutrophil apoptosis at 12 h post-injury. Specific CDK9 knockdown using morpholinos or CRISPR/cas9 also reduced neutrophilic inflammation at the tailfin 24 h after transection, accompanied by increased apoptosis levels at 8 h in the morpholino-treated group. Inhibition of an endogenous CDK9 inhibitor, LaRP7, had the opposite effect and increased neutrophil numbers; and could oppose the neutrophil-

reducing effect of AT7519 and CDK9 morpholino knockdown. Preliminary genetic knockdown studies into the roles of CDK7 and Mcl-1 have been carried out. Taken together, the results demonstrate CDK9 is important in the resolution of neutrophilic inflammation, indicating that manipulation of CDK9 activity could be a good target for therapeutic intervention in inflammatory disease.

Lay Abstract

Cells of the immune system work to protect the body against infection and help to heal damaged tissue. These processes are known as an inflammatory response. Immune cells circulate in the blood and move to places where they are needed in host defence. One such cell is the neutrophil, which quickly move to sites of inflammation, where they "eat" and destroy bugs that invade the body using digestive substances stored inside the cell. Neutrophils also release small substances that attract other immune cells to the inflammatory area, launching a co-ordinated response to the original stimulus. After this stimulus is cleared, neutrophils undergo a death process called apoptosis, to avoid the inflammation carrying on for too long in an uncontrolled manner. This can end up causing more damage to the tissue than the original inflammatory stimulus did. There are several diseases where this happens, including rheumatoid arthritis (RA) and acute respiratory distress syndrome (ARDS). For this reason, this project has investigated if drugs could be used to cause the death of neutrophils, and therefore help to resolve inflammation.

Specific drugs known as cyclin-dependent kinase inhibitor (CDKi) drugs have been shown to cause death of neutrophils. In rodent tests they have also been shown to help cure models of inflammatory disease; for example in one model, the antibiotic bleomycin sulphate is introduced into the lung, and causes an inflammatory response where neutrophils are recruited. It was thought that this was because the CDKi drugs inhibit a specific CDK, CDK9, which is required for the production of a pro-cell-survival molecule called Mcl-1. This theory was tested in this project, using transparent zebrafish embryos with fluorescently labelled neutrophils to carry out imaging of neutrophils, allowing the cell behaviour to be visualised inside a live animal. This model was used to show that CDKi drugs could reduce neutrophil numbers after wounding of the fish tailfin, and staining for dead cells showed that CDKi treatment increased the number of dead neutrophils. CDKi drugs did not affect the number of macrophages at the wound, which are required to take up and clear away apoptotic cells. Genetic technologies were used to target genes of the CDK9 gene pathway. Targeting CDK9 reduced neutrophil numbers post-wounding. Targeting the LaRP7 gene, which is a negative regulator of CDK9, have the opposite effect:

neutrophil numbers were increased. Preliminary studies into the role of other apoptosis pathway regulators (CDK7, Mcl-1) were performed. Overall, the project concluded that CDKi drugs targeting CDK9 may well be a good future therapeutic for inflammatory disease.

1. Chapter 1. Introduction

Inflammation is vital to protect the human body from invading pathogens, and also to promote healing of damaged tissue. In the vast majority of cases inflammation occurs and resolves without major issue in a self-contained manner. However, in many disease settings inflammation is a major cause of disease pathology. This is seen in diseases such as asthma, rheumatoid arthritis and sepsis (1-3).

The initial innate inflammatory response primarily involves cells of the myeloid lineage, particularly neutrophils, eosinophils and macrophages. These cells are recruited soon after the host is compromised by an infection or wound, and carry out several functions to clear the immune challenge. Later, cells of the adaptive arm of immunity (e.g. B or T lymphocytes) are recruited to carry out a more specific response. The development of these cell types is outlined in Figure 1.1.

The first sections describe what is known about mammalian inflammation; the last section will focus on zebrafish as an animal model for inflammation.

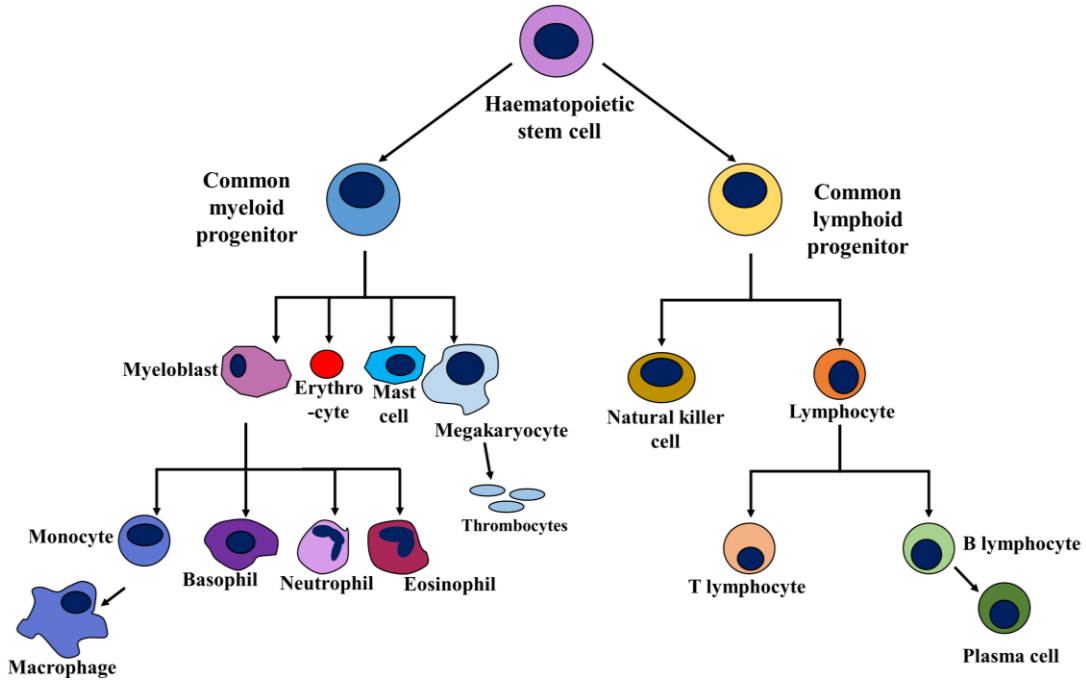

Figure 1.1. Mammalian Haematopoiesis

The development of white blood cells, from haematopoietic stem cells, divergence through the myeloid and lymphoid lineages, to form functional granulocytes and lymphocytes.

1.1. Inflammation at the Cellular and Molecular Level

1.1.1. Granulocytes

The inflammatory response occurs when cells in the host tissue become alerted to tissue damage or infiltration by pathogens. One of the first cells to respond in this mammalian inflammatory response is the neutrophil. Neutrophils arise from the common myeloid progenitor cell in the bone marrow, which differentiate to become granulocyte progenitors (Fig. 1.1.) (1). These progenitors then become blood-circulating neutrophils, eosinophils or basophils. Neutrophils are the most abundant white blood cell (approximately 70% of circulating leukocytes, 2-7.5x10^9 cells/L) in humans (1). They are typically thought to live in circulation for 7 – 10 h but inflammatory stimuli can increase this lifespan to as much as 48 h. Other studies have challenged the standard dogma of neutrophil lifespan; suggesting it can be as much as 5 days, although this is controversial (4, 5). Neutrophils possess a multi-lobed nucleus and their cytoplasm is filled with primary (e.g. myeloperoxidase, phospholipase A2, elastins, defensins), secondary (e.g. lysozyme, nicotinamide adenine dinucleotide phosphate-oxidase [NADPH] oxidase, cathelicidin) and tertiary granules (e.g. cathepsin, gelatinase), as well as secretory granules containing plasma proteins (1, 6). Pathogens are phagocytosed by neutrophils and the secreted contents of the granules can help to destroy pathogens. Neutrophils also secrete cytokines to send signals to other inflammatory cells to activate them and induce migration to tissue (e.g. tumor necrosis factor [TNF], interleukin [IL]-1β and IL-8) (7). In addition, neutrophils are known to produce extracellular traps (NETs) which trap pathogens (8). When regulation and resolution of these neutrophil responses does not occur, aberrant inflammation and disease occurs (see Section 2.1.2).

In addition to neutrophils, other inflammatory cells, i.e. eosinophils and basophils are also present in the blood of mammals (9). Eosinophils are thought to be effective tools against parasitic infection, in particular; and high levels are also found in individuals during allergic reactions, especially in Western society. They have many granule proteins specific to them such as major basic protein and eosinophil peroxidase. Basophils release histamine and cytokines which are thought to influence the immune response towards a T-helper 2 phenotype by interactions with dendritic

cells (DCs) (10). The lifespan of eosinophils in tissue can greatly exceed that of neutrophils, even as much as 6 days (9). Basophils survive for around 60 h – 70 h (9).

1.1.2. Neutrophils in disease

Neutrophils are a vital part of host defence, and their toxic granule contents and phagocytic capabilities are important for the destruction of invading pathogens. However their actions can in fact contribute to disease and pathology, due to their cytotoxic cell contents, which can damage tissues. For this reason, appropriate shutdown of the neutrophil response is essential. Examples can be found in many different disease models. In experimental pneumococcal meningitis in mice, over-expression of the survival protein B cell lymphoma-2 (Bcl-2) results in lower neutrophil apoptosis levels, and contributes to higher brain inflammation and tissue damage during infection (11). Inhibition of the pro-apoptotic p53/Puma pathway has been shown to extend neutrophil survival, and prevent resolution in a mouse model of bacterial sepsis, and increases mortality rates (12).

In the mammalian lung, it is known that neutrophils are a key cell in acute lung injury (ALI) with a large neutrophil infiltrate into the lung interstitium and bronchoalveolar space (13). The higher number of neutrophils present, the worse the disease pathology is found to be (14). Depleting neutrophils in mouse models of ALI results in a reduction in inflammatory markers and prevents development of disease (15).

It is recognised that inflammation in the heart can contribute to the development of atherosclerosis. Neutrophils are known to be involved in the early growth of atherosclerotic plaques, as neutrophil depletion correlates with a reduction in lesion size (16, 17). They also contribute to later plaque rupture, when the presence of reactive oxygen species and proteases are known to facilitate atherothrombosis (17, 18).

Recent data have even shown a role for neutrophils in the pathology of an Alzheimer's disease model in mice (19). Soluble amyloid-β was shown to cause activation of lymphocyte function-associated antigen-1 (LFA-1), resulting in adhesion

and transendothelial migration (TEM) into the brain and central nervous system. In the systemic disease sepsis, the role of neutrophils is unclear; however it has been shown that the function of neutrophils is greatly dysregulated, with neutrophil accumulation at sites remote from the inflammatory response and reduced neutrophils at the site of inflammation (20).

A role for neutrophils in autoimmune diseases has also been noted. In rheumatoid arthritis, neutrophils in the circulation were shown to be primed for reactive oxygen species (ROS) production, and become activated in the arthritic joints by engagement of Fc receptors on neutrophils by immune complexes like rheumatoid factor (21). Mice with depleted neutrophils were resistant to the effect of transferring pro-atherogenic serum, and depletion of neutrophils after serum transfer was able to reverse the joint inflammation (22). Therapies for the treatment of severe rheumatoid arthritis, including anti-TNF therapy, reduces the elevated TNF seen on neutrophils in rheumatoid arthritis patients; which may contribute to the efficacy of the treatment (23).

It is clear that neutrophils play an important role in many diseases, and their persistence in inflammatory diseases may be detrimental.

1.1.3. Migration of leukocytes to inflammatory sites

Granulocytes can be attracted to inflammatory sites by numerous signals, including interleukin-8 (IL-8) and formyl-methionyl-leucyl phenylalanine (fMLF), which bind to their corresponding receptors on the leukocyte. Pro-inflammatory lipid mediators (e.g. leukotriene B_4 [LTB_4]) are produced from the arachidonic acid biosynthesis pathway, and also induce granulocyte migration (24).

Detection of these signals attracts circulating granulocytes towards inflammatory site, promoting their adhesion to the endothelial wall and TEM across the vessel wall (25) (26). Adhesion is mediated initially by weak binding of selectin ligands (e.g. P-selectin glycoprotein ligand -1, PSGL-1) on leukocytes with selectins on activated endothelium. Stimulation of chemokine receptors by chemokines on the endothelium switches integrins on the leukocyte into a high-affinity conformation,

allowing them to bind to intracellular adhesion molecules 1 and 2 (ICAM-1 and ICAM-2), and vascular cell adhesion molecule 1 (VCAM-1) (26). This mediates migration via diapedesis processes to the site of inflammation, via migration through the border of endothelial cells (paracellular TEM), or less commonly, through endothelial cells (transcellular TEM). Live imaging evidence also exists to suggest that in mice, neutrophils can undergo reverse TEM from inflamed tissue back into the vasculature (27, 28). This has also been noted in zebrafish (29).

1.2. Resolution of Inflammation

Inflammation is vital for host defence, however it can be a damaging response and therefore must be carefully controlled. One of these levels of control is that neutrophils must undergo apoptosis to terminate and resolve inflammation. Apoptosis is a controlled, self-contained form of cell death. Apoptosis of neutrophils after they have completed their functions at the inflammation site is a vital part of this resolution, helping to dampen down the whole response. Other types of cell death include necrosis (where the cell contents are released to the surroundings), NETosis (DNA is expelled from inside the cell) and autophagy (when intracellular lysozymes digest cell contents from within).

Resolution of inflammation is orchestrated by various pro- and anti-inflammatory molecules. An overall view of the inflammation and resolution processes are shown in Figure 1.2. Various pro-apoptotic factors such as ROS can induce neutrophil apoptosis, over-riding neutrophil pro-survival factors such as granulocyte-macrophage colony stimulating factor (GM-CSF) or hypoxia, which is present in inflamed tissues.

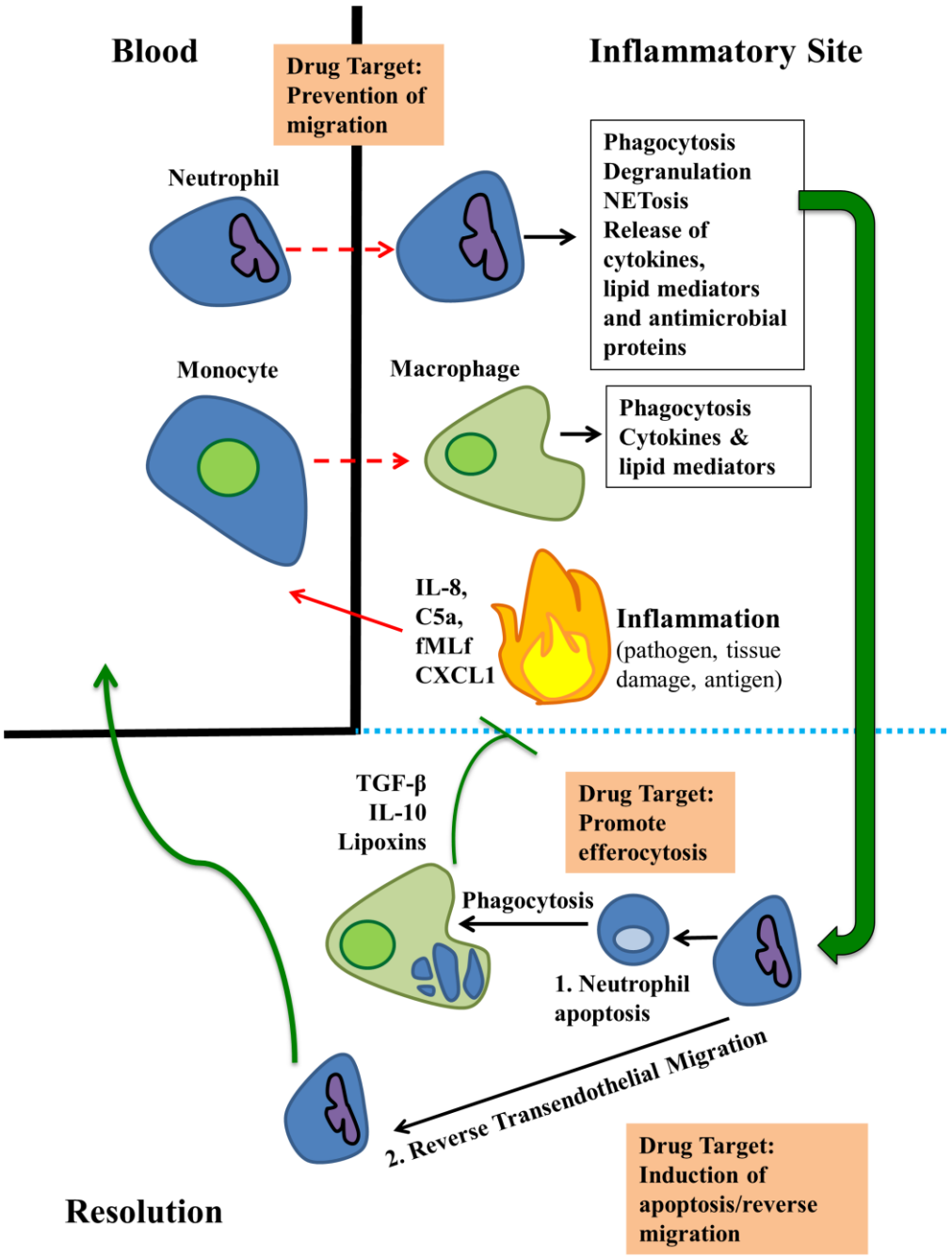

Figure 1.2. Cellular events in resolution of inflammation.

Neutrophils and monocytes are recruited from the blood, and can phagocytose and destroy bacteria and release pro-inflammatory mediators. Following this, neutrophils undergo apoptosis and macrophage switch to an anti-inflammatory phenotype, and ingest apoptotic neutrophils. Some neutrophils are also thought to migrate back to the circulation. Some of these processes are desirable pharmacological targets (orange boxes).

1.2.1. Neutrophil Apoptosis

Apoptosis is important from early in development. Originally termed "programmed cell death", it was described as an important part of the development of the transparent nematode *C. elegans*, allowing the direct observation of cell behaviour in development (30). In zebrafish, the development of sex organs was shown to be dependent on apoptosis (31).

Aspects of the apoptotic process are shown diagrammatically in Figure 1.3. Apoptosis is mediated by caspases, which are endoproteases that work by cleaving target proteins. Caspases are present as pro-caspases, which are activated by cleavage by other caspases. Caspases 3, 6, 7, 8, and 9 have been implicated in apoptosis, while others (e.g. caspases 1) are involved in the activation of inflammatory cytokines (32). Adaptor proteins cause the caspases to cluster together, and initiator caspases start off a process of downstream caspases cleaving each other. This results in release of cytochrome C from mitochondria, and then executioner caspases (such as caspase-3 and caspase-7) initiate proteolysis and DNAse of intracellular proteins in an organized manner (33). mRNA inside the cell is then rapidly degraded. This degradation results in cell shrinkage and chromatin condensation (pyknosis). The DNA becomes fragmented and the cell membrane buds into irregular blebs. Finally the cell breaks up into vesicles called apoptotic bodies. These apoptotic cells are cleared away by phagocytes such as macrophages. Failure of clearance results in cells proceeding to necrosis (34).

1.2.1.1. Activation of apoptosis

Activation of apoptosis can broadly occur by two pathways, although there is crossover. The extrinsic pathway is mediated by death receptors. These are expressed on the cell surface and bind to death receptor ligands (35). Examples of these ligands are TNF, Fas ligand (FasL) and TNF-related apoptosis-inducing ligand (TRAIL). These ligands are not specific to death pathways, for example TNF also plays a role in inflammatory responses and activation of nuclear factor κ-light-chain-enhancer of activated B cells (NF-κB). TNF only becomes pro-apoptotic in circumstances when NF-κB signalling is blocked. When these ligands bind to their receptors, the death-inducing signalling complex (DISC) is recruited, resulting in

caspase 8 activation. This is regulated by proteins such as DISC protein cellular FLICE (FADD-like IL-1beta-converting enzyme)-like inhibitor protein (c-FLIP), a caspase-8 homologue that lacks proteolytic activity; and inhibitor of apoptosis proteins (IAPs) that can block apoptosis. Proteins like second mitochondria-derived activator of caspases (SMAC)/direct IAP binding protein with low pI (DIABLO) can inhibit the actions of IAPs.

The second pathway is the intrinsic pathway, which results from caspase-9 activation by apoptotic protease activating factor-1 (Apaf-1). Apaf-1 changes conformation in cell stress. Pro-apoptotic proteins such as Bcl-2 homologous antagonist killer (Bak) and Bcl-2 associated X protein (Bax) create pores, allowing cytochrome C release from damaged mitochondria, which recruits procaspase-9 via caspase recruitment domains. In turn this creates an 'apoptosome' scaffold, in which caspase-9 is activated. This then leads to the activation of executioner pathways. The intrinsic and extrinsic pathways of apoptosis have a degree of overlap; the extrinsic pathway results in activation of the intrinsic pathway.

1.2.1.2. Regulators of Apoptosis

The apoptotic pathways are regulated by many molecules, some pro-apoptotic and others anti-apoptotic. In particular, the B cell lymphoma-2 (Bcl-2) family members regulate apoptosis by governing mitochondrial permeability and the release of cytochrome C into the cytosol. Bcl-2, Bax and Bak are present on the mitochondrial membranes, endoplasmic reticulum and nuclear envelopes. They permeabilise the mitochondrial membrane, facilitating the efflux of pro-apoptotic proteins such as Cytochrome C. Myeloid cell leukaemia 1 (Mcl-1) is a pro-survival protein which exists mainly in the cytosol. Mcl-1 sequesters Bax and Bak to help prevent the release of cytochrome C.

In neutrophils, the pro-survival protein Mcl-1 is highly expressed; to a much greater extent than other Bcl-2 family members. This means the neutrophil relies heavily on Mcl-1 for cell survival (36). Mcl-1 expression declines in isolated human neutrophils, eventually disappearing by 20 h post-culture which corresponds to high levels of apoptosis (37).

As with many genes, it is highly conserved between species, with mouse neutrophil survival also thought to rely on Mcl-1 (38). Mcl-1 is also expressed in zebrafish (39). It exists in two isoforms, the 40 kDa and 32 kDa isoforms.

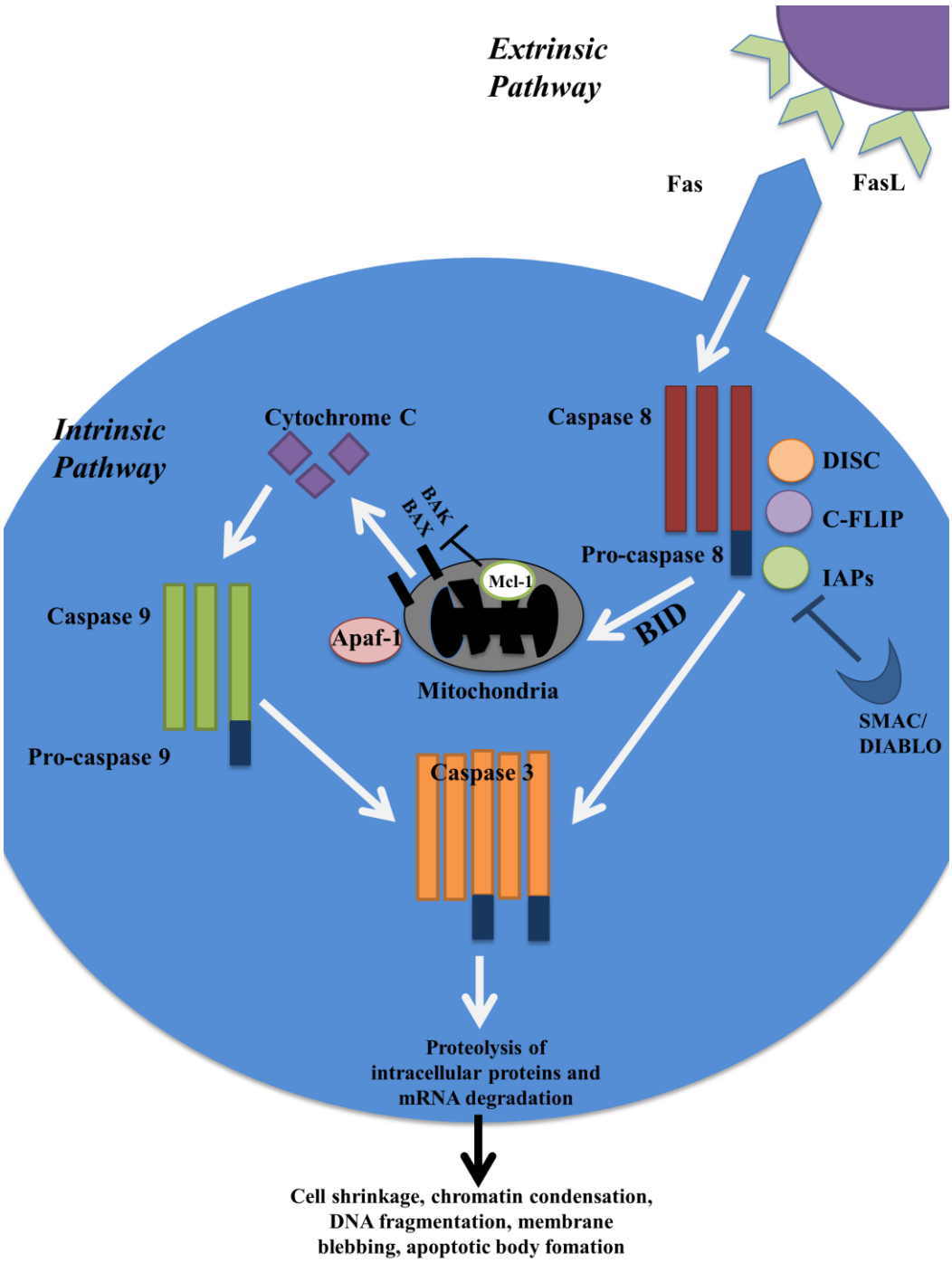

Figure 1.3. Apoptosis pathways in cells

Apoptosis can be activated by the intrinsic and extrinsic pathways. In the extrinsic pathway, external ligands signal to induce caspase 8 activation and activate executioner caspases (e.g. caspase 3), resulting in apoptosis. The intrinsic pathway occurs by release of cytochrome C from mitochondria, resulting in caspase 9 activation and then activation of executioner caspases. Many molecules exist to promote (e.g. SMAC/DIABLO) or inhibit (e.g. Mcl-1) apoptosis.

1.2.2. Macrophages during resolution of inflammation

1.2.2.1. Clearance of apoptotic neutrophils

Apoptotic neutrophils must be cleared away by phagocytes such as macrophages to prevent them eventually proceeding to secondary necrosis (where the apoptotic cell falls apart, releasing intracellular contents). The macrophage is attracted to find apoptotic neutrophils by signals such as sphingosine-1-phosphate which are released from neutrophils and bind macrophage receptors. They recognise molecules such as phosphatidylserine (PS) on the surface of apoptotic cells, via receptors such as TIM4 or BAI1 (40). In addition, molecules such as annexins (e.g. annexin A1) or Protein S can opsonise apoptotic cells via binding to PS, facilitating recognition by receptors such as tyro, axl and mer (TAM) receptors (41) (2, 42, 43). This process is an anti-inflammatory process, switching macrophages to the 'M2' anti-inflammatory phenotype, in which pro-resolution cytokines such as transforming growth factor β (TGFβ) and IL-10 are released (44-46). Apoptotic neutrophils can release factors that inhibit the recruitment of further neutrophils. Annexin A1 moves to the surface of neutrophils in apoptosis, where it can engage formyl peptide receptor 1 (FPR1), helping to regulate leukocyte migration and promote further apoptosis and phagocytosis of apoptotic cells (efferocytosis) (47-49).

1.2.2.2. Macrophages in tissue repair

Macrophages are thought to be key cells in the process of healing and restoration of tissue homeostasis following inflammation (50). Healing involves a co-ordinated response from macrophages and progenitors to replace tissue, promote angiogenesis and normal tissue oxygen, and prevent fibrosis developing. Macrophages exist in a dynamic state of inflammatory ('M1') vs anti-inflammatory, pro-healing ('M2'). Some hallmarks of M2 macrophages are up-regulation of Dectin-1, mannose receptor and production of ornithine and polyamines through arginase pathways, production of vascular endothelial growth factor (VEGF), fibroblast growth factors (FGF), platelet-derived growth factors (PDGF), and anti-inflammatory cytokines such as TGF-β (51). Macrophages can be skewed to the M2 phenotype by the presence of anti-

inflammatory factors like IL-4 or IL-13. M2 can be subdivided into a, b and c subtypes based on what stimulated them in the first place and what they express, although these are *in vitro* classifications and the situation *in vivo* is likely to be more plastic (52).

Growth factors promote cell proliferation in the cells around the affected area, and proteases like matrix metalloproteinases (MMPs) help to remodel the extracellular matrix. MMP12 from macrophages destroys the receptor-binding site of CXC chemokines which attract neutrophils, helping to dampen down inflammation (53). Various MMPs also cleave monocyte-attractant CC chemokines, rendering them unable to signal to the monocyte although they can still bind, hence they act as antagonists (54). In a similar way, decoy chemokine receptors such as D6 also promote resolution. D6-deficient mice display excessive neutrophilic responses after myocardial infarction, resulting in tissue damage (55). D6 has been shown to be important in switching macrophages to a pro-resolution phenotype. In a zymosan-induced peritonitis model, macrophages from D6-deficient animals had increased pro-inflammatory mediator production (56).

1.2.2.3. Macrophage production of pro-resolution mediators

Macrophages can also produce pro-resolution lipid mediators. Exploiting some naturally occurring pro-resolving molecules may be a good strategy to target some of these functions. This family of proteins can be both pro- and anti-inflammatory. The arachidonic acid pathway can synthesise pro-inflammatory molecules but also pro-resolution ones such as lipoxins, and derivatives from unsaturated fatty acids, such as resolvins and protectins (2). The production of these mediators is regulated by the cyclooxygenase (COX) enzymes, COX-1 and COX-2. These appear to be expressed differently in M1 and M2 macrophages, with 'M1' macrophages up-regulating COX-2, and 'M2' macrophages up-regulating COX-1. (57). For this reason, anti-inflammatory therapeutics targeting cyclooxygenases aim to target COX-2 selectively (58). Lipoxin A4 (LXA4), another member of this family, can mediate its' effects differently depending on the cell type it binds. In neutrophils, LXA4 inhibits neutrophil migration to sites of inflammation; as well as decreasing pro-inflammatory actions such as NF-κB activation and cytokine production. However in monocytes,

LXA4 promotes migration (2). In has been shown that Lipoxin A4 can be pro-resolving *in vivo* in models of acute lung inflammation (carrageenan-induced, and *E. coli*-induced), by indirectly promoting neutrophil apoptosis and driving clearance by phagocytes (59).

Macrophages can migrate away from the inflamed site via the draining lymph when the inflammatory response is resolved. Failure to do this contributes to prolonged inflammation; in atherosclerotic plaques, monocyte migration away from the plaque was associated with regression of lesions, whereas high numbers of retained macrophages correlates with progression of plaques (60). Macrophages are able to present antigen to adaptive immune cells, although not as effectively as dendritic cells (61). This has resulted in controversy in how exactly one defines a macrophage or dendritic cell – it has been suggested they are all part of the same plastic spectrum (62).

Due to the body of evidence suggesting that targeting neutrophil apoptosis and macrophage clearance might be a good strategy to induce resolution of inflammation, several drugs to target these events have been tested in inflammation models.

1.2.3. Drugs to target resolution

Potential therapeutics to target resolution should ideally perform some of the following functions:

1. Prevention of neutrophil migration
2. Promotion of efferocytosis
3. Induction of neutrophil apoptosis

The resolution processes and potential targets are outlined in the orange boxes of Figure 1.2.

1.2.3.1. Prevention of neutrophil migration

Many strategies to prevent neutrophil migration have been tested. Some drugs already in clinical use (e.g. the non-steroidal anti-inflammatory drugs (NSAIDs) naproxen, ibuprofen and oxaprozin) are known to prevent neutrophil migration to chemoattractants like CXC ligand 8 (CXCL8) and complement component 5a (c5a). An inhibitor of c-Abl kinase, ST1571, has been shown to inhibit neutrophil recruitment due to its effect on β2 integrin, actin polymerisation and hence migratory morphology of cells (63). However, a consequence of inhibiting neutrophil recruitment is that patients are likely to clinically present at the peak of inflammation, i.e. when neutrophils will already be recruited to the site of inflammation, and for this reason strategies to specifically drive apoptosis may be more beneficial.

The addition of synthetic annexin A1 derivatives in a model of lipopolysaccharide (LPS)-induced pleurisy in mice has been shown to reduce neutrophil migration to lung tissue in intestinal ischemia-reperfusion, during which the lung becomes inflamed (64), and also promotes neutrophil apoptosis (48). A 2011 paper indicates that *R*-roscovitine may also work by suppressing activation of leukocytes/endothelial cells, down-regulating adhesion molecules and preventing migration to inflammatory sites (65).

1.2.3.2. Increasing phagocytosis of apoptotic neutrophils

One possible drug strategy for inducing resolution of inflammation is increasing phagocytic clearance of apoptotic neutrophils, preventing the progression of apoptotic cells to secondary necrosis, as well as inducing the macrophage to switch to an anti-inflammatory phenotype (45). Glucocorticoid drugs have been shown to increase the capacity of macrophages to take up apoptotic cells (66).

1.2.3.3. Driving neutrophil apoptosis

Several pathways exist whose disruption may drive neutrophil apoptosis; for example, interference of pathways such as Extracellular signal-related kinase 1 and 2 (ERK1/2) and phosphoinositide 3-kinase (PI3K) signalling. Treatment with the ERK inhibitor

PD98059 was shown to drive neutrophil apoptosis and enhance resolution of a carrageenan-induced pleurisy model (67).

One strategy which is investigated within our laboratory group is the inhibition of cyclin-dependent kinases. In 2006 it was shown that the CDK inhibitor, *R*-roscovitine, could effectively drive neutrophil apoptosis *in vitro*, observed by increased Annexin V binding and cleaved caspase 3 expression in *R*-roscovitine-treated cells (68). There was a concurrent decrease in the expression of Mcl-1, a pro-survival protein, which is a vital part of neutrophil survival (36). *R*-roscovitine was then shown to reduce inflammatory cell numbers, oedema and inflammatory cytokines in a carrageenan-induced pleurisy model; and helped to restore normal tissue architecture in the lung (68). This was reversible using the caspase inhibitor Carbobenzoxy-valyl-alanyl-aspartyl-[O-methyl]-fluoromethylketone (zVAD-fmk). *R*-roscovitine was also effective in reducing inflammation in other disease models, including bleomycin-induced lung inflammation, and serum-induced arthritis (68). Further work showed that *R*-roscovitine could overcome pro-survival signalling by driving apoptosis and decreasing Mcl-1 levels after human neutrophil exposure to bacterial products such as lipopolysaccharide, or pro-inflammatory mediators such as TNF (69). The drug had no effect on Bim, a member of the Bcl-2 family that is pro-apoptotic, thus indicating that *R*-roscovitine may well be effective to tip the balance of pro- and anti-apoptotic factors in favour of apoptosis.

Further studies were performed to investigate which cyclin-dependent kinases were being targeted by *R*-roscovitine (70). In neutrophils, the most highly expressed genes were CDK7 and 9, and CDK2 to a lesser extent. *R*-roscovitine was shown to decrease phosphorylated RNA polymerase II, which is a downstream enzyme of CDK7 and 9, and is involved in transcription. *R*-roscovitine has also been shown to similarly affect eosinophil apoptosis (71).

Other molecules with similar structures to CDK inhibitor drugs have been described to cause apoptosis. Flavone compounds are members of the flavonoid family of compounds, characterised by the presence of a 2-phenylchromen-4-one (2-phenyl-1-benzopyran-4-one) backbone. The flavones wogonin, apigenin and luteolin have been shown to drive neutrophil and eosinophil apoptosis (72, 73).

The compound flavopiridol (FVP) is one of the most widely-tested CDK inhibitor drugs in lots of disease models, particularly for cancer, due to its activity against CDK1 (74). The use of FVP as a therapeutic for cancer has been disappointing, due to low efficacy and toxicity issues. However, FVP has other targets including CDK9. It has been shown to inhibit migration of neutrophils, in the setting of ConA-induced liver injury. Intravital imaging of the mouse cremaster muscle after intrascrotal TNF injection showed that FVP reduced transendothelial migration of leukocytes, with decreased ICAM-1 mRNA expression in endothelial cells (75). In this case, FVP was given before or together with inflammatory stimuli. However it has also been shown that FVP causes neutrophil apoptosis (37).

1.2.3.4. The CDKi compound AT7519

The synthetic CDK inhibitor AT7519 was generated by a high-throughput medicinal chemistry study, with several beneficial properties for therapeutic use (76, 77). The compound was effective in causing apoptosis in cancer cell lines (77-79). It also inhibited growth of xenografted neuroblastoma cells in mice (80). In a phase I trial of patients with solid tumours, the drug was well-tolerated (81).

AT7519 was shown to drive the apoptosis of isolated human eosinophils, and also increased eosinophil apoptosis when administered to a mouse model of allergic pleurisy inflammation (an eosinophil-mediated diseases, driven by challenge with ovalbumin) (82). Furthermore, AT7519 was shown to drive neutrophil apoptosis *in vitro*, even overcoming the pro-survival effect of LPS (38). This coincides with a reduced expression of Mcl-1. The effect was reversible using the caspase inhibitors zVAD-fmk and Q-VD-OPh. AT7519 was not shown to cause apoptosis of monocyte-derived macrophages, despite causing a downregulation of Mcl-1 – likely due to the lower reliance of macrophages on Mcl-1 for survival (83). LPS-mediated lung inflammation in mice could be reduced by intraperitoneal treatment with AT7519, with decreased inflammatory cytokines present (e.g. IL-6), an increased level of monocyte chemoattractant protein-1 (MCP-1), increased apoptotic neutrophils and ingested neutrophils inside macrophages in bronchoalveolar lavage fluid (BAL) (38). The same effect was seen when AT7519 was used when the mice were infected with *E. coli* intra-

tracheally (38). Interestingly, circulating neutrophil numbers were unaffected by AT7519, suggesting that targeting Mcl-1 to induce apoptosis is specific to inflammatory neutrophils. Furthermore, AT7519 was able to decrease bacteria titres in the lung and BAL, although the mechanisms for this are still not known (38).

1.2.4. Cyclin-dependent kinase 9 (CDK9) as a drug target in inflammation

1.2.4.1. Cyclin-dependent kinases

The above evidence suggested CDKs appear to be a good target for resolution of inflammation. CDKs are important in functions such as cell cycle, but also transcription. The first CDK was discovered in 1982 in yeast (84-86). It was shown that this CDK was important in the transition of cell cycle phases in cell division of the yeast *Saccharomyces cerevisiae* (cell division cycle [cdc] 28) and *Schizosaccharomyces pombe* (cdc2). Subsequently, cdc2 was found to be conserved in human cells and was eventually renamed CDK1 (87). Since then, the family of mammalian CDKs has expanded to include CDK1 – CDK20, after new discoveries and nomenclature of existing proteins has changed (88) (Table 1.1). CDKs are small serine-threonine kinases, around 30 – 40 kDa, which partner with cyclins in order to perform their phosphorylation activity. Yeast rely on a small number of CDKs and cyclins for functions such as cell cycle and transcription; however mammals have a much wider spectrum of CDKs which have evolved from the yeast CDKs and have taken on particular roles, in keeping with the complexity of the mammalian system (88). For example, different CDKs are activated at different points of the cell cycle; CDK1 in mitosis phase, and CDK2 in S phase. However, there is an element of redundancy; it is known that CDK1 is indispensable for cell division in yeast and mammals; however in mammals, CDK2 is dispensable for mitosis (but not meiosis). CDK2, 4 and 6 triple knockout mice still develop to mid-gestation, indicating CDK1 alone is sufficient for cell cycle to proceed; however CDK1 knockout embryos do not begin to develop, or undergo embryogenesis, as evidenced when CDK1 gene mutant heterozygote mice are crossed (89).

In addition to this functional redundancy, other proteins exist which possess CDK activity. One such example PFTK1, which bears no homology to CDKs but interacts with cyclin D3, and knockdown of PFTK1 causes arrest of cell cycle at G_1 phase. PFTK1 has since been designated CDK14 (90).

On the other hand, some CDKs, specifically, CDK7, 8 and 9 have been shown to regulate transcription and in fact play no role in cell cycle. The cyclin binding partners of CDK7, 8 and 9 (cyclin H, C and T, respectively) do not change in expression throughout the cell cycle, unlike the binding partners of other CDKs involved in the cell cycle.

Table 1.1. Cyclin-dependent kinases in mammals

CDK	Binding Partner	Function	Zebrafish homologue?
CDK1	Cyclin A, B & E	Cell cycle	✓
CDK2	Cyclin A, B, D & E	Cell cycle	✓
CDK3	Cyclin A,B,C & E	Cell cycle	✓
CDK4	Cyclin D	Cell cycle	✓
CDK5	CDK5R1 (p35), CDK5R2, cyclin D & Y	Cell cycle	✓
CDK6	Cyclin D	Cell cycle	✓
CDK7	Cyclin H	Transcription, CDK activation kinase	✓
CDK8	Cyclin C	Transcription	✓
CDK9	Cyclin T	Transcription	✓
CDK10	Cyclin M	Transcription, Cell cycle	✓
CDK11	Cyclin L	Transcription, Cell cycle	✓
CDK12	Cyclin L1, Cyclin K1	Transcription,	✓
CDK13	L type cyclins, Cyclin K	Transcription,	✓
CDK14	CDK5R1 (p35), CDK5R2, cyclin D & Y	Cell cycle	✓
CDK15	CDK5R1 (p35), CDK5R2, cyclin D & Y	Cell cycle	✓
CDK16	CDK5R1 (p35), CDK5R2, cyclin D & Y	Cell cycle	✓
CDK17	CDK5R1 (p35), CDK5R2, cyclin D & Y	Cell cycle	✓
CDK18	CDK5R1 (p35), CDK5R2, cyclin D & Y	Cell cycle	✓
CDK19	Cyclin C	Transcription	✓
CDK20	Cyclin H	Transcription	✓

1.2.4.2. Cyclin-dependent kinase 9 (CDK9)

CDK9 was first characterised in 1994, originally designated PITALRE (91). CDK9 is a cdc2-like Ser/Thr kinase. Its crystal structure has previously been determined (92). CDK9 is expressed within all mammalian tissues and particularly highly in terminally differentiated cells. Two isoforms have been described with different molecular weights at 42 and 55 kDa, shown by Western blotting (93). These isoforms both

interact with the same cyclins (T1 and T2) and RNA Pol II in the same way. However the 55 kDa isoform is present in only the nucleus, whereas the 42kDa isoform is present in both nucleus and cytoplasm (94). Isoforms are expressed to different extents in different tissues; e.g. the 55 kDa isoform is the most highly expressed in lung, liver and brain; whereas the 42 kDa isoform was the predominant isoform in the spleen and testis (95). Additionally, the 55 kDa isoform appears to be involved in the differentiation of hematopoietic cells, muscle cells and adipogenesis.

The cyclin binding partners of CDK9 are the cyclin T family consisting of T1, T2a and T2b (96). CDK9/cyclin T heterodimers are involved in transcription as part of the positive transcription elongation factor b (P-TEFb), consisting of RNA polymerase II and transcription factors such as transcription factor II B (TFIIB).

The P-TEFb complex was originally described in drosophila (97, 98). It stabilises the elongation of RNA transcripts, which are made by RNA Polymerase II (99). RNA polymerase II cannot cause RNA elongation on its own; due to inhibition by the negative transcription elongation factor (N-TEF). P-TEFb is able to displace N-TEF and phosphorylate the carboxyl terminal domain (CTD) of RNA polymerase II, facilitating elongation of RNA transcripts by RNA polymerase II (100).

The P-TEFb complex controls transcription factors such as NF-κB, resulting in the production of proteins such as inflammatory cytokines and pro-survival factors (such as Mcl-1). More is still being discovered about the P-TEFb complex and associated gene pathways; for example recent work showed the existence of a previously unknown binding partner, AFF1 (101). Other endogenous inhibitors of the P-TEFb complex exist, for example, the 7SK small nuclear ribonucleoprotein (snRNP). Part of this complex is the La-ribonucleoprotein family member 7 (LaRP7). (Fig. 1.4).

P-TEFb is involved in the transcription of several important proteins in neutrophils; and for this reason, work in our laboratory group has considered CDK9 to be a potentially useful therapeutic target. Mcl-1, the short-lived protein important in neutrophil survival, is transcribed as a result of CDK9 phosphorylation (102). Inhibiting CDK9 is associated with driving apoptosis, due to its role in transcription of pro-survival proteins (70). Not only is CDK9 inhibition directly associated with driving apoptosis, but may also liaise with other molecules to drive apoptosis. In a

cancer cell line, CDK9 inhibition alongside TNF apoptosis-inducing ligand (TRAIL) caused a synergistic effect, increasing the apoptosis-causing potential of TRAIL (103). This was due to the ability of CDK9 to drive transcription of cFLIP, in addition to Mcl-1, sensitizing the cells to TRAIL inhibition. Up-regulation of CDK9 activity results in Mcl-1 stability, and therefore increased resistance to CDK inhibitor treatment in a leukaemia cell line (104).

In addition, P-TEFb is also thought to play a role in other inflammatory processes such as cytokine transcription. It is involved in TNF-inducible NF-κB activation, and STAT3 signalling induced by IL-6 (105). Previous work also showed that CDK9 was necessary for the transcription of pro-inflammatory cytokines such as TNF, and even synergises with IL-6 to induce NK-κB activation (106, 107). It also appears that P-TEFb is required for IL-8 production (108).

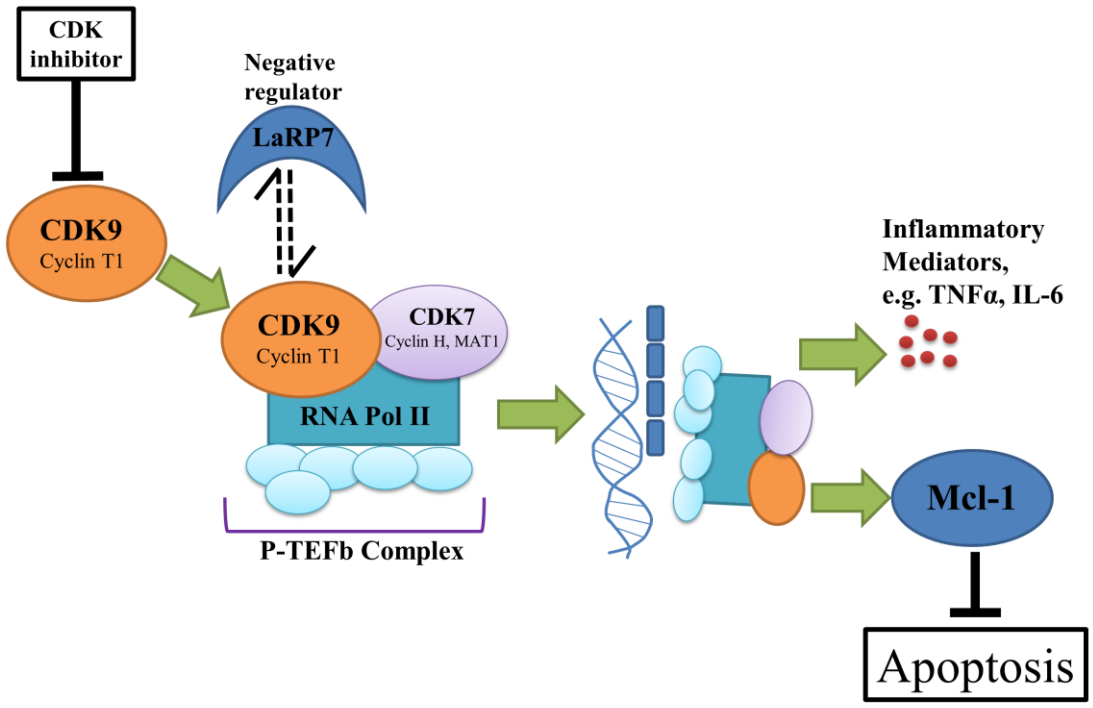

Figure 1.4. The P-TEFb pathway in mammalian cells

The P-TEFb complex consists of CDK9 and cyclin T1, which bind to RNA polymerase (pol) II along with other transcription factors (e.g. TATA-binding factor, TBP). P-TEFb is associated with the inhibitory 7SK snRNP, of which LaRP7 is part. Conformational changes induce the association of P-TEFb, allowing it to bind RNA pol II and initiate transcription of genes such as Mcl-1.

1.2.4.3. Cyclin-dependent kinase 7 (CKD7) in the P-TEFb complex

CDK7 is also part of the initiation of this transcription complex (see Fig 1.4) (109). RNA polymerase II transcription is initiated by phosphorylation by the transcription factor II H (TFIIH), which CDK7 is part of. This may also be a useful target for inhibition of transcription of neutrophil survival proteins.

However unlike CDK9, which is preferentially involved in transcription, CDK7 seems to be involved in the cell cycle in mammalian cells (110). It has both a CDK-activating domain (CAK), which phosphorylates cell cycle CDKs, as well as

forming part of TFIIH and phosphorylating RNA polymerase II. CDK7 levels do not fluctuate through the cell cycle though, and therefore may be involved in regulation rather than driving the cell cycle (111).

1.2.4.4. Difficulties of investigating the role of CDKs in mammals

Traditionally, neutrophil biology studies have been carried out in isolated human cells or mouse models. This is due to the ease of isolating human neutrophils from the blood, and the good homology between human and mouse genetics. Mouse models make it possible to investigate diseases similar to human diseases; for example lung inflammation models (e.g. bleomycin- or LPS-induced, or *E. coli* infection), and serum-induced arthritis as a model for RA.

CDK9 is clearly an important transcriptional regulator in development, as attempts to generate CDK9 deficient mice have been so far unsuccessful due to the low viability of the animals. CDK9 knockdown has also been shown to be lethal in *C. elegans* embryos, further supporting its role as a master regulator (112). A myeloid-specific CDK9 knockout has yet to be been created. Mouse embryogenesis has been shown to require cyclin T2 - which works together with CDK9 to form P-TEFb (113). A myeloid-specific Mcl-1 knockout mouse has been created, although it does exhibit neutropenia, making it a less useful model for studies of Mcl-1 in neutrophils during inflammation (83, 114).

CDK studies using human neutrophils have typically involved the use of CDK inhibitor compounds of varying specificities for individual CDKs. It is very difficult to achieve knockdown of any mammalian gene in primary neutrophils, due to the fact that they are terminally differentiated with a half-life of around 8 hours (115). Techniques such as small interfering RNA (siRNA) have been applied to neutrophils with limited success. The best compromise is to use neutrophil-like cell lines such as human promyelocytic leukaemia cell-60 (HL-60) (38); or for eosinophils, the eosinophil-like cell line, Eosinophilic leukaemia-1 (EoL-1) (116). However, these cells by their very nature have an altered survival profile, although they can be differentiated further to improve their neutrophil/eosinophil-like characteristics.

Knockdown of Mcl-1 in HL-60 cells was shown to cause increased apoptosis levels (38).

For the above reasons, the CDK9-P-TEFb-Mcl-1 hypothesis (shown diagrammatically on page 56) was investigated in a model more amenable to genetic manipulation, namely the zebrafish (*Danio rerio*). Applying this hypothesis to a whole-animal study will give greater insight in to the importance of these genes *in vivo*. Recent work has shown the importance of CDK9 and the P-TEFb complex in regulating the proliferation of cardiomyocytes after laser injury of the zebrafish heart; shown by morpholino targeting of CDK9 (described in Section 2.5), as well as pharmacological inhibition using FVP (117). This study shows that zebrafish are a good model in which to investigate the role of CDK9 *in vivo*.

1.3. Zebrafish as a model of resolution of Inflammation

1.3.1. Zebrafish embryos as an animal model

Zebrafish embryos have become increasingly recognised as a useful adjunct to traditional mammalian systems for investigating innate immune biology, namely primary cells and rodent models (115, 118, 119). They originally emerged as a tool in developmental biology, when it was recognised that their optically transparency and rapid development outside the mother makes it simple to image development *in vivo*. They develop a full range of immune cells, and are amenable to genetic and chemical manipulation. The zebrafish produces large numbers of eggs, facilitating experiments with large *n* values and strong statistics. Furthermore, as the zebrafish embryo can survive without a cardiovascular system for up to 7 days the feasibility of studying embryonic-lethal phenotypes is possible (120). Zebrafish are relatively cheap to house and maintain, making them a practical animal model. Some of the useful properties of zebrafish are detailed below.

1.3.1.1. Live imaging of zebrafish

The transparency of the zebrafish embryo makes them a perfect tool for *in vivo* imaging. Before 24 h, the embryo is completely transparent, ideal for imaging early developmental stages. After this, pigmentation develops, which can present an issue for imaging specific organs or regions of the embryo; however areas such as the tailfin are still free of pigmentation till much later stages of development. Lines of zebrafish are now widely used which lack these pigmented cells, such as *casper* or *golden*. Propylthiouracil (PTU) treatment at 1 dpf can delay pigmentation, however the potential side effects of this toxin on the immune response are unknown (115).

In zebrafish it is relatively simple to label cell populations and intracellular structures with fluorescent proteins. This, together with the transparency of the fish, allows *in vivo* imaging of these cells/structures (121). In addition, the wide range of fluorescent proteins available in recent times means that crossing different lines allows interactions between multiple labelled populations to be imaged within the same animal. One of the major differences between studying zebrafish and mammalian

neutrophils and macrophages is the cell numbers present. For example, a 3 days post fertilisation (dpf) zebrafish embryo will have roughly 200 neutrophils (122). This can make *ex vivo* work with these cells technically challenging, however does allow for clear *in vivo* imaging of cells and their interactions.

1.3.1.2. Zebrafish Immune Studies

Zebrafish develop a full range of haematopoietic cells, equivalent to those seen in mammals (123). However, there are some noteworthy differences, such as the presence of nuclei in erythrocytes (119). From around 30 hours post fertilisation (hpf), myeloid cells are seen which are capable of performing functions such as phagocytosis (124, 125). These cells can be imaged *in vivo* following the development of neutrophil-specific Tg(mpx:EGFP)^{i114} (126) and macrophage-specific Tg(MPEG1:mCherry), Tg(fms:mCherry) lines (127, 128). Images of these embryos at 3 dpf are shown in Figure 1.5.

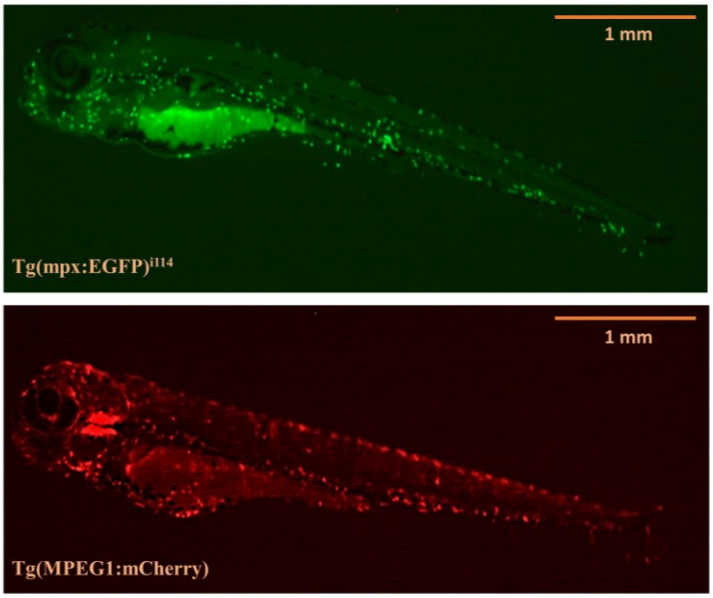

Figure 1.5. Images of Tg(mpx:EGFP)^{i114} and Tg(MPEG1:mCherry) zebrafish at 3 dpf

Whilst myeloid cells are seen at early stages from 1 dpf onwards, adaptive immune cells do not develop from about 10 dpf onwards in zebrafish (115). This allows exclusive and unimpeded imaging of the innate immune response at early stages, to assess cell behaviour without the confounding factor of other inflammatory cell types.

Zebrafish neutrophils possess many similar characteristics to mammalian neutrophils, such as polymorphic nuclei, primary and secondary granules, myeloid-specific peroxidase (a homologue of myeloperoxidase in mammals), and NADPH oxidase (125, 129). They can engulf and destroy bacteria (130) and it has been shown *ex vivo* that zebrafish neutrophils are capable of producing extracellular traps (131). Other components are conserved, such as IL-1 and CXCL8-CXCR2 signalling to induce neutrophil migration (132, 133). Rodents do not have the CXCL8 gene, making zebrafish a useful model to study CXCL8 function *in vivo* (134). Zebrafish also possess toll-like receptors (TLRs), and mediators such as complement and acute-phase proteins (135, 136).

Zebrafish macrophages have been shown to phagocytose bacteria and express L-plastin (124). They undergo frustrated phagocytosis when apoptotic cells are too large to phagocytose easily, and also form granulomas in response to infection with *Mycobacterium marinum*, a close relative of *Mycobacterium tuberculosis* (124, 137). Live imaging has permitted more insights into the behaviour of these cells *in vivo*; for example, it was shown that neutrophils engulf surface-associated bacteria, whereas macrophages can engulf fluid-borne bacteria (130). Macrophages are thought to play important roles in regeneration following tissue injury/loss (138, 139).

In addition to the existence of neutrophil and macrophage-like cells, there is a high degree of conservation between zebrafish and mammalian genes. Importantly for this project, the zebrafish possesses the full complement of CDK genes with a high degree of homology to humans. They have two isoforms of the Mcl-1 gene, with less homology to the human gene (compared to CDK gene conservation), however both have a role in cell survival (39, 140). Table 1.2 details the conservation of selected relevant protein sequences between species, calculated using Clustal Omega sequence alignment software (European Molecular Biology Laboratory, EMBL).

Table 1.2. Percentage similarity of selected protein sequences between species

Protein	Human:Mouse homology	Zebrafish: Human homology	Accession Number (Zebrafish)	Accession Number (Mouse)	Accession Number (Human)
CDK9	99.7%	94.4%	ENSDARG00000044811	ENSG00000136807	ENSG00000136807
CDK7	91.9%	96.8%	ENSDARG00000051916	ENSMUSG00000069089	ENSG00000134058
Mcl-1	82.9%	N/A	N/A	ENSMUSG00000038612	ENSG00000143384
Mcl-1a	N/A	58.8%	ENSDARG00000009779	N/A	N/A
Mcl-1b	N/A	56.4%	ENSDARG00000008363	N/A	N/A

1.3.1.3. Models of inflammation in zebrafish

Inflammation in zebrafish has generally been modelled by wounding or infection studies. Wounding of the tailfin has been used to image recruitment of neutrophils and macrophages to wounds (126). The tailfin is a good area to image due to the lack of pigmentation in this area. This has been done in various guises; removing the entire tailfin and part of the vasculature (126), removing only the tailfin (72), and 'nicking' the tailfin (141). This results in recruitment of neutrophils with a peak at 4-6 h post-injury. The injuries result in a variety of recruitment levels; around 30 neutrophils when the vasculature is injured, but less than 10 when the tailfin is nicked, although the duration of monitoring the inflammatory response was much shorter in this study (2.5 h) (141). However, what is clear is that the onset of the inflammatory response can be clearly observed, made easier with transgenic lines mentioned above. Macrophage recruitment is slower and rises progressively over the next 48 h post-wounding in the vasculature-injury model (127).

Different methods have been used to injure the tailfin in this model; sterile blades have been used previously (126), but also a laser can be used to punch a straight line of dots along the tailfin, resulting in the tailfin 'sloughing' off (142). The use of a laser is more precise and easier to reproduce injuries each time. Nicking' the tailfin has been carried out in the past using a 19 gauge needle and is technically challenging (141).

Other injury models have been used; for example laser injury of the heart and vasculature has been used to investigate inflammation and repair (143, 144) (145). Targeted laser ablations of cells in the brain have been used to show that Ca^{2+} waves are involved in the microglia response to this brain injury (146).

Zebrafish wounding studies have revealed new insights into inflammation biology. A wounding model was used to demonstrate for the first time that hydrogen peroxide is involved in attracting leukocytes to sites of inflammation (147). Reverse migration of neutrophils away from inflammatory injury sites was first observed in zebrafish (141, 148, 149). Primarily they reverse migrate through tissue, but it has been demonstrated that some neutrophils can 'reverse migrate' into the vasculature (149). This function has now been demonstrated in rodents It was shown that Hypoxia inducible factor 1α (HIF1α) expression is related to the incidence of reverse migration (150). This phenomenon contributes to resolution of inflammation in this model. It has been suggested these cells might play a role in influencing T cells in lymphatic organs (149).

Apart from wounding, inflammation can be induced by chemical means. Copper sulphate can be added to the water, destroying hair cells of the lateral line by causing oxidative stress (151). In addition, infectious disease can be modelled in the zebrafish. *Salmonella typhimurium* infection in zebrafish was used to further examine the role of CXCL8 in zebrafish (152). *Mycobacterium marinum* injection into the caudal vein of zebrafish results in a similar disease to human tuberculosis, with formation of granulomas (153). Labelling bacteria fluorescently allows the imaging of host-pathogen interactions *in vivo.* These inflammation models can then be manipulated at the genetic level, or by addition of chemicals/drugs (115).

1.3.1.4. Genetic Manipulation of Zebrafish

Many tools exist to alter genes in zebrafish (154). Due to the fact that embryonic stem cells have not been identified, targeted cell-specific deletions (as in mouse genetics) have not yet been possible. Stem cell-like cells have been found in zebrafish but this is still controversial (155). However, several other techniques are in common use, which are relatively simple to apply. In zebrafish it is common to use both forward genetic approaches (large scale mutagenesis followed by identification of specific genes related to a particular phenotype) and reverse genetics approaches (disrupting a known gene then analysing the phenotype). The benefits of some of these methods for gene targeting are compared in Table 1.3.

One such approach which zebrafish are very suitable for is large-scale genetic forward screens. Ethyl nitrosourea (ENU) can be used to generate random mutations to screen (156). This approach was used to identify a mutant of the *cleavage and polyadenylation specificity factor 1* (*cpsf1*) gene, which has a defect in haematopoietic stem cell development (157).

A targeted reverse genetics approach to the creation of mutants is the use of clustered regularly interspaced short palindromic repeats (CRISPR) RNA-guided cas9. This allows targeted mutations of genes of interest, with an efficiency rate of over 80% (158-160). It works by using an RNA guide to specifically bind the DNA region of interest. The oligonucleotide is attached to a protospacer adjacent motif (PAM) site, which recruits the cas9 enzyme. Cas9 cleaves DNA, resulting in DNA excision and frame shift mutations. This technique has been widely used to knockout genes of interest, and also to knock in genes (158). One recent study used vector delivery of CRISPR sequences to induce gene knockout in tissues; but due to the 80% efficiency rate (not all mutations will be frameshift), not all target cells will be affected (161).

Other reverse genetic techniques include transcription activator-like effector nucleases (TALENs). These consist of TAL effector DNA-binding domains fused to DNA cleavage domains, hence allowing specific excision of DNA sequences (162). TAL effectors are bacterial-derived proteins from Xanthomonas. For genetic knockdown, microinjection of morpholinos (which are synthetic antisense

oligonucleotides with sequences specific for the gene of interest) results in temporary gene knockdown (163).

Table 1.3. Advantages and disadvantages of different knockout methods.

Technology	Features/Advantages	Disadvantages
Forward genetics mutagenesis screens	Unbiased target discovery, may reveal previously	Laborious/time consuming (large scale analysis)

		unknown targets of interest.	Genetic redundancy (e.g. genome duplication) may mask potential phenotypes
Reverse genetics Morpholino-mediated gene knockdown		Immediate loss of gene function, does not require raising several generations Simple and quick to use	Possibility of off-target effects and toxicity Transient and sometimes incomplete knockdown
Reverse genetics Genome editing	Clustered regularly interspaced short palindromic repeats (CRISPR)/cas9	Heritable knockout in desired location RNA guided DNA endonuclease mediated-RNA/DNA hybridisation of 20bp motif Easy to use, highly efficient	Relatively new technology – any possible side-effects are not fully known yet and some may yet be discovered
	Transcription activator-like effector nucleases (TALENs)	Heritable knockout in desired location Protein guided DNA endonuclease, each TAL effector recognises a single DNA base	Laborious to engineer modules of TAL effectors
	Zinc finger nucleases (ZFNs)	Heritable knockout in desired location Protein guided DNA endonuclease, each zinc finger recognises a DNA base triplet	Laborious to engineer modules of TAL effectors Least specific gene editing method, as each zinc finger can bind different DNA triplets with different affinities

The creation of transgenic lines in zebrafish for *in vivo* studies of fluorescently-labelled cells is a well-established method. It has been made easier to create new lines by the use of 'tol2' approaches, which utilise the tol2 transposon element to promote DNA incorporation into cells, at a higher efficiency rate (20%) than previous methods such as BAC recombineering (164). However these approaches require the identification of cell-specific promoters, which does not yet exist for all cells. In

addition, ablation of these cells can be carried out by inclusion of the bacterial nitroreductase enzyme (NTR) gene, which catalyses the pro-drug metrodinazole (Mtz) to a cytotoxic product; or the Killer Red gene, a light-activated inducer of ROS which is toxic to cells (165, 166).

1.3.1.5. Chemical Manipulation in Zebrafish

One of the benefits of using zebrafish embryos is the ability to do large-scale drug testing, and systems to allow automation of these vast screens may well be used widely in the future (115). Chemical manipulation of the inflammatory response post-wounding has primarily been carried out by immersion of the embryo in the drug, diluted to the appropriate concentration (167). Drugs can also be injected directly into the embryo, allowing the concentration which is actually taken up into the embryo to be more carefully controlled compared to incubation. Several examples exist of drug manipulation of tailfin inflammatory responses; for example it was shown that Class III antiarrhythmic methanesulfonanilides inhibited leukocyte recruitment to sites of tailfin injury (141). The pan-hydroxylase inhibitor dimethyloxalogylglycine (DMOG), which inhibits an endogenous inhibitor of HIF1α, was shown to delay resolution of inflammation post-wounding (150). HIF1α is involved in extending neutrophil lifespan during conditions of hypoxia seen during inflammation.

Some studies have been carried out using CDKi compounds in zebrafish, to examine if they also drive neutrophil apoptosis in this *in vivo* setting, as seen in human cell lines and rodent models. Renshaw *et al* showed that the CDKi *R*- roscovitine reduces neutrophil numbers after tailfin wounding (which also transected the tailfin vasculature) (168). Meanwhile, the caspase inhibitor zVAD-fmk and the pro-inflammatory stimuli LPS had the opposite effect, with higher neutrophil numbers at 24 h post-wounding, and less apoptotic neutrophils, compared to control. The flavone wogonin, which has structural similarities to CDKi compounds, was also able to reduce neutrophilic inflammation post-wounding (72). This was reversible using the caspase inhibitor zVAD-fmk, showing that apoptosis is playing an important role here.

1.4. Hypothesis

The hypothesis of the project was that the P-TEFb pathway and Mcl-1 transcription are vital in regulating resolution of inflammation *in vivo.*

The aim of the study was to test this hypothesis by using genetic and pharmacological manipulations of the CDK9/CDK7, P-TEFb, Mcl-1 transcription pathway *in vivo* in a zebrafish inflammation model. From previous work with human neutrophils *in vitro*, these genes have been shown to be important in neutrophil lifespan (37, 68, 70), and the zebrafish offers a unique opportunity to probe the role of these genes *in vivo.* Figure 1.6 depicts aspects of the P-TEFb pathway and the green boxes highlight what is known about the role of these genes *in vitro* in human neutrophils, *in vivo* in mouse systems, and what is still unclear. Briefly, some research questions at the start of the project, and which chapter they were addressed in, were as follows:

(a) What is a good zebrafish injury model to probe the role of CDKs in neutrophil- and macrophage-mediated inflammation? *Chapter 3*
(b) What is the neutrophil and macrophage response profile in this model? *Chapter 3*
(c) Can the inflammation be increased by addition of bacterial products like lipopolysaccharide (LPS)? *Chapter 3*
(d) Do the zebrafish neutrophils share functional characteristics with mammalian ones? *Chapter 3*
(e) Do cyclin-dependent kinase (CDKi) drugs affect resolution of neutrophilic inflammation in zebrafish, and the general neutrophil population? *Chapter 4*
(f) Do CDKi drugs affect apoptosis of neutrophils in zebrafish inflammation? *Chapter 4*
(g) How are macrophages affected by CDK inhibition? *Chapter 4*
(h) Does genetic targeting of specific genes in the P-TEFb pathway (specifically CDK9, CDK7, Mcl-1 and the negative regulator LaRP7) affect neutrophils and macrophages during inflammation, and in the entire embryo? *Chapter 5*
(i) Does targeting CDK9 have an effect on neutrophil apoptosis? *Chapter 5*

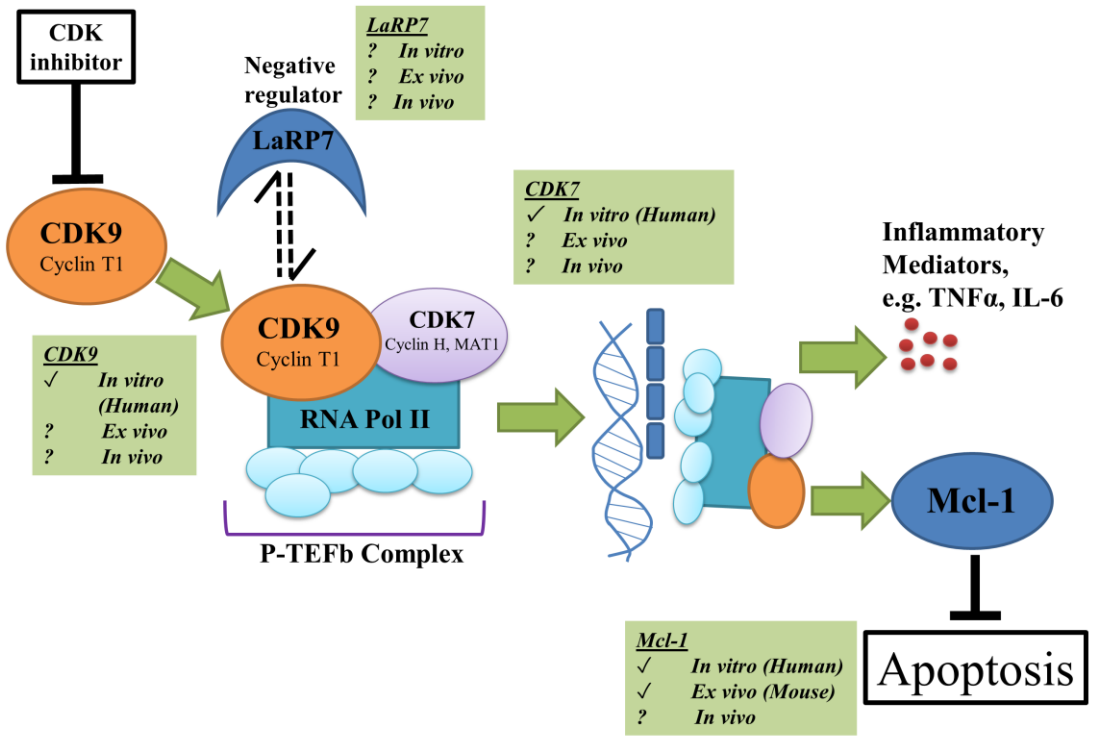

Figure 1.6. What is known about the P-TEFb pathway

CDK7 initiates mRNA transcription and CDK9 and RNA Polymerase II are important for elongation. This results in the transcription of several important genes in neutrophils such as Mcl-1, TNF and IL-6. The green boxes highlight genes of interest and where their role has been investigated with respect to their role in resolution of inflammation and neutrophils in particular models.

2. Chapter 2. Methods

The materials and methods described in this chapter relate to the general techniques applied throughout this study. Further details of specific reagents, including manufacturer, is given in Appendix A; and recipes for solutions are in Appendix B.

2.1. The zebrafish tailfin injury model

2.1.1. Zebrafish application and ethical review

All experiments were carried out in accordance with the accepted standards of humane animal care under the regulation of the Animal (Scientific Procedures) Act UK 1986 and EU Directive 2010/63/EU; animals were held in a UK Home Office approved facility. The animals used in these experimental studies were under the age of 5 days post fertilisation.

2.1.2. Zebrafish lines used in the study

Throughout the project, various genetically modified lines were used to aid the visualisation of inflammation.

- Tg(mpx:EGFP)^{i114} or Tg(mpx:mCherry)^{i114} (126) were used to image neutrophil populations *in vivo*.
- Tg(MPEG1:mCherry), Tg(MPEG1:EGFP) (128) and Tg(fms:mCherry) (127) were used to image macrophages.

The above lines were a kind gift from Professor Stephen Renshaw, University of Sheffield. In the project, new lines and mutants were also generated. CDK9 homozygote and heterozygote knockout fish were generated using CRISPR-Cas9 technology (158). Tg(LysC:mcl1a:cmlc2:EGFP) and Tg(LysC:mcl1b:cmlc2:EGFP) fish were created using the Tol2 transgenesis system, in which the cardio-myosin light chain promoter linked to EGFP is driven by Lysozyme C linked to Mcl-1a or Mcl-1b, respectively. Wild-type (WIK strain) were used for microinjecting plasmids (169) and CRISPR/cas9 constructs to generate new lines (159).

2.1.3. Zebrafish husbandry and breeding

Adult fish (classified as older than 90 days) (170) were housed according to standard operating procedures and maintained with a 14 hour (h):10 h light:dark photoperiod cycle at an ambient temperature of 28.5°C. The onset of the light cycle triggers spawning of these photoperiodic organisms. Eggs were collected by pair-mating one female and one male fish overnight and collecting the eggs in a sieve the next morning. The eggs were maintained at 28.5°C in an incubator until use. Experiments were conducted at 22°C but stored at 28.5°C between time points. All animals were used under the age of 5 days post fertilisation, which is the age when procedures carried out on the embryos require a Home Office licence. Staging of zebrafish to ensure they were always at similar developmental stages was conducted by eye, according to the guidelines of Kimmel *et al* (171). Collected eggs were maintained in either "systems water" containing 0.03% salt or Embryo Medium (see Appendix B for recipes) with 0.5 mg/L of the antifungal/antibacterial methylthioninium chloride (methylene blue) in deionised water, in 9 cm Petri dishes. Systems water or embryo medium was replenished every 24 h.

2.1.4. Zebrafish tailfin injury

Zebrafish (3 days post fertilisation [3 dpf]) were injured in a similar manner to the one described by Renshaw and colleagues (126). The fish were anaesthetised by immersion in 4.2 % MS-222 buffered tricaine solution (v/v, see Appendix B), equivalent to 20 μM, in a petri dish (60 mm x 15 mm) (172). Tricaine has been determined to be the most safe and effective anaesthetic for use in zebrafish (173). When the fish had ceased movement and was assessed to be anaesthetised (tested by stimulus and ataxia but with a good cardiovascular flow, as determined by Denvir et al (172), it was laid on an inverted petri dish using a 3 mL pastette. Excess water was removed using tissue paper to make the transection process easier. The transection process was performed using a dissecting scope (Leica MZ16F). The median tailfin was fully transected using a sterile scalpel (Fig. 2.1, green line) and the fish were then kept in 1 mL of embryo medium in a well of a 48 well plate. The wound was briefly examined using a dissecting scope to assess if the wound was in the correct place. This

model was selected for the project (Chapter 1, Fig 3.1), but other models were also tested.

In one model, the zebrafish embryo tailfin was fully transected in the same way as just described, but also involved cutting off the end of the body and embryonic vasculature system (Fig. 2.1, red line). A more mild injury was tested, involving nicking the side of the tailfin with a 19 G needle (Fig. 2.1, blue line). The area of the tailfin vasculature is more clearly highlighted using a purple line in Figure 2.1. No observable detrimental effects were observed with each wound type; such as alteration in heart rate, blood flow or gross morphology. The fish recovered from anaesthesia and showed normal swim behaviour. Any animals that appeared unhealthy were excluded from the experiment.

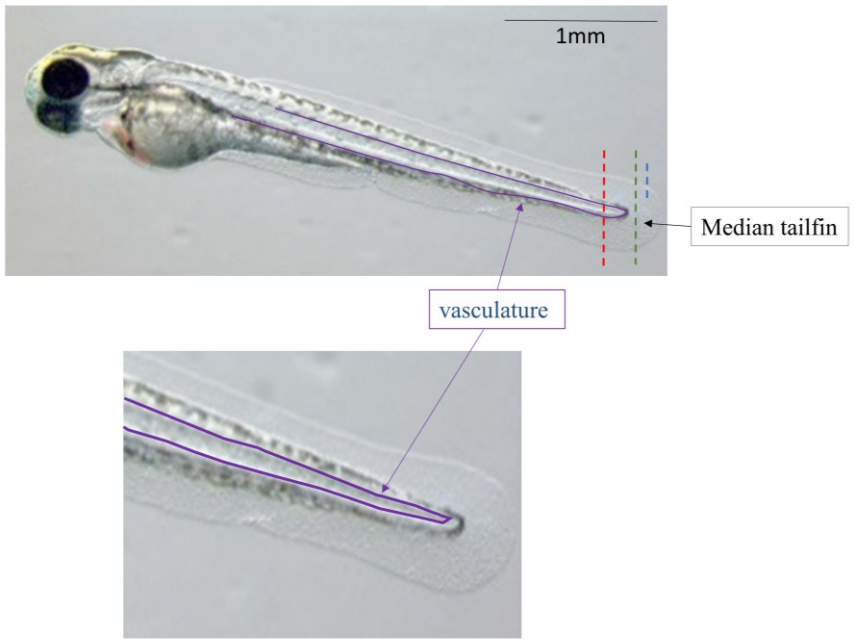

Figure 2.1. Tailfin transection of 3 dpf zebrafish.

Dotted lines depict transection sites. The purple line demonstrates more clearly the vasculature in the tailfin area. Red line: transection damaging vasculature; green line: transection without damaging the vasculature; blue line: tailfin nick using needle

2.1.5. Mounting embryos for imaging

For imaging using fluorescence microscopy, embryos were anaesthetised in 4.2% tricaine (v/v, see Appendix B) and imaged in embryo medium in a petri dish, or laid on the surface of a petri dish in a drop of embryo medium. For confocal microscopy, the embryos were mounted in agarose. Briefly; a solution of 1.5% agarose in system water was made and microwaved until boiling, then 1 mL was cooled for 1 minute (min) to 50°C in a 1.5 mL microcentrifuge tube. Each embryo was submerged in the agarose and positioned. A pastette was used to transfer an embryo into a well of an 8 well chamber cover glass slide. To each well, 500 µL of 4.2% embryo medium/Tricaine anaesthetic was added to help keep the embryo wet and under anaesthesia.

2.1.6. Imaging, measurement and analysis of inflammation

For general tailfin transection assays, images were taken on a Leica fluorescent dissecting stereoscope at 40x magnification (for whole embryo imaging) or 80x magnification (for imaging the tailfin), with EGFP (Ex. 488) and Texas Red filters (Ex. 596). An example image at 40x magnification is shown (Fig. 2.2, A). Images were taken on a Leica DFC300 FX Digital Colour Camera connected to LAS (Leica) software. Afterwards, ImageJ software (NIH, Bethesda) was used to create a selection area of 0.5 mm length. This was consistently applied to the same area at the fish tailfin, namely with the right hand vertical line placed where the notochord/vasculature ends (Fig 2.2, B). All the cells to the right of the left-hand vertical line of the box were counted. For whole embryo cell counting, the ImageJ multi-point tool was used. Images were taken in different focal planes to ensure that all cells were counted (as some cells might be obscured by cells directly above/below).

Confocal imaging or time lapse imaging was carried out using a Leica sp5 microscope. EGFP was excited at 488 nm; mCherry at 587 nm, and TUNEL at 570 nm. The images were taken at 100x magnification to image the inflammatory response, or at 400x magnification to acquire images of fixed, Terminal deoxynucleotidyl transferase dUTP nick end labelling (TUNEL)–stained embryos (as apoptotic DNA is smaller and more difficult to visualise).

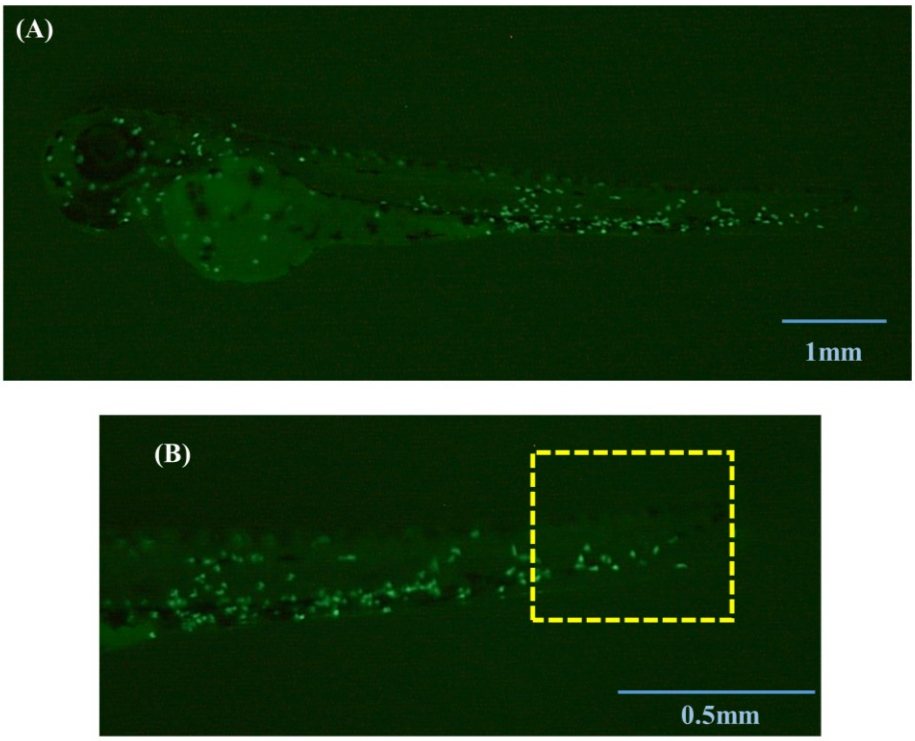

Figure 2.2. Tailfin transection and counting of cells

Tg(mpx:EGFP)^{i114} zebrafish with a transected tailfin. Images taken at 40x (A) and 80x (B) magnification.

2.2. Analysis of zebrafish neutrophil characteristics and function

2.2.1. Digestion of whole embryos for fluorescent activated cell sorting (FACS)

As many embryos as possible were used for a reasonable yield after sorting; in these studies about 500 embryos were used. Tg(mpx:EGFP)^{i114} embryos were transferred using a pastette into a 1.5 mL microcentrifuge tube. They were euthanized by immersion in 100% Tricaine stock solution (see Appendix B) for 15 min, until it was that activity and cardiovascular function had ceased. The approved Schedule 1 method

is detailed by Home Office A(SP)A'86 guidelines). The embryos were then briefly washed in Tris Buffered Saline (TBS, see Appendix B) and then 1 mL of Trypsin was added to disassociate the cells of the embryo. The embryos were put on a shaking heat block for 1 h at 37°C. Vigorous pipetting was carried out twice per tube, to help in the dissociation process. The resulting solution was then passed through a 40 μM filter in a 50 mL conical centrifuge tube, then centrifuged at 300 g for 5 min and resuspended in a flow cytometry tube in 300 μL of media (Roswell Park Memorial Institute [RPMI] cell medium [supplemented with 10% Foetal Bovine Serum [FBS], to aid the solution easily passing through the BD FACS Aria cell sorter]).

2.2.2. Isolation and digestion of adult zebrafish kidneys for FACS

The kidney of the adult Tg(mpx:EGFP)^{i114} zebrafish was digested and neutrophils isolated, to examine if a greater yield could be achieved than with digestion of embryos alone (Section 3.3.6). The adult zebrafish was killed by the Schedule 1 method as detailed by Home Office A(SP)A '86 guidelines (Section 2.2.1), followed by destruction of the brain. The fish was then supported and inverted, in a wet, tissue paper-moulded groove in a petri dish. A stereo dissecting microscope (for details, see Appendix A) was then used to visualise the inverted fish during the dissection process. Dissecting scissors were used to open the peritoneal cavity, and the intestinal tissue was removed by cutting the oesophagus and anus. The soft kidney was carefully removed using fine forceps, teasing it away from the peritoneal cavity (174). The kidney of Tg(mpx:EGFP)^{i114} zebrafish can easily be identified using EGFP fluorescence. Neutrophils labelled with EGFP could be visualised throughout the kidney of these animals. The kidney was dissociated by the addition of the kidney tissue to 1 mL of RPMI supplemented with 10% FBS, followed by gentle pipetting up and down. This was sufficient for good tissue dissociation. The mixture was then filtered through a 40 μM filter and collected in a 50 mL conical centrifuge tube, and centrifuged down at 300 g and resuspended in 300 μL of RMPI media in a flow cytometry tube.

2.2.3. Fluorescence-activated cell sorting (FACS) of EGFP$^+$ zebrafish neutrophils

Embryos or kidneys were digested as described in Sections 2.2.1 or 2.2.2. The cell populations in 300 µL RPMI in flow cytometry tubes were sorted on a BD FACS Aria II^{TM} cell sorter, based on EGFP fluorescence (Ex. 488). The sort takes approximately 40 min. The gating is shown in Chapter 1 (Fig. 3.7). The cells are collected in a 1.5 mL cytocentrifuge tube and used for imaging or *ex vivo* stimulation

2.2.4. Imaging of zebrafish embryo EGFP+ neutrophils isolated by FACS

FACS-isolated EGFP$^+$ cells were imaged in media in an 8 well chamber cover glass slide using a fluorescent microscope (EVOS FL Cell Imaging System). Time lapse images of these cells were made on the same microscope.

2.2.5. Stimulation of sorted EGFP$^+$ neutrophils using N-Formyl-Met-Leu-Phe (fMLF)

Shape change of sorted EGFP$^+$ neutrophils was assessed after fMLF stimulation (see page 89). fMLF is a potent chemotactic stimuli for neutrophils, inducing cell polarisation and therefore a shape change which can be measured by increase in forward scatter (175). The sorted EGFP$^+$ neutrophils were centrifuged at 300 g for 5 min and resuspended in 75 µL of Phosphate-Buffered Saline (PBS, see Appendix A) containing Ca^{2+} and Mg^{2+} in a 2 mL microcentrifuge tube in a 37°C shaking heat block (300 rpm). An additional 60 µL of PBS containing Ca^{2+} and Mg^{2+} was added, along with 15 µL of fMLF (10 nM) or PBS as a control. The tubes were incubated for a further 30 min at 37°C, then 75 µL of cells were added to 250 µL of PBS (without Ca^{2+}/Mg^{2+}) and placed on a flow tube on ice. The samples were then processed on an LSR Fortessa Flow Cytometer, and forward and side scatter profile was analysed.

2.3. Treatment of zebrafish embryos with pharmacological compounds

2.3.1. Incubation of zebrafish embryos with compounds

Zebrafish at 3dpf were transected as described in Section 2.1.4. At 4 h after the initial transection, each embryo was added to an individual well of a 48 well plate containing 500 µL of embryo medium (see Appendix B) with the appropriate concentration of compound or dimethyl sulfoxide (DMSO) vehicle control (≤1% DMSO, unless specifically stated otherwise). The compound concentrations used were listed in Table 2.1 below. The fish are repeatedly imaged at different time points over the 48 h post-transection (see Section 2.1.5), and inflammation is determined (see Section 2.1.6). Only healthy animals with normal swim behaviour are included in the analysis, as determined by eye (see Section 2.1.4).

Table 2.1. Compound incubation of 3 dpf zebrafish embryos

Drug	**Concentration Used**
AT7519	10 µM, 20 µM
Wogonin	25 µM, 50 µM
Luteolin	50 µM, 100 µM
Apigenin	50 µM, 100 µM
FVP	1 µM, 3 µM
SNS-032	10 µM, 20 µM, 50µM
zVAD-fmk	100 µM
QVD-OPh	1 µM, 10 µM, 50 µM

2.3.2. Microinjection of zebrafish embryonic yolk sac with compounds

The zebrafish embryo was anaesthetised in 4.2% (v/v) Tricaine (see also section 2.1.4). The embryo was then laid in the groove of a microinjection tray exposing the ventral surface for microinjection (Fig. 2.3, B). Excess water was removed to ensure the embryo does not float away when the needle is inserted. Then, 3 µL of compound or control solution (see Table 2.2) was loaded into a microcapillary needle, using 20 µL microloader tips. The loaded microcapillary needle was inserted in the needle holder of a Narishige IM-300 microinjector and held in place in a Narishige micromanipulator for reproducible microinjections. The microcapillary needle was calibrated by injecting a single pulsed bolus of experimental solution (for typical microinjector

settings, see Appendix A) into mineral oil on a 1 mm stage micrometer slide (Pyser SGI). The diameter of the bolus was measured using the 1 mm ruler on the micrometer. The injection time of the microinjector was adjusted as necessary until the bolus measured 0.1 mm. A bolus of this size corresponds to a 500 pL volume. The volumes listed in Table 2.2 were injected into the yolk sac of the embryo, using a Narishige microinjector and micromanipulator. This region is indicated in Fig. 2.3. The settings used for the needle puller, necessary to shape capillary needles, are listed in Appendix A. After injection, the animals were each isolated and maintained in a single well of a 48 well plate in 1 mL of system water. Over the 48 h post-transection the fish are serially imaged (see Section 2.1.4 and 2.1.5), and inflammation is counted (see Section 2.1.6). Unhealthy animals are removed from analysis as necessary (see Section 2.1.4).

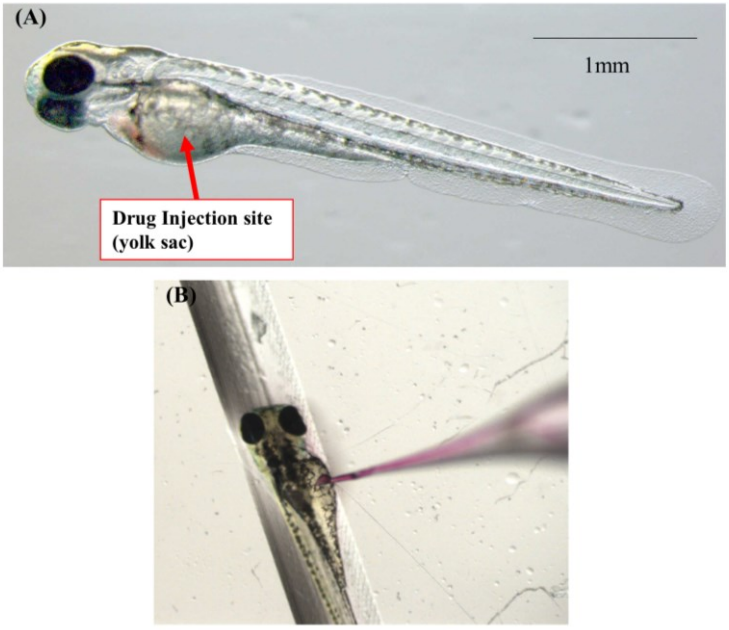

Figure 2.3. Microinjection into zebrafish yolk sac

Compounds such as AT7519 were injected into the zebrafish yolk sac (A). Fish were laid in a microinjection tray in the correct orientation for microinjection (B).

Table 2.2. Compound injection into zebrafish yolk sac

Drug	Manufacturer	Volume Injected	Concentration of stock	Mass injected
AT7519	Astex Therapeutics	1.5nL	10mM	0.5 ng
zVAD-fmk	Tocris Bioscience	2nL	100mM	93.5 ng
FVP	Sigma Aldrich	0.5nL	10mM	2.2 ng

2.4. Staining zebrafish for apoptosis

2.4.1. Fixing and preparing embryos for staining

Embryos were euthanized using 100% Tricaine by Schedule 1 methods (see Section 2.1.4). The embryos were transferred using a pastette into a 1.5 mL microcentrifuge tube, then briefly washed in TBS. The TBS was removed, then 1 mL of paraformaldehyde solution (PFA, 4%) was added to the tube. The tubes were kept at 4°C overnight. After 12 h of fixation, the PFA was removed. Alternatively, fixation was carried out for 1 h at room temperature. If staining was carried out on the same day, the embryos were washed 3 times with TBS prior to beginning the staining protocol. If the embryos were stored long term, the PFA was removed and 1 mL of 100% methanol was added to the tubes. They were then stored at -20°C. Prior to use, the embryos must be rehydrated by successive 5 min incubations in 75% Methanol/25% TBS, 50% Methanol/50% TBS then 25% Methanol/75% TBS. The embryos are then washed 3 times in TBS.

2.4.2. Tyramide signal amplification (TSA) and terminal deoxynucleotidyl transferase dUTP nick end labelling (TUNEL) staining

TUNEL staining was carried out in fixed Tg(mpx:EGFP)^{i114} conjunction with Tyramide Signal Amplification (TSA), in order to amplify the EGFP signal. The protocol is carried out with components from the Tyramide Signal Amplification

(TSA) Kit and the ApopTag® Red *In Situ* Apoptosis Detection Kit (for details, see Appendix A).

2.4.2.1. TSA Staining

The embryos were washed in 500 µL of Amplification Diluent from the TSA kit. They were then incubated in a 1 in 50 dilution of Fluorescein:Amplification Diluent. The tubes were wrapped in foil and incubated for 10 min at 28°C degrees. The embryos were washed 3 times for 10 min in TBS. The fluorescein stain was checked on a fluorescent stereomicroscope (see Appendix A). The embryos were then fixed for 20 min at room temperature (RT) in 4% PFA.

2.4.2.2. TUNEL staining

The TUNEL staining protocol began with a Proteinase K digestion. The embryos were incubated for 90 min at room temperature in 10 ng/mL of Proteinase K. The embryos were then washed twice for 5 min in TBS with 0.1% Tween20 (TBS-T), then fixed in 4% PFA for 20 min at room temperature (20°C). Another 3 washes with TBS-T were carried out followed by an incubation in 1:2 acetone:ethanol for 7 min at -20°C. Three 5 min washes in TBS-T were performed, then 50µL of Equilibration Buffer (ApopTag® Red kit) was added to each tube for 1 h at RT. The equilibration buffer was then removed, and to each tube 16 µL terminal deoxynucleotidyl transferase (TdT) enzyme and 30µL Reaction Buffer (both from ApopTag® Red kit) was added. The tubes were incubated for 90 min at 37°C. The liquid was then removed and 200 µL of Stop Buffer (ApopTag® Red kit) was added for 3 h at 37°C. The embryos were then washed for 3 times for 5 min in TBS-T. To each tube 62 µL anti-Dig Rhodamine and 68 µL of Blocking solution (both from ApopTag® Red kit) was added, and the tubes were incubated overnight on a shaker at 4°C. The next morning, 4 washes for 30 min in TBS-T were performed, then 4% PFA was added for 30 min at RT. Four final washes for 5 min in TBS-T were carried out. The embryos were then stored in 80% glycerol at -20°C until they were imaged. For imaging the embryos were also mounted in 80% glycerol.

2.5. Morpholino knockdown of genes of interest

2.5.1. Design of morpholino sequences

Morpholinos were ordered from Gene Tools LLC. These are 25 base-pair synthetic oligonucleotide sequences which block either mRNA splicing or translation. To design these sequences, the ENSEMBL ID of each transcript was entered into the Design Tool of the Gene Tools website (http://www.gene-tools.com/). For ATG-morpholinos, the morpholino is designed across the start codon of the gene and therefore block translation. For splice-targeting morpholinos, the desired potential target exons were listed and morpholinos are designed which span this exon-intron boundary. Optimal morpholino design should have a 40-60% Guanine (G)-Cytosine (C) content. The sequences should not have long stretches of self-complementarity, or more than 4 G nucleotides in a row (due to water solubility issues). Table 2.3 lists the target, sequence, fluorophore and details of previous publications of the morpholinos. Mismatched controls (similar sequences with random base pair changes) are also injected, to prove that the phenotype seen is due to the specific effect of the morpholino, and is not an artefact of the injection procedure.

Table 2.3. Morpholinos microinjected into zebrafish eggs throughout the project

Target	Type of Morpholino	Sequence	3' Fluorophore	Previously published?
CDK9	Splice blocking *a* *Exon 3/Intron 3*	GGTGCATTTTCTT ACCCCTTCTTTC	Lissamine	✓ (117)
CDK9	Splice blocking *b* *Exon1/Intron1*	GTAAAATATTCGT ACTTTTCACCGC	Lissamine	×
CDK9	Mismatched control	GGTCCATTTTGTT AGCCGTTGTTTC	Lissamine	✓ (117)
CDK9	ATG	CTTCCGGTTTTGTC GCGCTGCATCC	Lissamine	×
CDK7	Splice blocking *Exon 11/Intron 11*	ATAAAGTGTTTCT TTACCCTGTTCA	Lissamine	×
CDK7	Mismatched control	ATATACTGTTTGT TTACCGTCTTCA	Lissamine	×
Mcl-1a	ATG	GAGCCATATTTCA ATCGCTGATTAC	Lissamine	✓ (39)
Mcl-1b	ATG	CTGTTTTCAATTCC ACATAAACGCC	Lissamine	✓ (39)
Mcl-1	Mismatched control	GACCCATATTACA ATGGCTCAATAC	Fluorescein	×
LaRP7	Splice blocking *a* *Exon 3/Intron 3*	TCATCTCCATACT AAACCAAACTGT	Lissamine	✓ (117)
LaRP7	Splice blocking *b* *Exon1/Intron1*	CGTTTACGAATTT TACCAATGCCGA	Lissamine	×
LaRP7	Mismatched control	TGATGTCCATAGT AAACGAAACTCT	Lissamine	✓ (117)

2.5.2. Preparation of morpholino injection solution

Morpholinos were diluted to a stock solution of 1 mM in sterile water and kept at room temperature. They were then diluted further in sterile water for microinjection (microinjection technique is detailed in Section 2.3.2). The amount of morpholino injected into the zebrafish eggs in a volume of 1 nL are listed in Table 2.4, along with the dilution from the 1 mM stock solution. For each morpholino several amounts of morpholino were tested to ascertain the optimal amount, in which knockdown was achieved but the fish were healthy and not developmentally stunted (171). For the purpose of clarity, only the optimum amount used is shown here. Success of morpholino knockdown was assessed using Western blotting.

Table 2.4. Amount of morpholino injected into zebrafish eggs

Morpholino	Amount injected in 1nL volume	Dilution from Stock (1mM)
CDK9 Splice blocking *Exon 3/intron 3*	455.1pg	1 in 20
CDK9 Splice blocking *Exon 1/intron 1*	455 pg	1 in 20
CDK9 Mismatched control	461.1 pg	1 in 20
CDK9 ATG	130.7 pg	1 in 70
CDK7 Splice blocking *Exon 11/Intron 11*	1.8 ng	1 in 5
CDK7 Mismatched control	1.8 ng	1 in 5
Mcl-1a ATG	4.6 ng	1 in 2
Mcl-1b ATG	4.6 ng	1 in 2
Mcl-1 Mismatched control	4.4 ng	1 in 2
LaRP7 *Exon 3/intron 3*	911.5 pg	1 in 10
LaRP7 Mismatched control	923.5 pg	1 in 10
CDK9 + CDK7 Splice- blocking	303.4 pg + 1.2 ng	1 in 30 (both)
CDK9 + LaRP7 Splice-blocking	303.4 pg + 455.75 pg	1 in 30, 1 in 20
Mcl-1a + Mcl-1b	2.3 ng + 2.3 ng	1 in 4 (both)

2.5.3. Microinjection of morpholinos into zebrafish eggs

Morpholinos were microinjected into newly–laid zebrafish eggs, up to the 8-cell stage (171). The microinjection equipment was set up as described in Section 2.3.2. The volume of the injected bolus was determined to calculate the amount of morpholino added. Multiple eggs were laid into the grooves of a microinjection tray, using a pastette, and 1 nL of the morpholino was injected into the yolk sac of the zebrafish egg, shown in Figure 2.4 (A). Morpholinos do not need to be injected into the single cell of the developing embryo, unlike DNA injections, as the morpholinos can easily be taken up in the cytoplasmic stream of the yolk sac into the developing cells. The eggs were raised in petri dishes till 3 days post fertilisation. They were screened using a fluorescent microscope for positive uptake of the fluorescently-labelled morpholino, before further use in assays of interest (Fig 2.4, B).

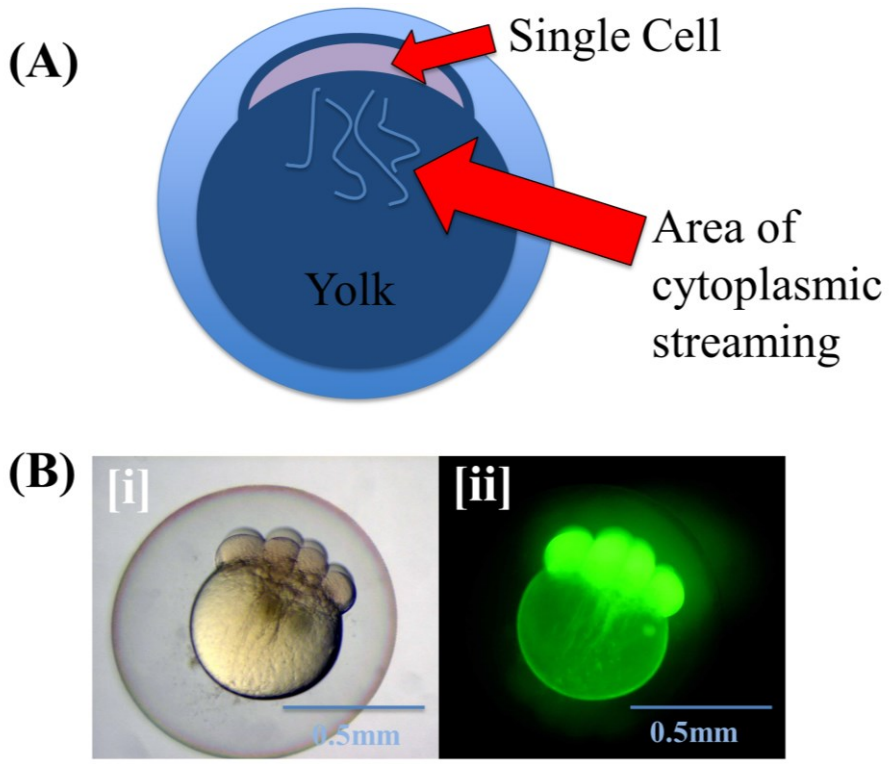

Figure 2.4. Microinjection of morpholinos into the zebrafish egg

The red arrow indicates the area of cytoplasmic streaming where the morpholino is injected (A). Brightfield (B [i]) and EGFP fluorescent (B [ii]) images of an egg successfully injected with an EGFP fluorescent morpholino.

2.5.4. Western blot to assess morpholino knockdown

Embryos were euthanized by Schedule 1 methods, fully described in Section 2.2.1. Briefly, embryos at 3 dpf were immersed in 100% Tricaine for 5 min. Each was then transferred by pastette into a 1.5 mL microcentrifuge tube. A solution was prepared of 790 µL Radioimmunoprecipitation Assay (RIPA) buffer plus 10 µL Protease Inhibitor Cocktail. To each tube 30 µL of this solution was added, and the embryos were dissociated with a pestle. The solution was then sonicated for 30 seconds (s) at 5 µW using a sonicator. The tubes were incubated for 30 min on ice, following which they were centrifuged for 15 min at 13,000 g. The supernatant (approximately 30 µL) is collected and transferred into a fresh 0.5 mL microcentrifuge tube. It was then stored at -20°C or ran immediately on a 5-12% Tris-Glycine gel.

A protein assay was carried out using the Pierce Bicinchoninic acid assay (BCA) Protein Assay kit. The kit consists of a BCA Working Reagent (50:1 Reagent A:Reagent B). Various BSA protein standards were made up in the range 125 – 2000 μg/mL as per manufacturer's instructions, by serial dilutions in distilled, deionised (dd)H_20 from a protein stock of known concentration. Then, 200 μL of the Working Reagent was added to 10 μL of standards or samples in a 96 well plate. The plate was covered with a lid and mixed on a plate shaker for 30 s then covered with foil and incubated for 30 min at 37°C. The plate was then measured at room temperature at 562 nm on a plate reader. A standard curve of Optical Density (OD) vs. protein concentration was created on a Microsoft Excel spreadsheet. This was used to calculate the unknown values of protein concentration of samples, based on the OD of the samples.

Sample buffer (4x) containing reducing agents (see Appendix B) and ddH_20 was added to the sample to make a volume of 40 μL, all containing the same amount of protein (confirmed from the protein assay standard curve). The samples were then incubated at 95°C for 5 min in a heat block to denature the protein. The Benchmark pre-stained protein ladder was used to estimate protein size. Following this, the samples and 1 well of protein ladder were loaded and run on a 4-12% sodium dodedcyl sulphate (SDS)-Polyacrylaminde gel electrophoresis (PAGE) gel to separate the proteins, at 110 V for 45 min in Running Buffer (recipe in Appendix B). The protein was then transferred onto a polyvinylidene fluoride (PVDF) membrane (pre-activated for 5 min in methanol) in Transfer Buffer (recipe in Appendix B) at 80 V for 1 h at 4°C. The membrane was then incubated in a 50 mL conical centrifuge tube containing 15 mL of 5% dried milk powder in TBS-T. The membrane was then incubated overnight on a roller in a 1 in 1000 dilution of the appropriate primary antibody (see Table 2.5). The membrane was washed 3 times in TBS-T then incubated in the appropriate secondary antibody for 1 h (see Table 2.5). The membrane was then washed 3 times in TBS-T then developed using an Electrochemiluminescence (ECL) kit. Briefly, 1 mL of Solution A was mixed with 1 mL of Solution B (both from the ECL kit) in a 50 mL conical centrifuge tube. The membrane was then developed onto a film, in the dark room using a developer. The size of the protein band was estimated

by comparing it to the size of the closest protein ladder bands, which are of known size.

Table 2.5. Antibodies used for western blotting

Antibody	Type	Protein Band Size
CDK9	Rabbit Polyclonal	43 kDa
CDK7	Rabbit Polyclonal	42/37 kDa
Mcl-1	Rabbit Polyclonal	40/32 kDa
LaRP7	Rabbit Polyclonal	67 kDa
Goat Anti-Rabbit	Horse Radish Peroxidase-conjugated secondary	N/A
Goat Anti Mouse	Horse Radish Peroxidase-conjugated secondary	N/A
B-Actin	Mouse Monoclonal	N/A

2.6. Heritable gene knockdown of CDK9 in zebrafish using clustered regularly interspaced short palindromic repeats (CRISPR)/cas9 gene editing

2.6.1. Design of gRNA guide oligonucleotide sequences

The use of the CRISPR/cas9 for gene editing is previously described in zebrafish (158-160). The gRNA guide oligonucleotide sequences were designed with an online CRISPR Design Tool (http://www.genome-engineering.org/crispr/?page_id=41). It is an algorithm based on a previously published analysis which selects good targets from a 23-1000 bp long region of interest. Good targets are DNA sequences which are followed by a PAM sequence (5'-NGG, 5'-NAG), as these are the sites targeted by the Cas9 enzyme. From this, two guide sequence templates were synthesised, as shown in Figure 2.5. The guide sequence and T7 primers were diluted to 200 μM stocks in ddH_20. The guide and T7 primer sequences were then annealed together by mixing them together in a solution where they were both at 15 μM concentration. The tube was then heated in a PCR machine for 5 min at 95°C, then cooled down to 22°C by

setting the machine to decrease temperature at 0.1°C per s. The reagents from the MEGAscript T7 kit are thawed to room temperature (except the enzyme mix which should be kept on ice). Each transcription reaction is done in a polymerase chain reaction (PCR) tube with 2 µL of ATP, CTP, GTP and UTP solutions; 2 µL of 10X Reaction Buffer, 2 µL of Enzyme Mix, and 2 µL of the annealed product. The tubes were mixed thoroughly and incubated for 3 h at 37°C. 1 µL of TURBO DNAse is added and mixed well, then the tubes were incubated at 37°C for 15 min. The MEGAclear kit was then used to further purify the RNA from the *in vitro* transcription reaction. The RNA sample was brought to a total volume of 100 µL with Elution Solution and then 350 µL of Binding Solution Concentrate was added and mixed gently again using a p1000 pipette. A further 250 µL of 100 % ethanol was added to the sample and mixed gently. The sample was then applied to a filter cartridge inside a collection and elution tube. The tube was centrifuged for 1 min at 13,000 g till the solution passed through the filter. The flow-through was discarded and the filter was washed by adding 500 µL of Wash Solution and centrifuging for 1 min at 13,000 g, then discarding the flow-through. This step was repeated, then a further 30 s 13,000 g centrifuge step was carried out to remove any remainder of the Wash Solution. The RNA was eluted from the filter by placing the filter into a new collection/elution tube and applying 50 µL of Elution Solution to the filter. The tube was incubated in a heat block set at 65°C for 10 min. The eluted RNA was then recovered by a 1 min centrifugation at 13,000 g. This elution step was repeated with another 50 µL of Elution Solution (to maximise RNA recovery). The DNA concentration in 1 µL of DNA solution was measured using a Nanodrop machine (for details, see Appendix A). With the Guide #2 template, the yield was consistently between 200-300 ng/µL. With the Guide #1 template, the yield was consistently around 50 ng/µL. This indicated that Guide #2 was probably the best template, however both Guide #2 and Guide #1 RNA were still used for microinjection into zebrafish eggs.

2.6.2. Cas9 *in vitro* transcription

An aliquot of Cas9 mRNA was provided as a kind gift from the laboratory group of Dr David Lyons. It was synthesised as previously described (159). Briefly; wild-type

Cas9 from *Streptococcus pyogenes* had nuclear localisation sequences and a C-terminal HA tag added by PCR using the following primers:
5'-
ATGGCCCCAAAGAAGAAGCGCAAGGTAGGTGGAGGTGGAGGAGGAGAT
AAGAAATACTCAATAGGCTTAG-3', and 5-
TCAAGCGTAGTCTGGGACGTCGTATGGGTAACCTCCTCCTCCTCCTCCTA
CCTTACGCTTCTTCTTTGGAGCACCTCCTCCTCCTCCTCCGTCACCTCCTA
GCTGACT-3'. The PCR product was then subcloned into the vector pCR8/GW/TOPO/TA and then recombined into the vector pCS2+/GW using LR Clonase II. The Cas9 was then linearized using *Not*I, then transcribed *in vitro* using the SP6 mMESSAGE mMACHINE kit.

Table 2.6. Primer Sequences

Primer	Sequence
T7	TAATACGACTCACTATAG
CDK9 Forward	GCCGAAAGAAAACGCGAAGT
CDK9 Reverse	ACGGGCCATATGGGGATTTC

A

Guide 1

5’

AAAGCACCGACTCGGTGCCACTTTTTCAAGTTGATAACGGACTA
*GCCTTATTTTAACTTGCTATTTCTAGCTCTAAAA***CAATACTACGA**
TGGCGTCGAGCTATAGTGAGTCGTATTACGC

3’

Guide 2

5’

AAGCACCGACTCGGTGCCACTTTTTCAAGTTGATAACG
*GACTAGCCTTATTTTAACTTGCTATTTCTAGCTCTAAAA***C**
GTCCGATCTTCGCCAGCTTCCTATAGTGAGTCGTA
TTACGC

3’

B

TCATTGTTTGTCTTC**CGGTCGGCAGGTGGTGGTAACGTGTTTTTGCGCCGCTGAAT**
CCGTCCTGGGAACCGCAGAGGAACAGCAAGGATGCAGCGCGACAAAACCGGAA
GCTCTGGCGGCGGTGAAAAGTACGAATATTTTACTAATTTTATACACTTAACGTTCAT
TTACACTGTTAAATCTCGCATTTTATTACATTTTAATATACAAAGCACACATTTGTACTGC
TATAACATAGCTAGTCTCCAAAGCGACGCTGTAAATGTGATGTTTGTGTGGGGGTCTGG
ATTTGTGTCTTTGTCGGGCCGAAAGAAAACGCGAAGTGATCCACACACTCAAAACAG
CGTCATAAAAGACCAAATAGTTCTTTAAAACAAGCTTAATTATAACATAAATCAGTAAA
TAGCGGATTTGTAGTTGTACTTAGCGTGATATGTGTAGGCGGAATGAAGTAATATCGCC
TTGTTGTAAAACATGAGTGTGTATTTGTGTTGTTTGTGTTCAG**GCCGGACAGAGAGA**
CCGCCATCATGTCCAAATACTACGATGGCGTCGAG**TTTCCCTTCTGTGATGAATTCT**
CCAAATATGAGAAGCTGGCGAAGATCGGAC**AGGGCACCTTTGG**GTGAGTATTTGAT
GTTTGTGTGTGTAAATATACCATAATGTTTATCATCCAGTAACAGACCATTTTCACATGG
CGTCCGGTTTCACTCCATGCAGTGTGTCGTTACTTCCGCCTACATAGAAATCCCCATAT
GGCCCGTTTCCACTGAGT

Primers Guide #1 Guide #2

Figure 2.5. Designing CRISPR guide sequences
Two gRNA anti-sense guide sequences were synthesised for *in vitro* transcription. In *italics* is the conserved gRNA scaffold, containing sites necessary for Cas9 enzyme recruitment. In **bold** is the region of the gene of interest which will be targeted, upstream of a PAM site in the gene. In red is the T7 primer binding site, necessary for recruitment of the T7 primer during *in vitro* transcription (A). The CDK9 genomic DNA sequence of the target areas. In **bold** are exons; in orange are primers designed for PCR and genotyping of the knockout region. In green is the Guide #1 site, in blue the Guide #2 site. The red lines indicate the restriction enzyme cut sites for Hpy99I (Guide 1) and Hpy188I (Guide 2) (B).

2.6.3. Microinjection of gRNA oligonucleotide and cas9 mRNA into zebrafish eggs

The following injection solution was prepared: 2 µL of Cas9 mRNA, 1 µL Phenol Red, gRNA oligonucleotide at a concentration of 15 ng/µL, and then made up to 10 µL with ddH_20. This solution (1 nL) was injected into the single cell of newly laid zebrafish eggs, as shown in Figure 2.6 (see sections 2.3.2 and 2.5.3 for further information on microinjection).

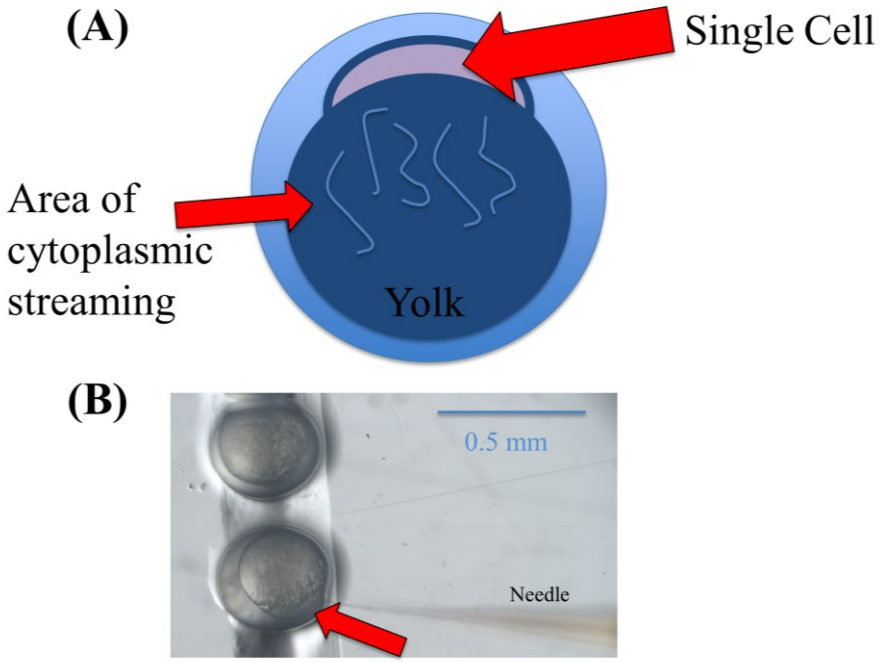

Figure 2.6. Microinjection of gRNA oligonucleotide and cas9 mRNA into zebrafish eggs

The red arrow indicates the region where the CRISPR/cas9 mRNA is injected (A). Image shows microinjection into the single cell, with the egg orientated so the single cell faces to the right to facilitate penetration by the needle.

2.6.4. Genotyping of CRISPR/cas9-injected animals and subsequent generations

Genotyping PCR assays were performed on whole single zebrafish embryos, or tail fin clips isolated from adults. Briefly, this was done by anaesthetising the adult fish in 4.2

% Tricaine in system water (see Section 2.1.4), and then laying the fish on wet tissue paper and removing the tip of the tailfin with a sterile scalpel (see Figure 2.7). This area is sufficient to allow extraction of enough genomic DNA (gDNA) for genotyping. Each tailfin sample was added to a PCR tube that was stored on dry ice, which helps the tissue to stick to the side of the tube. The embryos were euthanised in Tricaine (see Section 2.2.1), rinsed in PBS then singly distributed in PCR tubes. Excess liquid was removed. To each tube, 50 µL of a solution of 1:50 Proteinase K (20 mg/mL):TE Buffer was added. The tubes were then incubated overnight in a PCR machine at 55°C. This isolates the gDNA (170). The CDK9 primers in Table 2.6 were used to amplify the region in which a mutation would be predicted to occur in Guide #1 or Guide #2 injected animals. This is demonstrated in Figure 2.6. Each PCR tube was set up as follows to make a 25 µL reaction: 2 µL of genomic DNA, 12.5 µL of One*Taq* Quick-Load 2x Master Mix with Standard Buffer, 0.5 µL of each forward and reverse primer (diluted to 10 µM) and 9.5 µL ddH_20. The PCR settings used were as follows:

94°C	2 min	Initial Denaturation		
94°C	30 s	⎫		Denature
58°C	30 s	⎬	**x37**	Annealing
68°C	1 min	⎭		Extension
68°C	1 min	Final Extension		
4°C	Hold			

For genotyping, 12.5 µL of this PCR product was digested with 0.5 µL of Restriction Digest Enzyme Hpy99I (for Guide #1 template) or Hpy188I (for Guide #2 template), 1.5 µL of ddH_20 and 2 µL of Cutsmart Buffer. These enzymes cut within the Guide #1 or #2 target sites, shown in Figure 2.5.

2.6.5. Running agarose DNA gels

Agarose DNA gels were run to check the size of the PCR bands and restriction digest bands. A solution of TAE buffer and 2% Agarose was heated in the microwave till simmering. 2 µL of Sybr Safe Gel Stain was added per 100 mL of gel, then it was poured into a gel mould. Gene ruler 100 bp plus DNA ladder (5 µL) was loaded into

the first and last wells of each row, to allow assessment of the band size of the samples. The samples were loaded into the other wells. The gel was run at 100 V for roughly 45 min till the dye reached the edge of the gel.

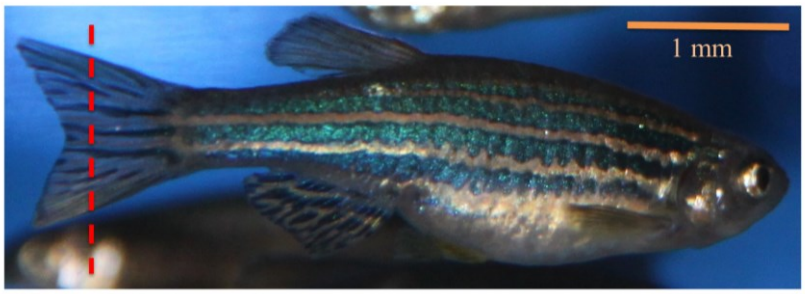

Figure 2.7. Fin clip of an adult zebrafish, for genotyping

An adult female zebrafish, with a red line to show the region of caudal fin which is removed using a scalpel for genotyping.

2.7. Creation of Mcl-1 over-expressing zebrafish using Tol2 gateway cloning

2.7.1. Cloning Mcl-1 into middle entry clone (pMe)

Vectors containing Mcl-1a and Mcl-1b fused to pEGFP-C1, and a vector containing the Lysozyme C (LysC) promoter, were given as a kind gift from Professor Stephen Renshaw, University of Sheffield. The Mcl-1a and Mcl-1b vectors were in an unsuitable vector for Tol2 cloning, so PCR was performed to amplify these areas of the plasmid and clone them into another vector.

The dried plasmid was shipped to Edinburgh on filter paper, then the patch containing the plasmid was cut out and the paper soaked in 30 µL of nuclease free water. The plasmid was transformed into TOP10^{TM} *E. coli* by adding 2 µL of this solution to an aliquot of Top10^{TM} chemically competent cells on ice for ½ h. The cells

were put on heat for 40°C for 30 s, so the bacteria take up the plasmid. The tubes were returned to ice for 1-2 min then 250 µL of SOC medium was added. The tubes were put on a 37°C shaker for 50 min and 150 µL of this solution was added to a Petri dish of Agar supplemented with kanamycin antibiotic (500 µL of 50 mg/mL Kanamycin in 500 mL of Agar). From each plate (Mcl-1a, Mcl-1b and LysC) 4 clones were picked by dipping a pipette tip in the clone and dropping the tip in a bacteria culture tube containing 5 mL of the same concentration of Lysogeny Broth (LB) medium and kanamycin. The tubes were kept overnight in a bacteria culture shaker at 37°C and then 700 µL of the culture was added to 300 µL of Glycerol for long term storage. The rest was centrifuged down repeatedly in a 2 mL microcentrifuge tube at 6800 g for 3 min, till only the bacterial pellet remained. This pellet was used to prepare plasmid DNA using the Qiagen Spin-Miniprep Kit. First, 250 µL of Buffer P1 from the kit was used to resuspend the bacterial cells, then next 250 µL of Buffer P2 was added and the tube was mixed by inverting it 10-12 times until the solution turned blue. The solution was incubated for 5 min then 350 µL of Buffer N3 was added, and the tube was mixed by inverting 10-12 times till the solution turned colourless. The tube was centrifuged for 10 min at 17,900 g, then the supernatant was applied to the QIAprep spin column. The supernatant was centrifuged at 17,900 g for 1 min then the flow-through was discarded. This was repeated till all the supernatant was gone and afterwards 500 µL of Buffer PB was added to the spin column and the tube centrifuged at 17,900 g for 1 min, and the flow-through was discarded. This step was repeated with 750 µL of Buffer PE. The spin column was transferred to a fresh collection tube and centrifuged for 1 min at 17,900 g to remove residual wash buffer. The spin column was placed in a fresh 1.5 mL microcentrifuge tube and the DNA was eluted by adding 60 µL of ddH_20 to the column, incubating at room temperature for 1 min, and centrifuging for 1 min at 17,900 g.

PCR was used to amplify 4 different sequences; *1:* Mcl-1a, *2:* Mcl-1b, *3:* peGFP-C1:Mcl-1a and *4:* peGFP-C1:Mcl-1b. The PCR reaction consisted of 5 µL of 10x buffer, 1 µL of PFU DNA Polymerase, 1 µL of dNTPs, 1 µL of DNA, and 2 µL of the appropriate forward and reverse primers, diluted to 10 µM, and 40 µL of ddH_20. For each condition the following primers were used: *1:* Mcl-1a forward and reverse primers, *2:* Mcl-1b forward and reverse primers, *3:* peGFP-C1 forward primer and

Mcl-1a reverse primer, and *4:* peGFP-C1 forward primer and Mcl-1b reverse primer (see Table 2.7). The following settings were used:

94°C	2 min	Initial Denaturation		
94°C	30 s			Denature
60°C	30 s		**x37**	Annealing
72°C	1 min			Extension
72°C	1 min	Final Extension		
4°C	Hold			

The PCRs were checked on a gel as in Section 2.6.5., with the exception that 6x loading dye was added to the samples, as the PFU DNA Polymerase did not contain loading dye already in a master mix. The PCR product was excised from the gel under UV light and digested using a QIAquick gel extraction kit (Qiagen), according to the manufacturer's protocol. The gel slice was weighed and 3 volumes of Buffer QG were added per 1 volume of gel. After the gel slice was dissolved, 1 gel volume of isopropanol was added to the sample and mixed. A QIAquick spin column was added to a 2 mL collection tube. The DNA was applied to the column and centrifuged for 1 min at 17,900 g, then the flow-through was discarded and 0.4 mL of Buffer QG was added to the QIAquick column. The column was centrifuged for 1 min at 17,900 g, then the flow-through was discarded. A wash step was performed by addition of 0.75 mL of Buffer PE (from kit) to the column and a 1 min 17,900 g centrifugation was performed. The column was left at room temperature for 5 min then centrifuged for 1 min to remove any residual wash buffer. The column was placed into a fresh 1.5 mL microcentrifuge tube. The DNA was eluted by addition of 50 µL ddH_20 to the column, incubation at room temperature for 1 min, then centrifuged for 1 min at 17,900 g. The DNA product was measured on the Nanodrop machine (See Appendix A for details), and the amount of ng needed for the BP reaction for each was calculated using the following formula:

$$Ng = (x \text{ fmoles})(\text{Base pairs})(660 \text{ fg/fmoles})(1ng/10^6 \text{ fg})$$

A BP reaction was set up to clone the PCR fragment into the Entry Vector (pDONR22). The following reaction was set up in PCR tubes: the appropriate amount

of DNA for 50 fmoles, along with 3 µL of 50 µg/µL vector and TE buffer up to 8 µL. 2 µL of BP Clonase was added to each tube, and then a 2 h incubation was performed at 25°C. The plasmid was transformed into *E. coli* as before and the cells were plated onto a kanamycin plate and incubated overnight at 37°C (described earlier in this section). Clones were picked and incubated overnight at 37°C. The DNA was prepared as before using the MiniPrep kit (described earlier in this section). The DNA was sent for sequencing to Eurofins Genomics using the Seq Smart DNA sequencing kit along with the M13 and T7 primers. M13 and T7 sites are present on the plasmid, facilitating sequencing. Appropriate restriction digests were performed at each step, to examine band size and ensure they were as expected.

2.7.2. LR reaction to create destination vector (pDest)

The LR reaction was carried out to combine the p5e LysC vector, the pMe vector (containing Mcl-1a, Mcl-1b, peGFP-C1:Mcl-1a OR peGFP-C1:Mcl-1b), p3e-PolyA and pDest vector). For the LR reaction, 1 µL of each vector (10 fmoles) and 1 µL of LR clonase was added together with TE buffer, up to 8 µL. This was incubated at 25°C overnight, then 1 µL of Proteinase K was added per reaction and the tubes were incubated for 10 min at 37°C.

2.7.3. Microinjection of vector and mRNA

Finally, an injection solution of 2 µL Danieau's Solution, 2 µL Rhodamine/Dextran solution, 1 µL Tol2 transposase mRNA (a kind gift from the lab of Dr Yi Feng), 2 µL of DNA, and 3 µL of ddH_20 as prepared and then 1 nL was microinjected into the 1 cell stage as described in Section 2.6.3.

Table 2.7. Primers used in Cloning of Mcl-1a and Mcl-1b

1-4: Sequences in red: Kozak Sequence; Sequences in **bold**: Mcl-1-specific sequence; Sequences in *Italics*: attB1 sequence (forward primers) or attB2R sequence (reverse primers)

Primer	**Sequence**
1. Mcl-1a Forward Primer	*GGGGACAAGTTTGTACAAAAAAGCAGGCT*GCCGC CACC**ATGGCTCTGAGTTTGGATTTTAG**
2. Mcl-1a Reverse Primer	*GGGGACCACTTTGTACAAGAAAGCTGGGT***TCACC GGATGAGGAAGGC**
3. Mcl-1b Forward Primer	*GGGGACAAGTTTGTACAAAAAAGCAGGCT*GCCGC CACC**ATGTTCGCTGGAAGAAACAAC**
4. Mcl-1b Reverse Primer	*GGGGACCACTTTGTACAAGAAAGCTGGGT***TCACC GTATCCAATAGGCAAG**
M13 Primer	GTAAAACGACGGCCAGT
T7 primer	CCCTATAGTGAGTCGTATTA

2.8. Neutrophil Isolation from human peripheral blood and treatment with R-roscovitine

This technique was performed with kind assistance from Dr Calum Robb. Around 40-160mL of blood was collected from donors in 50 mL microcentrifuge tubes with sterile sodium citrate (final conc. 0.38%). The blood was centrifuged at 300 *g* for 20 min and platelet-rich plasma removed. Leukocytes were separated from erythrocytes by dextran sedimentation over 25-30 min using pre-warmed (37°C) 0.6% (weight/volume) dextran T500. The upper leukocyte-rich layer was aspirated and volume adjusted to 50 mL using pre-warmed 0.9 % saline. The leukocytes were pelleted by centrifugation at 350 g for 6 min. Polymorphonuclear leukocytes underwent separation from mononuclear leukocytes using a discontinuous isotonic Percoll gradient (9:1 percoll:10 x Phosphate Buffered Saline [PBS] ratio). The gradients were as follows: 81%, 70% 55% Percoll in 1x PBS (without cations).

3 mL of 70% isotonic Percoll was layered on 3 mL of 81% isotonic Percoll in a 15 mL microcentrifuge tube. The leukocytes were re-suspended in 3 mL 55% Percoll. The gradients were centrifuged at 720g for 20 min. Mononuclear cells are in the upper 55:70% interface, and polymorphonuclear leucocytes at the 70:81% interface. Cell yield was calculated using a haemocytometer. Leukocytes were washed twice in pre-warmed 1x PBS (without cations), by filling the microcentrifuge tube containing cells with 50 mL of 1x PBS, then centrifuging at 300*g* for 5 min and discarding the

supernatant. Cell viability staining was performed using trypan blue to check that a purity of at least 98% neutrophils was obtained. Cells were re-suspended at $5x10^6$ cells/mL in Iscove's modified dulbecco's medium (IMDM) with 50 U/mL penicillin and 50 U/mL penicillin/streptomycin (10%) Pen/Strep) plus 10% autologous serum. The isolated neutrophils were cultured in flat-bottomed 96 well plates at $5x10^7$ cells/mL in IMDM with 10% autologous serum and 10% Pen/Strep in a humidified, 5% CO_2 incubator at 37ºC. 75 µl of $5x10^6$ cells/mL cell suspension to each well of a flat-bottomed 96 well plate. To treat with drug or control, 15µl of *R*-roscovitine, (at 10x concentration) or DMSO control and 60µl of IMDM/10% serum were added to the 75 µl of cells. The plate was covered and incubated at 37°C in an incubator at 5% CO_2 for 6 h.

Cytospins were prepared from the cells and stained to study their morphology. 100 µL of cell suspension was added into a cytospin chamber, and the chamber cytocentrifuged for 3 min at 30 g. The slide was removed and air-dried for 5 min. The slide was fixed in methanol for 2 min then drained and stained with an acid dye (Diff-Quik solution #1) for 2 min). It was then stained immediately with a basic dye (Diff-Quik solution #2). The slide was drained, rinsed with dH_20, and then dried and a drop of DPX mountant media was applied to the cells and a coverslip placed on top. Slides were viewed using a light microscope at 40x or 100x objectives.

The cells were resuspended in the 96 well plates, then 50 µL of cell suspension was transferred from each well into a flow cytometry tube with 250 µL Annexin V buffer. The tubes were incubated on ice for 5-10 min. Immediately prior to analysing the samples using a flow cytometer, 1µL of PI (1 mg/mL solution) was added to each sample. Samples were analysed on a flow cytometer using FL-1/FL-2 channel analysis. Viable cells are dual AnnV/PI negative; apoptotic cells are AnnV positive, PI negative; necrotic cells are dual AnnV/PI positive (depicted in the example in Figure 3).

2.9. Graphing, data analysis and statistical analysis

Graphs were created using Graphpad Prism 5, and the statistical analysis was also carried out using this software. The tests carried out were one-way or two-way Anova followed by post-hoc Newman-Keuls, or unpaired T-tests, as appropriate and indicated in the Results. Significance was determined as a p value of less than 0.5 ($p \leq 0.5$). FlowJo™ software was used to analyse flow cytometry data.

For image analysis, ImageJ Fiji (NIH Bethesda) was primarily used for analysing stereofluorescent and confocal images. Furthermore, Leica LAS Lite software was also used to analyse confocal images.

Tests were conducted to assess the effect of intra-observer and inter-observer variability. Some tailfin wound images were selected at random, and the neutrophils were counted using the method shown in Figure 2.2 (Chapter 2: Methods) and Figures 3.1 and 3.2 (Chapter 3: Establishing the Zebrafish Tailfin Transection Injury Model). Then, the same images were counted a day later (Intra-Observer test 2) and by a third party (Inter-Observer test, Fig, 2.8). This revealed no statistical difference ($p \geq 0.05$) in the cell numbers counted in each group, indicating that counting cells by eye was a reliable and reproducible method.

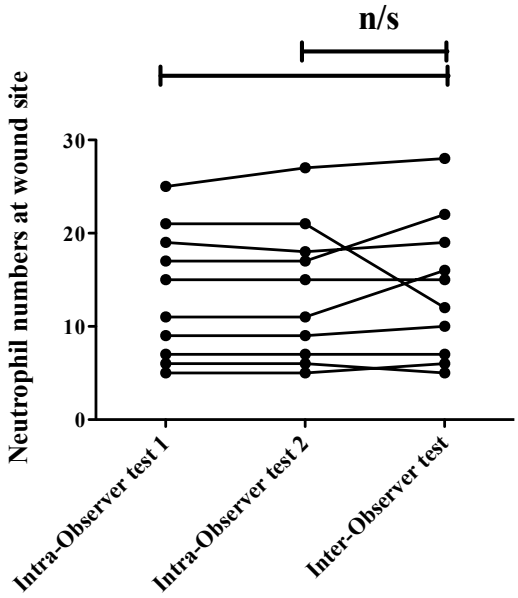

Figure 2.8. Intra-observer and inter-observer testing on tailfin neutrophils after wounding

Zebrafish neutrophils at the injury site post-wounding were counted in a selection of random images, then re-counted a day later (Intra-Observer test 2) then by a third party (Inter-Observer test). The differences between each group were analysed using one-way ANOVA.

3. Chapter 3. Establishing the Zebrafish Tailfin Transection Injury Model

3.1. Introduction

The early stages of this project involved establishing a suitable inflammatory model in the zebrafish with which to investigate the innate inflammatory response, and specifically to manipulate neutrophil apoptosis and macrophage efferocytosis. Often injury of the tailfin is used as an excellent model, as it is thin and transparent and therefore amenable to visualisation and image analysis. This is regarded as a sterile inflammation model, but it is possible to elicit a non-sterile inflammatory response by including infectious agents in the water or by microinjection. Previously other sources of stimulation have been used; for example, lipopolysaccharide (LPS) (168) and live *Pseudomonas aeruginosa* (141) have also been used alongside tailfin transection to increase inflammation.

The tailfin transection model was pioneered by Renshaw et al in 2006 (126). The group created a transgenic fish with fluorescently-labelled neutrophils (Tg[mpx:EGFP]^{i114}). These animals have transgenic expression of green fluorescent protein (EGFP) driven by expression of the myeloperoxidase promoter. In these animals, they transected the end of the embryonic tailfin and body, including part of the vasculature system (126). This induces an inflammatory response with rapid neutrophil recruitment to the site of wounding. The profile of this injury includes a 'peak' of neutrophils (roughly 20 cells) at 4-8 hours (h), which subsequently resolves by 24 h (126). An alternative model developed by Brown et al involved using a needle to 'nick' the tailfin, which induces a more subtle response with around 8 neutrophils recruited at 2 h after transection, measured by MPO staining (141). Variations on this theme were tested in the initial stages of this project, to ascertain the most suitable model for the manipulations that would subsequently be carried out. Consideration was also given as to which defined area to use for measuring the inflammatory response (i.e. should the area in which cell numbers were counted encompass the whole tailfin area or just the exact site of the wound?).

After the initial zebrafish neutrophil inflammation studies in the transgenic embryos made by Renshaw et al (126), fish were developed in which macrophages are specifically labelled. This was relatively difficult compared to development of the neutrophil-specific lines, due to the lack of a characterised macrophage-specific marker (176). The first line to be made was the Tg(fms:mCherry) line. This line was

initially used in this project, as it was already available in the zebrafish facility. In Tg(fms:mCherry) fish, macrophages are labelled by the M-CSF receptor promoter; but some other cells are also labelled, including xanthophores (yellow pigment cells) (127). This is not necessarily a problem, as distinction can be made based on the fact that macrophages are migratory whereas xanthophores are not. Later in this project, access to the Tg(MPEG1:mCherry) line became available (128). Macrophage-expressed gene 1 (MPEG1), is a macrophage-specific promoter, involved in perforin expression (177).

The phenotypic and functional characteristics of these labelled neutrophils and macrophages has been carried out in a variety of ways, such as whole-mount in-situ hybridisation and quantitative PCR to check what genes these cells express (176, 178). Another approach has been flow cytometric sorting of zebrafish neutrophils from whole embryos, to allow comparison of *ex vivo* zebrafish neutrophils to *ex vivo* mammalian neutrophils. Isolation of zebrafish neutrophils has been successfully performed (178) in order to carry out phenotyping assays; such as characterisation of cells with strong EGFP expression ($EGFP^{hi}$) and those with weak EGFP expression ($EGFP^{lo}$) populations which exist in the $Tg(mpx:EGFP)^{i114}$ line. The $EGFP^{lo}$ but not the $EGFP^{hi}$ population express colony stimulating factor 1 receptor (CSF1R), indicating that macrophages may express a small amount of myeloperoxidase (which is considered a neutrophil marker); or that these $EGFP^{lo}$ cells are a multipotent precursor cell. Isolating a population of cells in this way allows functional and phenotypic assays to be performed, although this is somewhat limited in zebrafish by the cell numbers that can be obtained, particularly from embryos, although this can be circumvented by obtaining large embryo numbers. More cells can be obtained by digesting the site of haematopoietic development (the kidney). Several assays exist that can be used to investigate granulocyte phenotype and function. These include antibody staining for specific markers (i.e. Ly6G) or the measurement of shape change (cell polarisation) by stimulation with formyl-methionyl-leucyl-phenylalanine (fMLF) (175). fMLF is a potent neutrophil chemoattractant which induces neutrophils to migrate by binding to the G-protein seven transmembrane formyl peptide receptor 1 (FPR1) (179). FPR1 ligands (N-formylated peptides and annexin A1 among others) are secreted by pathogens or released passively by dying host cells. Bacteria actively

release N-formylated peptides; and in cells dying via necrosis, where intracellular DNA is released, maternal mitrochondrial peptides are also released (which are rich in formylated DNA). It seems logical that they are pro-inflammatory, as mitochondria are thought to have arisen from proteobacteria becoming incorporated into eukaryotic cells. In this project, tests were conducted to develop the previously described zebrafish model (126) as a suitable model to test the study objectives of this project. fMLF was selected for testing the effect of stimulation on isolated zebrafish neutrophils.

Taken together, the initial studies allowed the rest of the project to proceed with confidence that there was a justification for using zebrafish as an animal model of neutrophilic inflammation. An inflammatory model was selected, and the neutrophil and macrophage response was characterised; paving the way for future manipulations and comparisons to be made to normal, baseline responses.

3.2. Research Questions

- What is a suitable and reliable zebrafish injury model for modelling neutrophil-driven inflammation?
- How should the area of inflammation be quantified?
- What is the normal profile of neutrophil and macrophage response to wounding?
- Can this be enhanced by other stimuli (i.e. non-sterile inflammation)?
- Do zebrafish neutrophils possess similar characteristic to mammalian neutrophils?

3.3. Results

3.3.1. Testing three different injury models

To set up this model, three alternative injuries were trialled (section 3.1.4, Fig. 3.1, 2.1). Firstly; the entire tailfin of Tg(mpx:EGFP)^{i114} was removed without damaging the vasculature using a scalpel, resulting in cell recruitment to the wound site (Fig. 3.1, A). In the second model, the tailfin was removed along with a portion of the vasculature using a scalpel (Fig. 3.1, B), resulting in a larger recruitment of neutrophils and a 'plug' of cells where the vasculature was damaged. In the third model, the tailfin was 'nicked' using a needle, resulting in a lower recruitment of neutrophils (Fig. 3.1, C). The recruitment of neutrophils in each injury was quantified (Fig. 3.1, D)

The tailfin transection model without vasculature damage was selected to carry through the project, as it produced a more reproducible injury with smaller error bars after quantification compared to the vasculature injury model (Fig. 3.1, A, D). The approved wound technique used in these studies will be called "tailfin transection", as only the median fin, beyond the body will be cut (i.e. the body is undamaged).

Figure 3.1

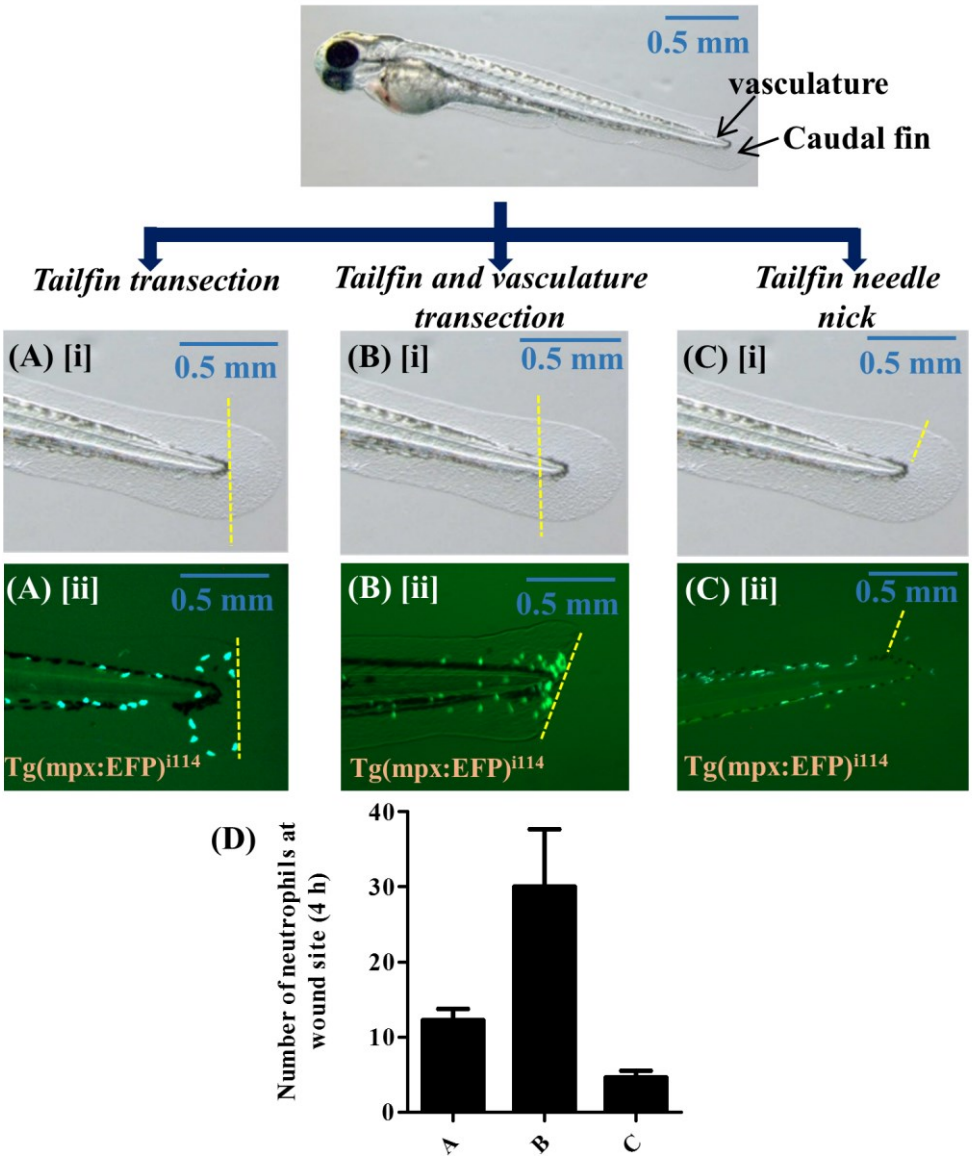

Figure 3.1. Comparison of the position of different zebrafish tailfin transections

Images depicting the position of full transection without damaging the vasculature (A), full transection including vascular injury (B), and a small 'nick' to the edge of the tailfin (C) in brightfield [i] or in Tg(mpx:EGFP)^{i114} fish with green neutrophils at 4 h post transection (taken using a fluorescent stereoscope with a GFP filter (Ex. 488) [ii]. Yellow line indicates area of transection with scalpel or nick with 19G needle. 4 h images for each injury from (A), (B) or (C) were quantified – shown in (D).

3.3.2. The area of tailfin measured to assess inflammation

Next, analysis was carried out to determine how the inflammatory wound cells should be counted (Fig. 3.2). This was done using defined areas created using ImageJ software, which was considered important so that counting was consistent throughout the project. The following areas (depicted in Fig. 3.2, A) were counted: *b* – length 0.16 mm from the tip of the body (i.e. cells directly at the wound), and *c* – length 0.5 mm from the tip of the body (i.e. cells at the wound plus cells migrating to the wound). This area was kept consistent by saving a 0.16 mm or 0.5 mm length box on ImageJ, and applying the box to all the images (taken at 8x magnification), by placing the right-hand line of the box at the edge of the pigmented area at the end of the fish body (this is marked with a red line (Fig. 3.2, A[i]).

Both areas (*b* and *c*) were quantified (Fig 3.2, B). From this, it was concluded that *c* (0.5 mm, incorporating both *a* and *b*) was the best area to count, as it shows a pronounced inflammatory response, which would likely be more amenable to manipulation. In addition, the area depicted by *a* is clearly a site of dynamic inflammation, as direct comparison of these images shows; so therefore *a* should be included (A). At 0 h, there are 5 cells (i.e. resident neutrophils) in the area designated *a*; however by 4 h there were 8 cells in the same area. This indicated it might be important to include this area, to incorporate cells that are migrating to the wound but have not quite reached the wound site yet. The motility of cells in this area is also observed when performing live imaging of neutrophil migration to the wound (Video 1). Further quantification of tailfin wounding inflammation was therefore quantified using the area designated by *c*.

Figure 3.2

(a + b)
(c)

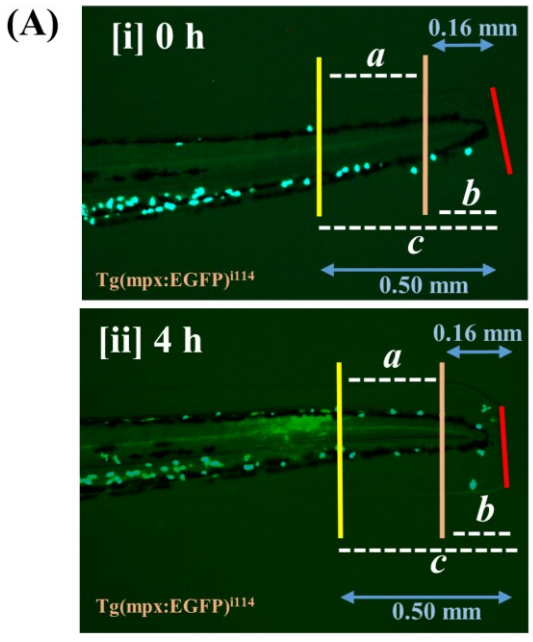
(A)
[i] 0 h
0.16 mm
a
b
c
Tg(mpx:EGFP)i114
0.50 mm
[ii] 4 h
0.16 mm
a
b
c
Tg(mpx:EGFP)i114
0.50 mm

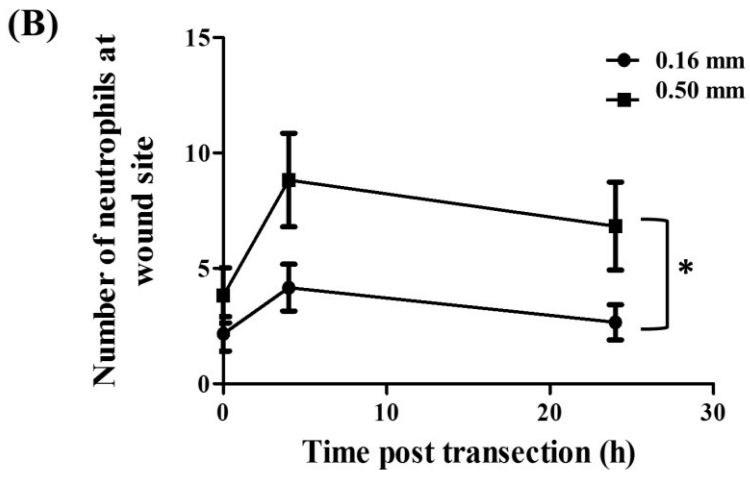
(B)
Number of neutrophils at wound site
15
10
5
0
0
10
20
30
Time post transection (h)
0.16 mm
0.50 mm
*

Figure 3.2. Comparison of area used to measure zebrafish tailfin transection model

Images of transected Tg(mpx:EGFP)^{i114} fish were taken immediately after transection at 0 h (A [i]) and again at 4 h (A[ii]). The red line indicates the transection. The cells in the area with length 0.16mm (from red line to orange line, *b*) and 0.5mm (from red line to yellow line, *c*) were counted and compared to measure the inflammatory response (B). 15 fish were quantified in this example from 3 independent experiments. Data expressed as mean ± S.E.M. * $p \leq 0.05$, ANOVA followed by post-hoc Newman Keuls test.

3.3.1. Quantifying the neutrophil response to tailfin transection

Next, the inflammatory response was characterised by wounding, then imaging at different time points after transection (examples in Fig. 3.3, A) and quantifying as shown (Fig. 3.3, B). This quantification (Fig. 3.3, C) revealed that neutrophil numbers rise sharply after the initial transection, peaking at around 4 h after the initial transection (13 ± 2). The inflammation continues over the next 24 h and even appears to increase further at around 44 h post-transection (17 ± 2 neutrophils) before starting to decline at 48 h, which was the age limit of imaging the fish according to Home Office guidelines. The inflammatory response for 15 h after transection is also shown in time lapse format in Video 2.

Figure 3.3

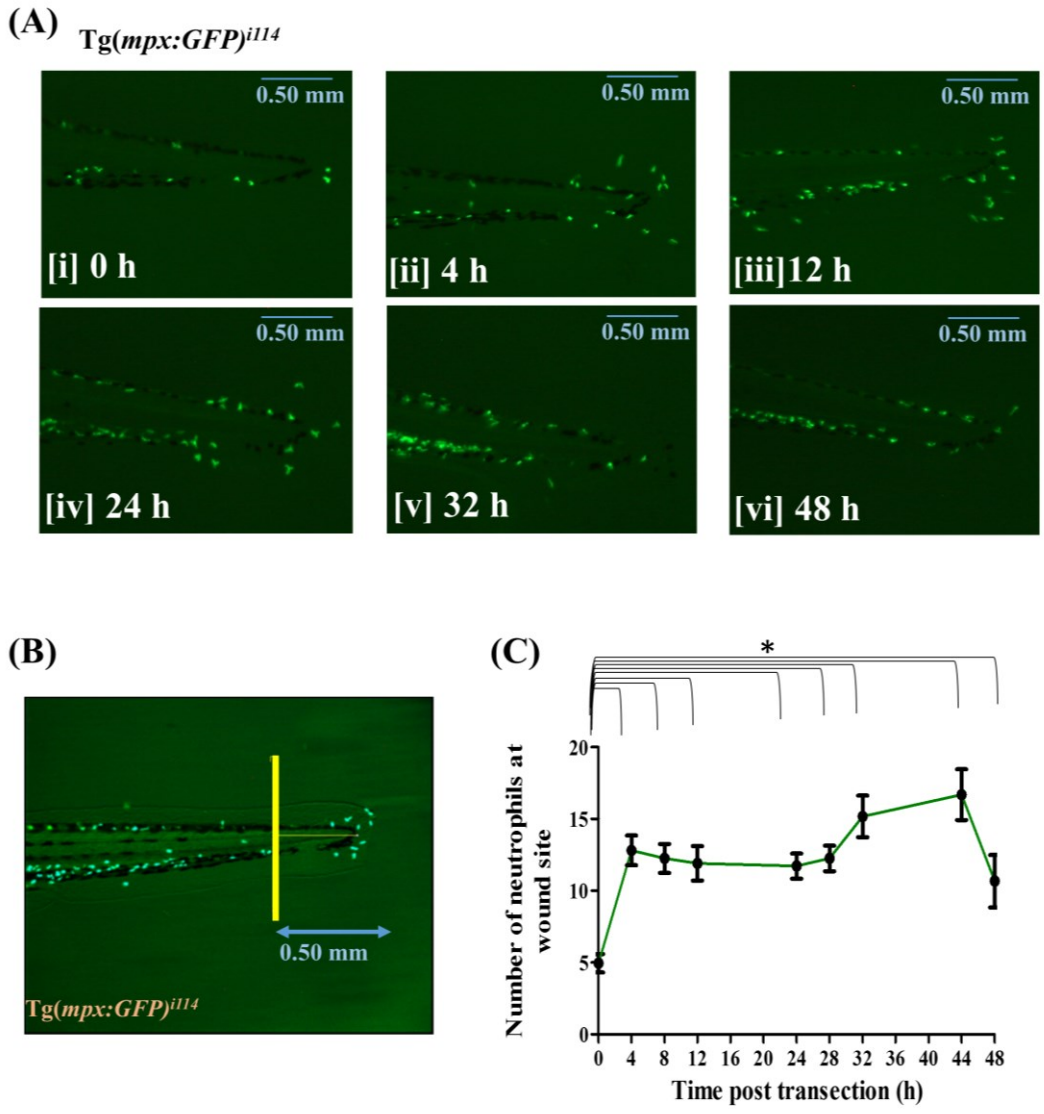

Figure 3.3. Neutrophil migration to wound sites of Tg(mpx:EGFP)^{i114} zebrafish after tailfin transection

Tg(mpx:EGFP)^{i114} fish with labelled neutrophils are wounded at the 0 h time point and then imaged serially over different time points (A) [i]-[vi], and quantified by counting the area shown [as determined in Fig. 3.2.] (B, C). (B) adapted from Lucas et al, FASEB J, 2013, to show the area used for quantifying inflammatory cells. Embryo 3 dpf, 4 hpi. ≥40 fish in 3 individual experiments. Data expressed as mean ± S.E.M. *$p \leq 0.05$, 0 h v all other time points; assessed by one-way ANOVA followed by post-hoc Newman-Kuels test

3.3.4. Selecting a macrophage-specific line for use in tailfin transection model

The same tailfin transection assay was carried out using the macrophage-labelled lines, Tg(fms:mCherry) and Tg(MPEG1:mCherry) (Fig 3.4, Section 1.3.1.2). Due to non-specific expression of the fms promoter, it can be difficult to count cells in these fish; there can be significant numbers of non-macrophage cells, for example in the 4 h time point image, in which macrophages (orange arrows) and resident non-macrophages (green arrows) are labelled (Fig 3.4, A[ii]).

Quantification revealed there may be over-estimation when counting the Tg(fms:mCherry) line, as numbers of macrophages counted at 24 h were higher in these animals compared to Tg(MPEG1:mCherry) – there were 26 ± 2 cells in the fms:mCherry group rather than 19 ± 4 (Fig. 3.4, D).

Macrophage numbers in the Tg(MPEG1:mCherry) peaked at 24 h post-transection then decreased over the next 48 h (Fig. 3.5). In general, the number of macrophages was always higher than neutrophil numbers. For example, at 12 h post-transection in this group of animals, there were a mean of 12 ± 2 neutrophils at the wound compared to 21± 2 macrophages (Fig. 3.5).

Figure 3.4

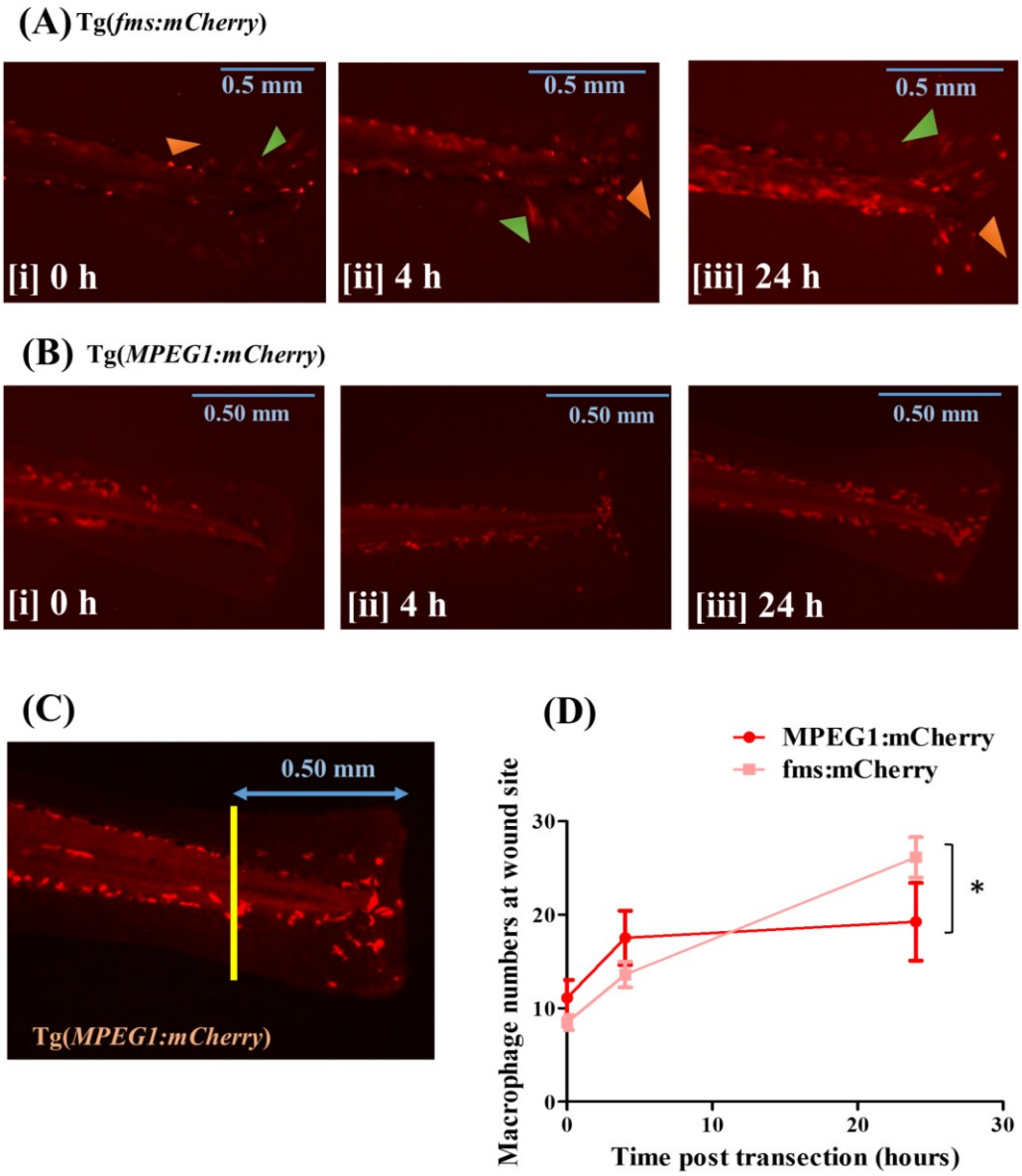

Figure 3.4. Macrophage migration to wound sites in Tg(fms:mCherry) and Tg(MPEG1:mCherry) zebrafish after tailfin transection

Fish were wounded at the 0 h time point and then imaged serially over different time points in Tg(fms:mCherry) (A) [i]-[iii] or Tg(MPEG1:mCherry) fish (B) [i]-[iii]. Green arrows in (A[ii]) indicate non-specific fms expressing-cells which don't migrate; orange arrows indicate macrophage cells which have migrated to the wound area. The inflammation was quantified by counting the area shown (everything to the right of the yellow line) (C). The macrophage numbers in Tg(fms:mCherry) and Tg(MPEG1:mCherry) fish after injury were directly compared (D). *Indicates a p value of ≤ 0.05. ≥26 fish, from 3 independent experiments. Data expressed as ± S.E.M.

Figure 3.5

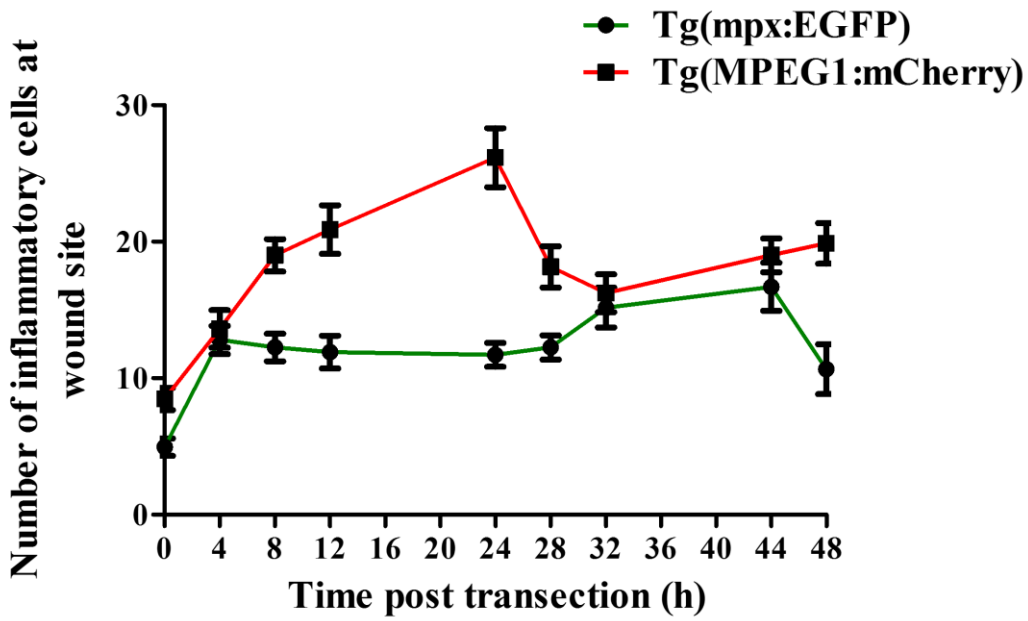

Figure 3.5. Comparison of neutrophil and macrophage recruitment following tailfin transection

An overlay graph comparing the numbers of neutrophils and macrophages recruited to the site of tailfin transection over different time points in the first 24 h post transection. Experiments were carried out in Tg(mpx:EGFP)^{i114} and Tg(MPEG1:mCherry) zebrafish for measurement of neutrophils and macrophages, respectively. ≥ 40 fish per group, from 3 independent experiments. Data expressed as ± S.E.M.

3.3.5. Addition of lipopolysaccharide (LPS) after zebrafish tailfin transection

After establishing these inflammation profiles, the transection experiment was performed, but with the addition of lipopolysaccharide immediately after transection.

Various concentrations of LPS were tested but did not show any effect on the neutrophil numbers after wounding in the Tg(mpx:EGFP)^{i114} fish (Fig. 3.6). For example, at 24 h post-transection, there was a mean of 11 ± 2 neutrophils in the control group compared to 10 ± 1 in the LPS-treated group. Further wounding experiments used did not include any additional stimulus such as LPS.

Figure 3.6

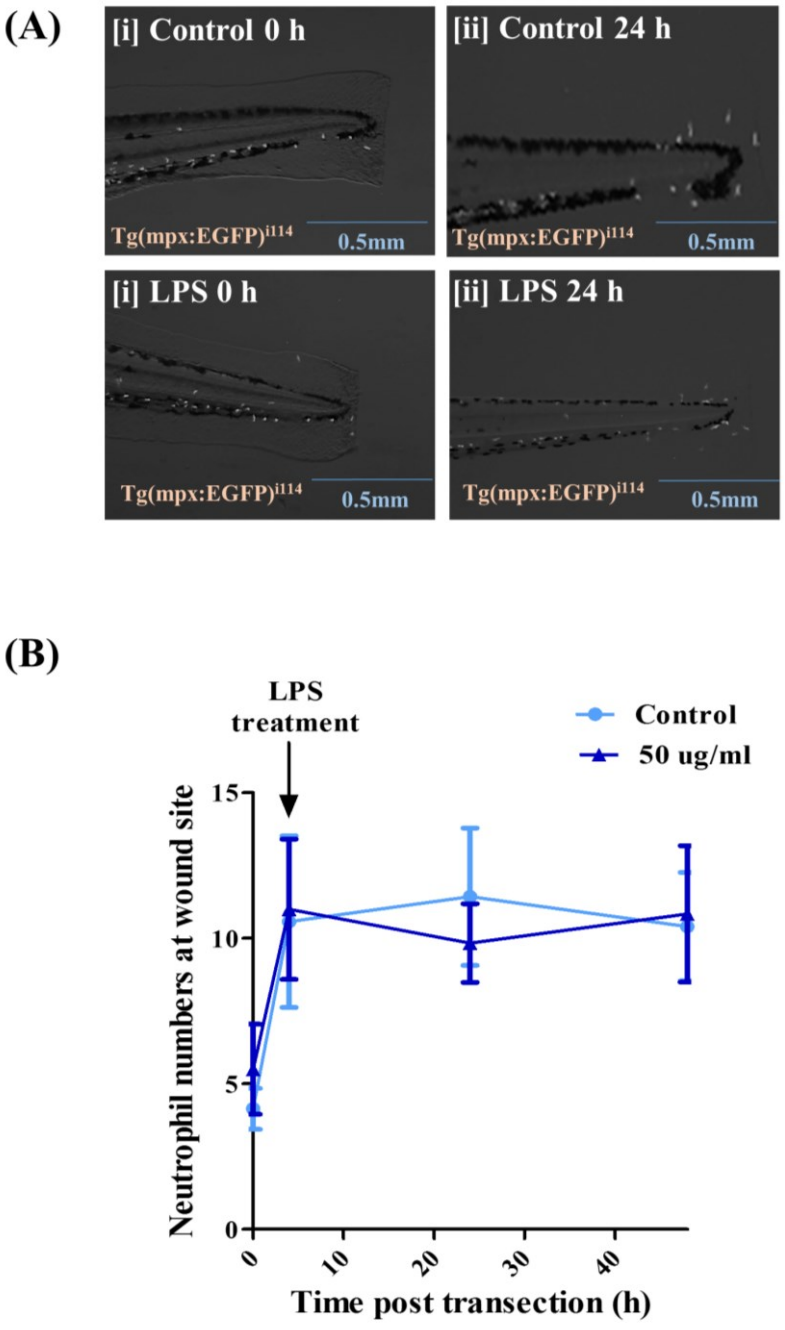

Figure 3.6. Tailfin transection and Lipopolysaccharide (LPS) Treatment
The tailfin of Tg(mpx:EGFP)^{i114} zebrafish was transected and LPS added to the water at 4 h post-transection, at a variety of concentrations (shown here is the highest, 50 µg/mL), and imaged at different time points post-transection (A) and quantified (B). ≥8 fish per group, from 2 independent experiments. Data expressed as mean ± S.E.M.

3.3.6. Sorting of EGFP$^+$ embryonic neutrophils and stimulation with fMLF

The similarities between mammalian and zebrafish neutrophils were explored by *ex vivo* stimulation. This was done by flow sorting cells from whole embryos (500 embryos were used here to obtain populations of roughly 3000 neutrophils). It is easy to distinguish a EGFP$^+$ population in a population of total embryonic cells (Fig. 3.7, A[ii]) compared to wild-type animals (A[i]). Imaging of these cells revealed that they migrate with a neutrophil-like morphology (Fig. 3.7, B, Video 3).

Sorted cells were stimulated *ex vivo* with fMLF. This stimulation caused an increased in forward scatter in the sorted EGFP$^+$ cells (Fig. 3.8, A, B[ii]) compared to untreated cells (Fig. 3.8, A, B[i]). Isolation of EGFP$^+$ neutrophils was also carried out by digesting 5 whole kidneys (the kidney is the site of haematopoietic development in zebrafish), and then flow sorting cells based on EGFP expression. Higher yields were possible than with embryonic fish (around 40,000 from 3 adult kidneys, data not shown).

Figure 3.7

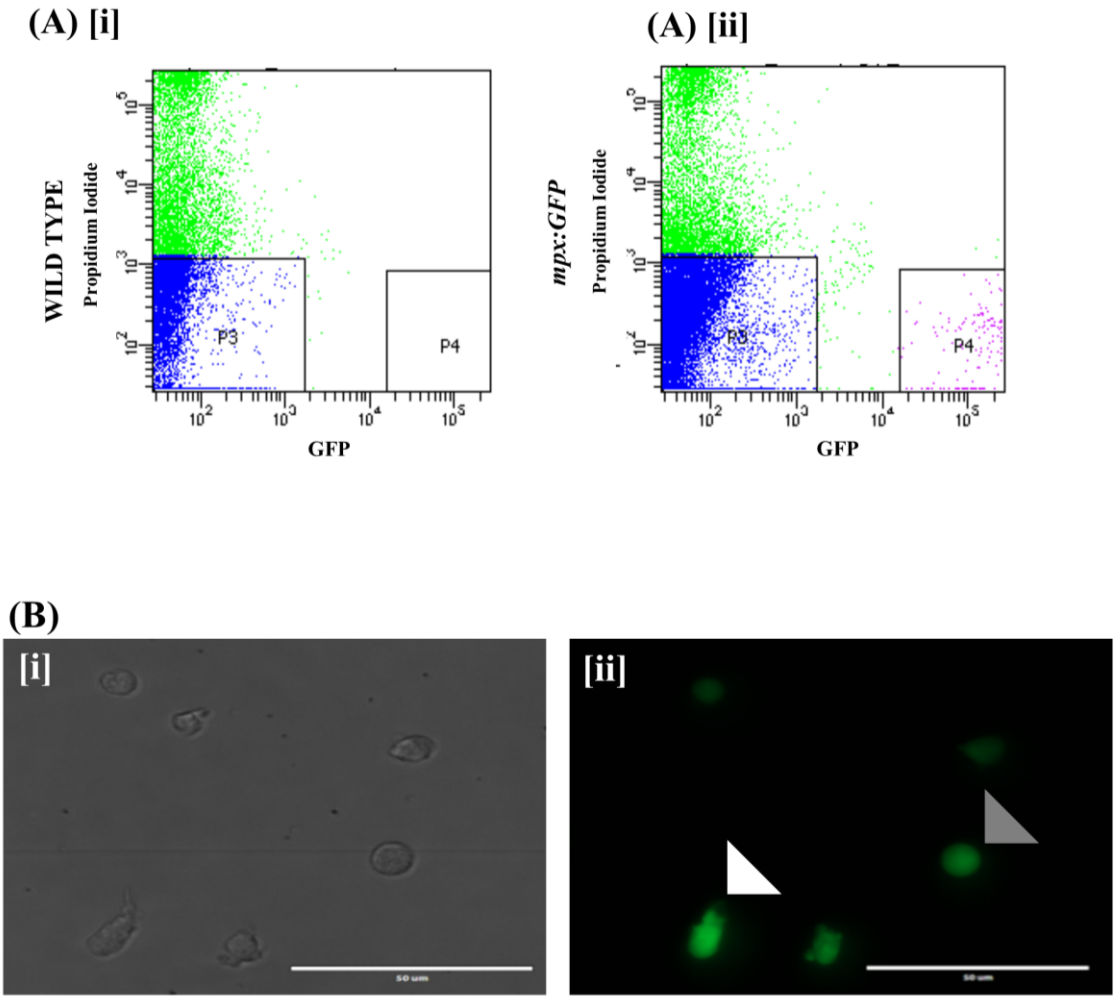

Figure 3.7. Fluorescence-activated cell sorting (FACS) of embryonic EGFP^{+} neutrophils *ex vivo*

Flow sorting was carried out on embryos from wild type (A[i]) and Tg(mpx:EGFP)^{i114} (A[ii]) fish, with the "P4" gate demonstrating a EGFP^{+} population in [ii]. Brightfield (B [i]) and EGFP^{+} cells (B [ii]) were imaged on a cover glass slide, with white arrows indicating a healthy cell and grey a potential apoptotic cell. Approximately 500 embryos were used to obtain around 3000 cells in this example.

Figure 3.8

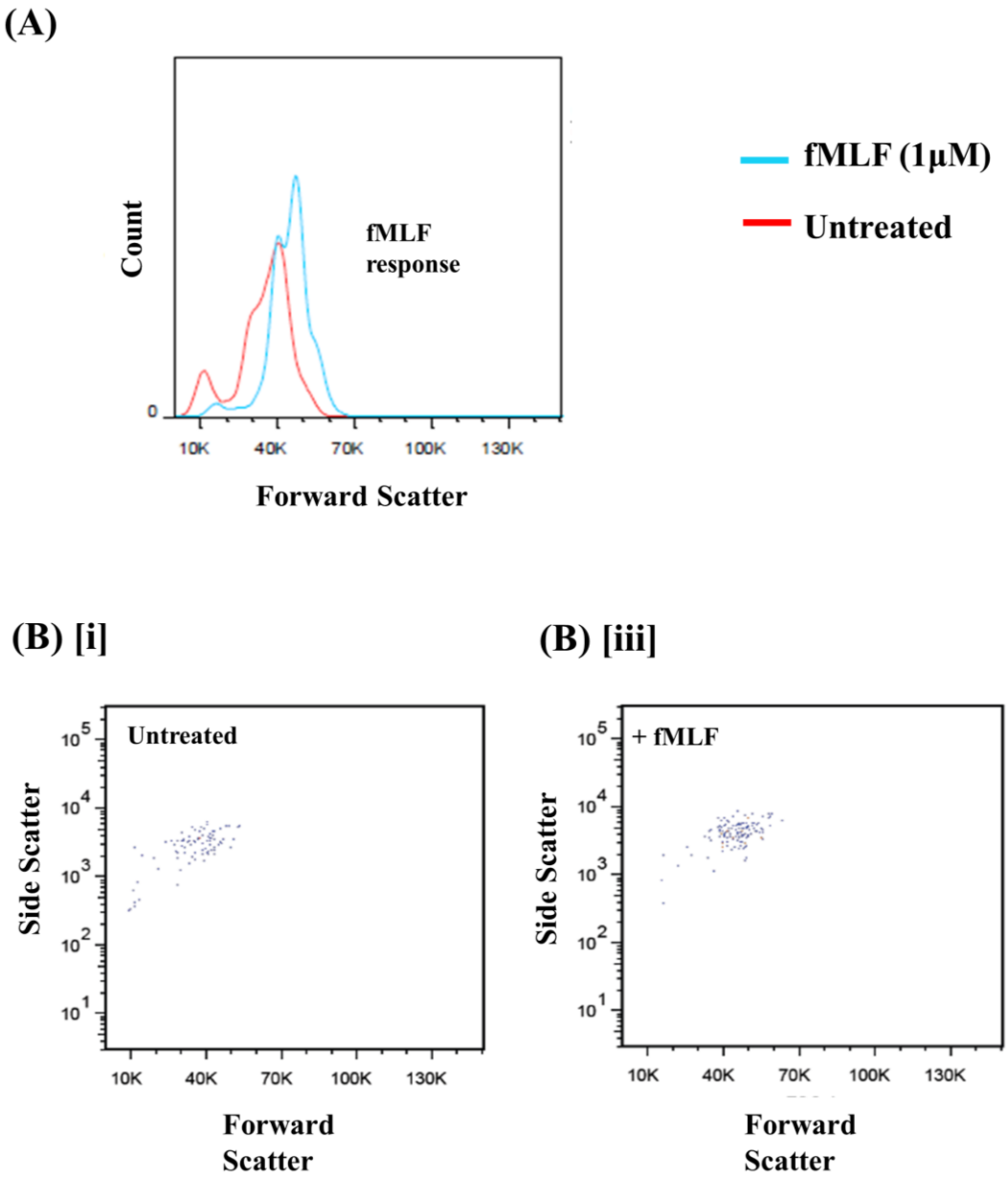
(A)
Count
fMLF
response
0
10K
40K
70K
100K
130K
Forward Scatter
fMLF (1µM)
Untreated
(B) [i]
Untreated
Side Scatter
10^5
10^4
10^3
10^2
10^1
10K
40K
70K
100K
130K
Forward
Scatter
(B) [iii]
+ fMLF
Side Scatter
10^5
10^4
10^3
10^2
10^1
10K
40K
70K
100K
130K
Forward
Scatter

Figure 3.8. Stimulation of isolated zebrafish neutrophils *ex vivo* with fMLF

Sorted $EGFP^{+}$ cells from 500 embryos were stimulated *ex vivo* with fMLF, or were untreated; and forward scatter was assessed in both groups, shown as a histogram of forward scatter (A) and also as dot plots (B[i], B[ii]). Representative of 3 independent experiments.

3.4. Discussion

Observations from Chapter 3

- Tailfin transection of the tailfin without damage to the body and vasculature is an ideal model for imaging neutrophil and macrophage accumulation (Fig. 3.1).
- The inflammatory response seen after tailfin transection is reproducible and allows a significant inflammatory response with manageable numbers.
- The best area of inflammatory response to measure was determined to be the area with length of 0.5 mm from the end of the body (Fig. 3.2).
- Neutrophil recruitment in the zebrafish peaks at around 4 h after tailfin transection, and macrophage recruitment peaks at around 24 h after transection. There is a second peak of neutrophil recruitment at 44 h post-transection.
- Inflammatory cell numbers in this tailfin injury model do not fully return to baseline level within 48 h post-transection.
- The area for counting these inflammatory cells should take into consideration migrating cells (both to and from the site of the wound), as well as cells directly at the wound.
- Addition of this variant of LPS did not affect neutrophilic responses after wounding in this model, when added at 4 hours post injury (hpi).
- The Tg(MPEG1:mCherry) zebrafish is a better model for macrophages compared to Tg(fms:mCherry), in which non-macrophage cells can also be labelled (Fig. 3.4).
- $EGFP^{+}$ neutrophils from zebrafish can be isolated and used for *in vitro* experimentation, for example imaging and stimulation.
- The flow-sorted zebrafish neutrophils respond to fMLF, by increasing their size. This response occurs in a similar manner in mammalian neutrophils.

Following these initial studies, a "tailfin transection" model, which removed only the tailfin portion of the median fin, without damaging the vasculature (Fig. 3.1, A[i]), was chosen for further experiments. This injury produced a reproducible wound with

consistent inflammation levels (Fig. 3.3). The most severe transection (Fig. 3.1, B), pioneered by Renshaw et al (126), was deemed difficult to count, due to the fact that large 'clumps' of cells accumulate at the area of vasculature wounding, to heal this area and 'plug' the damage to the blood vessel.

The milder 'needle nick' model (Fig. 3.1, C) was deemed to be not severe and acute enough; i.e. the effect of the genetic and pharmacological manipulations might not be seen if not enough cells are recruited. The numbers of neutrophils recruited in the 'nick' model have previously been shown to be quite low and also quite variable (between 0 to 8 cells) (141). Furthermore, in prior work by Brown et al in which they 'nick' the tailfin with a needle, it was concluded that *Pseudomonas aeruginosa* incubation was necessary in addition to wounding, in order to cause a greater number of leukocytes to migrate to the wound (141). This "nick" model is subtle although the authors report a clear statistical difference by both genetic and pharmacological manipulation of the inflammatory response, and it allowed the successful conclusion to a specific scientific question to be reached in a non-GM zebrafish line (141).

In conclusion, the tailfin transection model chosen results in an inflammatory response which is severe enough to manipulate, but also allows ease of quantification without the huge inflammatory response seen when the vasculature is damaged. The presence of so many cells can make it difficult to identify individual cells when tracking and counting. A similar model to the tailfin transection used in this study has been recently published, showing it to be a robust assay for drug screening of inhibitors of neutrophil recruitment (180).

In the tailfin transection model chosen, around 15 neutrophils are recruited at 4 h post-transection (Fig. 3.3, C). There are about 20 neutrophils recruited at the peak of inflammation in the tailfin/vasculature transection model (126); not dissimilar to the numbers recorded in the model chosen for this study (which does not damage the vasculature). In this study the authors counted only cells which were directly in the vicinity of the wound. Hence, the fact that the numbers of cells counted in this study are not hugely different from the Renshaw et al study can likely be attributed to the fact that the area chosen for counting in this study takes into account cells not directly associated with the wound. It was deemed important to include cells not immediately

next to the wound (i.e. area ‘a’ in Fig. 3.2), as the area next to the wound is a site of dynamic migration of neutrophils, and therefore these cells can be described as ‘inflammatory’. (Fig. 3.2, Video 2). This is clear from the fluctuations in cell numbers in area ‘a’ over time.

The recruitment of macrophages over time is more gradual, peaking at 24 h post transection (Fig. 3.3, C). This is in keeping with the standard dogma that neutrophils migrate faster than macrophages. In this study, macrophage numbers post-transection are consistently higher than neutrophil numbers. This is in contrast to previous studies, where macrophage numbers are lower and increase over time to become greater in number at the wound than neutrophils (127). Again, this is likely due to the differences in the area selected for counting, and also perhaps reflects the increased presence of macrophages during homeostasis; whereas neutrophils are primarily recruited during inflammation. In this study, the macrophages were counted using the same area that was chosen for counting neutrophils (Fig. 3.2). As the acute neutrophil response was deemed to be the focus of the study, the macrophage response was assessed in direct relation to this area.

One notable difference in the injury model of this study, compared to previous injury models, is that resolution does not fully occur by 48 h post-transection, which was the limit to which imaging was carried out. There are still residual inflammatory cells present at 48 h post-transection. This might be due to the fact that in the more severe model used by Renshaw et al., the injury is so acute that neutrophil migration and subsequent resolution occur much more quickly, as it is important for the overall survival of the embryo to heal the damaged vasculature speedily (126).

Interestingly, a ‘second wave’ of neutrophil infiltration seems to occur at 32-48 h post-transection. This is an observation that has been previously noted in mammals (181). This might reflect an infiltration of ‘M1’ macrophages at 24 h, releasing pro-inflammatory mediators such as IL-8 or TNF (182). Future studies would undertake an analysis of such cytokines and chemokines. Conversely, the increase in macrophages towards the 44-48 h time point could be attributed to a later infiltration of ‘M2’ macrophages, whose presence helps to dampen down inflammation and promote healing (52). Testing this hypothesis in the future could be

an interesting study; for example by examining the expression of markers of M1 and M2 macrophages by immunostaining.

The Tg(fms:mCherry) line was used for initial macrophage experiments but then results were then confirmed using the Tg(MPEG1:mCherry) line, due to the better specificity of the latter. Tg(fms:mCherry) zebrafish have labelled mCherry macrophages via expression of the macrophage colony stimulating factor (M-CSF) receptor promoter, whereas in Tg(MPEG1:mCherry) fish, macrophages are labelled via expression of the macrophage expressed gene 1 (MPEG1, perforin) (127, 128). It is possible to differentiate which cells are macrophages in the Tg(fms:mCherry) line, by comparing which cells have migrated after transection and which were resident xanthophores already present. However, the concern remained that non-specificity could obscure accurate counting; for example if a macrophage was present within the same plane of focus as the xanthophore cells. It is also quicker to carrying out counting when non-specific, non-migratory cells do not have to be excluded from the final count for each image, by returning to compare to the 0 h time point image each time.

These zebrafish lines have been well studied and used as a model of neutrophil and macrophage inflammatory responses. However, at the beginning of the project, some experiments were performed to define important characteristics of the zebrafish leukocytes to justify their use as a model for mammalian leukocytes. Work on mammalian neutrophils is typically done *in vitro* with cells directly isolated from blood, or *ex vivo* with cells from animals treated with inflammatory stimuli.

In this project, cells were isolated from whole zebrafish embryo, and imaging and phenotyping assays were carried out. This revealed that zebrafish neutrophils exhibit some characteristics of mammalian neutrophils; for example the neutrophils respond to stimulation with fMLF by increasing their forward scatter. Sorted neutrophils also migrate with a similar morphology to sorted human neutrophils. The use of flow sorting itself to isolate populations of human neutrophils has been shown not to cause neutrophil activation (175). These data (showing zebrafish neutrophils respond to fMLF) indicate that the neutrophils from zebrafish are similar to mammalian neutrophils, alongside other published evidence showing that the neutrophils have multi-lobed nuclei and can perform phagocytosis (125). In the future,

a similar assay will be performed for sorted macrophages. One example of a potential assay is measurement of the induction of ROS which can be stimulated by reagents such as phorbol myristate acetate (PMA) (183).

Some *ex vivo* assays were difficult to perform, such as antibody staining of sorted cells. This was due to limitations in the total cell numbers that can be isolated, and the washing steps involved in staining protocols results in continual loss of cells. Zebrafish neutrophils can be harvested in larger numbers from adult zebrafish kidneys (kidneys are the site of haematopoietic development in zebrafish) (119). However, this poses the problem that the adult neutrophils are presumably fully developed cells, which may differ from the embryonic neutrophils on which all the future imaging experiments were to be performed.

Previously, use of LPS has been shown to increase inflammation levels post-wounding (168). However, in this system it did not have any effect. There could be several reasons for this; firstly many types of LPS exist which differ slightly depending on the exact isolation procedure (184). These elicit different responses upon addition of cell cultures or animal models. Hence it is difficult to compare this experiment directly to other studies, without knowing exactly which type of LPS was used. To further these experiments, varying doses of several types of LPS should be tested. Perhaps the more severe vasculature transection model allows for increased access of LPS to the wound site, helping to aggravate the response (168). It may also be that it is necessary to pre-treat with LPS before transection to see an effect.

One challenge with this model, common to many *in vivo* models, is the issue of reproducibility. With practise it is possible to injure the animal in roughly the same place each time, but there will be some variability in the exact position of the injury. This can be improved using a laser to position the line of injury more exactly; however variability always occurs naturally *in vivo*. However, the use of sufficient n numbers will reduce variability. Laser injury and scalpel injury of the tailfin has been shown to result in similar numbers of neutrophils being recruited when the tailfin was transected; however there are more macrophages at 48 h post-transection in the scalpel-transected animals compared to laser-transected (Nicolette Mineo, unpublished data). Laser injury, possibly with a cauterised wound, works on the basis of a line of laser ‘dots’

being made down the tailfin, resulting in sloughing of the excess tissue. Perhaps this type of injury requires more 'M2' macrophages for healing compared to the scalpel transection injury, as it consists of lots of small wounds.

These initial studies provided the framework for future experiments in which tailfin transection was used to cause an inflammatory response, which could be manipulated pharmacologically and genetically.

4. Chapter 4. Pharmacological CDK inhibition in Zebrafish Embryos

4.1. Introduction

The zebrafish embryo is a good model for drug and chemical screening, due to the numbers of embryos produced from a single cross, allowing large-scale screenings. This facilitates experiments with large sample sizes consisting of individual zebrafish (n values); and due to the transparency of the embryo, the effect of chemicals on different organs can easily be assessed (185). Furthermore, vast automated screening is also a possibility in some of these systems by automated measurements of parameters such as fluorescence intensity (122, 186). Drugs identified in zebrafish screens are now advancing to therapy in human disease, for example, the small lipid mediator dmPGE2, which was identified in a zebrafish screen, is now in clinical trials for patients who are undergoing hematopoietic stem cell transplantation (187).

In this study, CDK inhibitor (CDKi) compounds were tested in the zebrafish tailfin injury model (established in Chapter 3) to examine the role of CDKs in the resolution of innate inflammation. For this, the CDKi compound AT7519 was selected as it is a small molecule inhibitor with good CDK9 specificity; the half maximal inhibitory concentration (IC50, i.e. the amount needed to inhibit a biological process by half) of AT7519 for CDK9 is ≤10 nm. AT7519 is in Phase I and II clinical trials as a potential cancer treatment for chronic lymphocytic leukaemia (CLL) and mantle cell lymphoma (77, 81, 188), and appears to be well tolerated by humans.

Previous work from our laboratory group has shown the CDKi *R*-roscovitine (which inhibits multiple CDKs, including CDK9, CDK2 and CDK5), causes neutrophil apoptosis *in vitro* and drives resolution of inflammation *in vivo* in mouse models (e.g. bleomycin-induced lung inflammation) (68). *R*-roscovitine has subsequently been used in zebrafish and was shown to cause a reduction in neutrophilic inflammation at sites of zebrafish tailfin injury (168). AT7519 is more CDK9-specific and has also been shown to be more potent than *R*-roscovitine in terms of driving neutrophil apoptosis. AT7519 also drives resolution in mouse models of inflammation, for example in the ovalbumin-induced pleurisy allergy model, and endotoxin- or *E. coli*-induced lung inflammation (38, 82). For these reasons, it was selected as the main compound of choice for experiments in this study.

Other compounds have gained interest which also work in a similar manner to traditional CDKi drugs, by out-competing ATP in the ATP-binding pocket of CDK9. Some examples are found in the flavone group of chemicals, which are a class of flavonoids which possess a 2-phenylchromen-4-one backbone (189). The flavone wogonin is a compound isolated from *Scutellaria baicalensis,* and is an active ingredient in the Chinese herbal medicine sho-saiko-to (190). Wogonin has been shown to drive apoptosis of cancer cells by inhibition of CDK9 and down-regulation of Mcl-1 (191). These compounds also increase sensitivity of cells to other anti-cancer drugs which inhibit other Bcl-2 family members such as Bcl-2 and Bcl-xL (192). Work from our group showed that wogonin can also cause neutrophil apoptosis *in vitro* and resolve mouse models of neutrophilic inflammation (e.g. LPS-induced lung inflammation), and eosinophilic allergic airway inflammation. (38, 73). It was also shown that wogonin drives neutrophil apoptosis in zebrafish tailfin injury (72). A related compound, flavopiridol (FVP), has also been shown to accelerate neutrophil apoptosis and drives a reduction in Mcl-1 protein levels (37).

Some of these pharmacological compounds were tested to see if they could drive resolution of inflammation after zebrafish tailfin transection. The treatment was administered at 4 h because this is when the initial inflammatory response after transection peaks (Chapter 3, Fig. 3.3). This is to mimic a clinical setting – patients with inflammatory disease are likely to present once inflammation has been established. This would show whether the model is useful and relevant for investigating CDKs and their role during inflammation, and if targeting CDKs will have an effect in this system. As the zebrafish can be readily used for continuous *in vivo* imaging of inflammation, it allows for new insight into the mechanism by how the CDKi drugs may drive resolution. Furthermore, this could prove to be a valuable model for further drug screening of compounds.

4.2. Research Questions

- Do CDKi compounds affect the total number of neutrophils in the zebrafish embryo (i.e. haematopoiesis) and neutrophil numbers at the tailfin in a zebrafish tailfin wounding inflammation model?
- Do CDKi compounds affect neutrophil apoptosis during inflammation?
- Do CDKi compounds affect macrophages during inflammation?
- Do existing compounds with structures similar to CDKi (e.g. flavones) also affect neutrophils during resolution of inflammation?

4.3. Results

4.3.1. Incubation of Tg(mpx:EGFP)^{i114} zebrafish embryos with AT7519 post-tailfin transection

Tg(mpx:EGFP)^{i114} zebrafish embryos, which had undergone tailfin transection 4 h earlier, were incubated with 20 μM AT7519. Images were taken at various time points before and after treatment to allow assessment of the effect of AT7519 on the neutrophil inflammatory response. There was no statistical difference ($p \geq 0.05$) in the neutrophil numbers at the wound site after 24 h of treatment with AT7519 (20 ± 2 cells) or the vehicle control DMSO (≤1%, 16 ± 2 cells, Fig 4.1, A, B). For clarity, only one of the AT7519 concentrations tested is shown (20 μM).

As solubility can be an issue with some compound treatments, the experiment was repeated with the addition of 2% DMSO to the compound to ensure the drug was dissolved as much as possible. A dose-response test revealed 2% was the highest DMSO concentration the embryos could be bathed in, without compromising their health; higher concentrations resulted in unresponsiveness or death (data not shown). Again no statistical difference ($p \geq 0.05$) in neutrophil numbers at the wound site was discernible at 24 h after treatment in the AT7519-treated group (12 ± 1 cells) compared to the DMSO-treated group (10 ± 1 cells, Fig 4.1, C, D).

Figure 4.1

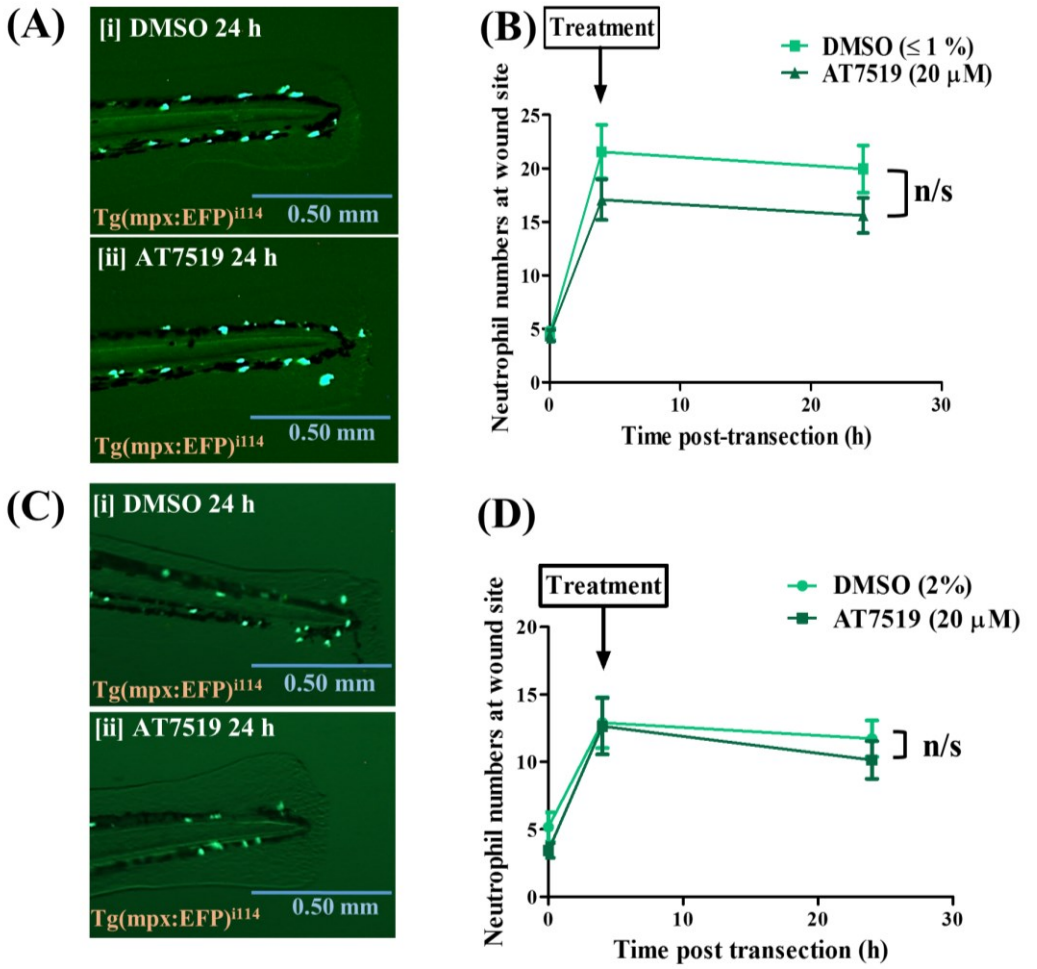

Figure 4.1. Incubation of zebrafish embryos with the CDK inhibitor, AT7519
Tg(mpx:EGFP)^{i114} 3dpf zebrafish embryos were incubated with 20 μM AT7519 (A [i]) or ≤1% DMSO (A [ii])$^{\#}$, and representative images were taken at 24 h after transection and quantified (B). 24 h DMSO vs 24 h AT7519; $p \geq 0.05$.
Zebrafish were also incubated with 2% DMSO + 20 μM AT7519 (C [ii]) or DMSO alone (C [i]); representative images were taken at various time points after transection and treatment at 24 h and then quantified (D).
n/s: $p \geq 0.05$, analysed by ANOVA. ≥16 fish per group in 3 independent experiments. Data expressed as ± S.E.M.
Preliminary AT7519 incubation study data (A, B) were obtained from Masters by Research (Biomedical Sciences) Thesis of Ms Laura Hoodless, 2012

4.3.2. Microinjection of AT7519 into Tg(mpx:EGFP)^{i114} zebrafish embryos post tailfin-transection

AT7519 was administered by microinjection into the zebrafish yolk sac at 4 h post-tailfin transection.

At 24 h after transection, there was a significant ($p \leq 0.05$) reduction in neutrophils at the wound site in the embryos injected with 0.5 ng of AT7519 compared to control, as demonstrated by the example images and when quantified over different time points (Fig. 4.2, A, B, C[i]). Specifically, there was a mean of 12 ± 1 cells in the DMSO group, and 8 ± 1 cells in the AT7519 group after 24 h (Fig. 4.2, C[ii]). This was apparent not only by examining neutrophil numbers at 24 h, but also by calculating the percentage change in neutrophil numbers from 4 to 24 h (Fig. 4.2, C[iii]), which reveals changes in individual animals. The percentage reduction in neutrophil numbers in the DMSO group was a mean of 12% compared to 52% in the AT7519 group. The AT7519 data were also re-calculated by removing from the analysis fish deemed as "non-responders". This was deemed as fish with less than 13 neutrophils at the wound site at 4 hpi (Fig. 4.2, D). This calculation resulted in an enhanced inflammatory response (16 ± 1 neutrophils at 4 h) and 14 ± 2 neutrophils in the DMSO group at 24 h compared to 7 ± 1 in the AT7519 group.

The number of neutrophils in the entire animal at 24 h after drug treatment was counted by inspection of images of the tailfin of these fish (Fig 4.3, A) then counting total cells (Fig 4.3, B). There was no statistically significant difference between the DMSO (116 ± 5 cells) and the AT7519-treated groups (130 ± 10 cells).

The total embryonic neutrophils numbers were also examined by flow cytometry, by measurement of the percentage of $EGFP^+$ cells in a pool of embryos. This revealed no significant difference ($p \geq 0.05$) in total neutrophil numbers between DMSO and AT7519-treated (Fig 4.3, C). In the DMSO group, a mean of 0.26% of the total cells were $EGFP^+$ neutrophils; and in the AT7519 group, 0.21% of the cells were $EGFP^+$ neutrophils.

Figure 4.2

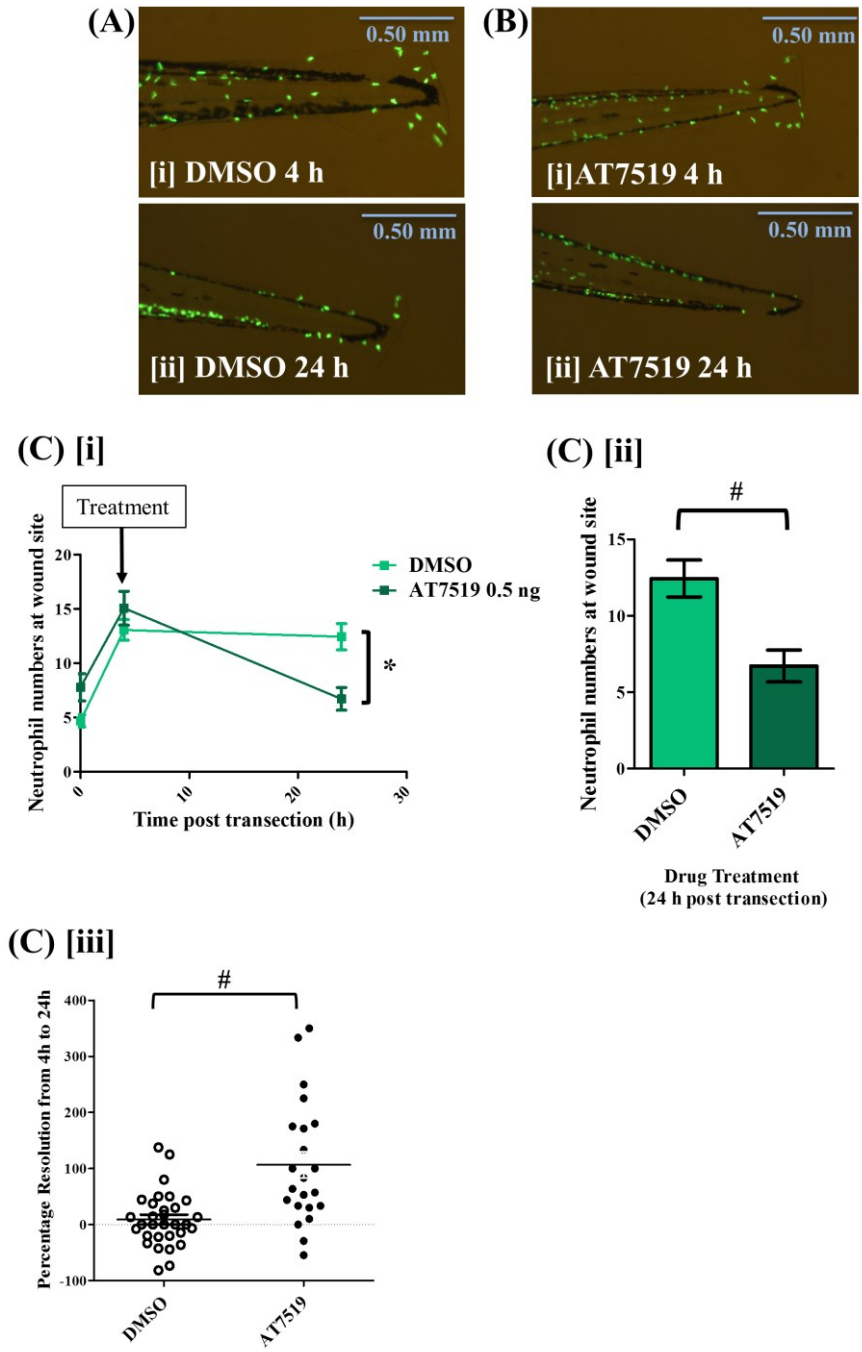

Figure 4.2. Microinjection of zebrafish embryos with AT7519

The yolk sac of Tg(mpx:EGFP)^{i114} 3 dpf embryos is microinjected with AT7519 or DMSO 4 h after tailfin transection. Example images from DMSO- (A) and AT7519-treated (B) fish are shown from 24 h after transection. Cell numbers at the wound site are shown (C [i, ii]) and the percentage change per individual embryos from 4 h to 24 h is shown (C [iii]). ≥ 20 fish per group in 4 independent experiments. Data expressed as ± S.E.M. *$p \leq 0.05$ analysed by ANOVA followed by post-test Newman Keuls. $^{\#}p \leq 0.05$ analysed by unpaired t-test

Figure 4.3

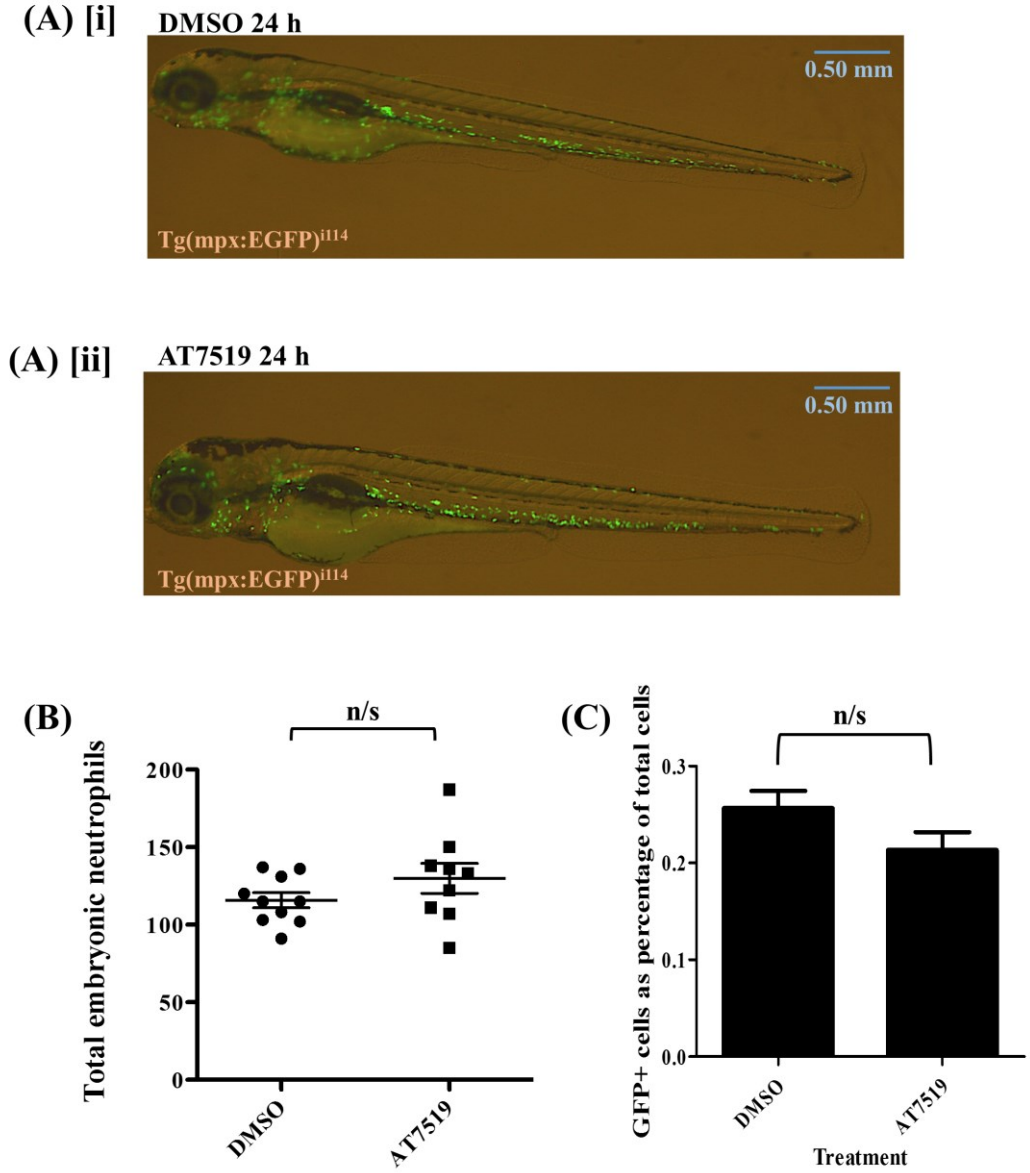

Figure 4.3. Total neutrophils in Tg(mpx:EGFP)^{i114} zebrafish after microinjection with AT7519 or DMSO

The total neutrophils in images of the whole embryo were counted 24 h after treatment with 0.5 ng of DMSO [i] or AT7519 [ii] (A), and then quantified (B). ≥10 fish per group from 3 independent experiments. Whole embryos treated with DMSO or AT7519 were digested and the percentage of EGFP+ total cells in the entire embryo digest was measured (C). ≥20 fish per group from 3 independent experiments. n/s: $p \geq 0.05$, analyzed by unpaired t-test. Data expressed as ± S.E.M.

4.3.3. Pre-injection with AT7519 before tailfin transection of Tg(mpx:EGFP)^{i114} zebrafish embryos

Next, the embryos were pre-injected with 0.5 ng AT7519 or DMSO 0.5 h before tailfin transection. The fish were imaged immediately after transection and at 4 h post-transection (Fig. 4.4, A). The cells at the inflammation site were quantified, showing that AT7519 pre-treatment significantly ($p \leq 0.05$) inhibited neutrophil influx to the wound site after transection, compared to control; with 14 ± 1 cells at the wound site in the DMSO-treated group at 4 h, compared to 10 ± 1 in the AT7519 group (Fig. 4.4, B).

Figure 4.4

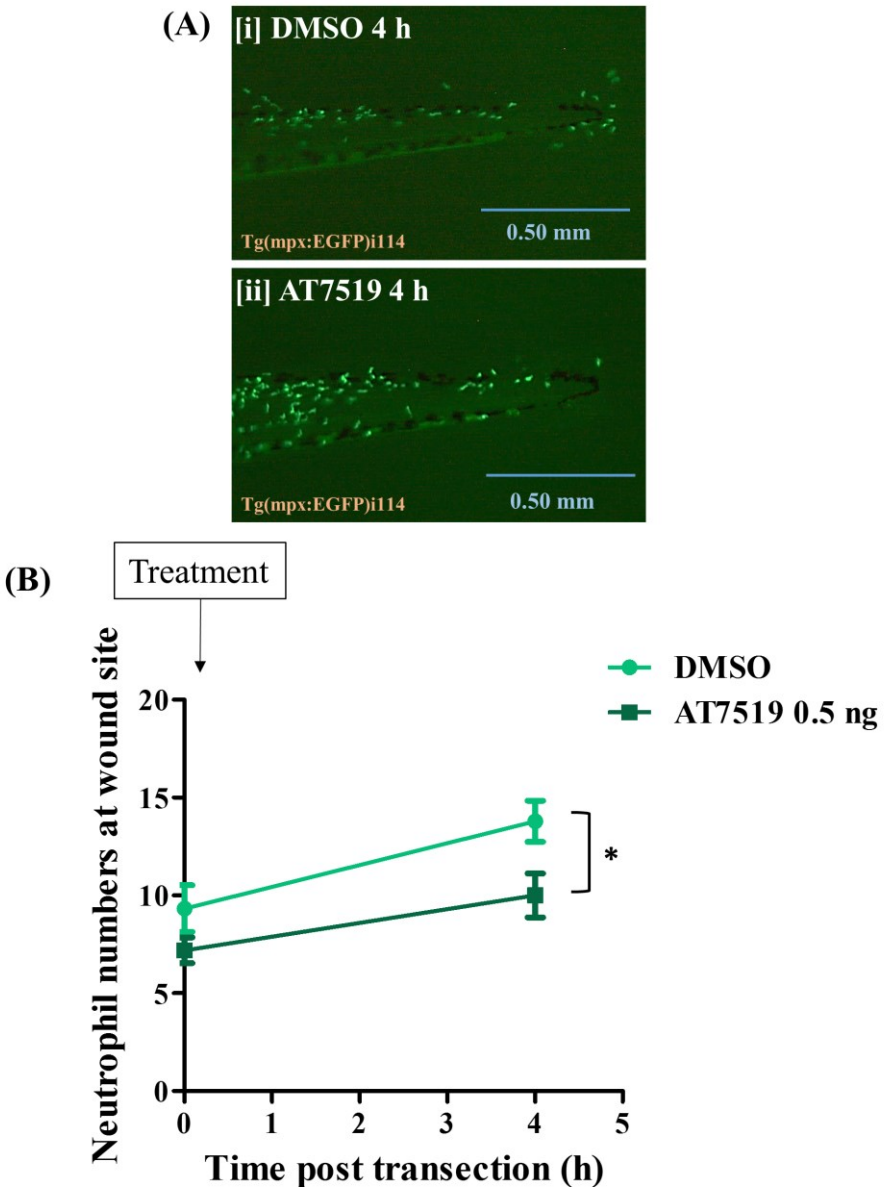

Figure 4.4. Pre-treatment of zebrafish embryos with AT7519 before tailfin transection

Tg(mpx:EGFP)^{i114} 3dpf zebrafish embryos were injected with 0.5 ng DMSO [i] or AT7519 [ii], then the tailfin was transected 0.5 h later. The embryos were imaged at 0 h and again at 4 h (A), and quantified (B). *$p \leq 0.05$, 4 h DMSO vs 4 h AT7519, analysed by ANOVA then post-test Newman-Keuls. ≥40 fish per group from 3 independent experiments. Data expressed as ± S.E.M.

4.3.4. Effect of AT7519 microinjection on Tg(MPEG1:mCherry) zebrafish embryos

The effect of AT7519 and DMSO on macrophage recruitment to sites of wounding was assessed by microinjection of 0.5 ng of AT7519 or DMSO into Tg(MPEG1:mCherry) embryos with fluorescent macrophages.

The fish were injured using the tailfin transection model and treated with DMSO/AT7519 at 4 h post-wounding, following which the embryos were imaged at various time points. The example images shown are from the 24 h post-injury time point (Fig. 4.5, A), and the macrophage numbers at 0, 4 and 24 h were quantified (Fig. 4.5, B), showing no significant difference ($p \geq 0.05$) in macrophage numbers at the wound between DMSO (16 ± 1 cells) and AT7519-treated groups (15 ± 1 cells). The other time points also showed no significant difference.

Figure 4.5

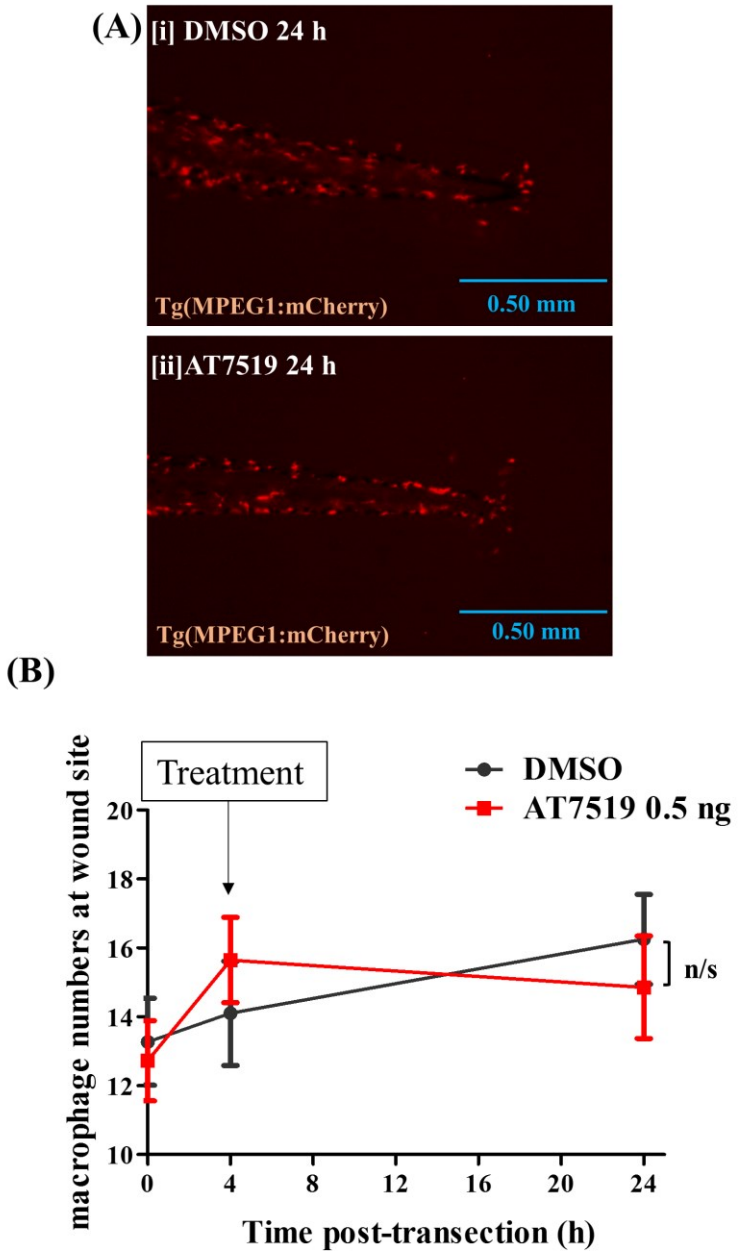

Figure 4.5. Tailfin transection of Tg(MPEG1:mCherry) zebrafish
The tailfin of Tg(MPEG1:mCherry) were transected and then microinjected with 0.5 ng DMSO (A [i]) or AT7519 (A[ii]) at different time points after transection. Shown here are the 24 h post-transection images. The macrophages at the tailfin at different time points post-injury were quantified (B). ≥ 22 fish per group from 3 independent experiments. Data expressed as ± S.E.M. n/s: $p \geq 0.05$, analysed by ANOVA.

4.3.5. TUNEL staining of tailfin transection zebrafish embryos microinjected with 0.5 ng AT7519 or DMSO

Apoptosis of neutrophils was measured by terminal deoxynucleotidyl transferase dUTP nick end labelling (TUNEL) performed in conjunction with tyramide signal amplification (TSA). This labelled apoptotic cells red, and neutrophils green, and the transected region of the tailfin was then imaged. An example is shown in Figure 4.6 [A]. The staining must be carried out on fixed embryos; which means the same embryos cannot be tracked over time.

The number of apoptotic neutrophils (cells which are both $EGFP^+$ and $TUNEL^+$ positive) at different time points post-transection after DMSO/AT7519 treatment was quantified (Fig. 4.6, B[i]). At 12 h post-transection (but no other time point), there was a significantly ($p \leq 0.05$) increased number of apoptotic neutrophils in the AT7519 (a mean of 3 $EGFP^+$ $TUNEL^+$ cells) compared to the DMSO control (a mean of 1 $EGFP^+$ $TUNEL^+$ cell). The 12 h time point post-transection (i.e. 8 h post-AT7519 treatment) is highlighted separately as there is a significant ($p \leq 0.05$) difference in apoptotic neutrophils in the tailfin at this time (Fig. 4.6, B[ii]). Shown are example images from 12 h post transection in DMSO (Fig. 4.6, C[i]) and AT7519 (Fig. 4.6, C[ii]) – treated fish.

The percentage of total $EGFP^+$ neutrophils which were also $TUNEL^+$ was calculated (Fig. 4.6, D[i]). At 12 h post-transection, there was a significantly ($p \leq 0.05$) higher percentage of apoptotic neutrophils in the AT7519-treated group (23%) compared to DMSO control (10%, Fig. 4.6, D[i] and highlighted in Fig. 4.6, D[ii]).

Figure 4.6

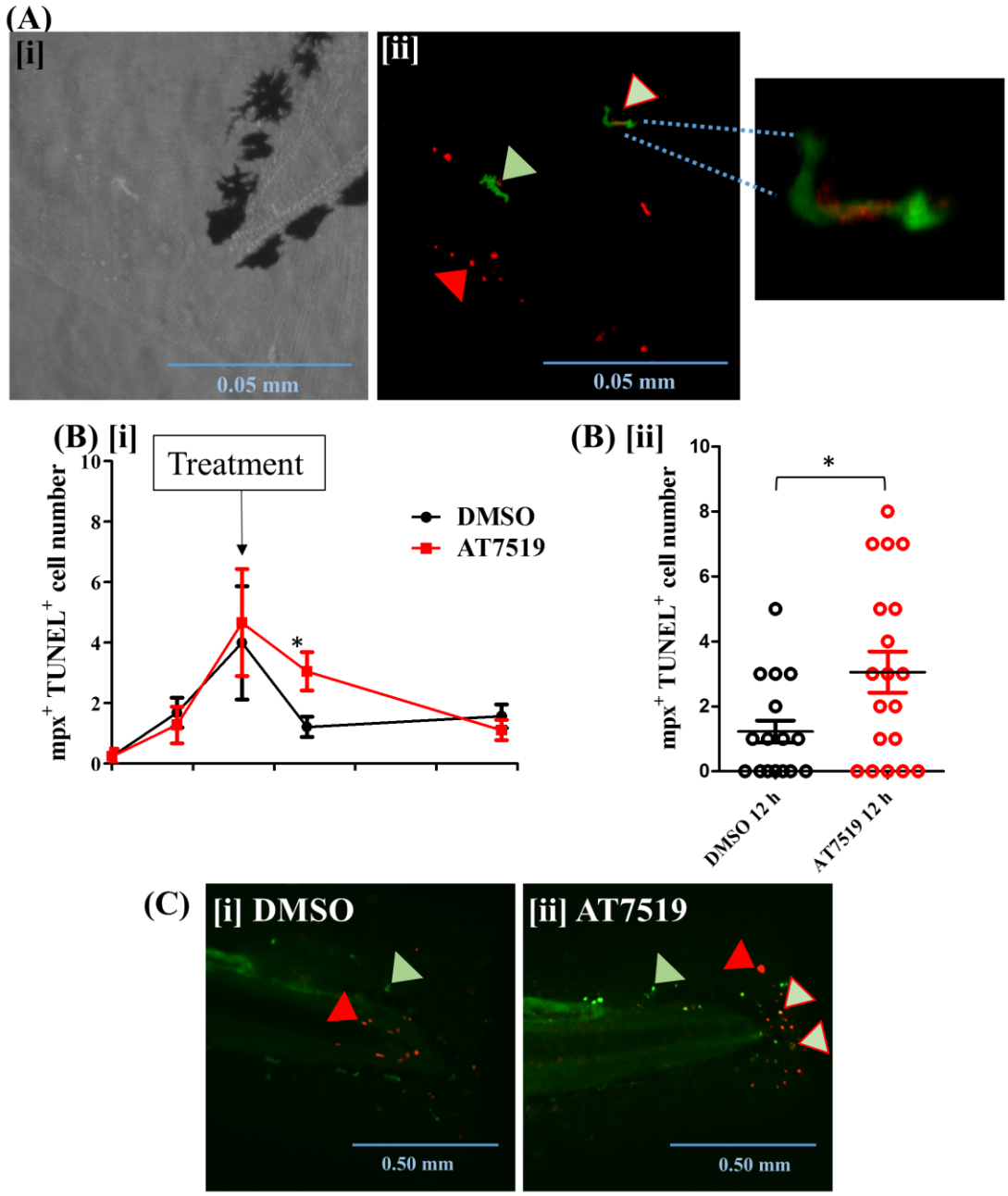

Figure 4.6 legend overleaf

Figure 4.6

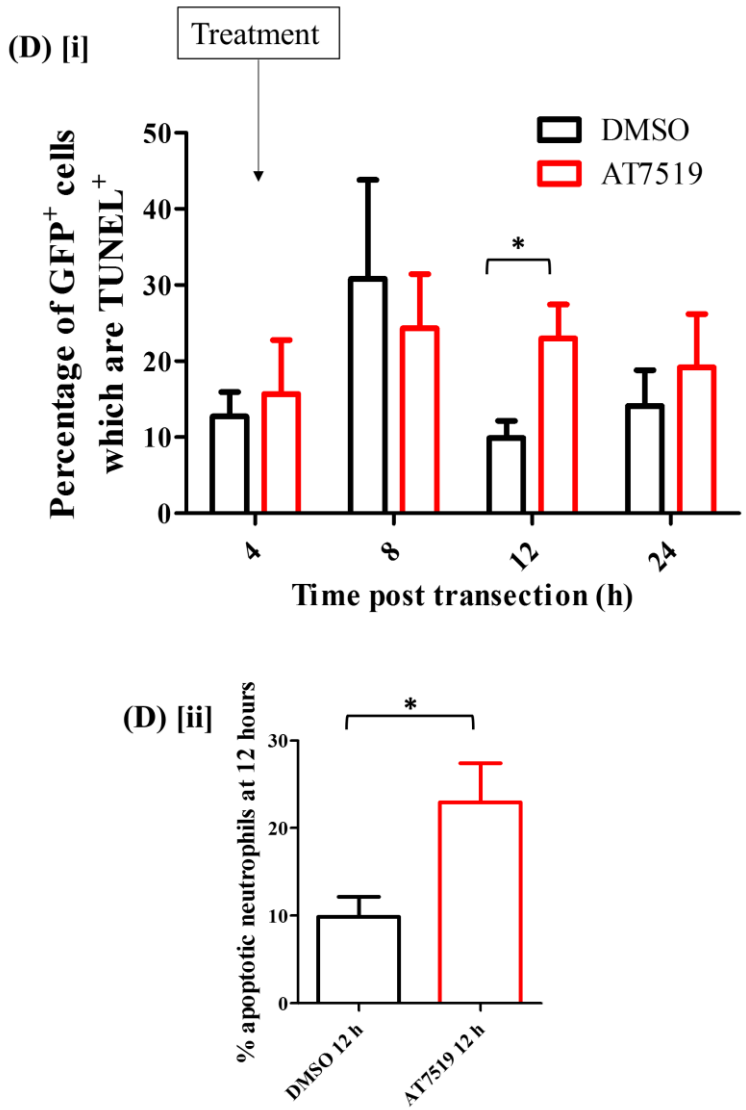

Figure 4.6. TUNEL staining of zebrafish embryos microinjected with DMSO or AT7519

TSA/TUNEL staining was performed on Tg(mpx:EGFP)^{i114} zebrafish, labelling neutrophils in green, and apoptotic cells in red. In this tailfin transection example (A [i], a neutrophil is designated by a green arrow, apoptotic cells by a red arrow, and apoptotic neutrophils (double positive) by a green and red arrow (A [ii]). The number of double positive cells over different time points was quantified (B [i]) and the 12 h post-transection time point was highlighted as one of interest (B [ii)]. An example image of the 12 h post-transection time point is shown in animals treated with DMSO (C [i]) and AT7519 (C [ii]) at 4 h post-transection. The number of double positive cells as a percentage of the total EGFP^{+} neutrophil population was calculated (D [i]), and the 12 h time point is highlighted (D [ii]). ≥16 embryos per group in 3 independent experiments. *p≤0.05 12 h DMSO vs 12 h AT7519, unpaired t test. Data expressed as ± S.E.M.

4.3.6. Effect of AT7519 on uptake of neutrophils by macrophages

Tg(mpx:EGFP)^{i114} fish were crossed with Tg(MPEG1:mCherry) fish to create embryos in which neutrophils and macrophages could be visualised together in the same animals. The embryos were transected and imaged at various time points before and after microinjection with 0.5 ng DMSO or AT7519 at 4 h. In the example is the 24 h time point in DMSO or AT7519 –treated groups (Fig. 4.7, A).

The number of co-localised cells at the injury site was counted (Fig. 4.7, B). This gave an impression of the level of phagocytosis of neutrophils by macrophages at the site of wounding. There was a statistically significant increase ($p \leq 0.05$) within each group (DMSO or AT7519) of uptake of neutrophils between 0 h and 24 h. In the DMSO-treated group, there was a mean of 1 co-localised EGFP^{+} neutrophil within a macrophage. At 24 h, this rose to 3 co-localised cells. In the AT7519-treated group, there was a mean of 1 neutrophil inside a macrophage at 0 h and by 24 h there was 2. However, there was no statistical difference ($p \geq 0.05$) between DMSO and AT7519 at any given time point.

Figure 4.7

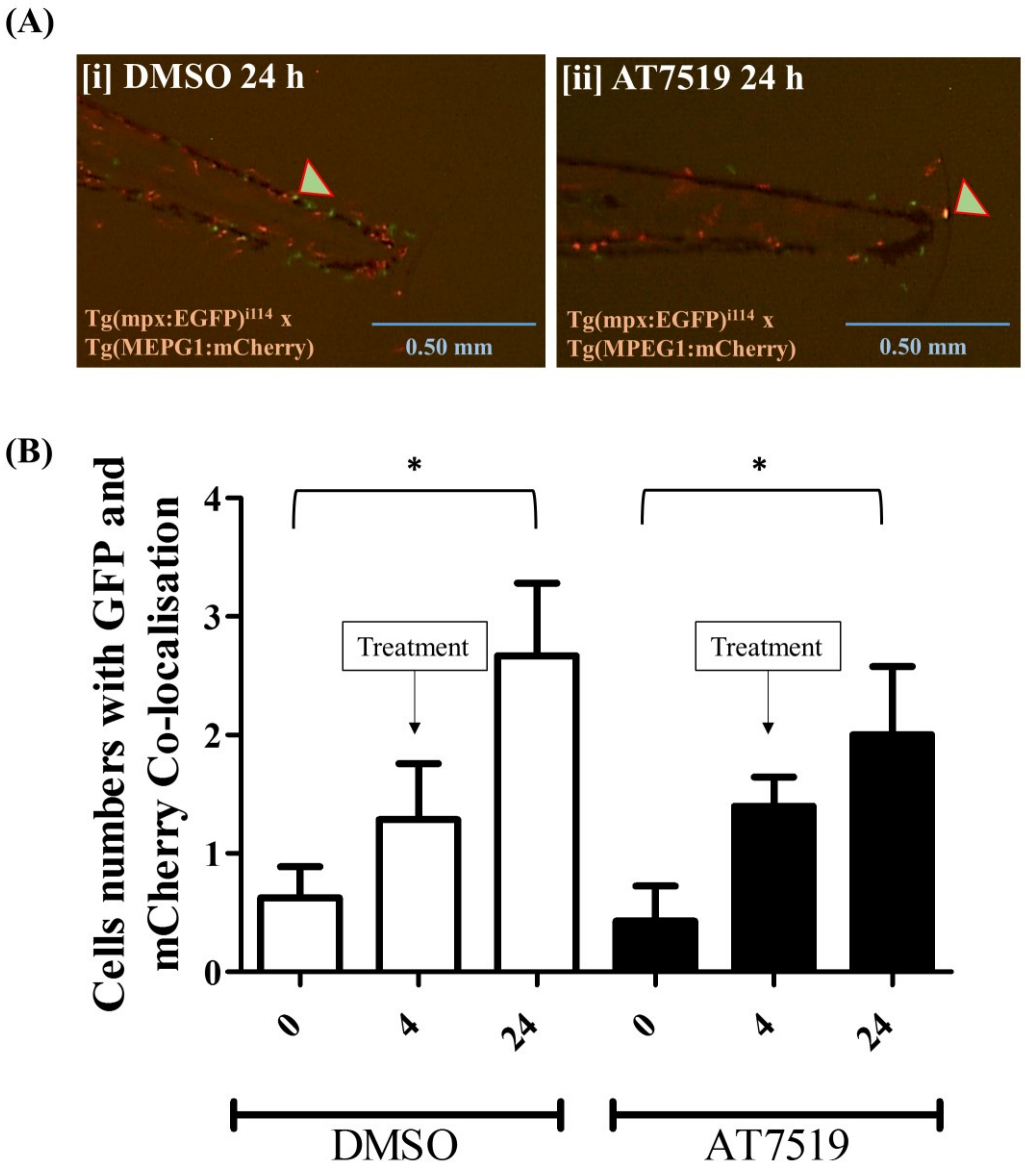

Figure 4.7. Colocalisation of EGFP^{+} neutrophils and mCherry^{+} macrophages in Tg(mpx:EGFP)^{i114} x Tg(MPEG1:mCherry) zebrafish embryos treated with DMSO and AT7519 after tailfin transection.
Example images shown from embryos 24 h post-tailfin transection, treated with DMSO (A[i]) or AT7519 (A[ii]). Green and red arrows indicate co-localisation of EGFP^{+} neutrophils and mCherry^{+} macrophages. The numbers of co-localised cells at 0 h, 4 h, and 24 h were quantified and graphed (B). ≥10 fish in each group in 3 independent experiments. Data expressed as ± S.E.M. $p \leq 0.05$, DMSO/AT7519 0 h vs 24 h, analysed by ANOVA followed by post-hoc Newman-Keuls test.

4.3.7. Effect of bath treatment with flavopiridol on neutrophilic inflammation after tailfin wounding

Another CDKi compound, FVP, was tested which is known to have potent activity against CDK9. Similar to before, the Tg(mpx:EGFP)^{i114} embryos were incubated with 1 μM of FVP or DMSO (<1%) at 4 h post-transection. The concentration shown was obtained by carrying out dose-response experiments (data not shown). The embryos were then imaged at various time points after the tailfin transection; example images at 24 h are shown here (Fig. 4.8, A).

Neutrophilic inflammation was significantly ($p \leq 0.05$) reduced after 24 h (but no other time points) in FVP-treated embryos (9 ± 1 neutrophils at 24 h), compared to DMSO vehicle control (13 ± 1 neutrophils at 24 h, Fig. 4.8, B[i]). The individual numbers at the 24 h time point are shown in Figure 4.8, B[ii]. The embryos were also injected with FVP or DMSO at 4 h post-transection, but this did not have a significant effect ($p \geq 0.05$) on neutrophil numbers at the injury site; the DMSO group had a mean of 8 ± 1 neutrophils, and the FVP group had 7 ± 1 (Fig. 4.8, C).

Figure 4.8

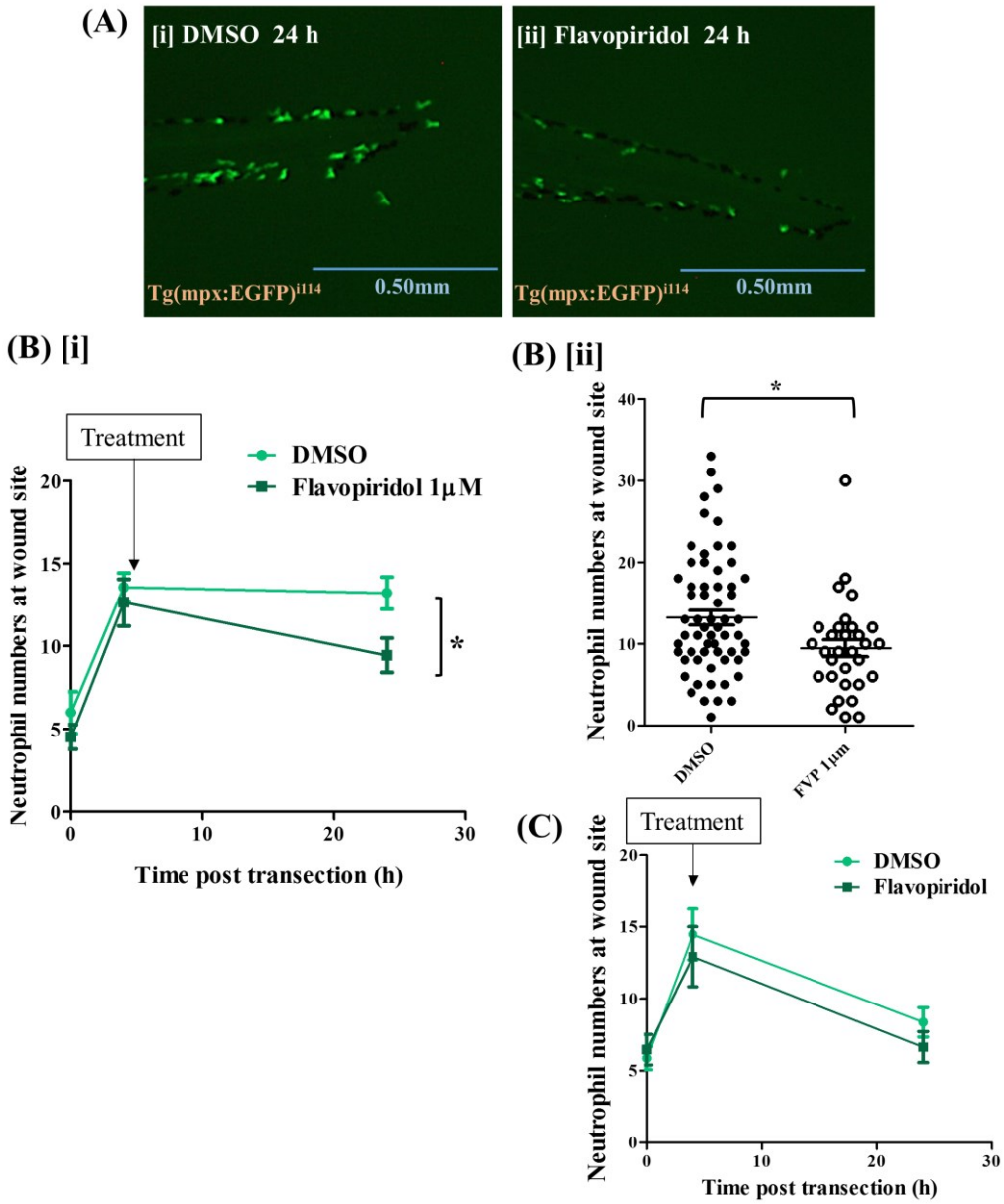

Figure 4.8. Treatment of zebrafish embryos with flavopiridol (FVP) or DMSO following tailfin transection.

3 dpf Tg(mpx:EGFP)^{i114} embryos were incubated with FVP (1 µM) or DMSO (<1%), at 4 h post-transection. Example images at 24 h post transection and treatment are shown for DMSO (A[i]) and FVP-treated (A[ii]) animals, and these data are quantified in (B [i]). The 24 h time point is also shown with each circle corresponding to cell numbers in an individual animal (B [ii]) ≥31 fish per group. 2.19 ng of FVP or DMSO in a 0.5 nL volume was also administered to the embryonic yolk sac by microinjection and inflammation at the wound site was quantified (C). ≥13 fish per group in 3 independent experiments. Data expressed as ± S.E.M. *p ≤ 0.05, DMSO 24 h vs FVP 24 h, analysed by ANOVA followed by post-hoc Newman Keuls test.

4.3.8. Effect of flavone compounds on zebrafish embryos after tailfin transection

The flavone compounds wogonin, luteolin and apigenin were tested in the tailfin transection model in Tg(mpx:EGFP)^{i114} embryos by bath treatment. At 24 h following tailfin transection and wogonin (50 μM) incubation, neutrophil numbers at the wound site were significantly reduced (compared to the DMSO control), as demonstrated in the example images (Fig. 4.9, A). At 24 h post-injury, there were 17 ± 2 neutrophils in the DMSO (≥ 1%) control group, compared to 9 ± 1 in the wogonin-treated (Fig. 4.9, B[i]).

Tg(mpx:EGFP)^{i114} fish were also pre-injected with the pan-caspase inhibitor zVAD-fmk 0.5 h prior to wogonin incubation at 4 h following tailfin transection (Fig. 4.9, B[ii]). ZVAD-fmk was able to reverse the resolution driven by treatment with wogonin alone after 24 h of treatment. In the wogonin-treated group, there was 2 ± 1 neutrophils and in the zVAD-fmk + wogonin group, there was a mean of 10 ± 2 neutrophils; similar to the control DMSO group which had 12 ± 2 neutrophils. In the zVAD-fmk alone group, there was a mean of 10 ± 2 neutrophils, not significantly different from the DMSO group.

The embryos were also transected and incubated with the flavone compounds luteolin and apigenin, but there was no significant difference ($p \geq 0.05$) between luteolin, apigenin and DMSO-treated groups at 24 h post transection (Fig. 4.9, C).

Figure 4.9

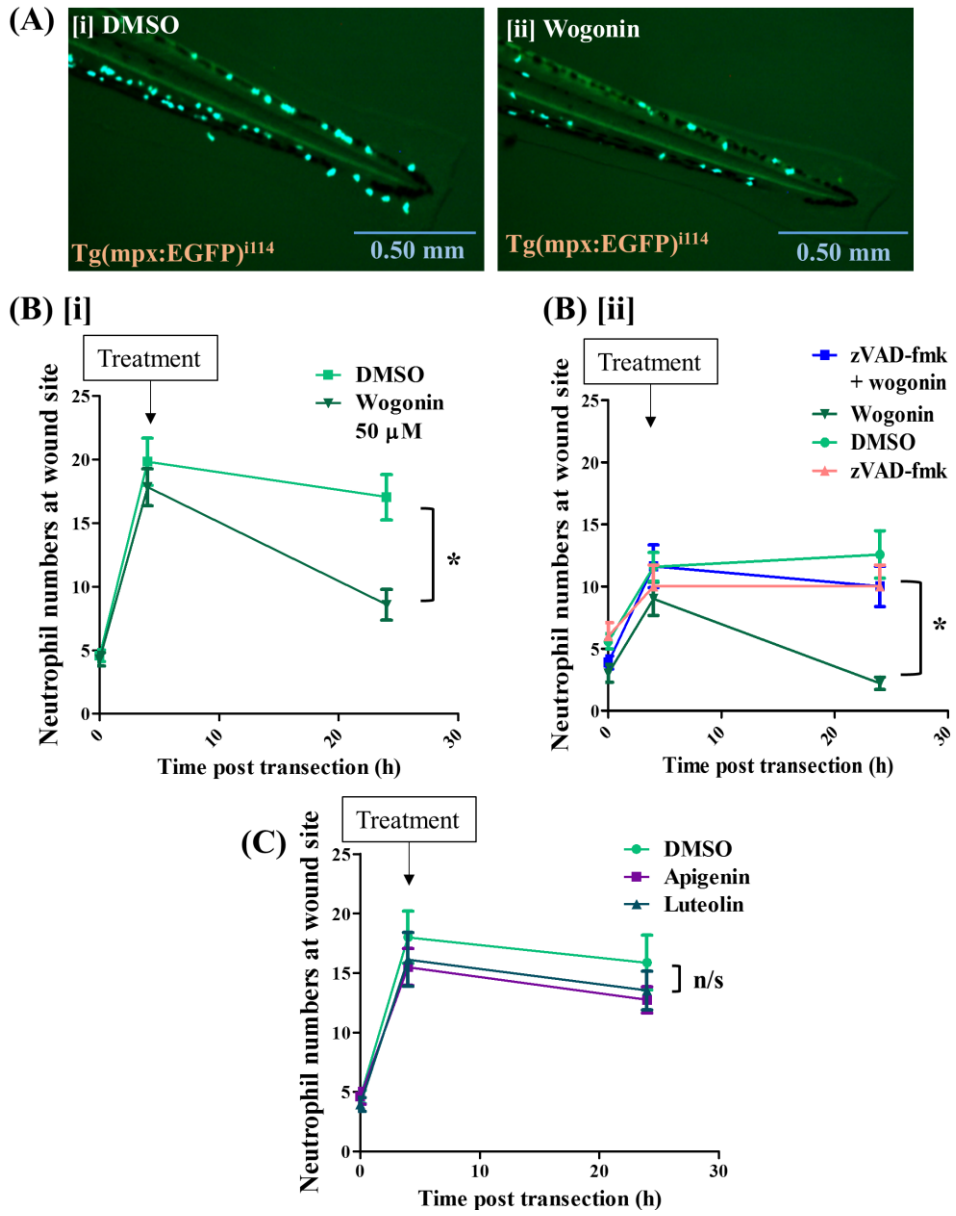

Figure 4.9. Bath treatment of zebrafish embryos with the flavones wogonin, luteolin and apigenin after tailfin transection

3dpf Tg(mpx:EGFP)^{i114} zebrafish embryos underwent tailfin transection and were treated at 4 h with 50 µM of wogonin or DMSO (≤ 1%) and imaged at various time points. Shown here is the 24 h post-transection time point (A) in DMSO [i] and wogonin [ii] – treated fish, which was quantified as shown in (B). Zebrafish embryos were also incubated with wogonin, or injected with Z-VAD-fmk, or both together (B [ii]). The embryos were incubated with the flavones apigenin or luteolin, also at 50 µM, and inflammation was measured at different times post-transection (C). Data expressed as ± S.E.M. ≥ 30 fish per group in 3 independent experiments. *p ≥ 0.05, DMSO 24 h vs wogonin 24 h, analysed by ANOVA followed by post-test Newman-Keuls

4.3.9. Treatment of zebrafish embryos with the CDKi R-roscovitine after tailfin transection

Zebrafish embryos were also treated with a compound previously studied in this model, *R*-roscovitine. Zebrafish embryos at 3 dpf underwent tailfin transection and were then incubated by bath treatment with 20 μM of *R*-roscovitine at 4 h post-tailfin transection. Example images of the 24 h post-treatment time point are shown (Fig. 4.10, A).

Treatment with *R*-roscovitine did not significantly ($p \geq 0.05$) affect neutrophilic inflammation at the site of injury after 24 h compared to control, with 17 ± 1 neutrophils in the DMSO-treated group, and 15 ± 2 neutrophils in the *R*-roscovitine-treated group (Fig. 4.10, B).

Figure 4.10

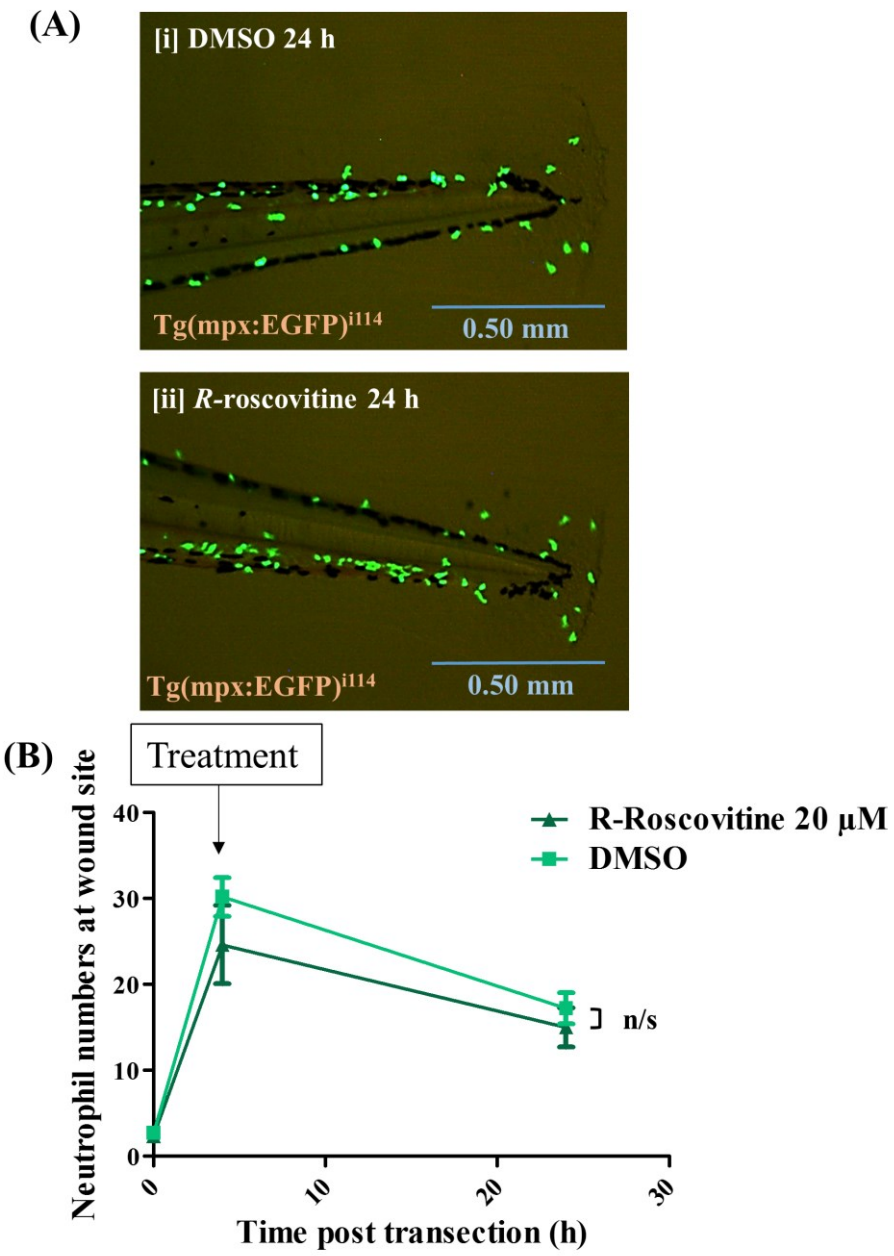

Figure 4.10. Bath treatment of zebrafish embryos with *R*-roscovitine after tailfin transection

Tg(mpx:EGFP)^{i114} embryos at 3 dpf were incubated with 20 µM *R*-roscovitine or ≤ 1% DMSO at 4 h post-tailfin transection, and imaged at various time point post-transection. Example images are of the 24 h time point in DMSO [i] and *R*-roscovitine [ii] – treated fish (A). The neutrophils at the wound at different time points after transection were quantified (B). Data are shown as ± S.E.M. n/s: $p \geq 0.05$, assessed by one-way ANOVA. ≥8 fish per group, from 2 independent experiments

4.3.10. Effect of R-roscovitine on isolated human neutrophils

Human neutrophils were isolated from peripheral blood and treated with *R*-roscovitine; to test if the compound was effective in human neutrophils, as it had no effect on zebrafish neutrophils (Fig. 4.10). Apoptosis of these neutrophils was assessed by flow cytometry using annexin V (AnnV, which binds phosphatidylserine on the outer membrane of apoptotic cells) and propidium iodide (PI) staining (labels necrotic cells by binding extracellular DNA).

These studies showed that 3.67% of neutrophils were apoptotic after 6 h in the control group, compared with 31.7% apoptotic neutrophils in the *R*-roscovitine treatment (Fig. 4.11, A). This was also clear when the cells were stained with DiffQuick™ - in the *R*-roscovitine-treated group, more cells were present which had typical apoptotic morphology (e.g. cell shrinkage and nuclear condensation). This is shown in the representative images of control and *R*-roscovitine-treated groups [i and ii, respectively] with a healthy neutrophil indicated by a white arrow and an apoptotic one with a black arrow.

Figure 4.11

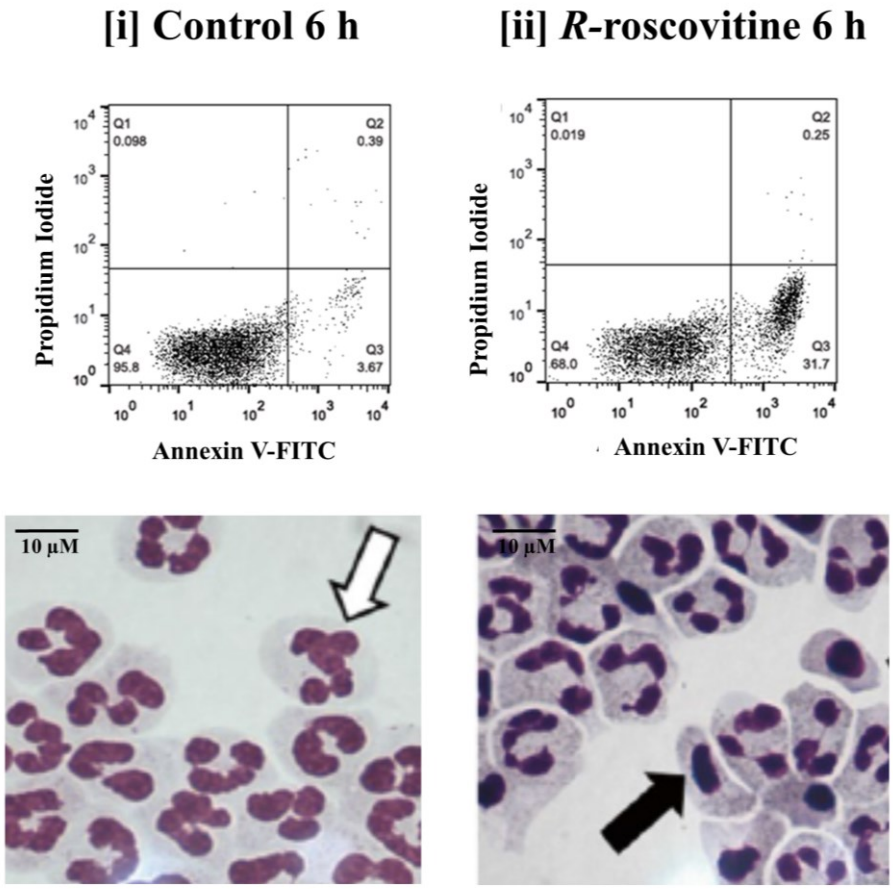

Figure 4.11. Treatment of human neutrophils with *R*-rosovitine
Flow cytometry plots are shown of isolated human neutrophils were treated with *R*-rosocovitine (20 µM), [ii]) or left untreated [i]. Cells which were stained with annexin V-FITC (AnnV) were designated apoptotic; propidium iodide (PI)-positive cells were counted as necrotic, and unstained cells as viable. 1000x magnified images were taken of haematoxylin and eosin (H & E) – stained cytospin slides, with the white arrow showing a viable cell, and a black arrow labelling an apoptotic cell. Representative flow plots and images are depicted here (Images adapted from Hoodless et al, 2015, Methods Mol Biol).

4.4. Discussion

Observations from Chapter 4

- Treatment of zebrafish embryos by incubation with AT7519 in the embryo medium does not affect neutrophilic inflammation at wound sites, even with an increase in % DMSO.
- Microinjection of AT7519 into zebrafish embryos at 4 hours post transection resulted in reduced accumulation of neutrophils at the injury site at 24 h post-transection.
- After AT7519 injection, macrophages accumulated at the wound at a similar manner to the DMSO control-injected fish.
- Injection of AT7519 did not affect the total number of neutrophils in the zebrafish embryos.
- AT7519 increases the number of apoptotic cells at the wound site at 12 h post-transection (8 h post AT7519 treatment).
- There is not a significant different in numbers of neutrophils co-localised with macrophages after AT7519 treatment in fish which have undergone tailfin transection.
- FVP reduces neutrophil numbers following wounding, when it is incubated in the embryo medium with Tg(mpx:EGFP)^{i114} zebrafish.
- Wogonin, but not luteolin or apigenin, drives resolution of zebrafish tailfin transection inflammation in a caspase-dependent manner following bath treatment.
- *R*-roscovitine has no effect on neutrophilic inflammation in this model when incubated with the fish in embryo water, but drives human neutrophil apoptosis *in vitro*.

Using a combination of incubation and microinjection administration, these pharmacological manipulation studies showed the importance of CDKs in regulation of neutrophilic inflammation; as the CDKi compounds AT7519, FVP and wogonin all reduced neutrophilic inflammation at the tail injury site. Further experiments revealed

AT7519 increased neutrophil apoptosis in zebrafish *in vivo*, agreeing with previous findings showing that it drives apoptosis of isolated mammalian neutrophils (38).

One important point that was resolved during these experiments was the importance of route of administration of these compounds. This is probably related to the solubility of the compounds. The lack of expected effect of AT7519 on neutrophils in zebrafish when administered in the bathing water prompted further investigation, and testing of a different route of administration (Fig. 4.1, 4.2). Therefore, the compound was microinjected directly into the fish, via the yolk sac; which is the source of nutrition for the embryo at this early stage of development. This was necessary despite the fact that AT7519 is known to be a water-soluble drug (77). However, the solution that embryos are bathed in contain a mix of salts (see Appendix B (170)), and it is not known how this might affect solubility. In addition, in incubation experiments, the compounds must enter the fish by routes such as the skin, gut, or gills, and it might be that a high amount of the drug does not reach the inflammatory site. Past studies have shown that drugs which were inactive when placed in the water were then shown to be effective when microinjected into the yolk sac in a drug screen for bradycardia (193). This demonstrates that there is likely to be an issue with solubility and drug delivery with some compounds. Hence, in these studies, AT7519 was also microinjected. In terms of large-scale drug screens, a bath incubation treatment is the simplest method for carrying out drug experiments. However microinjecting drugs is still relatively fast (when compared with rodent drug injections), and still allows for a large n value of embryos to be treated in a single day.

The food source for the early embryo at 3 dpf is the yolk sac rather than external food sources (171), meaning that the likelihood of effective drug absorption is perhaps higher in microinjected animals. Other possible sites of injection include injecting directly into the vasculature, but this can be technically challenging. A possible refinement to this experiment in the future would be to include a fluorescent dye along with the drug, in order to definitively image the areas of the fish where the drug is present after treatment. However care would have to be taken to control for any side-effects of the dye. In addition, the gastrointestinal tract is fully open at 4 dpf, meaning

that some compounds would work more effectively at 4 dpf rather than 3 dpf, as used in the project.

Conversely, FVP affected neutrophilic inflammation to a greater extent when incubated with the embryos, rather than microinjected (Fig. 4.8). It is already known that FVP can affect cardiomyocyte proliferation when incubated with zebrafish embryos (117), so is likely to be absorbed well. The lack of effect from microinjection may be attributed to the lack of optimisation of concentrations – perhaps the microinjected concentration was not comparable to the amount used in the incubation experiments.

In contrast, *R*-roscovitine did not have an effect on neutrophil numbers post-wounding (Fig. 4.10); although previously this compound has been shown to reduce neutrophil numbers after zebrafish tailfin transection at the same concentration, when also administered at 4 h post-injury (168). One explanation is that the injury caused here was not severe enough to allow the effect of the drug to be apparent. Also, damaging the vasculature perhaps allows good drug absorption directly to the site of wounding. Microinjection of *R*-roscovitine may prove to yield a bigger effect than incubation, in a similar manner to the AT7519 study. A more wide screen of concentrations and time points may also be insightful – perhaps this concentration was not optimal, or the effect was seen at an earlier time point.

Due to the finding that *R*-roscovitine was not effective in enhancing resolution in the Tg(mpx:EGFP)^{i114} tailfin transection model used here, the compound was tested to examine if it was effective in inducing apoptosis on isolated human neutrophils. The fact that *R*-roscovitine could still induce human neutrophil apoptosis indicated there was no issue with the activity of the drug itself; therefore route of delivery and the age of the embryo are important factors to consider.

On the other hand, AT7519 effectively reduced neutrophil numbers post-wounding when injected at 4 h post-injury (Fig 4.2). It also prevented recruitment of cells when it was administered immediately at the onset of inflammation (Fig. 4.4). However, in terms of translational medicine for patients, compounds that target inflammation are probably unlikely to be administered until the inflammatory response

is underway and already established. In the case of zebrafish tailfin injury, this peak is 4 – 6 h.

In previous work in the model used by Renshaw et al, neutrophil inflammation had to reach a certain level (30 neutrophils) to be treated with the compound Tanshinone IIA and included in future analysis (122), to ensure that only zebrafish which have a robust neutrophil response are included (occasionally some fish do not respond to tailfin injury by showing leukocyte migration to the wound, or respond poorly). In the current study, a similar analysis was not undertaken – it was deemed inappropriate to exclude healthy animals from the overall analysis, as it would narrow the field of animals studied to only ones with very specific phenotypes.

AT7519 did not affect total embryonic neutrophils, indicating the neutrophil-reducing effect is specific to inflammatory neutrophils (Fig.4.3). Two methods to measure this were carried out (counting images and flow cytometry), as direct counting of total cells by eye can be challenging due to the numbers of neutrophils present, and some cells are obscured by pigmentation in the embryo in certain areas (such as the head). In the future, due to difficulties with imaging cells in a whole organism in 3 dimensions (if some cells are obscured by pigmentation, or reside in a different focal plane but directly above or below other cells), other techniques could be employed for whole embryo cell counting. For example, there now exist automated imaging tools that can quantify all cells in an embryo in multiple embryos.

TUNEL staining was carried out to examine if apoptosis is a mechanism by which neutrophil numbers are increased after AT7519 treatment. TSA-stained $EGFP^+$ cells were counted as neutrophils, and neutrophils that also had evidence of TUNEL staining were classed as apoptotic neutrophils. This was displayed in Figure 4.6 as apoptotic neutrophil numbers and also as percentage of total neutrophils which were also $TUNEL^+$; because the cell numbers recruited in the wound injuries are relatively low and at any given 'snapshot' in time it is difficult to image apoptotic neutrophils when there are so few neutrophils to begin with. Hence, depicting these data as a percentage allows an overall picture of the levels of neutrophil apoptosis relative to the entire neutrophil population at the injury site. It appeared that AT7519 may mediate its effects on neutrophils by increasing levels of apoptosis. At 12 h post-

transection, there is an increased level of neutrophil apoptosis (TSA- and TUNEL-stained cells). This is in keeping with the time course studied; by 24 h, the effect of driving apoptosis in this model becomes reflected in the reduced neutrophil numbers. One important aspect of future work would be to use another method of assessing apoptosis, to confirm these observations. TUNEL staining is a well-validated method in this model (122), however perhaps other methods could be utilised, such as Mitocapture^{TM}, a dye which allows apoptosis to be assessed by measuring change in mitochondrial potential (70, 194). In isolated human and mouse neutrophil studies, annexin V/propidium iodide binding, measured by flow cytometry, is traditionally used to measure apoptosis (Fig. 4.11) (68). However, such a technique would be challenging in this model due to the difficulties associated with isolating sufficient numbers of cells and to then perform a staining protocol with several washing steps, where cells are being lost constantly.

Although CDK9 inhibitors affect neutrophil apoptosis, the effect on other cell types cannot be discounted and must be fully investigated. For example, one study shows that FVP affects endothelial cells to assist resolution in a liver inflammation model (concanavalin A-induced hepatitis), by inhibiting TNF induced endothelial cell/leukocyte interaction (75).

To strengthen the studies undertaken here, some work looking at molecules downstream of CDK9 could be examined. For example; EGFP^{+} neutrophils from embryos treated with AT7519 could be sorted using fluorescence activated cell sorting (FACS), and the expression of anti-apoptotic proteins (such as Mcl-1) could be measured by qPCR or western blotting. This would help to confirm that CDKi compounds are affecting neutrophils directly.

Although it has been suggested here that apoptosis is a mechanism by which AT7519 can drive resolution after zebrafish tailfin injury, the effects of the compound on reverse migration cannot be excluded. It has been shown that the compound Tanshinone IIA can drive neutrophil reverse migration in this model (122). This will be a source of further investigations in this project – to assess the contribution of apoptosis vs cells that leave the wound site.

Any increase in apoptosis of neutrophils should be accompanied by effective phagocytosis; as apoptotic neutrophils can proceed to secondary necrosis, where the release of toxic intracellular components can lead to damage to tissues (195). Treatment with AT7519 did not affect recruitment of macrophages or alter their numbers during the resolution phase.

Even though AT7519 does not affect macrophage recruitment to the site of injury, the effect of the compound on macrophage functionality (specifically uptake of neutrophils) was unknown. To further assess the effect of AT7519 on macrophage functionality, Tg(mpx:EGFP)^{i114} x Tg(MPEG1:mCherry) embryos were treated with AT7519 and were imaged at different time points. Neutrophils that appeared to be engulfed by macrophages were counted. However, apoptosis and subsequent efferocytosis is rapid and hard to image using still imaging, when there are so few neutrophils to begin with (as is the case in zebrafish). The uptake of neutrophils by macrophages from 4 to 24 h does not appear to be accelerated by the addition of AT7519 (Fig. 5.7). However, it will be important to fill in the gaps in between these times as apoptosis levels appeared to peak earlier (12 h), and time lapse imaging may be more useful still, although the use of time lapse is less practical to do experiments with large n values. In the future, tracking software could be applied to the time-lapse videos to obtain measurements of other parameters such as neutrophil migration speed and directionality post-wounding (121). Also, a stain for apoptosis should be included, to ensure that it is in fact phagocytosed apoptotic neutrophils that exist inside these macrophages. This comes with the disadvantage that the staining procedure is a terminal one, meaning that time lapse imaging cannot be carried out in conjunction with the apoptosis stain. Hence, a combination of still imaging and time lapse should be employed in the future.

In these types of studies new roles can be found for previously existing compounds. Wogonin is a herbal Chinese medicine, found to reduce Mcl-1 in cancer cells by CDK9 inhibition, and may be a potential anti-cancer treatment. Therefore in our laboratory group wogonin and the related flavones luteolin and apigenin were tested in neutrophils, which are known to be sensitive to Mcl-1 (72). These compounds are known to have CDKi-like structures, so were tested to investigate if they work in a similar manner to the other CDKi. Wogonin was shown to drive neutrophil apoptosis

in vitro. In this project, these compounds were then tested in the *in vivo* setting of the zebrafish. This showed wogonin effectively reduced inflammation *in vivo*, but luteolin and apigenin did not. These experiments were only performed using bath treatment so this warrants further investigation. This reduction in neutrophil numbers was reversible by microinjection of zVAD-fmk, a caspase inhibitor, suggesting wogonin mediates its effects by driving apoptosis. However, injection of zVAD-fmk does not increase neutrophil numbers higher than control levels when injected alone; suggesting that it only works on cells in which the caspases have become activated (for example, by the addition of a pro-apoptotic agent such as a CDKi compound).

These findings translated into the *in vivo* mammalian setting, in which wogonin was subsequently shown to attenuate allergic airways (ovalbumin-induced) inflammation and LPS-induced lung inflammation (38, 73). This is a good example of how drug studies in zebrafish can eventually translate into mammalian systems. Pre-testing in the zebrafish allows the reduction in the usage of higher organisms such as mice. It also shows how it can be useful to revisit existing therapeutics, which might have structural similarities to synthetic compounds and may have previously unknown useful properties in disease. These compounds may be already tested in humans, often for many years, and are known to be safe. The use of zebrafish also allows large-scale studies of the effect of drugs and compounds *in vivo*. Toxicology tests can rapidly be carried out by a simple bath treatment, with parameters such as mortality and gross changes in morphology being analysed. Using a large number of embryos means several different concentrations can be tested in one experiment, making it much quicker to determine the concentration ranges which do not have detrimental effects on overall fish health.

Taken together, these studies allowed the identification of selected CDK inhibitors, known to have activity against CDK9, which can drive resolution in the tailfin transection model of inflammation.

5. Chapter 5. Genetically Targeting Genes of the P-TEFb pathway.

5.1. Introduction

The P-TEFb complex is a transcription complex, activated by the activity of CDK7 and 9, resulting in the transcription of anti-apoptotic proteins such as Mcl-1, amongst others (Chapter 1, Fig. 1.4). In this chapter, several genes of the P-TEFb complex are targeted to assess what affect this has on inflammation.

In mammalian primary neutrophils it is very challenging to directly knockdown genes of interest, due to the fact that neutrophils are terminally differentiated and non-proliferative, as well as having a short lifespan and being prone to undergo apoptosis (196, 197). These problems can be circumvented using zebrafish as an animal model, both *in vitro* but more importantly as an *in vivo* model. One of the significant benefits of using zebrafish as an animal model is their excellent amenability to genetic manipulation and *in vivo* imaging of any manipulation. This has been carried out using morpholinos and more recently, transcription activator-like effector nucleases (TALENs) and clustered regularly interspaced short palindromic repeats (CRISPR)/cas9 technologies. (158, 162, 198).

Morpholinos cause a transient knockdown of a specific gene target, whereas TALENs and CRISPR/cas9 causes stable, heritable targeted knockouts of mutagenized genes, as the region of interest is excised. Both morpholino and CRISPR technologies were employed in this project, to target members of the P-TEFb pathway. Zebrafish possess the components of this pathway including CDKs 7 and 9, and RNA polymerase II; and also two isoforms (a and b) of the anti-apoptotic gene Mcl-1 transcribed by P-TEFb (199, 200). These genes share significant homology with mammalian CDKs in terms of protein sequence (see Chapter 1, Introduction, Table 1.2). A recent study in zebrafish has shown that the activity of this complex is important in the proliferation of cardiomyocytes following injury (117). However, aside from this, these genes have not been extensively studied in zebrafish.

To date, in mice, a CDK9 knockout is embryonic lethal (201), but potential exists to generate a myeloid-specific knockout. CDK9, a multi-functional kinase, has been targeted in the zebrafish previously to investigate its role in erythropoiesis, possibly due to its behaviour as a binding partner to Ldb-1, a transcriptional co-factor

important in mammalian haematopoiesis (202). CDK9 morpholinos have also been used to target the translation process; for example, a morpholino was used to target CDK9 just upstream of the polyA tail, preventing CDK9 translation (203).

Alongside CDK9, another component of the P-TEFb pathway is CDK7, previously demonstrated to be present in human neutrophils and implicated as potentially important in human neutrophil survival (70). In this study, the authors showed that CDK7 was shown to be highly expressed in neutrophils, and was down-regulated by *R*-Roscovitine treatment. Knockout of CDK7 in mice is embryonic lethal but the Cre-recombinase system has been used to cause knockout in adult tissues (such as skin, liver and kidney) with little detrimental effect on adult physiology (204). CDK7 also exists in zebrafish, but has itself not been targeted directly in zebrafish; merely its binding partners. A dominant negative form of Cyclin H (the CDK7 binding partner) has been cloned and the mRNA injected into zebrafish eggs. This resulted in stunted development of zebrafish (defective eye and head development and small size) (205), indicating CDK7 has a role in embryonic development.

Downstream of CDK9 and CDK7 is the transcription of the pro-survival protein Mcl-1. Mcl-1 has two isoforms in zebrafish (known as Mcl-1a and Mcl-1b) compared to a single gene in mammals (39, 140). Knocking down these isoforms individually using morpholinos was shown to have no effect on the phenotype of zebrafish, even when the highest possible concentration of morpholino was injected; but knocking down both together was shown to be lethal (39). In the double Mcl-1a and Mcl-1b knockdown, only 50% of embryos survived longer than 8 hours post fertilisation (hpf). Knocking out Mcl-1 in a myeloid-specific manner results in an almost complete deficiency of neutrophils (98% reduction compared to wild type) in mice (206). The Mcl-1 knockout mouse is embryonic lethal (207).

Negative regulation of the P-TEFb complex also exists in mammals and zebrafish. LaRP7 is a component of the 7SKsnRNP, required for its stability and function (208-210). The 7SKsnRNP complex recruits and sequesters P-TEFb in a catalytically inactive form. In these genetic studies, LaRP7 was also chosen as a target as it should have the opposite effect to targeting CDK9, as it is a negative regulator of P-TEFb. Knockout of LaRP7 eventually results in embryonic death in mice at day 16,

likely due to cell cycle dysregulation in primordial germ cells (211). CDK9 and LaRP7 have been targeted genetically in zebrafish in relation to their role in cardiomyocyte proliferation post-injury (117).

Together, these studies should provide direct genetic evidence whether or not the mechanism by how CDK inhibitors affect neutrophilic apoptosis and inflammation is mediated through inhibition of CDK9 and CDK7 via the P-TEFb pathway. The use of zebrafish circumvents some of the difficulties of using mouse knockouts in this pathway, which are embryonic lethal.

5.2. Research Questions

- What effect does genetically targeting CDK9 (using morpholinos and/or CRISPR/cas9) have on the development and morphology of zebrafish embryos?
- How does targeting CDK9 in zebrafish affect haematopoiesis and the neutrophil and macrophage response to tailfin wounding?
- Does targeting CDK7 affect neutrophil and macrophages during inflammation?
- Does knocking down LaRP7 have the opposite effect on inflammation to knocking down CDK9?
- Does targeting the *a* and *b* isoforms of Mcl-1 also affect neutrophil and macrophage inflammation?
- Are CDK9, CDK7, LaRP7and Mcl-1 key regulators of innate inflammation and resolution in zebrafish?

5.3. Results

5.3.1. Effect of CDK9 knockdown on zebrafish gross morphology and development

Zebrafish eggs at 0 dpf were microinjected with splice site morpholinos for the CDK9 exon 3/intron 3 boundary (CDK9 morpholino *a*) or the CDK9 exon 1/intron 1 boundary (CDK9 morpholino *b*). Details of concentrations used for all morpholinos are detailed in section 2.5.2. A translation-blocking morpholino targeting the ATG start codon was also used, along with control oligonucleotide sequences. Western blotting at 3 dpf showed that splice-blocking [i] and translation blocking [ii] in zebrafish embryos resulted in partial CDK9 knockdown (Fig. 5.1, A). The band size of CDK9 protein was 42 kDa. There also appeared to be a partial reduction in the Mcl-1 40 kDa isoform.

The fish injected with 455 pg of either the *a* or *b* splice morpholinos exhibited normal body morphology with no visible growth defects, however injection of 130.7 pg of the ATG morpholino resulted in embryos which were small (compared to control groups), with a deformed body-axis and peri-cardial oedema. (Fig. 5.1, B). There was also a reduced survival in eggs at 1 dpf in the ATG morpholino group (46 % ±8) compared to the splice morpholino *a* (73 % ±6) and control groups (82 % ±2, Fig. 5.1, C). Consequently only the splice-blocking morpholinos were taken further.

Figure 5.1

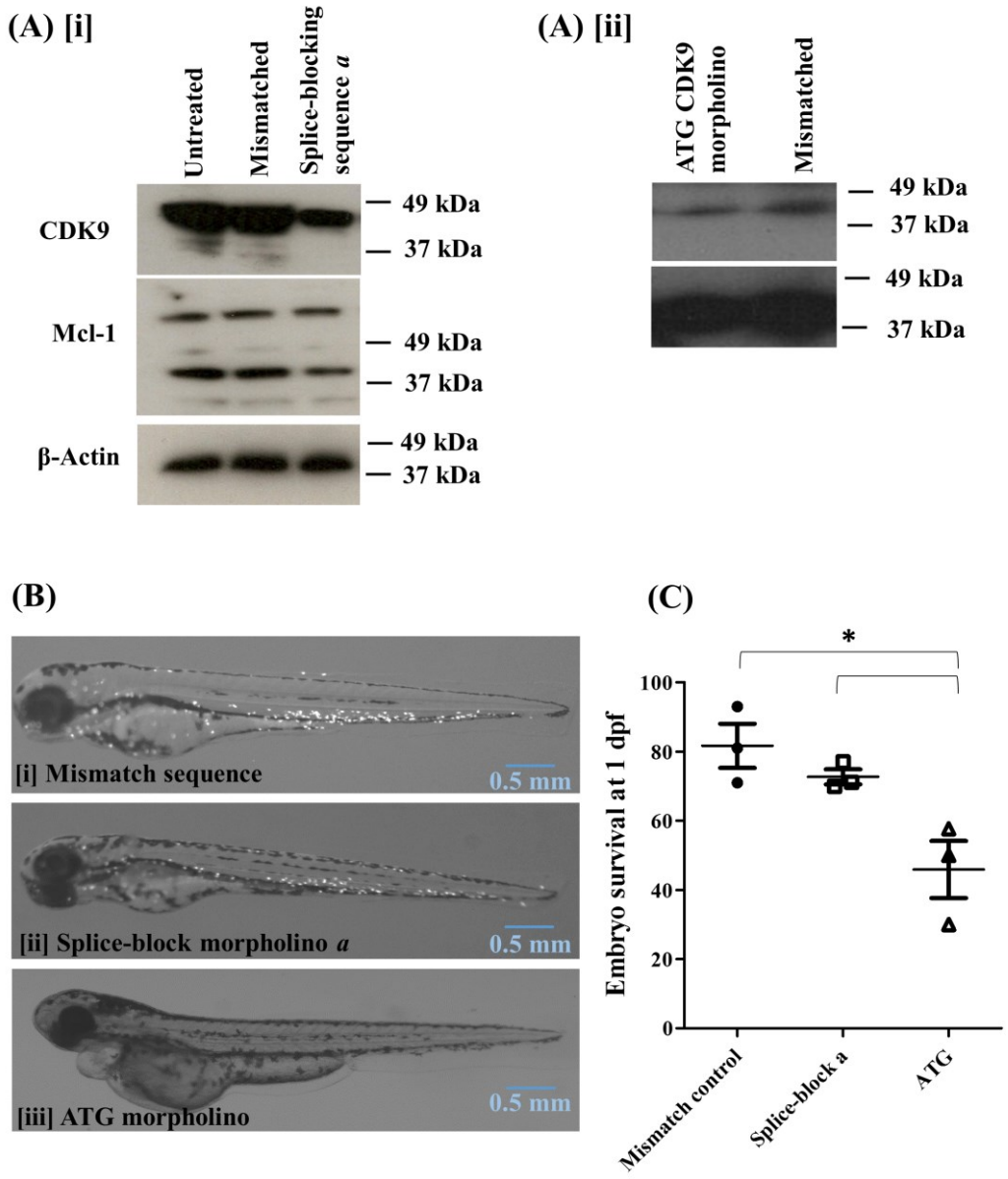

Figure 5.1. Effect of CDK9 knockdown on zebrafish gross morphology and development

Western blotting was performed to assess CDK9, Mcl-1 and β-actin expression in digested embryos at 3 dpf. The embryos were untreated or had been microinjected with a CDK9 splice-blocking morpholino *a* or *b* or a mismatched control sequence [i] or a translation-blocking ATG morpholino and control [ii] at 0 dpf (A). Gross morphology of 3 dpf zebrafish embryos (B) injected at 0 dpf with a mismatched control morpholino sequence [i], CDK9 splice-blocking morpholino *a* [ii], and the ATG morpholino [iii]. Representative images taken at 40x magnification. The percentage survival of eggs in dishes of mismatch control, CDK9 splice or ATG morpholino-injected embryos was calculated from 3 dishes of 50 embryos from 3 independent experiments (C). Data expressed as ± S.E.M and analysed by ANOVA.

5.3.2. Effect of CDK9 knockdown in zebrafish embryos after tailfin transection

Zebrafish eggs at 0 dpf were injected with morpholinos specific for the CDK9 exon/intron boundaries, or a similar control sequence. The details of each morpholino are given in Chapter 2, Table 2.3, and are designated as *a* or *b*. The highest amount of morpholino was injected which resulted in morphologically healthy animals which swim normally, with no visible growth defects (in this case, 455.1 pg) (172).

Example images are shown of zebrafish at 3 dpf previously injected with splice-morpholino *a* or a mismatch control sequence (Fig. 5.2, A).

For splice-morpholino *a*, knockdown of CDK9 resulted in a statistically significant ($p \leq 0.05$) reduction in neutrophils (16 ± 5 neutrophils in the control group compared to 9 ± 1 in the CDK9 knockdown group) at 24 h post-transection (Fig. 5.2, B[i]). At 4 h post-transection the difference between the morpholino *a* and control group were not significant.

Splice-morpholino *b* microinjection resulted in embryos which had a reduced number of neutrophils at 24 h post-transection, compared to control (26 ± 3 cells compared to 19 ± 1 in the splice-morpholino group).

As splice morpholino *a* appeared most effective at reducing neutrophil numbers, further experiments used this morpholino.

Figure 5.2

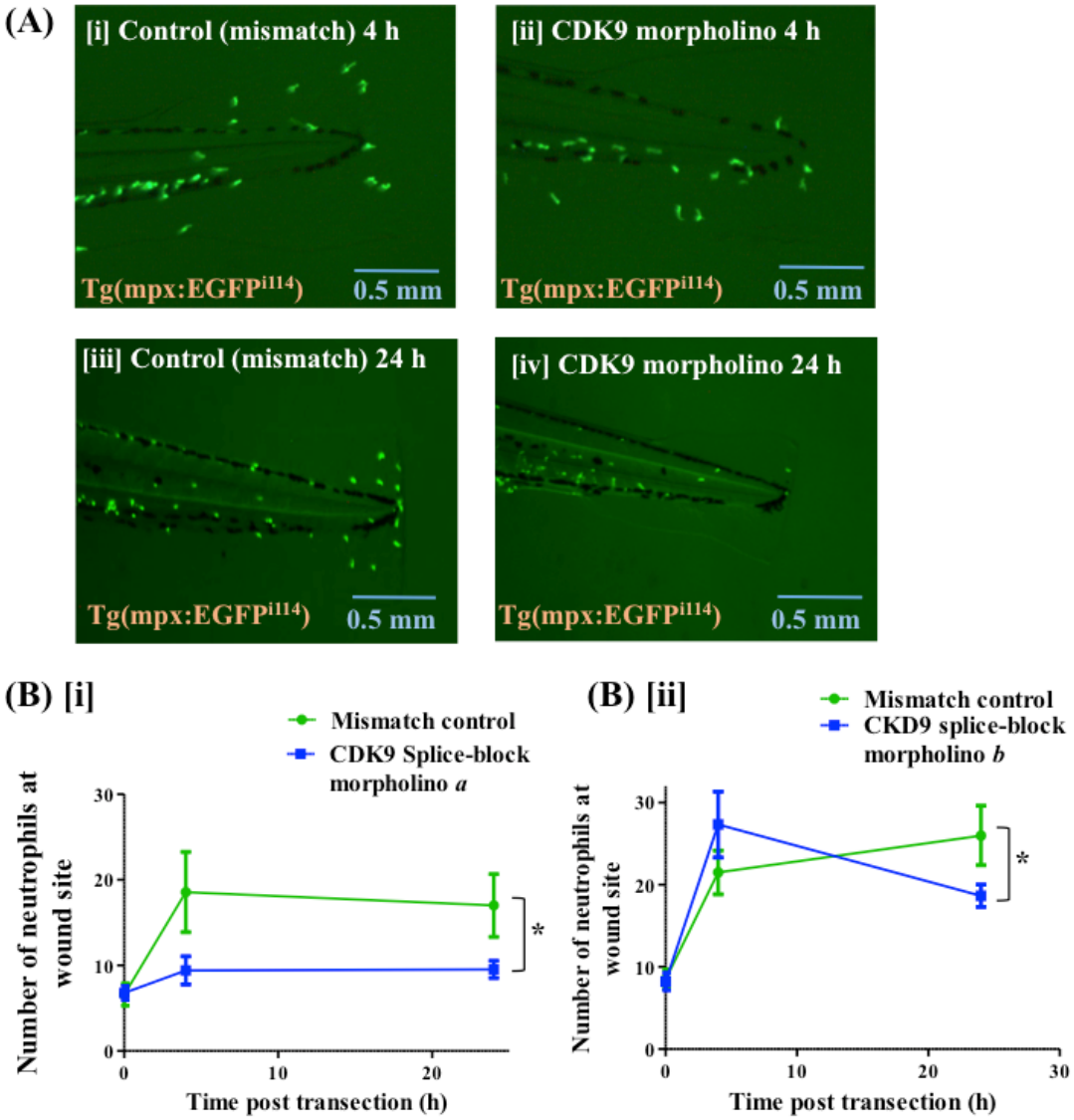

Figure 5.2. Knockdown of CDK9 in zebrafish embryos using morpholinos. At 3 dpf, the tailfins of CDK9 splice-blocking morpholino *a* and *b*-injected or mismatched control sequence-injected embryos underwent tailfin transection, and were imaged at various points over time. Shown is an example of 24 h post-transection (A). Transection experiments were performed and quantified using two splice-block morpholino sequences (*a* and *b*), each shown in (B [i]) and (B [iii]). n≥38 fish per group in 3 independent experiments. *p ≤ 0.05, assessed by unpaired t-test of 24 h splice blocking morpholino embryos vs 24 h mismatched control sequence embryos. Data expressed as ± S.E.M.

5.3.3. The effect of CDK9 knockdown on the total neutrophil numbers in Tg(mpx:EGFP)^{i114} embryos

Whole embryos microinjected with CDK9 splice morpholino *a* or a control sequence were imaged [i, ii] and the total neutrophils quantified by counting the cells in the images [iii] in 3 dpf embryo injected with CDK9 splice morpholino *a* (Fig. 5.3, A, B). This showed there was no significant difference ($p \geq 0.05$) in neutrophil numbers between the two different groups; with 84 ± 7 neutrophils in the control group and 81 ± 7 neutrophils in the CDK9 splice morpholino *a* group.

The fish were also digested and the percentage of $EGFP^+$ cells in the total embryonic cells was measured by flow cytometry. There was no significant difference ($p \geq 0.05$) in the percentage of total cells that were neutrophils in the CDK9 knockdown embryos (0.21 % ± 0.04) and control animals (0.23 % ± 0.04, Fig. 5.3, B).

Figure 5.3

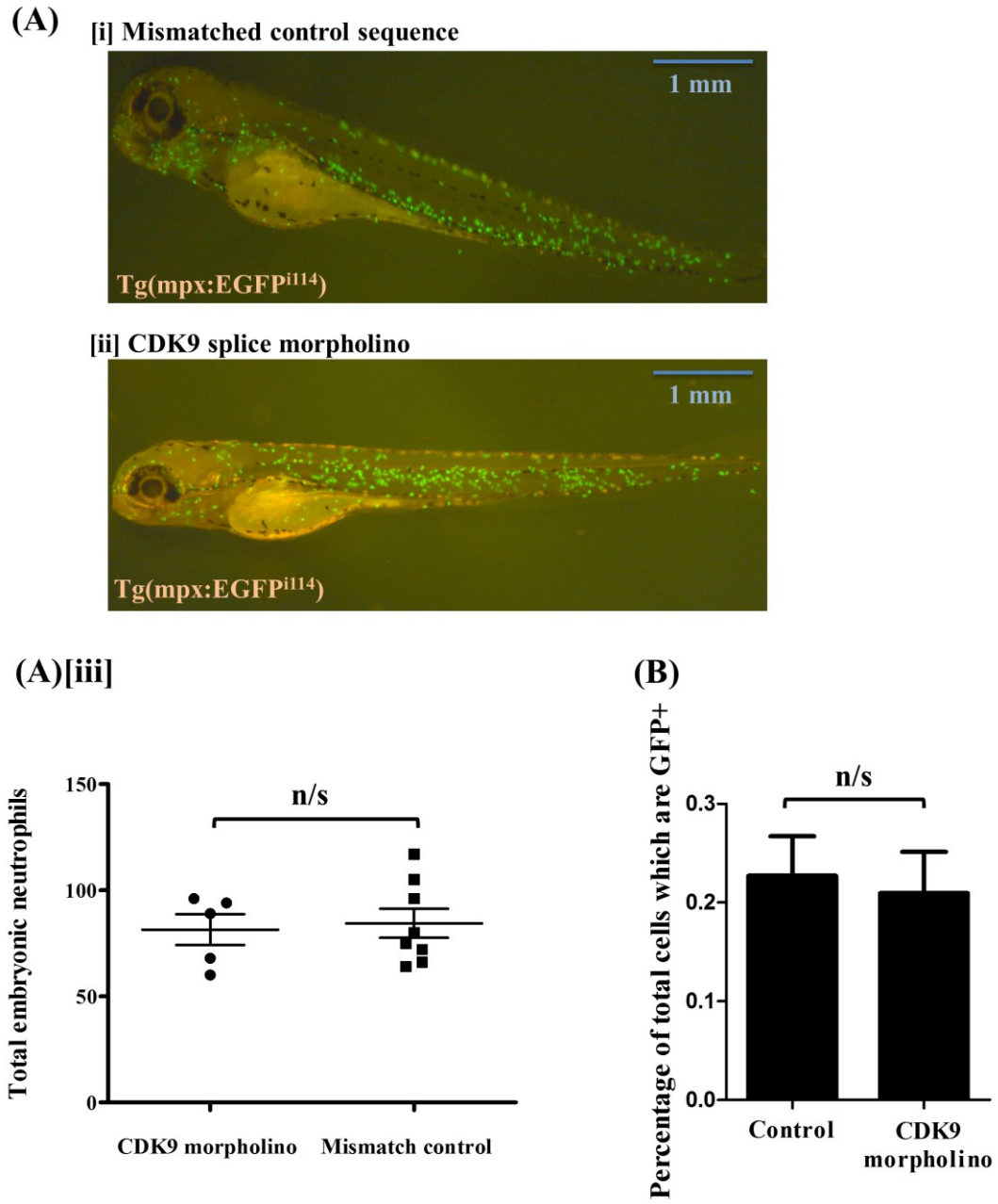

Figure 5.3. Total neutrophils in zebrafish after CDK9 knockdown

Tg(mpx:EGFP)^{i114} embryos were injected at 0 dpf with a CDK9 splice morpholino *a* or a mismatched control sequence, then raised to 3 dpf. Entire embryos were imaged (A [i, ii] and the cells in each embryo quantified (A [iii]). Whole embryos (10 per group) were also digested, and the amount of EGFP^{+} neutrophils in each group was assessed by flow cytometry (B). Statistical significance was assessed by an unpaired t-test. Data are shown as ± S.E.M.

5.3.4. The effect of CDK9 on neutrophil apoptosis after tailfin transection of Tg(mpx:EGFP)^{i114} zebrafish embryos

Tailfin transection was performed on 3 dpf embryos which had been injected at 0 dpf with CDK9 splice-blocking morpholino *a* or a control mismatched morpholino. Then tyramide signal amplification (TSA) and terminal deoxynucleotidyl transferase dUTP nick end labelling (TUNEL) was performed on embryos fixed at different time points (0, 4, 8, and 24 h) after transection. The number of TSA^+ cells (neutrophils), $TUNEL^+$ cells (apoptotic cells) and TSA^+TUNEL^+ cells were quantified. The double positive cells were counted by using confocal Z-stacks to image co-localisation of TSA and TUNEL (rather than just overlap of TSA and TUNEL in different planes). Shown is an example of 8 h time point images in control and morpholino groups (Fig. 5.4, A).

The cell numbers are shown here as percentage of total TSA neutrophils which are also $TUNEL^+$, to give a better insight of the contribution of apoptosis at each time point (Fig. 5.4, B). At 8 h post-transection, there was an average of 11 ± 4% apoptotic neutrophils in the tailfin in the splice-block morpholino group (black bar), compared to 5 ± 4% in the mismatch group (white bar). At 24 h post-injury, there were 0 apoptotic neutrophils observed in the splice-block group, but 30 ± 15% of neutrophils were apoptotic in the mismatch group.

Figure 5.4

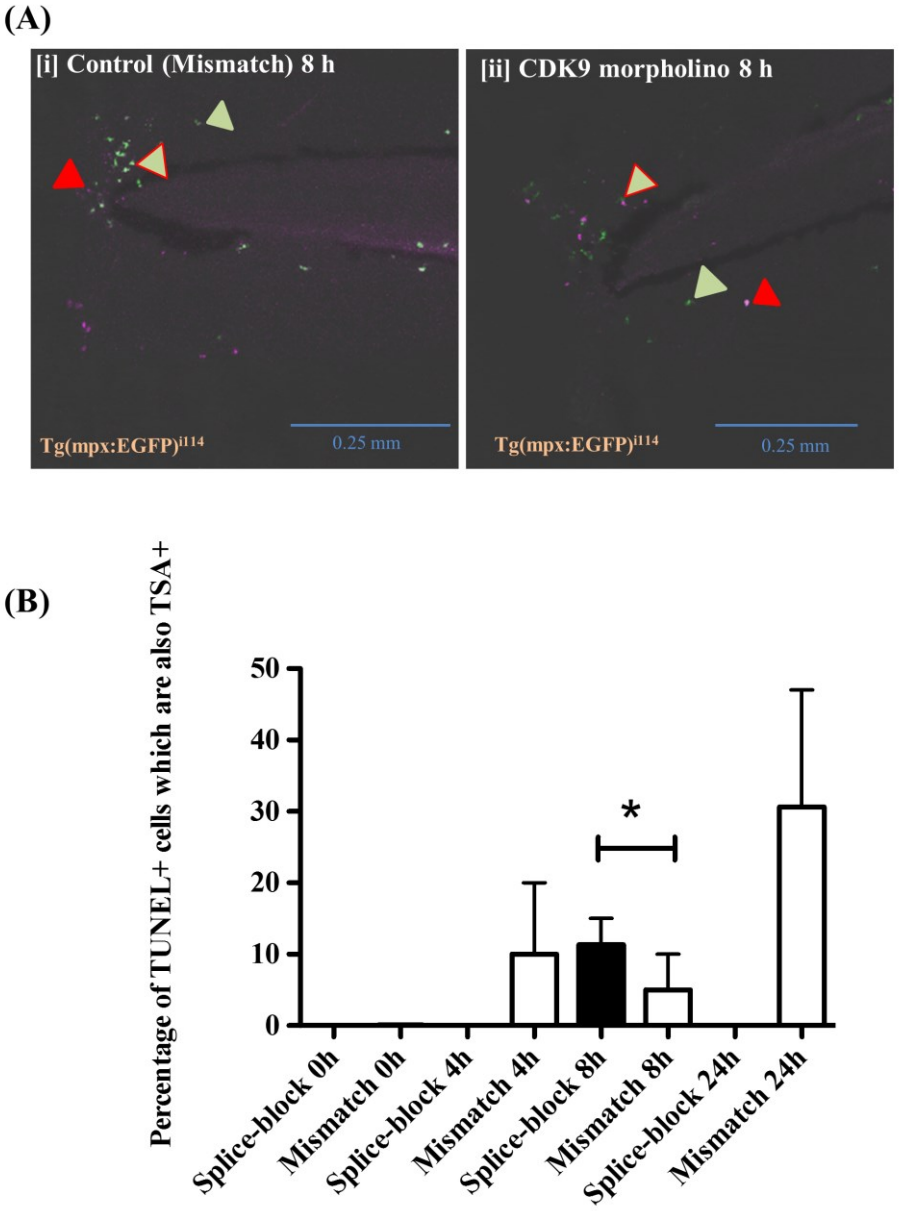

Figure 5.4. Apoptotic neutrophils in CDK9 morpholino-injected zebrafish embryos

Tg(mpx:EGFP)^{i114} embryos which had been microinjected with a morpholino to knockdown CDK9 (*a*), or a mismatch control sequence, underwent tailfin transection and fish were fixed at different time points for TSA/TUNEL staining. Shown are example images from 8 h post transection in control [i] or morpholino-injected fish (A [ii]). Each image was counted and the percentage of total TSA cells which were also TUNEL^{+} (assessed by examining confocal Z-stack images) was calculated (B). Green arrows depict neutrophils, red apoptotic nuclei, and green/red arrows double positive cells. 3 independent experiments. *$p \leq 0.05$. Statistical significance assessed by ANOVA.

5.3.5. CDK9 knockdown effect on macrophage numbers following tailfin transection

The effect of CDK9 knockdown on macrophages was assessed by injecting the CDK9 splice morpholino *a* into the Tg(MPEG1:mCherry) line at 0 dpf. At 3 dpf, the tailfin of these embryos was transected and imaged at various time points.

Shown are the 4 and 24 h time points for the morpholino *a*- [i] and control-injected groups [ii, Fig. 5.5, A, B). The macrophage response to transection was significantly lower at 4 h post transection in the splice-injected group (12 ± 1 cells), compared to control (20 ± 2 cells); however by 24 h the groups were similar – 24 ± 2 cells for CDK9 splice-sequence, and 20 ± 1 cells for the mismatch sequence (Fig 5.5, C).

Figure 5.5

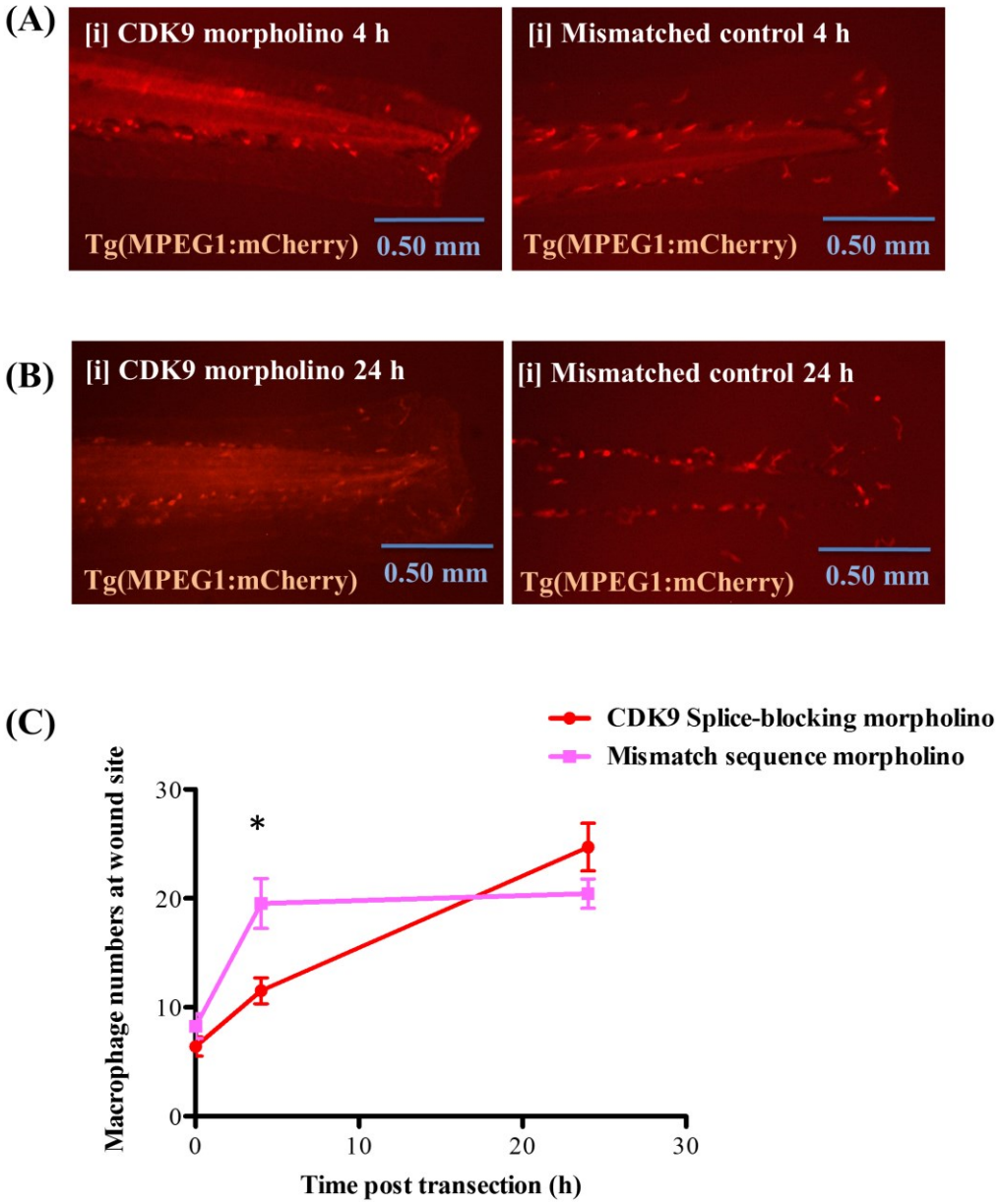

Figure 5.5. Effect of CDK9 knockdown on macrophages.
Newly laid Tg(MPEG1:mCherry) zebrafish eggs were injected with a CDK9 splice-blocking morpholino *a* or mismatched control sequence, then raised to 3 dpf. The embryo tailfin was transected and the fish imaged at various time points; shown are example images of the 4 h (A) and 24 h (B) time points for morpholino [i] and control [ii] fish. Numbers of macrophages at the wound were counted and shown graphically (C). n ≥ 20 fish per group in 3 independent experiments. Data shown as ± S.E.M. *p<0.05, assessed by ANOVA followed by post-hoc Newman Keuls test.

5.3.6. Utilising CRISPR/cas9 to knockout CDK9 in zebrafish

Only partial knockdown of CDK9 was achievable in this system by the use of the splice-specific morpholinos to target CDK9; the ATG start codon morpholino was found to be embryonic lethal, even at very low concentrations of ATG morpholino. Therefore, CRISPR/cas9 gene knockout techniques were applied to create homozygous and heterozygous CDK9 knockout animals. Tg(mpx:EGFP)^{i114} eggs were injected with a sequence designed to target exon 2 of CDK9 (all details in Chapter 2, Methods).

For genotyping, restriction digestions of a CDK9 PCR product were carried out using the Hpy188i enzyme. The digest site is shown in Figure 2.5. (Chapter 2, Methods). In wild type embryos, the PCR product (415 bp) is fully digested into 270 bp and 145 bp bands with the Hpy188i restriction enzyme (as the cut site is intact) (Fig. 5.6, A[i]). In heterozygous mutants, the PCR product is partially digested, as the cut site is present but not to the same extent as in the wild type. In homozygous mutants, the Hpy188i cut site is completely abolished, resulting in no digestion of the PCR product and one 415 bp band. In fin clips from the F1 Tg(mpx:EGFP)^{i114} x mpx:EFGP^{i114}-CRISPR injected) generation, a mix of wild type and heterozygous were present, at a ratio of 1:3 wild type:heterozygous (Fig. 5.6, A[i]).

The DNA of genotyped adult F1 fish was then sequenced over the CDK9 region (Fig 5.6, A[ii]). The heterozygote fish from this batch all had a 5'-3' GGAC base pair deletion, which are the last four base pairs of the CRISPR target site, shown in red text. This was translated to the protein sequence, showing an early stop codon occurs in the mutants (Fig. 5.6, B).

Figure 5.6

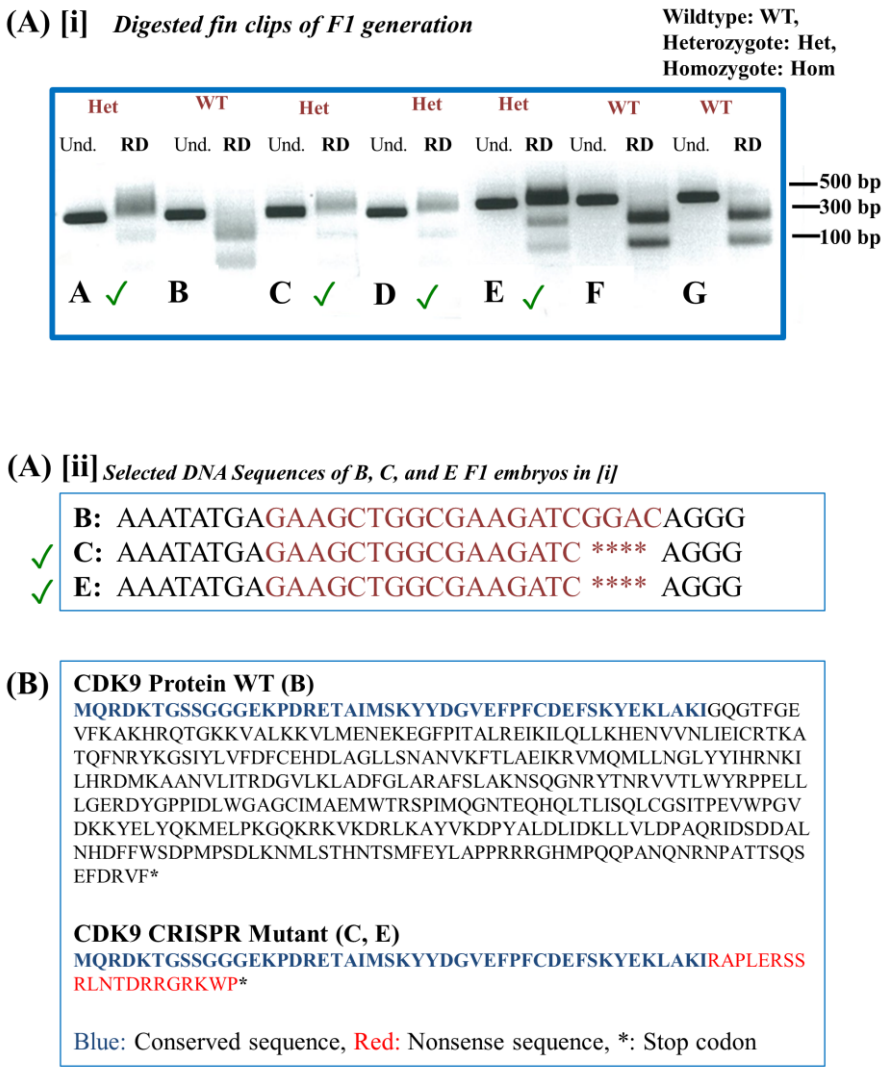

Figure 5.6. Generating F1 heterozygote CDK9 knockout zebrafish using CRISPR/cas9.

The CDK9 region in these assays was amplified by PCR (undigested ['Und'] bands) and the PCR product digested using Hpy188i restriction enzyme (restriction digest 'RD' bands). Fin clips from F1 fish (from a Tg[mpx:EGFP]^{i114} x CRISPR-injected WIK wild type cross) were digested and PCR and RD was performed (A), to show which F0 CRISPR-injected fish were producing heterozygote F1s. Fish were designated as heterozygotes when the PCR product was not fully digested into 2 smaller bands. Each fish was given a code (A-G) and the green ticks designate heterozygote fish. Some of these fin clips were sent for DNA sequencing; the sequence of the CDK9 exon 1 region is shown with the CRISPR target sequence in red (A [ii]). The protein sequence was determined from the DNA sequence, showing the conserved region between mutant and wild type (WT), and the early stop codon and nonsense sequence in the mutant (B).

5.3.7. Phenotype of CRISPR/cas9 CDK9 knockout homozygote and heterozygote Tg(mpx:EGFP)^{i114} zebrafish embryos

Two of the mutant fish were crossed and the resulting embryos genotyped, showing a mix of wild type, heterozygote-mutant and homozygote-mutant fish present in the F2 generation (Fig. 5.7, A). Embryos were digested for western blotting, showing that some of the F2 embryos have ablation of the 42 kDa isoform of CDK9 (Fig. 5.7, B).

Having confirmed that it was possible to generate homozygote and heterozygote CDK9 mutants, the phenotype of these animals was assessed. The homozygote mutants, although viable at the embryonic stage, have a deformed body-axis morphology and do not swim normally, compared to wild type (Fig 5.7, C[i], [iii]). The heterozygote mutants have normal body morphology with no curvature, normal heart function and normal swim behaviour (Fig. 5.7, C[ii]). Future assays of inflammation included heterozygotes as well as homozygote and wild type embryos.

Figure 5.7

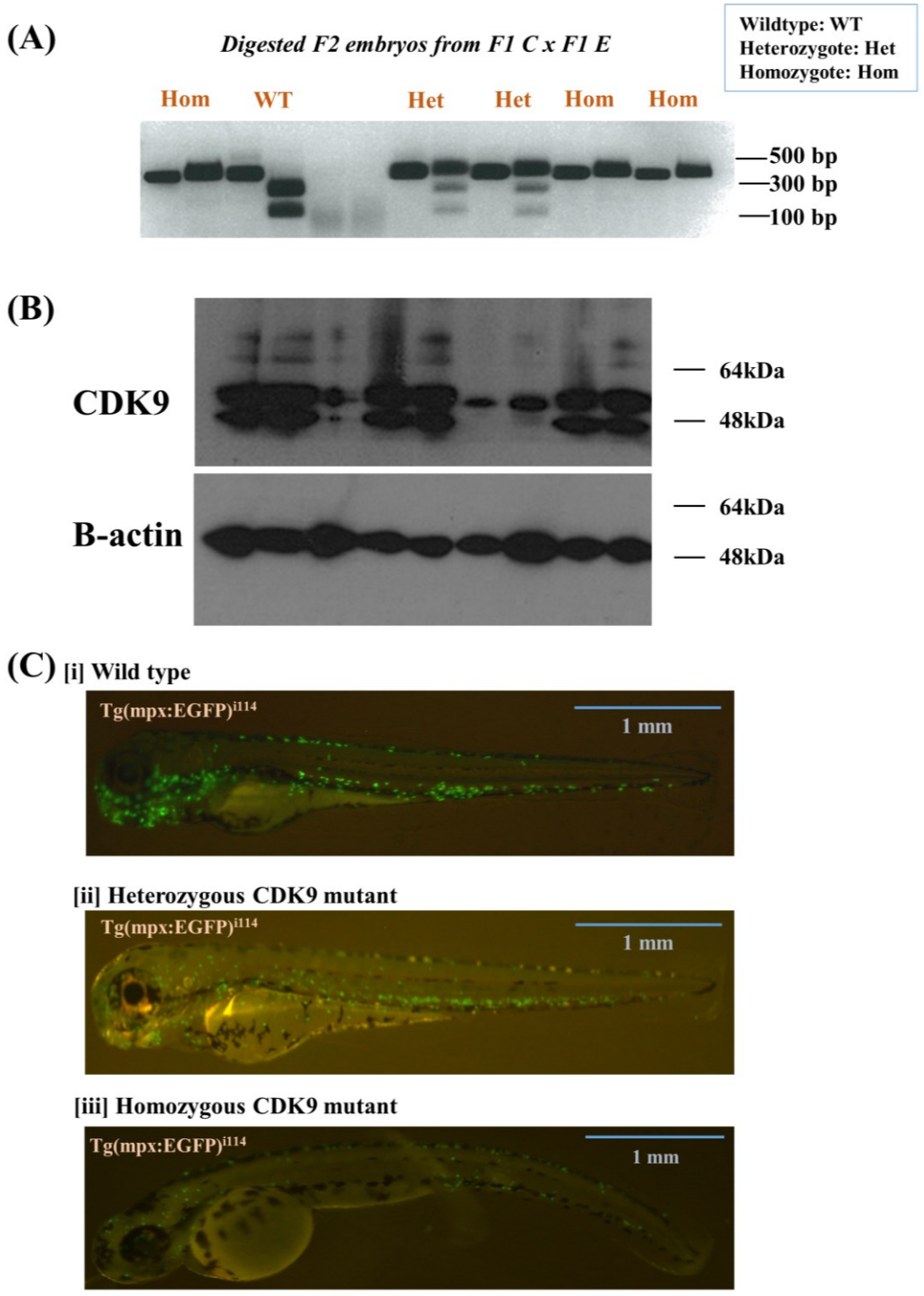

Figure 5.7. Generating F2 CDK9 knockout zebrafish using CRISRPR/cas9. Heterozygote F1s were crossed and the F2 generation was genotyped using PCR and restriction digestion, as in Figure 5.5. (A), and protein expression in a batch of embryos measured by western blotting (B). Representative images of wild type [i], heterozygous mutant [ii] and homozygous mutant [iii] embryos (C) were taken to assess the morphology of the mutants.

5.3.8. Neutrophil numbers in Tg(mpx:EGFP)^{i114} CRISPR/cas9 CDK9 knockout homozygote and heterozygote zebrafish embryos

The total (whole animal) embryonic neutrophils at 3 dpf were assessed in homozygote and heterozygote CDK9 mutants, and wild type fish. This showed there were significantly less ($p \leq 0.05$) total neutrophils between wild type (157 ± 12 cells) and heterozygote (131 ± 6 cells) embryos, and wild type and homozygote embryos (60 ± 6 cells, Fig. 5.8, A). See also images in Figure 5.7 (C).

The tail fin of these embryos were transected and the neutrophils at the injury site at different times were quantified (Fig. 5.8, B). This showed that the homozygote CDK9 knockout had significantly less ($p \leq 0.05$) neutrophils at the wound at 4, 8 and 24 h post-transection compared with the wild type and heterozygote mutant groups, with 4 ± 1 cells at 24 h post-transection compared to 11 ± 2 cells in the wild type group.

The heterozygote mutants had significantly less ($p \leq 0.05$) neutrophils at the wound site (and 8 ± 1 cells respectively) compared to wild type embryos (11 ± 2) at 24 h post-transection, but similar numbers at 0, 4 and 8 h time points. Images of the injured tailfin in wild type, heterozygous and homozygous CDK9 mutants at 24 h post-transection are shown to highlight the observed differences (Fig. 5.8, C).

Figure 5.8

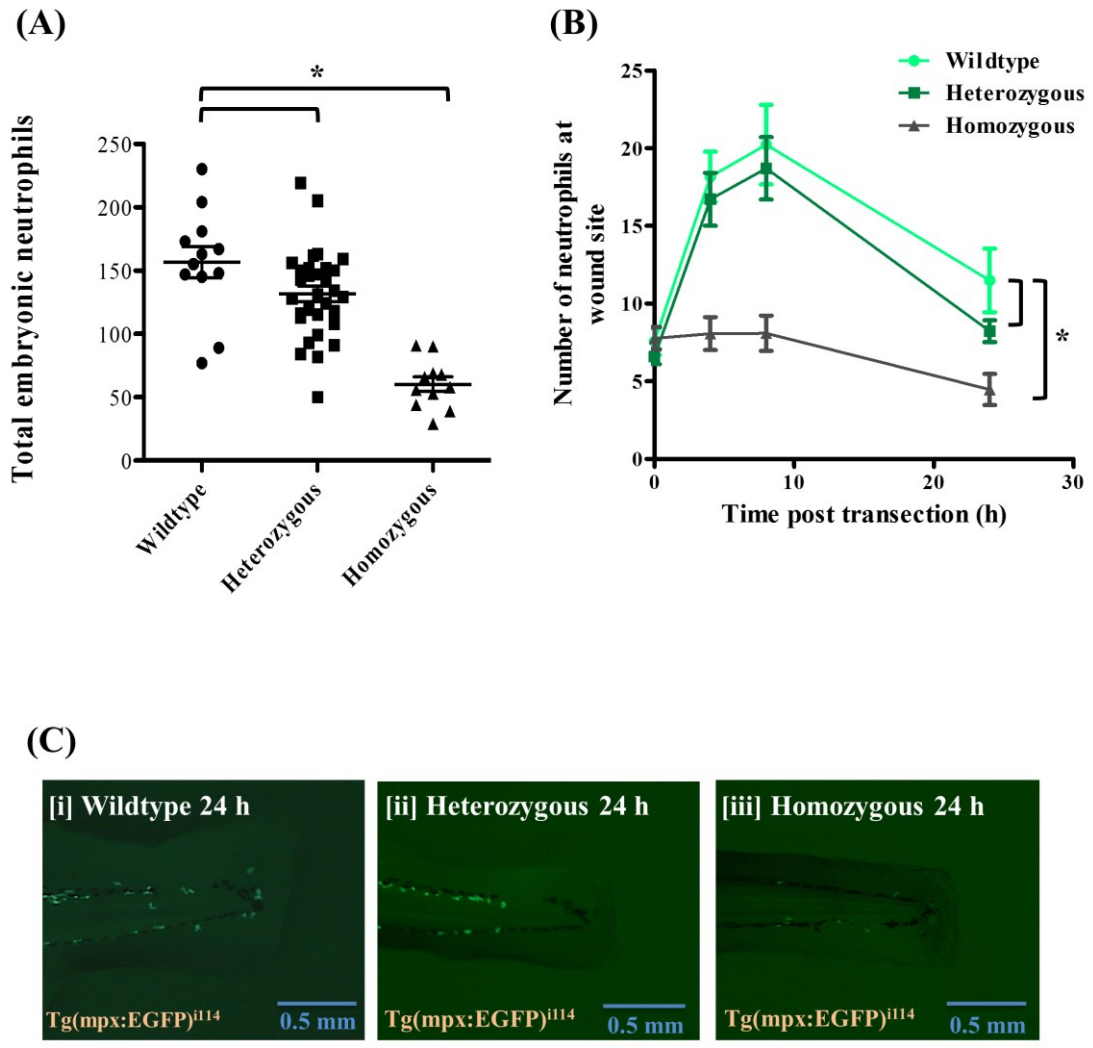

Figure 5.8. Inflammation in CDK9 homozygote/heterozygote-knockout zebrafish embryos

After imaging, the individual fish were digested and genotyped as in Fig. 5.4., to determine if they were wild type, heterozygous or homozygous for the CDK9 knockout. Total neutrophil numbers in Tg(mpx:EGFP)^{i114} embryos at 3 dpf were counted (A). The tailfin of embryos were transected and imaged at various time points after transection. The neutrophils at the tailfin were quantified (B). Example images shown of the 24 h time point (C). ≥47 fish per group from 3 independent experiments. *$p<0.05$. Statistical significance was assessed by ANOVA followed by a post-hoc Newman-Keuls test. Data are expressed as ± S.E.M.

5.3.9. Recruitment of neutrophils to wound site in wild type or CRISPR/cas9 CDK9 knockout fish, as a percentage of total embryonic neutrophils

In each fish, the wound-recruited neutrophils as a percentage of total embryonic neutrophils was calculated (Fig. 5.9). There was no significant difference ($p \geq 0.05$) between wild type, heterozygous and homozygous CDK9 knockouts in percentage of neutrophils which are recruited. For example, at 24 h post-injury, 5 ± 1 % of total neutrophils were recruited to the wound, compared to 7 ± 1 % in the heterozygous CDK9 knockout and 9 ± 2 % in the homozygote.

Figure 5.9

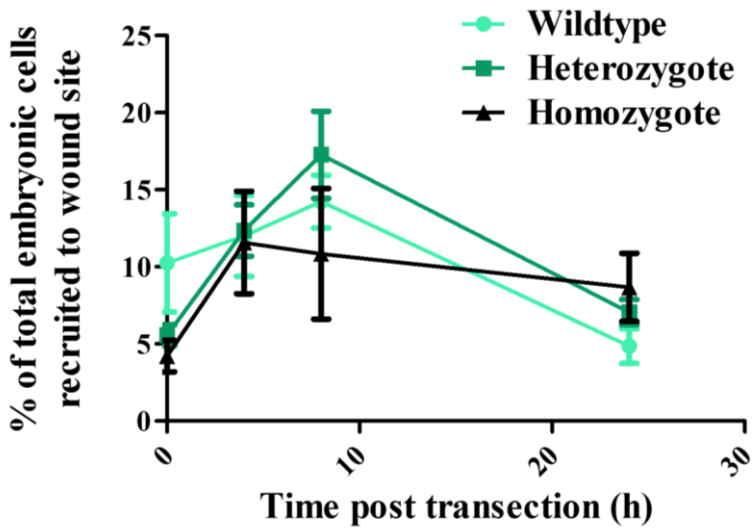

Figure 5.9. The percentage of total neutrophils that are recruited to the wound in CDK9 knockout embryos

CRISPR/cas9 was used to generate CDK9 knockout fish. Wild type, heterozygote and homozygote CDK9 knockout embryos underwent tailfin transection at 3 dpf.

In each embryo at each time point post-transection, the total embryonic neutrophils and wound site neutrophils are counted and the percentage of total neutrophils recruited to the wound was calculated. No statistical difference was noted using ANOVA ($p \geq 0.05$)

5.3.10. The effect of CDK7 knockdown on neutrophil numbers in zebrafish following tailfin transection

A splice-blocking morpholino to target the CDK7 exon 11/intron 11 boundary was injected into newly laid Tg(mpx:EGFP)^{i114} eggs at 0 dpf, along with a mismatched control sequence. Western blotting showed a reduction in CDK7 protein in embryos at 3 dpf injected with the CDK7 morpholino, compared to control sequence or untreated embryos (Fig. 5.10, A).

The 3 dpf morphant embryos underwent tailfin transection and were imaged at various time points, as shown in the representative images (Fig. 5.10, B) and the neutrophils at the wound site were quantified (Fig. 5.10, C). Neutrophil numbers were not significantly different ($p \geq 0.05$) in the CDK7 knockdown group compared to the control group; in the CDK7 knockdown group there was a mean of 17 ± 2 neutrophils at 24 h post-transection, compared with 18 ± 4 neutrophils in the mismatch-injected group. The 0 and 4 h time points were also not significantly different ($p \geq 0.05$) between morpholino and control groups.

Figure 5.10

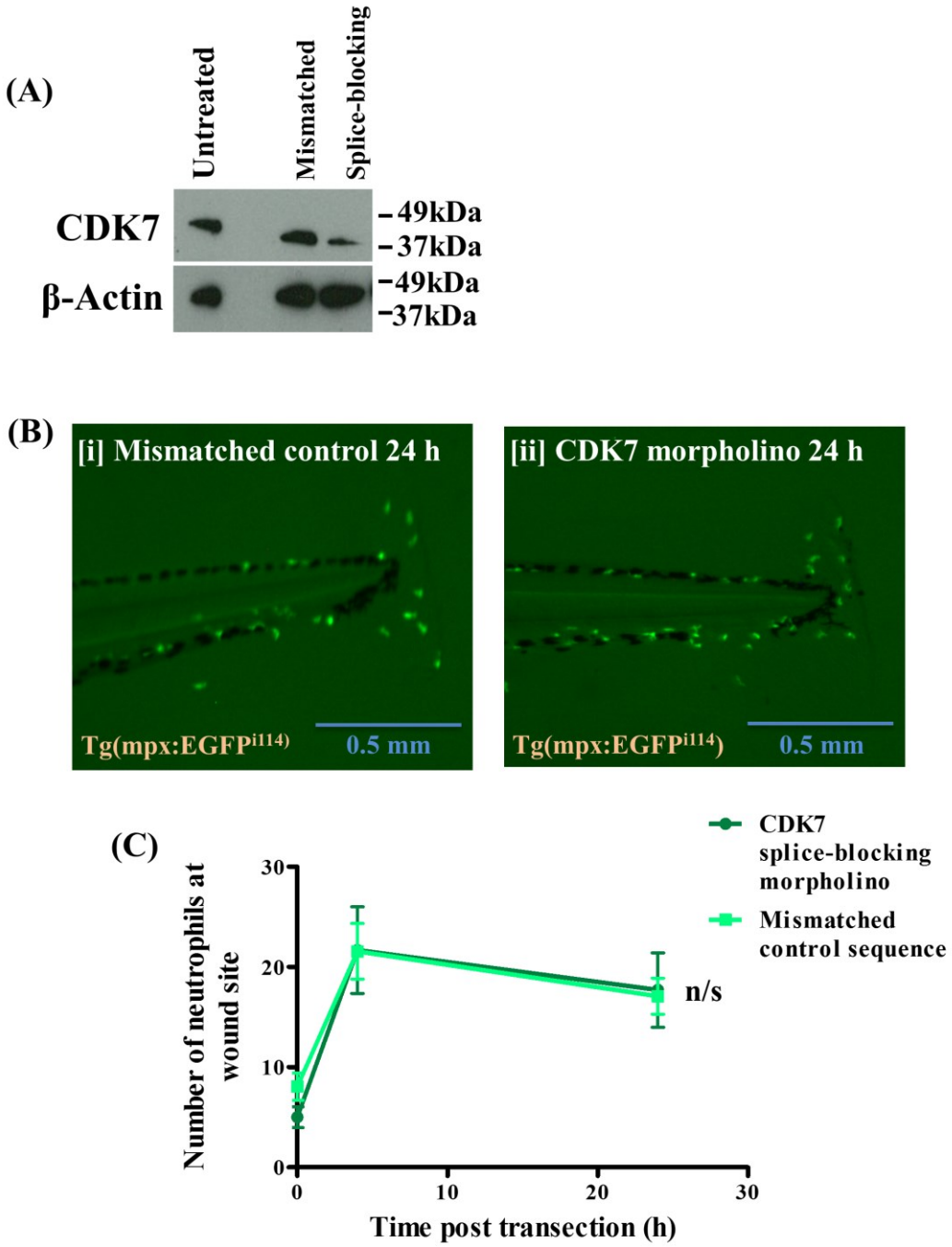

Figure 5.10. CDK7 knockdown in zebrafish embryos using morpholinos
Zebrafish embryos were microinjected with a CDK7 morpholino or mismatch sequence at 0 dpf. Embryos were digested for western blotting to assess knockdown (A). At 3 dpf, embryo tailfins were transected and the inflammation at the tailfin was imaged in control [i] and morpholino [ii] –injected groups (B), and then quantified (C). ≥16 fish per group, from 3 independent experiments. n/s: $p \leq 0.05$, assessed by ANOVA

5.3.11. The effect of knocking down CDK7 on macrophage numbers

A CDK7 splice morpholino or control mismatch sequence was microinjected into Tg(MPEG1:mCherry) zebrafish eggs at 0 dpf. At 3 dpf, successfully-injected embryos were selected by fluorescence and underwent tailfin transection.

At 0, 4 and 24 h the numbers of macrophages were counted, showing no significant difference ($p \geq 0.05$) in macrophage numbers at any time point after injury (Fig. 5.11). At 4 h, there was a mean of 21 ± 1 macrophages in the CDK7-morpholino group, compared to 22 ± 3 cells in the control group. At 24 h, the CDK7-morpholino had a mean of 25 ± 3 cells at the wound, compared to 23 ± 1 in the control group.

Figure 5.11

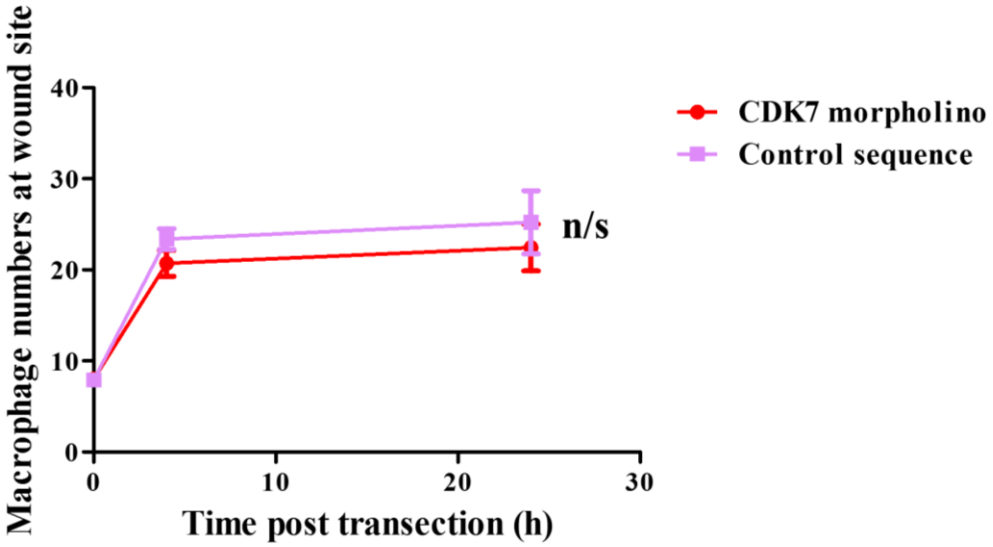

Figure 5.11. The effect of CDK7 knockdown on macrophage numbers.

CDK7 morpholinos and a control mismatch sequence were microinjected into newly laid Tg(MPEG1:mCherry) zebrafish eggs at 0 dpf. At 3 dpf the tailfin was transected and the numbers of macrophages were counted at 0, 4 and 24 h post-transection. ≥ 20 embryos per group in 3 independent experiments.

5.3.12. The effect of knocking down both CDK9 and CDK7 on neutrophilic inflammation post-wounding in zebrafish embryos

The CDK9 and CDK7 splice morpholinos were co-injected together into Tg(mpx:EGFP)^{i114} eggs (0 dpf). At 3 dpf, the embryos were transected and the inflammation was imaged and quantified at different times (Fig 5.12).

In the morpholino-injected group there was no significant difference between the morpholino and control-injected group, with an average of 18 ± 2 neutrophils at 24 h post-transection in the morpholino group, compared to the control-injected group which had an average of 17 ± 3 neutrophils. The 0 and 4 h time points did not show a significant difference between control and CDK9/CDK7 knockdown groups.

Figure 5.12

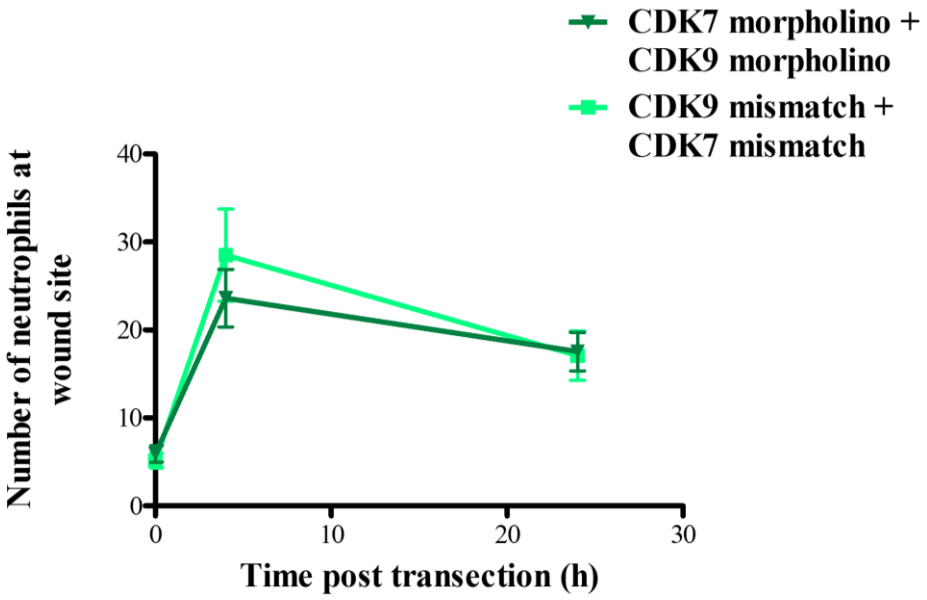

Figure 5.12. Microinjection of zebrafish embryos with CDK9 and CDK7 morpholinos.

Newly laid Tg(mpx:EGFP)^{i114} eggs (0 dpf) were injected with CDK9 splice *a* and CDK7 morpholinos or control mismatch sequences. The fish were imaged at various time points after tailfin transection and the inflammatory response at the wound was quantified. ≥14 fish per group in 3 independent experiments. Data expressed as ± S.E.M. Statistical significance was assessed by ANOVA followed by post-test Newman-Keuls.

5.3.13. The effect of knocking down LaRP7 on Tg(mpx:EGFP)^{i114} zebrafish embryos post-tailfin transection

A morpholino was injected into Tg(mpx:EGFP)^{i114} eggs to knock down LaRP7, or a control mismatched sequence. The success of knockdown of the 70 kDa isoform in 3 dpf zebrafish was assessed using western blotting (Fig. 5.13, A). Knockdown of LaRP7 significantly increased neutrophilic inflammation at 24 h post-tailfin wounding in Tg(mpx:EGFP)^{i114} zebrafish at 3 dpf, shown by the representative 24 h images (Fig. 5.13, B) and also when quantified (Fig. 5.13, C[i]).

At 4 and 8 h post-transection there was not a significant difference ($p \geq 0.05$) between LaRP7 morpholino and control sequence-injected groups in terms of neutrophil numbers. However, at 24 h post-transection there were significantly more neutrophils in the morpholino-injected group (21 ± 4 cells) compared to the control-treated group (10 ± 43). There was no significant difference ($p \geq 0.05$) between the LaRP7 morpholino- and control sequence-injected groups in terms of total neutrophils in the whole 3 dpf embryo, counted by eye (Fig. 5.13, C[ii]).

Figure 5.13

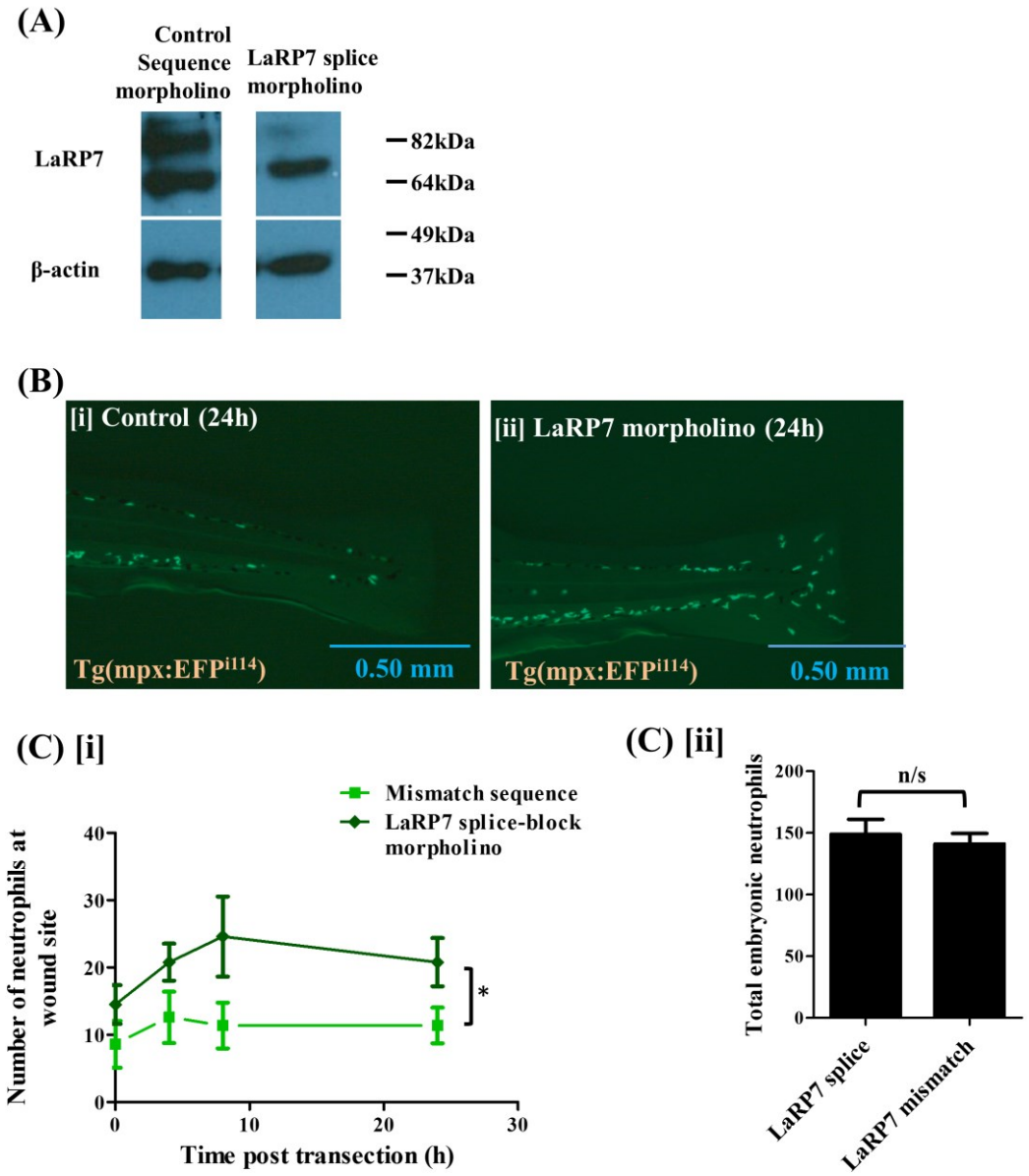

Figure 5.13. Microinjection of zebrafish eggs with LaRP7 morpholino
At 0 dpf, Tg(mpx:EGFP)^{i114} zebrafish eggs were injected with a morpholino to knock down LaRP7. Western blotting was performed of embryos injected with the LaRP7 morpholino or a control mismatched sequence for LaRP7 and β-actin (A). At 3 dpf, morpholino- [ii] or mismatch–injected [i] fish underwent tailfin transection. Images were taken at various time points (shown here are example images at 24 h, B) and the inflammatory response was quantified (C [i]). The total neutrophil numbers in whole embryos were quantified (C [ii]). Data shown as ± S.E.M. ≥10 fish per group in 3 independent experiments. *$p \leq 0.05$. Data analysed by ANOVA followed by post-hoc Newman Keuls, or unpaired t-test.

5.3.14. The effect of knockdown of LaRP7 and CDK9 morpholinos in Tg(mpx:EGFP)^{i114} zebrafish embryos after tailfin transection

Next, the LaRP7 and CDK9 (*a*) splice morpholinos were co-injected, to examine the effect of knocking down CDK9 as well as one of its negative regulators (Fig. 5.14, A). Western blotting was used to assess successful knockdown of both genes at the concentration used (Fig. 5.14, B), which was less than the concentration used for single injections, due to toxicity issues when both sequences were co-injected.

There was no significant difference ($p \geq 0.05$) in neutrophil numbers between the zebrafish injected with LaRP7 and CDK9 morpholinos, compared to control-sequence animals injected with two mismatch sequences, at all time points (Fig. 5.14, C[i]); for example, in the 24 h post-injury time point with an average of 10 ± 1 neutrophils at 24 h in the morpholino-treated group and 8 ± 1 neutrophils in the control group.

As a control, zebrafish eggs were injected with the morpholino specific for CDK9 or LaRP7, together with the control sequence of the other gene. In these studies, zebrafish injected with the CDK9 morpholino and the LaRP7 mismatch sequence had significantly decreased neutrophils (a mean of 8 ± 0.5) at 24 h after tailfin transection in comparison to the LaRP7 morpholino with the CDK9 mismatch control (11 ± 1 cells, Fig. 5.14, C[ii]). The 24 h time point for all these 4 conditions (LaRP7 and CDK9 morpholinos, LaRP7 and CDK9 mismatch sequences, CDK9 morpholino and LaRP7 mismatch sequence, and CDK9 mismatch and LaRP7 morpholino, Fig. 5.14, C[iii]).

Figure 5.14

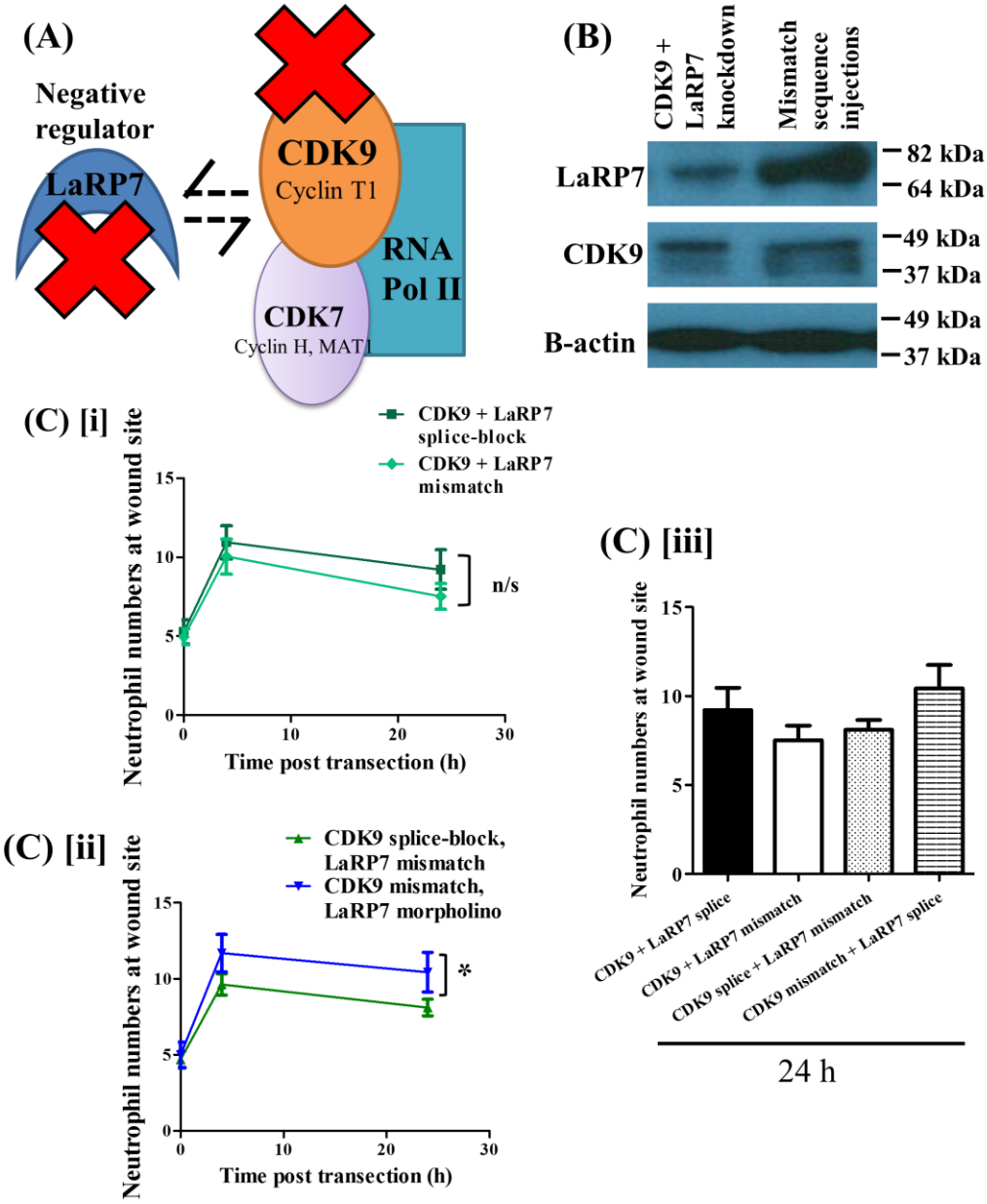

Figure 5.14. Co-injection of LaRP7 with CDK9 morpholino
The CDK9 (*a*) and LaRP7 morpholinos, or CDK9 and LaRP7 mismatch sequences were injected together into 0 dpf Tg(mpx:EGFP)^{i114} zebrafish eggs. The parts of the P-TEFb pathway targeted are depicted in (A). Western blotting was used to show the knockdown levels (B). Neutrophil migration to sites of wounding in these zebrafish was imaged and counted (C [i]). At 0 dpf, zebrafish eggs were also co-injected with CDK9 morpholino + LaRP7 mismatch control sequence, or CDK9 mismatch sequence + LaRP7 morpholino. At 3 dpf, the zebrafish tailfin was transected and the neutrophilic inflammation was imaged and quantified (C [ii]). Data expressed as ±S.E.M. ≥ 30 fish per group in 3 independent experiments. Data analysed by one-way ANOVA followed by post-test Newman Keuls. *$p \leq 0.05$.

5.3.15. Treatment with AT7519 in LaRP7 knockdown Tg(mpx:EGFP)^{i114} embryos that have undergone tailfin transection

The AT7519 CDKi compound was tested together with the LaRP7 morpholino. Zebrafish eggs at 0 dpf were injected with the LaRP7 morpholino or control sequence at 0 dpf. At 3 dpf, the embryos underwent tailfin transection and were then treated with AT7419 at 4 h post-transection.

The addition of AT7519 significantly ($p \leq 0.05$) reduced neutrophil numbers at 24 h post-transection in the mismatch control injected-group (4 ± 1) compared to the morpholino-injected group (9 ± 1 cells, Fig. 5.15, [ii]). However, the addition of AT7519 did not affect LaRP7 splice-morpholino injected fish, which had the same neutrophil numbers compared to the control group (9 ± 1 neutrophils, mismatch sequence + DMSO, Fig. 5.15, [i]).

At 4 h post-transection, immediately prior to AT7519 or DMSO treatment, the LaRP7 splice-blocking morpholino group had significantly ($p \leq 0.05$) more neutrophils than the mismatch-injected groups (17 ± 2 and 11 ± 1 cells, respectively. Fig 5.15 [i]).

Figure 5.15

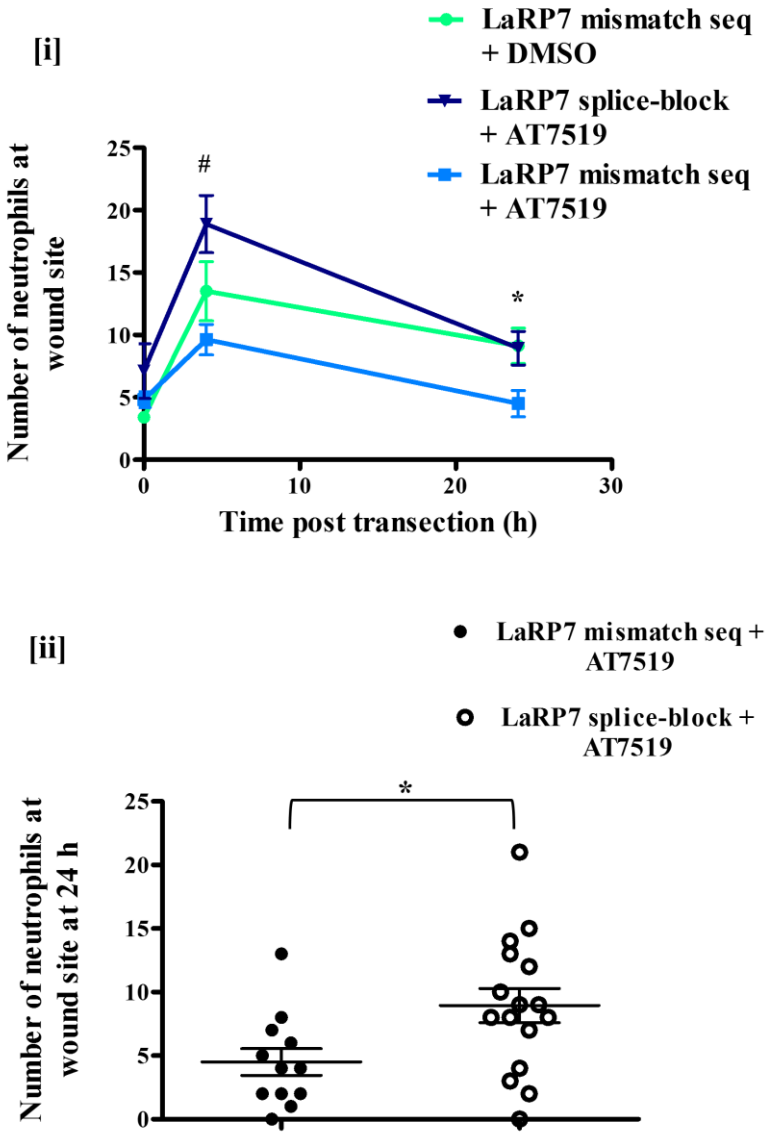

Figure 5.15. Treatment with AT7519 at 4 hpi in LaRP7-morpholino injected zebrafish after tailfin transection

Tg(mpx:EGFP)^{i114} zebrafish eggs were injected with a splice-blocking morpholino against LaRP7 or a control mismatch sequence. At 3 dpf, these zebrafish underwent tailfin transection and were treated with AT7519 or DMSO vehicle control at 4 h post-transection. The fish were imaged and tailfin neutrophils were quantified [i]. The 24 h post-transection time point is highlighted in AT7519-treated fish with either LaRP7 splice-blocking- or mismatch control sequence- injected fish [ii]. ≥15 fish per group in 3 independent experiments. Data expressed as ± S.E.M. *$p \leq 0.05$, analysed by ANOVA or unpaired t-test. *$p \leq 0.05$ LaRP7 mismatch + AT7519 vs LaRP7 splice-block +AT7519 and LaRP7 mismatch + DMSO. $^{\#}p \leq 0.05$, LaRP7 splice-block + AT7519 vs LARP7 mismatch + AT7519

5.3.16. The effect of knocking down Mcl-1a and/or Mcl-1b on neutrophils in Tg(mpx:EGFP)^{i114} zebrafish embryos

Due to the fact that Mcl-1 is thought to be transcribed as a result of CDK9 activity, the two isoforms of Mcl-1, Mcl-1a and Mcl-1b, were targeted with translation-blocking (ATG) morpholinos whose sequences had been previously published (39). Western blotting was used to show successful partial knockdown of Mcl-1a and Mcl-1b, after probing with an anti-Mcl-1 antibody and β-actin as loading control (Fig. 16 [A]).

Knocking down Mcl-1a [i] and Mcl-1b [ii] individually had no significant effect ($p \geq 0.05$) on the neutrophil numbers at the site of tailfin wounding in 3 dpf fish at any time point post-transection (Fig. 5.16, B). For example, at 24 h post-transection in the Mcl-1b knockdown group there was 13 ± 3 cells compared to 10 ± 2 cells in the control sequence-injected group.

Next, the morpholinos were co-injected together, in case one isoform compensates for the loss of the other. In the co-injected fish, no significant difference ($p \geq 0.05$) was seen in morpholino or control groups in the neutrophilic inflammation after wounding (Fig. 5.17, B). At 24 h, there were 10 ± 1 neutrophils in the control group; compared to 11 ± 1 neutrophils in the Mcl-1a and b injected groups. Example images are shown in Figure 5.17, A.

Figure 5.16

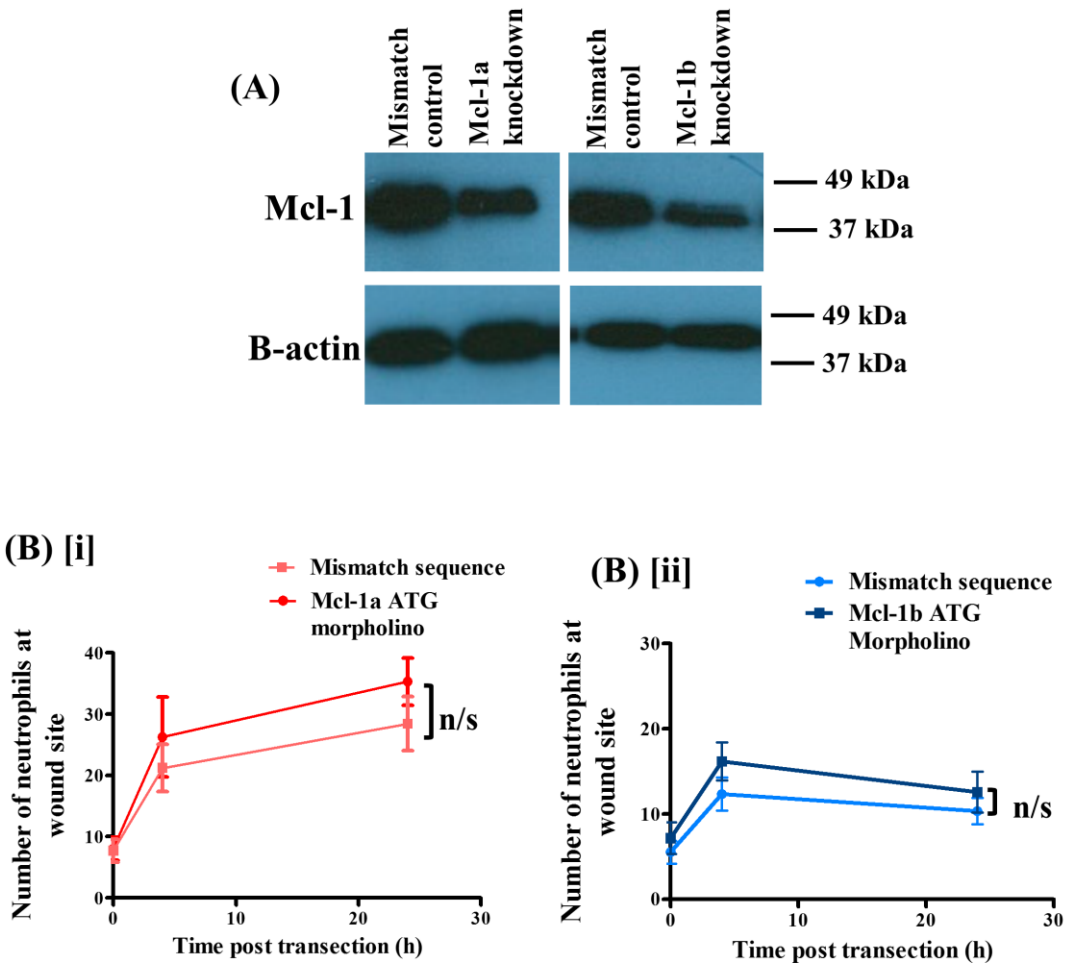

Figure 5.16. Knocking down Mcl-1a and Mcl-1b using morpholinos
4.6 ng of Mcl-1a or Mcl-1b ATG morpholino or a control sequence was injected into newly laid Tg(mpx:EGFP)^{i114} zebrafish eggs at 0 dpf. The knockdown levels were assessed by western blotting and proving with an anti-Mcl-1 antibody and β-actin antibody as loading control (A). At 3 dpf the zebrafish underwent tailfin transection, the tailfin wound was imaged at various time points and the inflammatory response was quantified (B) in Mcl-1a [i] or Mcl-1b [ii] knockdown fish. ≥ 22 fish per group in 3 independent experiments. Data shown as ± S.E.M. Statistical difference analysed by ANOVA.

Figure 5.17

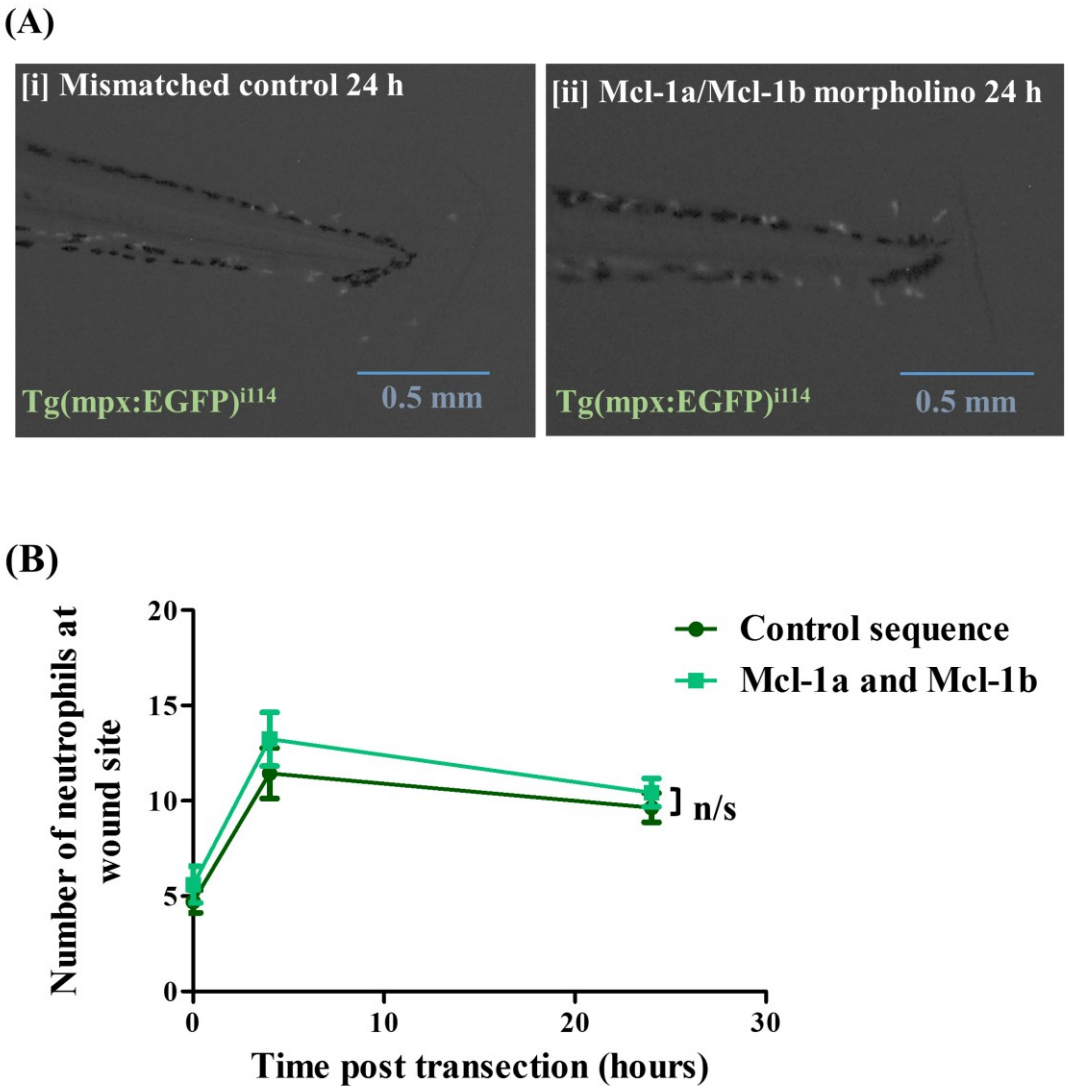

Figure 5.17. Co-injection of morpholinos to knockdown Mcl-1a and Mcl-1b

4.6 ng of Mcl-1a and Mcl-1b ATG morpholinos were injected together into Tg(mpx:EGFP)^{i114} embryos, and the fish tailfin was transected at 3 dpf and imaged at various time points. The neutrophil inflammatory response was quantified by counting cells at the wound. At least 22 fish per group in 3 independent experiments, ± S.E.M. Data analysed by ANOVA.

5.4. Discussion

Observations from Chapter 5

- Knocking down CDK9 is possible in zebrafish embryos using morpholinos and reduces accumulation of neutrophil numbers at 24 h post-wounding, due to increasing neutrophil apoptosis levels post-injury (shown by TUNEL staining).
- Knocking down CDK9 does not affect total neutrophil numbers.
- Homozygous CDK9 knockout embryos, and CDK9 ATG morphants exhibit significant defective body morphology.
- Homozygous CDK9 knockout embryos have less neutrophils, both in the whole embryo and at the tailfin after wounding.
- Heterozygous CDK9 knockout animals are viable with a normal morphology, have slightly less total neutrophils but have a reduced neutrophil response to wounding.
- CDK9 knockout using CRISPR/cas9 does not affect the percentage of total neutrophils that are actually recruited to the wound.
- Targeting CDK9 using morpholinos does not affect macrophage accumulation at the site of injury 24 h post transection, but does affect the initial recruitment.
- Knockdown of LaRP7 using morpholinos results in an increased neutrophil inflammatory response to tailfin wounding.
- LaRP7 knockdown can reverse the effect of CDK9 morpholino knockdown on neutrophil numbers after tailfin wounding, restoring neutrophil numbers to normal levels.
- AT7519 restores neutrophil numbers at the wound site in the LaRP7 splice morpholino zebrafish to control levels.
- Genetic manipulation of CDK7 in zebrafish using morpholinos has no effect on neutrophil and macrophage numbers at the wound site post-wounding.
- Knocking down Mcl-1a or Mcl-1b in zebrafish, or both simultaneously, does not affect neutrophil numbers post-wounding.

This section of the project allowed the role of particular genes to be probed in greater detail, in particular CDK9, CDK7 and Mcl-1. These genes have been hypothesised to be important in the mechanism by which CDK inhibitor drug targets can drive neutrophil apoptosis. Importantly, it is difficult to target these genes in primary human neutrophils, due to the short lifespan of neutrophils in culture, which is an important aspect in the choice of zebrafish as an *in vivo* model system.

The main genetic target of these studies was CDK9, as evidence indicates that it is an important regulator of neutrophil lifespan. CDK9 is also known to play a role in zebrafish as a regulator of cardiomyocyte proliferation (117). CDK9 knockdown using splice-blocking *a* and *b* morpholinos had the effect of attenuating neutrophil inflammatory responses at the injury site 24 h following wounding, indicating CDK9 is important in resolution of inflammation (Fig. 5.2). Splice morpholino *a* was more effective and therefore was chosen as the focus for the rest of the project. Interestingly, the morpholino did not affect the total neutrophils in the whole embryo, suggesting it does not affect haematopoiesis (Fig. 5.3). This suggests that neutrophils during inflammation appear to be more sensitive to the effect of CDK9 splice-blocking morpholino knockdown, perhaps relating to the fact that CDK9 is also thought to be involved in transcription of inflammatory mediators (212).

Knocking down CDK9 using splice-blocking morpholinos and treatment with CDKi drugs (Chapter 4) has a direct effect on neutrophils at the wound site after tailfin transection. However, the CDK9 ATG morpholino caused developmental defects when used here (Fig. 5.1), as it did in the study by Matrone et al (117), making the embryos not useful for experimentation purposes. In this project, the CDK9 ATG-targeting morpholino caused such drastic side effects that only very low concentrations yielded viable embryos. However, this comes with the disadvantage that the fluorescent tag is then heavily diluted, making it difficult to screen for positive embryos. Using western blotting to assess successful knockdown can be done after the experiment is run; but this is not so practical for large-scale transection studies, and also the morpholino is less effective over time as it is a transient knockdown. One strategy to combat morpholino toxicity is the co-injection of a morpholino against the pro-apoptotic protein p53, but this is not suitable in studies where apoptosis is important (213). For this reason, most parts of these studies focused on the use of

splice-blocking morpholinos with appropriate controls. To compensate for the fact that CDK9 ATG morpholino was less useful, a second splice-site targeting CDK9 morpholino was also used. The Mcl-1 morpholinos targeted the Mcl-1 ATG start codons, as they were used in a previous zebrafish study and the gross morphology of these animals was well described (39).

It is sometimes observed that different methods to target a gene result in different phenotypes; for example, morphants (where a gene is transiently knocked down using techniques like morpholinos) often have a different phenotype to genetic knockout mutants. The techniques differ in the fact that the morpholino causes a temporary knockdown which wears off through the various cell divisions. In one study, zebrafish mutants of the *egfl7* gene were generated using TALENs. *egfl7* morphants show vascular defects, whereas the mutants have no such phenotype (214). This has been attributed to compensation mechanisms. Extracellular matrix genes and *vegfab* are up-regulated in these TALEN mutants, but mutants generated by CRISPR/cas9 do not have this same gene up-regulation. Mouse mutants of the same gene have no phenotype. In the same study, in the zebrafish *vegfaa* mutant there is upregulation of the paralogue *vegfab*, but not so in the morphants (214). Targeting CDK9 in human fibroblasts and astrocytes using a pharmacological inhibitor (FVP), or siRNA targeting, or transduction with a dominant negative form of CDK9 all resulted in a different global effect on cell gene expression, as measured by microarray (215). It is therefore important to target genes using different methods.

These types of studies highlight the difficulties in interpretation of genetic manipulation data, and made it important to use another genetic method (such as CRISPR/cas9) as well as morpholinos to target CDK9, in order to compare the phenotype of the mutants and morphants. There are concerns about non-specificity and toxicity of morpholinos at high concentrations, and it is difficult to cause full CDK9 knockdown using this method, as the embryos die or do not develop properly when the high concentrations likely required to cause complete knockdown are injected. However, a partial knockdown can be achieved with the embryo still developing normally (Fig. 5.1).

Hence, in this study a CDK9 knockout animal was generated using CRISPR/cas9 technology to target CDK9 (160) (Fig. 5.6). This is described as a good system to create stable, heritable knockouts with an efficiency rate of approximately 70% (159). In this project, knocking out CDK9 using CRISPR was successfully achieved in the neutrophil labelled Tg(mpx:EGFP)^{i114} zebrafish. The homozygote mutant embryos, however, had a curved body morphology and poor long-term survival, although were still viable under 5 dpf (Fig. 5.7). This is in agreement with the morpholino studies, which revealed that only partial splice-site knockdown of CDK9 could be achieved in order to have healthy, viable animals, and use of the ATG CDK9 morpholino resulted in defective embryonic development. CDK9 is reported to be a master gene regulator, too important for healthy embryo development to be completely obliterated, observed also in this study with the CRISPR/cas9 CDK9 homozygote embryos and when larger amounts of morpholino are injected. Targeting CDK9 in a knockout mouse is embryonically lethal; suggesting it plays an important role in mouse development as well (113). It is known to be important in regulating genes during *Drosophila melanogaster* development (216).

Whether any of the zebrafish homozygous CDK9 CRISPR/cas9 mutants survive to adulthood will be a subject of further studies in the laboratory, including histopathological analysis. A mix of heterozygous and homozygous mutants of the F2 generation are being raised, and once they have reached adulthood, these fish will be fin-clipped and the tissue specimen genotyped using the assay described, to reveal whether any of the adult fish carry the homozygous mutation (Fig. 5.6).

The homozygous mutant embryos had a reduced number of neutrophils at the tailfin following transection, compared to wild type Tg(mpx:EGFP)^{i114} embryos (Fig. 5.8). In contrast to the morpholino data, there were also a reduced total number of neutrophils in the whole embryo in the CRISPR mutants, particularly in the homozygous CDK9 knockout. This indicates CDK9 is important in haematopoiesis in zebrafish.

Due to the morphology of the homozygous mutants, more specific attention was given to the inflammation phenotype of the heterozygous mutants. The heterozygous CDK9 mutant neutrophil response to wounding is similar to that of the

CDK9 splice morpholino knockdown animals – there are reduced neutrophils at 24 hpi (Fig. 5.8). This indicates the importance of CDK9 during resolution, and suggests that when there is a full CDK9 knockout, all time points of the inflammatory response are affected.

The reduced neutrophil numbers at the wound in homozygote and heterozygote mutant knockouts may be attributed to the reduction in total neutrophils seen in these embryos (Fig 5.8). The percentage of the total neutrophils that were actually recruited to the wound was calculated, to determine if the function of the neutrophils was impaired in the knockout embryos (Fig. 5.9). However, wild type and hetero-/homo-zygote knockout embryos are similar in terms of the percentage of total neutrophils that are recruited; suggesting the neutrophils present are functional and migrate. This reduction in total neutrophils is not seen in the CDK9 morpholino-knockdown, probably due to the less substantial knockdown in the morphants. To examine this further, tracking individual cells would have to be carried out.

Taken together, these data suggest that knocking out CDK9 completely is not a suitable resolution strategy, but partial targeting (as a pharmacological agent would be) may well be a good option for targeting neutrophilic inflammation. In addition, pharmacological intervention is given at the peak of the inflammatory response rather than being present from the beginning. Understanding the phenotype of the mutants will be the source of further study in this project.

From the CDK9 morpholino data, it was unclear if the neutrophils were more susceptible to apoptosis, or if there was a defect in the migration of the neutrophils to the injury site. To attempt to answer this, TUNEL staining of CDK9 knockdown embryos was performed to measure apoptosis levels (Fig. 5.4). There were an increased number of apoptotic neutrophils in the tailfin of the CDK9 splice-blocking morpholino group at 8 h post-transection compared to the control group. This indicates inflammatory neutrophils are more prone to undergo apoptosis when CDK9 has been knocked down. This 8 h post-injury time point was similar to the AT7519 apoptosis data, in which maximum TUNEL staining of neutrophils was seen at 12 h post transection (Chapter 4, Fig. 4.6). This 8 h time point also coincided with the beginning of a progressive increase in the presence of macrophage cells at the site of

injury in CDK9 knockdown animals; a point which will be expanded on later. Future work will also involve performing TUNEL assays on the CRISPR CDK9 mutants.

An issue with TUNEL staining is it requires fixing embryos at specific time points after transection, making it easy to 'miss' apoptotic events. One other way to confirm the possible link of migration or apoptosis would be increased confocal microscopy with tracking of individual cells (121). It has been shown *in vivo* that it takes approximately an hour for a neutrophil in the Tg(mpx:EGFP)^{i114} line to change into apoptotic morphology till the EGFP signal fades. A good strategy to assess apoptosis better would be the generation of a line in which apoptotic cells become fluorescently labelled, by apoptosis specific markers (e.g. externalised phosphatidylserine). This would allow definitive assessment of which cells were apoptotic. Previous work from this study and others has shown that maximum apoptosis occurs at 12 hours post-treatment with CDKi compounds, but the time course of neutrophil apoptosis when morpholinos are used to target molecules involved in apoptosis is not previously studied.

Furthermore, based on the CDK9 homozygous knockout data showing less neutrophils through the whole inflammatory response (Fig. 5.8), a future direction to this project would be the measurement of neutrophil recruitment. Although increased apoptosis was seen in the CDK9 splice-blocking morpholino group (Fig. 5.4), the effect may also be due to defective migratory potential due to the role of CDK9 in cytokine and/or adhesion molecule transcription (212). The CDK9 splice-blocking morpholino may affect chemotactic gradients such as H_20_2 gradients or calcium waves, which are known to be important in neutrophil chemotaxis in zebrafish (146, 147). It is possible to measure these chemotactic gradients in zebrafish using live imaging, for example the HyPer fish allows live imaging of the hydrogen peroxide chemotactic gradient by yellow fluorescent protein (YFP) expression (147).

Cytokines such as TNF and IL-8 are described in zebrafish (217, 218), and TNF-transgenic fish have been recently created which may be useful to examine the effect of targeting CDK9 on the levels of inflammatory mediators (219). Expression of cytokine mRNA in the tailfin could also be measured by dissecting the wounded tailfin area, and using q-PCR to measure the expression of these cytokine transcripts.

Zebrafish which express GFP under transcriptional control of NF-κB have also been generated, permitting the imaging and measurement of NF-κB activation (220). This would allow the effect of CDK9 inhibition on NF-κB to be assessed; it would be expected that reduced NF-κB levels would result in reduced cytokine production.

CDK9 knockdown using the splice-blocking morpholino *a* resulted in a slower initial recruitment of macrophages to the wound site, compared to the control groups and previously published macrophage recruitment data (127). This might be due to the fact that CDK9 is involved in transcription of macrophage-attracting inflammatory mediators (105). However, by 24 h post-injury, the number of macrophages is not significantly different between the CDK9 splice-blocking morpholino- and control sequence-injected groups, although there is a non-significant trend of increased numbers in the CDK9 splice-blocking morpholino group which may even increase further at later time points, and this will be investigated in a future study. This observation could perhaps be attributed to increased apoptosis of the neutrophils, resulting in release of factors to attract macrophages (221). However, previous work in LPS-induced lung inflammation in mice has shown that CDKi treatment drives macrophages to take up more apoptotic neutrophils rather than there being an increased recruitment of macrophages (38). It is important from a therapeutic point of view that targeting CDK9 drives neutrophil apoptosis but does not detrimentally affect macrophages during the resolution phase. This is because macrophages are required for effective clearance of apoptotic neutrophils. As well as the 'M1' pro-inflammatory phenotype, 'M2' pro-healing macrophages are important in clearance during resolution. A way to demonstrate the role of macrophages here would be use of the irf8$^{-/-}$ knockout line which lack embryonic macrophages, and test whether this leads to persistence of neutrophilic inflammation (222).

The CRISPR/cas9 mutants were initially made in the Tg(mpx:EGFP)^{i114} line, to examine the effect of CDK9 mutation on neutrophils, since it was hypothesised that neutrophils are sensitive to CDK9 inhibition. A source of further study will be to cross the CDK9 CRISPR/cas9 mutants to the macrophage-labelled Tg(MPEG1:mCherry) line, to see if there is also a similar initial delay in macrophage recruitment in the mutants which becomes similar to baseline by 24 h, as seen with the morphants. Time-lapse confocal microscopy may reveal if there is a link between apoptosis and the delay

in macrophage recruitment. In human *in vitro* studies, CDK inhibitor drugs do not drive apoptosis of monocyte-derived macrophages, but the percentage of macrophages which have ingested apoptotic bodies is increased (38). It seems that macrophages are able to phagocytose the increased numbers of apoptotic neutrophils present in these settings.

In the future, a CDK9 over-expressing fish could be generated using Tol2 transgenesis, by driving CDK9 expression under control of neutrophil-specific promoter such as myeloperoxidase. This might be an insightful addition to the repertoire, to examine the role of CDK9 in neutrophils *in vivo* but in the opposite manner to knocking CDK9 out. This would avoid the side-effects of CDK9 global knockout, which might be detrimental to other tissues; for example it is known that CDK9 is highly expressed in mammalian lung tissue (223). Although all the roles of CDK9 in zebrafish tissue are unclear, it has been shown to be involved in erythroid development and cardiomyocyte proliferation, by use of morpholino knockdown of CDK9 (224). Even though it is mainly described as a transcriptional regulator, CDK9 has also been thought to play a role in the cell cycle with roles in G1 and M phase in *Drosophila melanogaster,* which may also help to explain why it appears necessary for development (225).

As well as the *in vivo* studies, the genetic targeting of CDK9 also allows for potentially useful *ex vivo* cell studies. The effect of the CDK9 knockout/knockdown on neutrophil characteristics would be interesting to assess in future studies; for example: do neutrophils isolated (using FACS) from CDK9 knockout animals still migrate, and respond to fMLF stimulation by undergoing shape change, as observed in sorted neutrophils in Chapter 1 (Fig. 3.8)?

Along with CDK9, another important part of the P-TEFb complex is CDK7, which forms part of the TFIIH to helps initiate RNA pol II phosphorylation (226). For this reason, it was also a target of interest in this study. Knockdown of CDK7 with splice-blocking morpholinos did not affect neutrophils or macrophages during tailfin inflammation at any time point (Fig. 5.10), despite successful partial knockdown while maintaining healthy morphology of the animals. There could be a several reasons for this; the morpholino used was a splice-blocking morpholino, which typically causes a

less severe knockdown than ATG (translation-blocking) morpholinos, as ATG morpholinos bind to the transcriptional start codon. Indeed, full CDK7 knockdown was not achieved using splice-block morpholinos in these studies. Due to the toxicity of the CDK9 ATG morpholino, a CDK7 ATG morpholino was not tested here, as it was hypothesised that CDK7 would similarly be hard to fully knockdown due to its role in transcription (226). Perhaps, therefore, CDK7 does not play a role in transcription in zebrafish; very few studies have investigated CDK7 itself in zebrafish, however it is known that cyclin H, the binding partner to CDK7, is necessary for development. This was shown in a study in which a dominant negative form of cyclin H was expressed in zebrafish (205). Cyclin H and CDK7 are expressed throughout development in zebrafish in tissues such as the brain and liver, shown by *in situ* hybridisation. However, no link has been shown between CDK7 and haematopoiesis in any model (mammalian or fish). To answer questions about the importance of CDK7 in this system, a future study could use the CRISPR/cas9 system to generate a CDK7 mutant, as opposed to the morpholino strategy of causing transient, partial knockdown.

It was also hypothesised that CDK7 might work in conjunction with CDK9, and that any loss of CDK7 would be masked by compensation by CDK9. To test this, the CDK7 and CDK9 splice-blocking morpholinos were co-injected to investigate if the CDK7 morpholino would enhance the effect of the CDK9 morpholino (i.e., did CDK7 require the synergistic effect of reduced CDK9 in order to affect neutrophil apoptosis?). However, the co-injection of these morpholinos had no effect on the post-wounding neutrophil response, compared to control (Fig. 5.12). This could be attributed to the difficulties in establishing the proper concentrations to use. When both are co-injected at the same concentration as the single injection concentration, there are off-target toxicity effects which are typical when excess morpholino is injected, resulting in death or altered body morphology (227). Hence lower amounts of both morpholinos (compared to the single injection experiments) were injected to find concentrations in which the embryo had normal body morphology. These concentrations may not be high enough to cause a noticeable phenotype on the zebrafish neutrophils; for example, in this study, there were around 20 neutrophils in the CDK9 + CDK7 morpholino group (Fig 5.12) but in the group treated with only a

splice-blocking CDK9 morpholino (at a higher concentration), there are much less neutrophils (around 10 cells, Fig 5.2). In addition, the two morpholino sequences may be interacting with each other to reduce efficacy. In the future, the CDK7 morpholino could be injected into the CDK9 CRISPR mutants to try and circumvent these problems. In these studies the neutrophil recruitment in these batch of embryos was on average slightly higher than normal, strengthening the argument to define a "minimum-maximum" neutrophil response criteria to exclude low/high responders.

In order to further investigate the importance of the P-TEFb complex, the P-TEFb inhibitor LaRP7 was targeted using splice-blocking morpholinos. LaRP7 has been shown in human cells to act as a negative regulator of P-TEFb (210), and is part of the 7SK transcriptionally inactive complex form of P-TEFb. Driving enhanced LaRP7 expression is a potentially good therapeutic strategy as it is a specific endogenous regulator of P-TEFb. Indeed, Larp7 and the 7SK snRNP had anti-tumor functions in some kinds of cells, including *Drosophila* hematopoietic cell lineages (228). LaRP7 has been found in zebrafish and its knockdown destabilises the 7SK complex, indicating it works in the same way in fish as mammals (229). Knockdown of LaRP7 has been shown to oppose knockdown of CDK9 in a zebrafish morpholino study, resulting in cardiomyocyte proliferation after laser injury of the heart (117). Knockdown of LaRP7 using splice-blocking morpholinos induced significant developmental defects in the fish in the study by *Barboric et al*, however the amount of morpholino injected in their study was 3 times higher than in this study (229).

LaRP7 increased neutrophilic inflammation above the baseline level at 24 hpi (Fig. 5.13), having reduced the function of this negative regulator. Although with still elevated numbers in the LaRP7 group the difference was not statistically significant at 4 h and 8 h, possibly due to the increasing importance of CDK9 during resolution phase. The effect of LaRP7 knockdown on macrophages is still to be assessed – does more neutrophils result in higher macrophage recruitment? The amount of LaRP7 morpholino injected here was optimised so the effects of knockdown can be assessed without affecting the morphology of the fish. Partial LaRP7 knockdown was achieved using the morpholino, and this had the effect of increasing the inflammatory response higher than baseline (Fig. 5.13).

Inhibiting LaRP7 restored a normal neutrophil phenotype to the CDK9 splice-block morphants, as there was no difference in neutrophils in fish with co-injected LaRP7 and CDK9 morpholinos and those injected with controls; however, fish injected with only the splice-blocking LaRP7 morpholino (plus control sequence) had more neutrophils than fish injected with only the splice-blocking CDK9 morpholino (plus control sequence, Fig. 5.14). The difference between the LaRP7 and CDK9 single knockdown groups was not as substantial as in previous experiments (Fig 5.2, 5.13). This was likely to be because less morpholino of each type was injected in the co-injection experiments (due to toxicity issues), and knockdown of both genes was probably reduced; similar to the CDK9/CDK7 co-injection study. In the future it might be more useful to employ ATG translation-block morpholinos for these experiments, which are known to cause more effective knockdown. Further work will examine if LaRP7 knockdown can enhance the expression of CDK9.

The same strategy was employed with AT7519 used to target CDK9 instead of the morpholino, in LaRP7 knockdown or control embryos. Embryos with the LaRP7 knockdown (showing enhanced neutrophil numbers) were then treated with AT7519 at 4 h post-transection, and had similar neutrophil numbers at 24 post-wounding compared to control animals (mismatch sequence + DMSO, Fig. 5.15). However, the animals with a mismatch control sequence that were injected with AT7519 had reduced neutrophils at 24 h compared to the other groups. At 4 h post-transection, immediately prior to treatment with AT7519, the LaRP7 splice-block treated group had an increased number of neutrophils compared to the mismatch sequence-injected groups, as would be predicted from the ability of LaRP7 knockdown to increase neutrophils numbers. AT7519 addition returns the enhanced neutrophil numbers in the LaRP7 splice morpholino group to the same as the control group. This sharp decrease indicates that the LaRP7 morpholino group are especially sensitive to the effect of AT7519. Over-expression of LaRP7, by addition of a similar small molecule or another means of promoting its expression, might be a good future therapy to target CDK9 activity. It would be a useful study to create a LaRP7 CRISPR/cas9 mutant to examine its phenotype in comparison to the CDK9 mutant.

P-TEFb activity results in transcription of the anti-apoptotic protein Mcl-1 in neutrophils. It is known in zebrafish that both Mcl-1 isoforms must be knocked down

to affect fish survival (39). However, targeting Mcl-1a or Mcl-1b with ATG morpholinos had no effect on neutrophil numbers following wounding. This perhaps is due to the fact that Mcl-1 is a short lived protein with high turnover in neutrophils, and perhaps more is transcribed quite quickly after the morpholino begins to wear off (230). The fact that only partial knockdown was obtained indicates that even more morpholino should be injected in the future in the single knockdown embryos. In addition, in the embryos used in the Mcl-1a knockdown experiment, the recruited neutrophils was higher than normal and increased towards 24 hpi; even in the control group. This perhaps indicates the batch of fish used doing these studies had an aberrant response, validating a future need for defining a 'maximum' response.

Previous work using zebrafish survival as a readout showed that knockdown of both Mcl-1a and Mcl-1b is necessary for a phenotype to be seen; and this was the case here too. Single morpholinos can be injected at the highest possible concentration (9.2 ng per 1 nL), whereas in co-injected fish, death of eggs was seen when higher amounts than 4.6 ng was injected.

One way to examine the role of Mcl-1 in zebrafish neutrophils would be to image the eggs more closely in the first two days after morpholino injection, to examine the rate of neutrophil development. Perhaps other survival proteins are being transcribed as a result of the P-TEFb pathway, with Mcl-1 not being so crucial in zebrafish neutrophils compared to mammalian neutrophils. Zebrafish are known to possess the full range of Bcl-2 family members described in mammals, and perhaps one of these can compensate for loss of Mcl-1 in neutrophils (39). This could be studied by performing qPCR on isolated cells from CDK9 knockdown embryos to assess the levels of mRNA of other Bcl-2 family members (e.g. Bcl-2). Any family members which appear to have altered expression after CDK9 knockdown/knockout, or knockdown of the P-TEFb inhibitor LaRP7, could then be directly targeted and the effect on neutrophil survival assessed. The role of Mcl-1 will be investigated further now an Mcl-1a mutant has recently been obtained from the Wellcome Trust Sanger Institute Zebrafish Mutation Project (231), and an Mcl-1b mutant may well be discovered in the future or otherwise could be created in the laboratory.

In addition to this, the role of Mcl-1 is beginning to be further probed; during the study Mcl-1a/Mcl-1b over-expressing plasmids were created using Tol2 gateway cloning, and have been successfully sequenced. Plasmids containing the Mcl-1a and Mcl-1b sequence were obtained from Prof. Stephen Renshaw, University of Sheffield. They have been found to be integrated into the genome upon microinjection into single cell embryos. The plasmids were designed with the cardiac myosin light chain 2 (cmlc2)-GFP gene incorporated so successful plasmid integration can be assessed by screening for embryos with green fluorescent cardiac myosin cells (Fig. 5.18). The over-expression is driven by the Lysozyme C promoter so therefore should be mainly neutrophil-specific (232). The plasmid was microinjected and the embryos screened at 3 dpf. Those which possess a green heart were selected and are being raised for future studies.

This new line will allow an assessment of how increased Mcl-1 affects neutrophil and macrophage recruitment after wounding, as theoretically apoptosis should be decreased in these animals. One immediate study in the laboratory is to finish screening Mcl-1 over-expressing founders and breed them with Tg(mpx:EGFP)^{i114} embryos so they can be used in the tailfin transection assay, with the opposite hypothesis to the knockdown experiments: over-expression of Mcl-1 should increase inflammation.

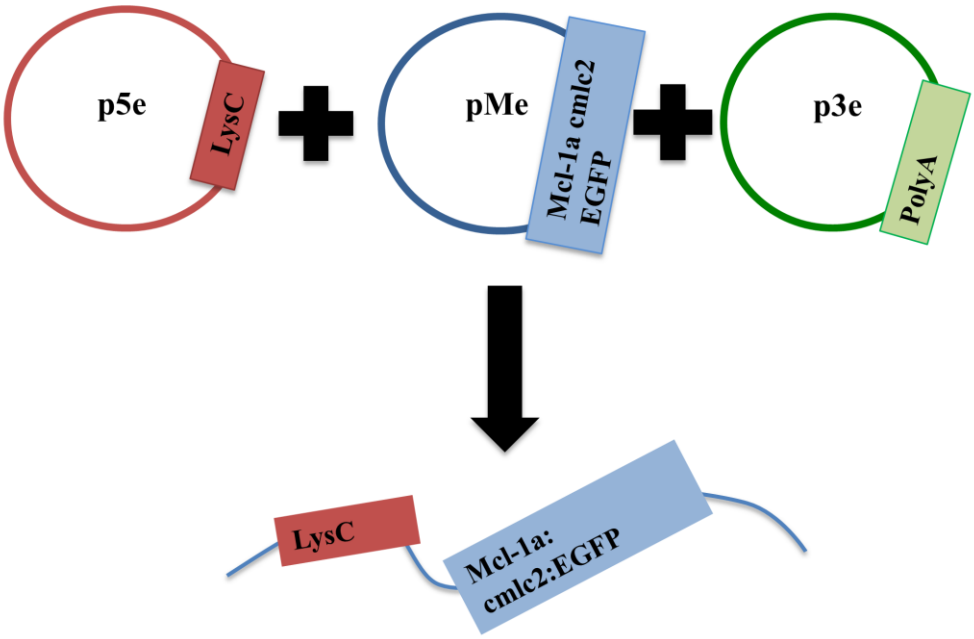

Figure 5.18. Generation of Mcl-1 over-expressing zebrafish
Plasmids containing sequences for Lysozyme C, Mcl-1a:cmlc2:EGFP and a polyA 3e entry clone, which were recombined into a single plasmid [i]. This was carried out for Mcl-1b too.

Genetic manipulations in zebrafish allows specific targeting but can also present a different set of problems, in particular due to the side-effects of manipulating genes in an entire animal. For now, tissue-specific knockout does not exist in zebrafish, due to the lack of identified stem cells; some groups have claimed to have identify these in zebrafish but these findings are still unclear (155). Recent work has utilised Tol2 gateway cloning to specifically target CRISPR/cas9 to particular cells, in this case the *urod* heme biosynthesis gene in red blood cells (by using plasmids targeting the *gata1* gene) (161). However, not all cells are affected, as this system causes different mutations in each individual cell, and several might be silent rather than frameshift mutations.

Taken together, these studies show the importance of CDK9 in resolution of inflammation *in vivo*. This was shown from both splice morpholino and CRISPR/cas9 mutant data. In the mutants but not the morphants, total neutrophils are unaffected. The role of CDK7 and Mcl-1 (using morpholinos) in this system are currently less clear, but can be a source of future studies. Knocking down LaRP7 has the opposite effect to knocking down CDK9, due to its role as negative regulator of P-TEFb, a role which it also seems to perform in zebrafish. AT7519 treatment reduces the enhanced neutrophils seen in the LaRP7 morpholino group.

6. Chapter 6. Overall discussion and future directions.

In this study, an *in vivo* zebrafish injury model was established with which to further probe the role of genes of interest in neutrophil apoptosis. Pharmacological CDKi agents known to drive neutrophil apoptosis *in vitro* in human neutrophils, and in mouse inflammatory models, were investigated and some were found to have a similar effect *in vivo* in zebrafish (AT7519, wogonin, FVP) (38, 68, 70, 72) (Fig. 4.2, 4.8, 4.9). From this, it was hypothesised that molecules shown to be important in neutrophil apoptosis *in vitro* (CDK9, CDK7, Mcl-1) might be important *in vivo* and the zebrafish was an ideal model with which to interrogate this possibility (115). The role of some of these genes, investigated in previous studies and this current study, are shown diagrammatically (Fig. 6.1). Overall, the study showed that targeting CDK9 enhanced the resolution of neutrophilic inflammation *in vivo* in the zebrafish (Fig. 5.2, 5.8), shown by genetic manipulation using morpholinos and CRISPR/cas9. Knocking down LaRP7, the negative P-TEFb regulator, had the opposite effect and increased inflammation post-wounding (Fig. 5.10), and could even reverse the neutrophil-reducing effect of the CDK9 morpholino post-tailfin transection (Fig. 5.11). The effect of LaRP7 knockdown could be overcome by addition of the CDKi AT7519 at 4 hpi (Fig. 5.12). The role of CDK7 and Mcl-1 in this model was still unclear at the end of the project u (5.10, 5.16 and 5.17).

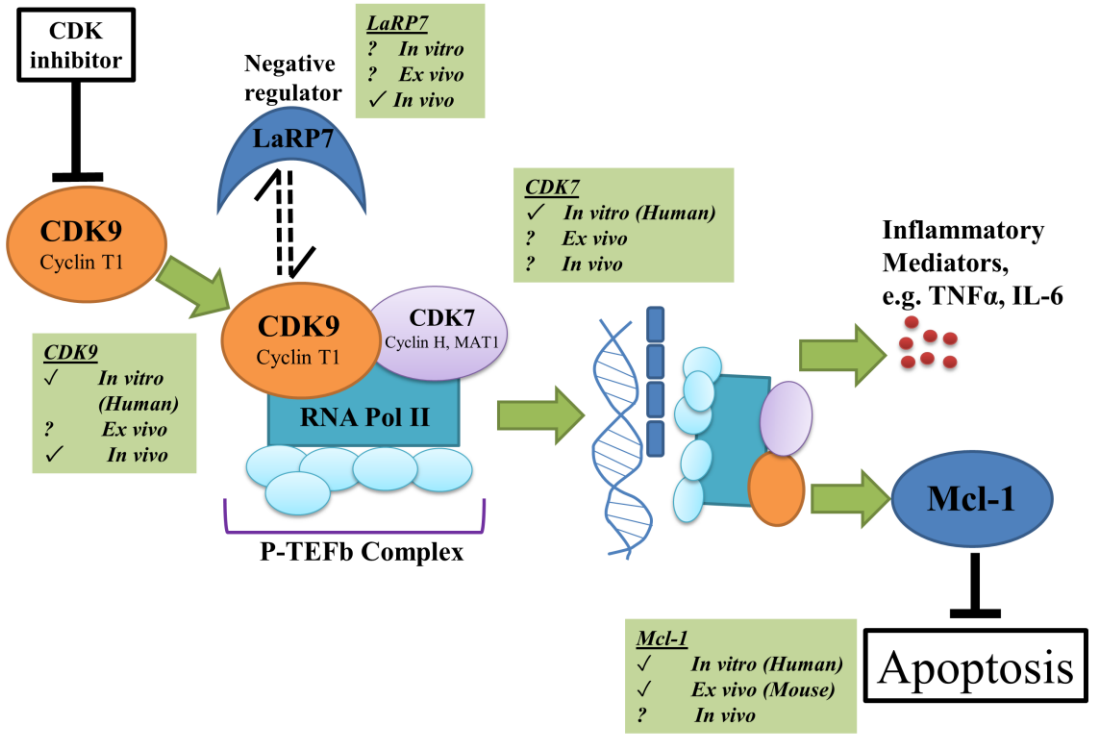

Figure 6.1. The role of P-TEFb transcription complex in human, mouse and zebrafish inflammation and apoptosis.
Schematic of the P-TEFb transcription pathway. Green boxes depict important proteins and whether or not their role in neutrophil apoptosis has been confirmed *in vivo* in human neutrophil studies, *ex vivo* in mouse neutrophils, and *in vivo* in zebrafish. '?' indicates that the role of this gene in this particular model is still unclear.

6.1. CDK9 as a therapeutic target in inflammatory diseases

In acute inflammatory diseases (e.g. acute lung injury [ALI]), where neutrophilic inflammation is an important part of the disease pathology, a sensible strategy would be to induce neutrophil apoptosis. This would reduce numbers of neutrophils producing pro-inflammatory factors. In addition, uptake of apoptotic neutrophils exerts an anti-inflammatory phenotype on macrophages, driving them to produce pro-

resolution cytokines such as IL-10 (45, 212). Targeting CDK9 and associated family members could potentially prove to be a good target for inflammatory diseases, particularly those dominated by neutrophils. P-TEFB is a universal transcription factor required for transcription of many genes (223). Hence, targeting its activity (via inhibition of CDK9) would seem like a non-specific therapeutic target. However, CDK9 is expressed most highly in terminally differentiated tissues, suggesting it carries out specialised cellular roles (233). In addition, if there is a redundancy in the role of CDK9 in transcribing other genes, it might be possible to target it for particular functions (e.g. driving apoptosis) without affecting other cellular functions to a great extent. CDK9 inhibition would be a good strategy for treatment of acute neutrophilic inflammatory disease, or for use in chronic situations in which neutrophils contribute to disease 'flares'. An understanding of the entire P-TEFb complex may well reveal other therapeutic targets; for example, LaRP7 is an endogenous inhibitor of the P-TEFb complex which may increase resolution of inflammation (99, 210). Perhaps enhancement of the actions of LaRP7 could be a therapeutic strategy for the future; by administration of LaRP7 or a synthetic small molecule with a similar mode of action.

In addition to this study, existing data indicate that CDKi drugs might be an effective strategy for inducing neutrophil apoptosis. In many mouse models of inflammation in different tissues, CDKi drugs have been shown to induce neutrophil apoptosis (38, 68). In diseases such as acute lung injury, patients usually present when inflammation is at its peak. This means that targeting neutrophil migration alone may not be a successful strategy; possible therapeutics should target neutrophils that are already there (and also perhaps enhance reverse migration). In the drug treatment tailfin injury experiments, this scenario was mirrored by administration of CDKi drugs at 4 h post-transection; the peak of neutrophilic inflammation in zebrafish (9).

6.2. Zebrafish as a model for inflammatory diseases

Zebrafish are a good model for investigating many aspects of neutrophil biology (115, 234). The ease of imaging of neutrophil behaviour is unprecedented in any other animal model. The injury model selected here proved to be a robust assay for measuring neutrophil inflammation, which occurs rapidly similar to mammalian

inflammation. Aside from this, the neutrophils themselves appear to share characteristics with mammalian cells. Sections of the haematopoietic site (the kidney) in adult fish reveal cells bearing hallmarks of neutrophils (multi-lobed nuclei) and macrophages (phagosomes in cytoplasm) (125). Coupled with the transparency of the embryo, they are an ideal model to image the real time behaviours of neutrophil and macrophages *in vivo*. Some disadvantages are that these are embryonic animals, and therefore these cells might not be fully developed. Presumably the environment of haematopoietic development in the kidney in the adult differs from that of the embryo, which has a pronephros embryonic kidney at these early stages. (235). The high degree of conservation in cells (for example the response to fMLF, shown in Fig. 3.8) indicates that many of the lessons learned in zebrafish can be applicable to mammalian models. Additionally, many genes such as CDK9 have high levels of conservation (Introduction, Table 1.2).

One drawback to this model is that mouse models can give information about the impact on individual organs compared to the embryo of the zebrafish, which has some still undeveloped organs (e.g. the kidney). In a lung inflammation experiment in mice, lung tissue, BAL, blood and lymphoid tissue such as the spleen can all be harvested for the measurement of parameters such as cell numbers and histological sections for analysis of tissue structure (38). This allows the effect of pharmacological treatments on these many different tissues to be assessed. However, in rodent systems the subtle cell-cell interactions are difficult to image *in vivo*, and simple genetic manipulations are not possible.

Like zebrafish, using primary isolated human neutrophils is a relatively simple and quick way to assess the effect of pharmacological manipulations on neutrophils directly (1). However, the short-lived nature of neutrophils is not amenable to genetic manipulation; they die within 24 h in culture. Hence, using both human, rodent and zebrafish models concurrently can give complementary data that can inform future experiments, as we have previously demonstrated using the compound wogonin, which proved to be effective in reducing mouse lung inflammation following initial trials in isolated human neutrophils and zebrafish (72) (38).

One issue, common to all transgenic lines in all models, is the specificity of cell labelling. Traditionally myeloperoxidase (labelled in Tg[mpx:EGFP]^{i114} zebrafish) is thought to be specific to neutrophils; however, it has been shown that macrophages in atheroma appear to express myeloperoxidase (236). In the MPEG1:mCherry line, perforin-2 expression labels macrophages (237), however, perforin-2 expression has been shown to be inducible in other cells such as fibroblasts (238). It is likely that there exists no perfect marker for individual cell types.

6.3. Pharmacological versus genetic approaches to investigate the role of CDK9 and P-TEFb in inflammation

In these studies, pharmacological and genetic approaches were used to target the same pathways. Some parallels could be drawn between the phenotype of the fish injected with the CDKi compounds, and the morpholino-injected fish (Chapter 4 and 5 data). Both manipulations reduced neutrophil numbers by increasing apoptosis, indicating the importance of CDK9 in neutrophil apoptotic pathways. There are important differences, in that the CDK9 morpholino is present from the 1-cell stage of the embryo. The drug and morpholino experiments are therefore not directly comparable, as the morpholino/CRISPR targeting is present from the beginning of development, whereas the drug treatments are present from the peak of inflammation (after tailfin transection). However, AT7519 pre-treatment prior to transection could also affect recruitment to the wound site. Whether this is down to effects on neutrophil apoptosis or migration is still unclear. This experiment was only carried out to 4 h post-transection, but it would be interesting to image these fish for longer and determine whether AT7519 pre-treatment results in a similar phenotype to the CDK9 knockdown animals.

One possible direction for the future is to examine CDK9 knockout from 3 dpf (the time of transection) would be the creation of a conditional knockout mutant, for example using a *Cre Lox* system (239). This could help to overcome issues of embryonic lethality, such as the phenotype of the homozygote embryos.

Despite the fact that the genetic manipulations can have off-target effects, this is also true of treatments with drugs and other compounds, and for drug usage in humans, a full understanding of the side effects is important. CDK inhibitor drugs generally target a range of CDKs in a variety of different potencies. Future therapies would hopefully target CDK9 active sites more specifically, which is made more possible with the development of small molecule inhibitors. It should be noted that morpholinos can also result in off-target effects; for example, by non-specific binding to other sequences. Hence, it is considered important to assess genetic manipulation via a second method.

Small molecule inhibitors of Mcl-1 itself have been challenging to create due to the need to disrupt high affinity bonds in Mcl-1, however these inhibitors are beginning to emerge (240). Hence, upstream molecules such as P-TEFb have generally been targeted in order to target Mcl-1 (241). Mcl-1 knockout mice are embryonically unviable (207). In this way, the use of the zebrafish might be a good strategy for investigating Mcl-1, as there exist two isoforms of Mcl-1 in zebrafish, and individual isoforms can be targeted (39).

The effect of CDK9 inhibition on neutrophil migration will be examined in the future, by measuring parameters such as the production of pro-inflammatory chemotactic agents at the tailfin post-injury (147). Alternatively, fluorescence activated cell sorting could be used to sort neutrophils from CDK9 knockout/knockdown zebrafish, then stimulating them *ex vivo* with a substance such as fMLF, to see if they respond, for example, by alteration in their forward scatter by flow cytometry measurement (see Chapter 3, Fig. 3.8). Alternatively, the effect of this stimulation could be measured *ex vivo* by imaging cell morphology and migration.

Taken together, the pharmacological studies allow the assessment of the effects of compounds on cell populations of interest in the zebrafish. The genetic studies here give insight in the role of specifically CDK9 and other genes in a way which pharmacological manipulations cannot. These studies are complementary despite the differences observed.

6.4. CDK9 in other model systems

In the future it will be interesting to examine the role of CDK9 in other inflammation models apart from the wounding model used in the thesis, to ensure the pro-resolution role of CDK9 occurs in other examples of inflammation. For example, an investigation of the phenotype of CDK9 knockdown/knockout zebrafish upon response to infection would be an interesting experiment. Targeting CDK9 in mice pharmacologically has been shown to have beneficial effects on bacterial clearance in the lung, and even resulted in a reduced bacterial load, even with the effect on driving neutrophil apoptosis (38). This could be possibly due to increased phagocytosis of bacteria by macrophages, which may be enhanced by increased apoptotic neutrophil numbers. This hypothesis could be carefully examined in fish, using fluorescently-labelled bacteria in Tg(mpx:EGFP)^{i114} and Tg(MPEG1:mCherry), allowing real-time imaging of what happens to the bacteria after CDK inhibitor treatment. Several infection models have been established in zebrafish, such as *E. Coli* and *M. Marinum* infection (137, 242). In addition to this, different methods of injuries could be used; for example, cryoinjury can be used to induce tissue damage (243). This injury is not localised like tailfin injury, so would be a system for examination of the role of CDK9 in a more diffuse injury.

6.5. Does targeting CDK9 affect reverse migration of neutrophils?

Neutrophil reverse migration is an umbrella term to describe the migration of neutrophils away from an inflammatory site, but sometimes also migration across the endothelium in the bloodstream, and sometimes appearing at a site remote from the original inflammatory site (29). This was first reported by Brown *et al* in 2007. The contribution of reverse migration to mammalian resolution remains unclear. It is thought that the majority of neutrophils will undergo apoptosis at the site of inflammation. However, studies *in vitro* and in mouse intravital imaging wound models have demonstrated that transendothelial migration of neutrophils can occur (27, 244), with around 10% of neutrophils shown to do this. The function of this is still unknown but may influence the adaptive immune response in lymphatic sites remote from the original inflammation site. Reverse transmigrated neutrophils may

also contribute to inflammation in organs separate from the inflammatory site. Some of the mechanisms of this are being delineated; for example, LTB_4 is thought to mediate the ability of neutrophils to reverse transmigrate, via stimulation of neutrophil elastase which cleaves JAM-C adhesion molecules (28).

Investigation of neutrophil reverse migration can be performed effectively in zebrafish, using the mpx:kaede transgenic line (115, 122). In this line, $EGFP^+$ neutrophils can be photoconverted to RFP^+ neutrophils. Hence, $EGFP^+$ neutrophils at the wound at the peak of inflammation (4 h) can be photoconverted, and then the RFP^+ neutrophils can be tracked – as RFP^+ neutrophils not present at the wound anymore must have reverse migrated. A recent study used this system to examine the phenotype of reverse migrated neutrophils (245). This revealed that reverse-migrated neutrophils had less spherical, more 'activated' morphologies, and mount normal responses to secondary insults.

Interestingly, a recent zebrafish study showed that reverse migration of neutrophils can be pharmacologically enhanced by the compound Tanshinone IIA. (122). Tanshinone IIA is an anti-inflammatory compound derived from a Chinese medicinal herb. It also has pro-apoptotic effects on neutrophils. This suggests that a good pharmacological strategy would be one that targets both apoptosis and reverse migration. In this study, a further step will be to investigate the effect of the CDKi drugs and genetic targeting of CDKs on parameters such as reverse migration. It would also be interesting to assess what happens to the excess neutrophils in the LaRP7 morpholino-injected animals- do they undergo enhanced reverse migration?

6.6. Does targeting CDK9 affect regeneration of the tailfin?

The zebrafish has become a popular model to investigate tissue regeneration, due to its ability to regenerate a large range of tissues such as the heart and spinal cord after lesioning; which does not occur in mammals (246). Similarly, the tailfin is able to grow back following transection. In tailfin injury models, new genes important in regeneration have been identified, such as fibroblast growth factor 20 (fgf20). Due to

the role of CDK9 in transcription, it would be interesting to assess how targeting CDK9 using morpholinos or pharmacological agents will affect the ability of tissues to regenerate after tailfin transection. An adverse effect on regeneration/healing would affect the possible therapeutic usage of the drug. It was shown that macrophages are key to tailfin regeneration (138, 139), and as the CDK9 manipulations do not affect macrophages, it is hypothesised the manipulations would not affect regeneration. It was even shown that removing neutrophils could accelerate tailfin regeneration (247) Hence, enhancing the resolution of inflammation using CDK inhibition may also affect tissue regeneration.

6.7. Ablating cell populations of interest

A powerful strategy to investigate cellular roles in the resolution of inflammation is to ablate specific cell populations, as described above in the regeneration studies (247). A future direction of this project could be to examine the effects of macrophage ablation on the resolution of inflammation after CDK inhibitor drug treatment or CDK9 knockdown. This would reveal the contribution of macrophages to resolving inflammation in this model. A number of questions arise including: i) does neutrophilic inflammation resolve differently without the presence of macrophages to clear apoptotic debris, especially when an external apoptosis-driving drug is added? Or ii) would other mechanisms such as reverse migration be able to compensate for this?

Knockouts of specific cells can be made on the basis of driving deletion of particular promoters. A macrophage deficient fish has been made by mutating the interferon regulatory factor 8 (irf8) (248). Irf8 was shown to regulate macrophage development (222). These fish later develop macrophages at later stages, suggesting irf8 only plays a role in primitive macrophage formation. These animals could be used to assess the contribution of macrophage phagocytosis to the resolution of inflammation induced by targeting CDK9.

One approach to target specific cells can be made by linking cell-specific promoters to the nitroreductase gene (*nfsB*) (166). The pro-drug metronidazole is converted to a cytotoxic drug upon nitroreductase expression. Addition of metronidazole to fish expressing *LysC (*labelling mainly neutrophils) or *fms* (labelling mainly macrophages) together with *nfsB* results in a good ablation of neutrophils and macrophages, respectively (138). The advantage of this is that the cell populations are not absent from the beginning of development, and therefore any unforeseen consequences on development can be avoided. However, these strategies rely on addition of a drug, which may in itself be having other side effects; and the drug may not fully reach the areas which require depletion (166). Some cells require longer incubations to be depleted than others. These animals were used to show the *Straphylococcus aureus* is likely to use neutrophils as a pathogen reservoir (249).

Another clever strategy to affect neutrophils previously used was the creation of CXCR4 mutants, which results in a retention of neutrophils in the haematopoietic site. This is true in both mammals and zebrafish (250). Knocking down stromal cell-derived factor 1 (SDF1) could reverse this phenotype in fish, suggesting that SDF1 was responsible for this retention. This is the mutation present in the immunodeficiency syndrome WHIM (warts, hypogammaglobulinemia, infections and myelokathexis). This mutation in zebrafish provides a way to examine 'neutropenia' and hence macrophage behaviour without the presence of neutrophils; however of course there is a defect in an important chemokine receptor in this system.

6.8. Conclusions

The zebrafish is a powerful model system, used here to examine the role of CDKs and neutrophil apoptosis in resolution of inflammation. Drugs that inhibit CDK9 may prove to be a good strategy to dampen down the inflammatory response. Evidence from mouse models supports this hypothesis, and the ability of CDK9-targeting drugs was shown here to have a neutrophil-reducing effect *in vivo* in the zebrafish. The genetic evidence presented in this study allows us to pinpoint exactly which genes are involved in this, giving justification for more specific targeting of CDK9 in the future.

The synthesis of new small molecules allows the creation of more selective inhibitors, and may allow targeting of important active sites in the structure of CDK9 in the future.

7. Bibliography

1. Duffin, R., A. E. Leitch, S. Fox, C. Haslett, and A. G. Rossi. 2010. Targeting granulocyte apoptosis: mechanisms, models, and therapies. *Immunol. Rev.* 236: 28–40.
2. Ortega-Gómez, A., M. Perretti, and O. Soehnlein. 2013. Resolution of inflammation: an integrated view. *EMBO Mol Med* 5: 661–674.
3. Alessandri, A. L., L. P. Sousa, C. D. Lucas, A. G. Rossi, V. Pinho, and M. M. Teixeira. 2013. Resolution of inflammation: mechanisms and opportunity for drug development. *Pharmacol. Ther.* 139: 189–212.
4. Pillay, J., I. den Braber, N. Vrisekoop, L. M. Kwast, R. J. de Boer, J. A. M. Borghans, K. Tesselaar, and L. Koenderman. 2010. *In vivo* labeling with H_2O_2 reveals a human neutrophil lifespan of 5.4 days. *Blood* 116: 625–627.
5. Tofts, P. S., T. Chevassut, M. Cutajar, N. G. Dowell, and A. M. Peters. 2011. Doubts concerning the recently reported human neutrophil lifespan of 5.4 days. *Blood* 117: 6050–6052.
6. Faurschou, M., and N. Borregaard. 2003. Neutrophil granules and secretory vesicles in inflammation. *Microbes Infect.* 5: 1317–1327.
7. Kasama, T., Y. Miwa, T. Isozaki, T. Odai, M. Adachi, and S. L. Kunkel. 2005. Neutrophil-derived cytokines: potential therapeutic targets in inflammation. *Curr Drug Targets Inflamm Allergy* 4: 273–279.
8. Mócsai, A. 2013. Diverse novel functions of neutrophils in immunity, inflammation, and beyond. *J. Exp. Med.* 210: 1283–1299.
9. Geering, B., C. Stoeckle, S. Conus, and H.-U. Simon. 2013. Living and dying for inflammation: neutrophils, eosinophils, basophils. *Trends Immunol.* 34: 398–409.
10. Otsuka, A., and K. Kabashima. 2015. Contribution of Basophils to Cutaneous Immune Reactions and Th2-Mediated Allergic Responses. *Front Immunol* 6: 393.
11. Koedel, U., T. Frankenberg, S. Kirschnek, B. Obermaier, H. Häcker, R. Paul, and G. Häcker. 2009. Apoptosis Is essential for neutrophil functional shutdown and determines tissue damage in experimental pneumococcal meningitis. *PLoS Pathog* 5: e1000461–13.
12. Garrison, S. P., J. A. Thornton, H. Häcker, R. Webby, J. E. Rehg, E. Parganas, G. P. Zambetti, and E. I. Tuomanen. 2010. The p53-target gene puma drives neutrophil-mediated protection against lethal bacterial sepsis. *PLoS Pathog* 6: e1001240.
13. Grommes, J., and O. Soehnlein. 2011. Contribution of neutrophils to acute lung injury. *Mol. Med.* 17: 293–307.
14. Matthay, M. A., W. L. Eschenbacher, and E. J. Goetzl. 1984. Elevated concentrations of leukotriene D4 in pulmonary edema fluid of patients with the adult respiratory distress syndrome. *J. Clin. Immunol.* 4: 479–483.
15. Abraham, E., A. Carmody, R. Shenkar, and J. Arcaroli. 2000. Neutrophils as early immunologic effectors in hemorrhage- or endotoxemia-induced acute lung injury. *Am. J. Physiol. Lung Cell Mol. Physiol.* 279: L1137–45.
16. Drechsler, M., R. T. A. Megens, M. van Zandvoort, C. Weber, and O. Soehnlein. 2010. Hyperlipidemia-triggered neutrophilia promotes early atherosclerosis. *Circulation* 122: 1837–1845.
17. Soehnlein, O. 2012. Multiple roles for neutrophils in atherosclerosis. *Circ. Res.* 110: 875–888.
18. Ionita, M. G., P. van den Borne, L. M. Catanzariti, F. L. Moll, J.-P. P. M. de Vries, G. Pasterkamp, A. Vink, and D. P. V. de Kleijn. 2010. High neutrophil numbers in human carotid atherosclerotic plaques are associated with characteristics of rupture-prone lesions. *Arterioscler. Thromb. Vasc. Biol.* 30: 1842–1848.
19. Zenaro, E., E. Pietronigro, V. D. Bianca, G. Piacentino, L. Marongiu, S. Budui, E. Turano, B. Rossi, S. Angiari, S. Dusi, A. Montresor, T. Carlucci, S. Nanì, G. Tosadori, L. Calciano, D.

Catalucci, G. Berton, B. Bonetti, and G. Constantin. 2015. Neutrophils promote Alzheimer's disease-like pathology and cognitive decline via LFA-1 integrin. *Nat. Med.* 21: 880–886.
20. Kovach, M. A., and T. J. Standiford. 2012. The function of neutrophils in sepsis. *Curr. Opin. Infect. Dis.* 25: 321–327.
21. Wright, H. L., R. J. Moots, and S. W. Edwards. 2014. The multifactorial role of neutrophils in rheumatoid arthritis. *Nat Rev Rheumatol* 10: 593–601.
22. Wipke, B. T., and P. M. Allen. 2001. Essential role of neutrophils in the initiation and progression of a murine model of rheumatoid arthritis. *J. Immunol.* 167: 1601–1608.
23. Wright, H. L., B. Chikura, R. C. Bucknall, R. J. Moots, and S. W. Edwards. 2011. Changes in expression of membrane TNF, NF-kappaB activation and neutrophil apoptosis during active and resolved inflammation. *Ann. Rheum. Dis.* 70: 537–543.
24. Viola, J., and O. Soehnlein. 2015. Atherosclerosis - A matter of unresolved inflammation. *Semin. Immunol.* 27: 184–193.
25. Sullivan, D. P., and W. A. Muller. 2014. Neutrophil and monocyte recruitment by PECAM, CD99, and other molecules via the LBRC. *Semin Immunopathol* 36: 193–209.
26. Zarbock, A., K. Ley, R. P. McEver, and A. Hidalgo. 2011. Leukocyte ligands for endothelial selectins: specialized glycoconjugates that mediate rolling and signaling under flow. *Blood* 118: 6743–6751.
27. Woodfin, A., M.-B. Voisin, M. Beyrau, B. Colom, D. Caille, F.-M. Diapouli, G. B. Nash, T. Chavakis, S. M. Albelda, G. E. Rainger, P. Meda, B. A. Imhof, and S. Nourshargh. 2011. The junctional adhesion molecule JAM-C regulates polarized transendothelial migration of neutrophils *in vivo*. *Nat. Immunol.* 12: 761–769.
28. Colom, B., J. V. Bodkin, M. Beyrau, A. Woodfin, C. Ody, C. Rourke, T. Chavakis, K. Brohi, B. A. Imhof, and S. Nourshargh. 2015. Leukotriene B4-neutrophil elastase axis drives neutrophil reverse transendothelial cell migration *in vivo*. *Immunity* 42: 1075–1086.
29. Lucas, C. D., L. J. Hoodless, and A. G. Rossi. 2014. Swimming against the tide: drugs drive neutrophil reverse migration. *Sci Transl Med* 6: 225fs9.
30. Ellis, R. E., J. Y. Yuan, and H. R. Horvitz. 1991. Mechanisms and functions of cell death. *Annu. Rev. Cell Biol.* 7: 663–698.
31. Uchida, D., M. Yamashita, T. Kitano, and T. Iguchi. 2002. Oocyte apoptosis during the transition from ovary-like tissue to testes during sex differentiation of juvenile zebrafish. *J. Exp. Biol.* 205: 711–718.
32. McIlwain, D. R., T. Berger, and T. W. Mak. 2013. Caspase functions in cell death and disease. *Cold Spring Harb Perspect Biol* 5: a008656–a008656.
33. Adams, J. M. 2003. Ways of dying: multiple pathways to apoptosis. *Genes Dev.* 17: 2481–2495.
34. Fink, S. L., and B. T. Cookson. 2005. Apoptosis, pyroptosis, and necrosis: mechanistic description of dead and dying eukaryotic cells. *Infect. Immun.* 73: 1907–1916.
35. Flusberg, D. A., and P. K. Sorger. 2015. Surviving apoptosis: life-death signaling in single cells. *Trends Cell Biol.* 25: 446–458.
36. Milot, E., and J. G. Filep. 2011. Regulation of neutrophil survival/apoptosis by Mcl-1. *ScientificWorldJournal* 11: 1948–1962.
37. Wang, K., P. Hampson, J. Hazeldine, V. Krystof, M. Strnad, P. Pechan, and J. M. 2012. Cyclin-dependent kinase 9 activity regulates neutrophil spontaneous apoptosis. *PLoS ONE* 7: e30128.
38. Lucas, C. D., D. A. Dorward, M. A. Tait, S. Fox, J. A. Marwick, K. C. Allen, C. T. Robb, N. Hirani, C. Haslett, R. Duffin, and A. G. Rossi. 2014. Downregulation of Mcl-1 has anti-inflammatory pro-resolution effects and enhances bacterial clearance from the lung. *Mucosal Immunol* 7: 857–868.
39. Kratz, E., P. M. Eimon, K. Mukhyala, H. Stern, J. Zha, A. Strasser, R. Hart, and A. Ashkenazi. 2006. Functional characterization of the Bcl-2 gene family in the zebrafish. *Cell Death Differ.* 13: 1631–1640.
40. Park, D., A.-C. Tosello-Trampont, M. R. Elliott, M. Lu, L. B. Haney, Z. Ma, A. L.

Klibanov, J. W. Mandell, and K. S. Ravichandran. 2007. BAI1 is an engulfment receptor for apoptotic cells upstream of the ELMO/Dock180/Rac module. *Nature* 450: 430–434.
41. Rosenbaum, S., S. Kreft, J. Etich, C. Frie, J. Stermann, I. Grskovic, B. Frey, D. Mielenz, E. Pöschl, U. Gaipl, M. Paulsson, and B. Brachvogel. 2011. Identification of novel binding partners (annexins) for the cell death signal phosphatidylserine and definition of their recognition motif. *J. Biol. Chem.* 286: 5708–5716.
42. Poon, I. K. H., C. D. Lucas, A. G. Rossi, and K. S. Ravichandran. 2014. Apoptotic cell clearance: basic biology and therapeutic potential. *Nat. Rev. Immunol.* 14: 166–180.
43. Lemke, G. 2013. Biology of the TAM receptors. *Cold Spring Harb Perspect Biol* 5: a009076–a009076.
44. Fadok, V. A., D. L. Bratton, A. Konowal, P. W. Freed, J. Y. Westcott, and P. M. Henson. 1998. Macrophages that have ingested apoptotic cells in vitro inhibit proinflammatory cytokine production through autocrine/paracrine mechanisms involving TGF-beta, PGE2, and PAF. *J. Clin. Invest.* 101: 890–898.
45. Michlewska, S., I. Dransfield, I. L. Megson, and A. G. Rossi. 2009. Macrophage phagocytosis of apoptotic neutrophils is critically regulated by the opposing actions of pro-inflammatory and anti-inflammatory agents: key role for TNF-alpha. *FASEB J.* 23: 844–854.
46. Fox, S., A. E. Leitch, R. Duffin, C. Haslett, and A. G. Rossi. 2010. Neutrophil apoptosis: relevance to the innate immune response and inflammatory disease. *J Innate Immun* 2: 216–227.
47. Scannell, M., M. B. Flanagan, A. deStefani, K. J. Wynne, G. Cagney, C. Godson, and P. Maderna. 2007. Annexin-1 and peptide derivatives are released by apoptotic cells and stimulate phagocytosis of apoptotic neutrophils by macrophages. *J. Immunol.* 178: 4595–4605.
48. Vago, J. P., C. R. C. Nogueira, L. P. Tavares, F. M. Soriani, F. Lopes, R. C. Russo, V. Pinho, M. M. Teixeira, and L. P. Sousa. 2012. Annexin A1 modulates natural and glucocorticoid-induced resolution of inflammation by enhancing neutrophil apoptosis. *J. Leukoc. Biol.* 92: 249–258.
49. Perretti, M., and E. Solito. 2004. Annexin 1 and neutrophil apoptosis. *Biochem. Soc. Trans.* 32: 507–510.
50. Saclier, M., H. Yacoub-Youssef, A. L. Mackey, L. Arnold, H. Ardjoune, M. Magnan, F. Sailhan, J. Chelly, G. K. Pavlath, R. Mounier, M. Kjaer, and B. Chazaud. 2013. Differentially activated macrophages orchestrate myogenic precursor cell fate during human skeletal muscle regeneration. *Stem Cells* 31: 384–396.
51. Wang, N., H. Liang, and K. Zen. 2014. Molecular mechanisms that influence the macrophage m1-m2 polarization balance. *Front Immunol* 5: 614.
52. Novak, M. L., and T. J. Koh. 2013. Macrophage phenotypes during tissue repair. *J. Leukoc. Biol.* 93: 875–881.
53. Dean, R. A., J. H. Cox, C. L. Bellac, A. Doucet, A. E. Starr, and C. M. Overall. 2008. Macrophage-specific metalloelastase (MMP-12) truncates and inactivates ELR+ CXC chemokines and generates CCL2, -7, -8, and -13 antagonists: potential role of the macrophage in terminating polymorphonuclear leukocyte influx. *Blood* 112: 3455–3464.
54. McQuibban, G. A., J.-H. Gong, J. P. Wong, J. L. Wallace, I. Clark-Lewis, and C. M. Overall. 2002. Matrix metalloproteinase processing of monocyte chemoattractant proteins generates CC chemokine receptor antagonists with anti-inflammatory properties *in vivo*. *Blood* 100: 1160–1167.
55. Cochain, C., C. Auvynet, L. Poupel, J. Vilar, E. Dumeau, A. Richart, A. Récalde, Y. Zouggari, K. Y. H. W. Yin, P. Bruneval, G. Renault, C. Marchiol, P. Bonnin, B. Lévy, R. Bonecchi, M. Locati, C. Combadière, and J.-S. Silvestre. 2012. The chemokine decoy receptor D6 prevents excessive inflammation and adverse ventricular remodeling after myocardial infarction. *Arterioscler. Thromb. Vasc. Biol.* 32: 2206–2213.
56. Pashover-Schallinger, E., M. Aswad, S. Schif-Zuck, H. Shapiro, P. Singer, and A. Ariel. 2012. The atypical chemokine receptor D6 controls macrophage efferocytosis and cytokine

secretion during the resolution of inflammation. *FASEB J.* 26: 3891–3900.
57. Martinez, F. O., S. Gordon, M. Locati, and A. Mantovani. 2006. Transcriptional profiling of the human monocyte-to-macrophage differentiation and polarization: new molecules and patterns of gene expression. *J. Immunol.* 177: 7303–7311.
58. Badrey, M. G., H. M. Abdel-Aziz, S. M. Gomha, M. M. Abdalla, and A. S. Mayhoub. 2015. Design and Synthesis of Imidazopyrazolopyridines as Novel Selective COX-2 Inhibitors. *Molecules* 20: 15287–15303.
59. Kebir, El, D., L. József, W. Pan, L. Wang, N. A. Petasis, C. N. Serhan, and J. G. Filep. 2009. 15-epi-lipoxin A4 inhibits myeloperoxidase signaling and enhances resolution of acute lung injury. *Am. J. Respir. Crit. Care Med.* 180: 311–319.
60. Llodrá, J., V. Angeli, J. Liu, E. Trogan, E. A. Fisher, and G. J. Randolph. 2004. Emigration of monocyte-derived cells from atherosclerotic lesions characterizes regressive, but not progressive, plaques. *Proc. Natl. Acad. Sci. U.S.A.* 101: 11779–11784.
61. Galli, S. J., N. Borregaard, and T. A. Wynn. 2011. Phenotypic and functional plasticity of cells of innate immunity: macrophages, mast cells and neutrophils. *Nat. Immunol.* 12: 1035–1044.
62. Hume, D. A. 2008. Differentiation and heterogeneity in the mononuclear phagocyte system. *Mucosal Immunol* 1: 432–441.
63. Tong, H., B. Zhao, H. Shi, X. Ba, X. Wang, Y. Jiang, and X. Zeng. 2013. c-Abl tyrosine kinase plays a critical role in β2 integrin-dependent neutrophil migration by regulating Vav1 activity. *J. Leukoc. Biol.* 93: 611–622.
64. Guido, B. C., M. Zanatelli, W. Tavares-de-Lima, S. M. Oliani, and A. S. Damazo. 2013. Annexin-A1 peptide down-regulates the leukocyte recruitment and up-regulates interleukin-10 release into lung after intestinal ischemia-reperfusion in mice. *J Inflamm (Lond)* 10: 10.
65. Berberich, N., B. Uhl, J. Joore, U. K. Schmerwitz, B. A. Mayer, C. A. Reichel, F. Krombach, S. Zahler, A. M. Vollmar, and R. Fürst. 2011. Roscovitine blocks leukocyte extravasation by inhibition of cyclin-dependent kinases 5 and 9. *Br. J. Pharmacol.* 163: 1086–1098.
66. McColl, A., S. Bournazos, S. Franz, M. Perretti, B. P. Morgan, C. Haslett, and I. Dransfield. 2009. Glucocorticoids induce protein S-dependent phagocytosis of apoptotic neutrophils by human macrophages. *J. Immunol.* 183: 2167–2175.
67. Sawatzky, D. A., D. A. Willoughby, P. R. Colville-Nash, and A. G. Rossi. 2006. The involvement of the apoptosis-modulating proteins ERK 1/2, Bcl-xL and Bax in the resolution of acute inflammation *in vivo*. *Am. J. Pathol.* 168: 33–41.
68. Rossi, A. G., D. A. Sawatzky, A. Walker, C. Ward, T. A. Sheldrake, N. A. Riley, A. Caldicott, M. Martinez-Losa, T. R. Walker, R. Duffin, M. Gray, E. Crescenzi, M. C. Martin, H. J. Brady, J. S. Savill, I. Dransfield, and C. Haslett. 2006. Cyclin-dependent kinase inhibitors enhance the resolution of inflammation by promoting inflammatory cell apoptosis. *Nat. Med.* 12: 1056–1064.
69. Leitch, A. E., N. A. Riley, T. A. Sheldrake, M. Festa, S. Fox, R. Duffin, C. Haslett, and A. G. Rossi. 2010. The cyclin-dependent kinase inhibitor R-roscovitine down-regulates Mcl-1 to override pro-inflammatory signalling and drive neutrophil apoptosis. *Eur. J. Immunol.* 40: 1127–1138.
70. Leitch, A. E., C. D. Lucas, J. A. Marwick, R. Duffin, C. Haslett, and A. G. Rossi. 2012. Cyclin-dependent kinases 7 and 9 specifically regulate neutrophil transcription and their inhibition drives apoptosis to promote resolution of inflammation. *Cell Death Differ.* 19: 1950–1961.
71. Duffin, R., A. E. Leitch, T. A. Sheldrake, J. M. Hallett, C. Meyer, S. Fox, A. L. Alessandri, M. C. Martin, H. J. Brady, M. M. Teixeira, I. Dransfield, C. Haslett, and A. G. Rossi. 2009. The CDK inhibitor, R-roscovitine, promotes eosinophil apoptosis by down-regulation of Mcl-1. *FEBS Lett.* 583: 2540–2546.
72. Lucas, C. D., K. C. Allen, D. A. Dorward, L. J. Hoodless, L. A. Melrose, J. A. Marwick, C. S. Tucker, C. Haslett, R. Duffin, and A. G. Rossi. 2013. Flavones induce neutrophil

apoptosis by down-regulation of Mcl-1 via a proteasomal-dependent pathway. *FASEB J.* 27: 1084–1094.
73. Lucas, C. D., D. A. Dorward, S. Sharma, J. Rennie, J. M. Felton, A. L. Alessandri, R. Duffin, J. Schwarze, C. Haslett, and A. G. Rossi. 2015. Wogonin induces eosinophil apoptosis and attenuates allergic airway inflammation. *Am. J. Respir. Crit. Care Med.* 191: 626–636.
74. Aleem, E., and R. J. Arceci. 2015. Targeting cell cycle regulators in hematologic malignancies. *Front Cell Dev Biol* 3: 16.
75. Schmerwitz, U. K., G. Sass, A. G. Khandoga, J. Joore, B. A. Mayer, N. Berberich, F. Totzke, F. Krombach, G. Tiegs, S. Zahler, A. M. Vollmar, and R. Fürst. 2011. Flavopiridol protects against inflammation by attenuating leukocyte-endothelial interaction via inhibition of cyclin-dependent kinase 9. *Arterioscler. Thromb. Vasc. Biol.* 31: 280–288.
76. Wyatt, P. G., A. J. Woodhead, V. Berdini, J. A. Boulstridge, M. G. Carr, D. M. Cross, D. J. Davis, L. A. Devine, T. R. Early, R. E. Feltell, E. J. Lewis, R. L. McMenamin, E. F. Navarro, M. A. O'Brien, M. O'Reilly, M. Reule, G. Saxty, L. C. A. Seavers, D.-M. Smith, M. S. Squires, G. Trewartha, M. T. Walker, and A. J.-A. Woolford. 2008. Identification of N-(4-piperidinyl)-4-(2,6-dichlorobenzoylamino)-1H-pyrazole-3-carboxamide (AT7519), a novel cyclin dependent kinase inhibitor using fragment-based X-ray crystallography and structure based drug design. *J. Med. Chem.* 51: 4986–4999.
77. Squires, M. S., R. E. Feltell, N. G. Wallis, E. J. Lewis, D.-M. Smith, D. M. Cross, J. F. Lyons, and N. T. Thompson. 2009. Biological characterization of AT7519, a small-molecule inhibitor of cyclin-dependent kinases, in human tumor cell lines. *Mol. Cancer Ther.* 8: 324–332.
78. Squires, M. S., L. Cooke, V. Lock, W. Qi, E. J. Lewis, N. T. Thompson, J. F. Lyons, and D. Mahadevan. 2010. AT7519, a cyclin-dependent kinase inhibitor, exerts its effects by transcriptional inhibition in leukemia cell lines and patient samples. *Mol. Cancer Ther.* 9: 920–928.
79. Santo, L., S. Vallet, T. Hideshima, D. Cirstea, H. Ikeda, S. Pozzi, K. Patel, Y. Okawa, G. Gorgun, G. Perrone, E. Calabrese, M. Yule, M. Squires, M. Ladetto, M. Boccadoro, P. G. Richardson, N. C. Munshi, K. C. Anderson, and N. Raje. 2010. AT7519, A novel small molecule multi-cyclin-dependent kinase inhibitor, induces apoptosis in multiple myeloma via GSK-3beta activation and RNA polymerase II inhibition. *Oncogene* 29: 2325–2336.
80. Dolman, M. E. M., E. Poon, M. E. Ebus, I. J. M. den Hartog, C. J. van Noesel, Y. Jamin, A. Hallsworth, S. P. Robinson, K. Petrie, R. W. Sparidans, R. J. Kok, R. Versteeg, H. N. Caron, L. Chesler, and J. J. Molenaar. 2015. Cyclin-dependent kinase inhibitor AT7519 as a potential drug for MYCN-dependent neuroblastoma. *Clin. Cancer Res.* clincanres.0313.2015.
81. Mahadevan, D., R. Plummer, M. S. Squires, D. Rensvold, S. Kurtin, C. Pretzinger, T. Dragovich, J. Adams, V. Lock, D. M. Smith, D. Von Hoff, and H. Calvert. 2011. A phase I pharmacokinetic and pharmacodynamic study of AT7519, a cyclin-dependent kinase inhibitor in patients with refractory solid tumors. *Ann. Oncol.* 22: 2137–2143.
82. Alessandri, A. L., R. Duffin, A. E. Leitch, C. D. Lucas, T. A. Sheldrake, D. A. Dorward, N. Hirani, V. Pinho, L. P. de Sousa, M. M. Teixeira, J. F. Lyons, C. Haslett, and A. G. Rossi. 2011. Induction of eosinophil apoptosis by the cyclin-dependent kinase inhibitor AT7519 promotes the resolution of eosinophil-dominant allergic inflammation. *PLoS ONE* 6: e25683.
83. Dzhagalov, I., A. St John, and Y.-W. He. 2007. The antiapoptotic protein Mcl-1 is essential for the survival of neutrophils but not macrophages. *Blood* 109: 1620–1626.
84. Lee, M., and P. Nurse. 1988. Cell cycle control genes in fission yeast and mammalian cells. *Trends Genet.* 4: 287–290.
85. Nurse, P., and P. Thuriaux. 1980. Regulatory genes controlling mitosis in the fission yeast Schizosaccharomyces pombe. *Genetics* 96: 627–637.
86. Beach, D., B. Durkacz, and P. Nurse. 1982. Functionally homologous cell cycle control genes in budding and fission yeast. *Nature* 300: 706–709.
87. Lee, M. G., and P. Nurse. 1987. Complementation used to clone a human homologue of the fission yeast cell cycle control gene cdc2. *Nature* 327: 31–35.

88. Malumbres, M. 2014. Cyclin-dependent kinases. *Genome Biol.* 15: 122.
89. Santamaría, D., C. Barrière, A. Cerqueira, S. Hunt, C. Tardy, K. Newton, J. F. Cáceres, P. Dubus, M. Malumbres, and M. Barbacid. 2007. Cdk1 is sufficient to drive the mammalian cell cycle. *Nature* 448: 811–815.
90. Shu, F., S. Lv, Y. Qin, X. Ma, X. Wang, X. Peng, Y. Luo, B.-E. Xu, X. Sun, and J. Wu. 2007. Functional characterization of human PFTK1 as a cyclin-dependent kinase. *Proc. Natl. Acad. Sci. U.S.A.* 104: 9248–9253.
91. Graña, X., A. De Luca, N. Sang, Y. Fu, P. P. Claudio, J. Rosenblatt, D. O. Morgan, and A. Giordano. 1994. PITALRE, a nuclear CDC2-related protein kinase that phosphorylates the retinoblastoma protein in vitro. *Proc. Natl. Acad. Sci. U.S.A.* 91: 3834–3838.
92. Baumli, S., G. Lolli, E. D. Lowe, S. Troiani, L. Rusconi, A. N. Bullock, J. E. Debreczeni, S. Knapp, and L. N. Johnson. 2008. The structure of P-TEFb (CDK9/cyclin T1), its complex with flavopiridol and regulation by phosphorylation. *EMBO J.* 27: 1907–1918.
93. Shore, S. M., S. A. Byers, W. Maury, and D. H. Price. 2003. Identification of a novel isoform of Cdk9. *Gene* 307: 175–182.
94. Shore, S. M., S. A. Byers, P. Dent, and D. H. Price. 2005. Characterization of Cdk9(55) and differential regulation of two Cdk9 isoforms. *Gene* 350: 51–58.
95. Romano, G. 2013. Deregulations in the cyclin-dependent kinase-9-related pathway in cancer: implications for drug discovery and development. *ISRN Oncol* 2013: 305371–14.
96. Peng, J., Y. Zhu, J. T. Milton, and D. H. Price. 1998. Identification of multiple cyclin subunits of human P-TEFb. *Genes Dev.* 12: 755–762.
97. Marshall, N. F., and D. H. Price. 1995. Purification of P-TEFb, a transcription factor required for the transition into productive elongation. *Journal of Biological Chemistry* 270: 12335–12338.
98. Marshall, N. F., J. Peng, Z. Xie, and D. H. Price. 1996. Control of RNA polymerase II elongation potential by a novel carboxyl-terminal domain kinase. *Journal of Biological Chemistry* 271: 27176–27183.
99. Romano, G., M. Kasten, G. De Falco, P. Micheli, K. Khalili, and A. Giordano. 1999. Regulatory functions of Cdk9 and of cyclin T1 in HIV tat transactivation pathway gene expression. *J. Cell. Biochem.* 75: 357–368.
100. Price, D. H. 2000. P-TEFb, a cyclin-dependent kinase controlling elongation by RNA polymerase II. *Mol. Cell. Biol.* 20: 2629–2634.
101. Lu, H., Z. Li, Y. Xue, U. Schulze-Gahmen, J. R. Johnson, N. J. Krogan, T. Alber, and Q. Zhou. 2014. AFF1 is a ubiquitous P-TEFb partner to enable Tat extraction of P-TEFb from 7SK snRNP and formation of SECs for HIV transactivation. *Proc. Natl. Acad. Sci. U.S.A.* 111: E15–24.
102. Chen, R., M. J. Keating, V. Gandhi, and W. Plunkett. 2005. Transcription inhibition by flavopiridol: mechanism of chronic lymphocytic leukemia cell death. *Blood* 106: 2513–2519.
103. Lemke, J., S. von Karstedt, M. Abd El Hay, A. Conti, F. Arce, A. Montinaro, K. Papenfuss, M. A. El-Bahrawy, and H. Walczak. 2014. Selective CDK9 inhibition overcomes TRAIL resistance by concomitant suppression of cFlip and Mcl-1. *Cell Death Differ.* 21: 491–502.
104. Yeh, Y.-Y., R. Chen, J. Hessler, E. Mahoney, A. M. Lehman, N. A. Heerema, M. R. Grever, W. Plunkett, J. C. Byrd, and A. J. Johnson. 2015. Up-regulation of CDK9 kinase activity and Mcl-1 stability contributes to the acquired resistance to cyclin-dependent kinase inhibitors in leukemia. *Oncotarget* 6: 2667–2679.
105. Brasier, A. R. 2008. Expanding role of cyclin dependent kinases in cytokine inducible gene expression. *Cell Cycle* 7: 2661–2666.
106. Darbinian, N., B. E. Sawaya, K. Khalili, N. Jaffe, B. Wortman, A. Giordano, and S. Amini. 2001. Functional interaction between cyclin T1/cdk9 and Puralpha determines the level of TNFalpha promoter activation by Tat in glial cells. *J. Neuroimmunol.* 121: 3–11.
107. Falco, G. D., L. M. Neri, M. D. Falco, C. Bellan, Z. Yu, A. D. Luca, L. Leoncini, and A. Giordano. 2002. Cdk9, a member of the cdc2-like family of kinases, binds to gp130, the

receptor of the IL-6 family of cytokines. *Oncogene* 21: 7464–7470.
108. Li, L.-L., S.-T. Hu, S.-H. Wang, H.-H. Lee, Y.-T. Wang, and Y.-H. Ping. 2010. Positive transcription elongation factor b (P-TEFb) contributes to dengue virus-stimulated induction of interleukin-8 (IL-8). *Cell. Microbiol.* 12: 1589–1603.
109. Ghamari, A., M. P. C. van de Corput, S. Thongjuea, W. A. van Cappellen, W. van Ijcken, J. van Haren, E. Soler, D. Eick, B. Lenhard, and F. G. Grosveld. 2013. *In vivo* live imaging of RNA polymerase II transcription factories in primary cells. *Genes Dev.* 27: 767–777.
110. Fisher, R. P. 2005. Secrets of a double agent: CDK7 in cell-cycle control and transcription. *J. Cell. Sci.* 118: 5171–5180.
111. Garrett, S., W. A. Barton, R. Knights, P. Jin, D. O. Morgan, and R. P. Fisher. 2001. Reciprocal activation by cyclin-dependent kinases 2 and 7 is directed by substrate specificity determinants outside the T loop. *Mol. Cell. Biol.* 21: 88–99.
112. Shim, E. Y., A. K. Walker, Y. Shi, and T. K. Blackwell. 2002. CDK-9/cyclin T (P-TEFb) is required in two postinitiation pathways for transcription in the *C. elegans* embryo. *Genes Dev.* 16: 2135–2146.
113. Kohoutek, J., Q. Li, D. Blazek, Z. Luo, H. Jiang, and B. M. Peterlin. 2009. Cyclin T2 is essential for mouse embryogenesis. *Mol. Cell. Biol.* 29: 3280–3285.
114. Steimer, D. A., K. Boyd, O. Takeuchi, J. K. Fisher, G. P. Zambetti, and J. T. Opferman. 2009. Selective roles for antiapoptotic MCL-1 during granulocyte development and macrophage effector function. *Blood* 113: 2805–2815.
115. Henry, K. M., C. A. Loynes, M. K. B. Whyte, and S. A. Renshaw. 2013. Zebrafish as a model for the study of neutrophil biology. *J. Leukoc. Biol.* 94: 633–642.
116. Reis, A. C., A. L. Alessandri, R. M. Athayde, D. A. Perez, J. P. Vago, T. V. Ávila, T. P. T. Ferreira, A. C. S. de Arantes, D. de S. Coutinho, M. A. Rachid, L. P. Sousa, M. A. Martins, G. B. Menezes, A. G. Rossi, M. M. Teixeira, and V. Pinho. 2015. Induction of eosinophil apoptosis by hydrogen peroxide promotes the resolution of allergic inflammation. *Cell Death Dis* 6: e1632.
117. Matrone, G., K. S. Wilson, S. Maqsood, J. J. Mullins, C. S. Tucker, and M. A. Denvir. 2015. CDK9 and its repressor LARP7 modulate cardiomyocyte proliferation and response to injury in the zebrafish heart. *J. Cell. Sci.*
118. Lieschke, G. J., and P. D. Currie. 2007. Animal models of human disease: zebrafish swim into view. *Nat. Rev. Genet.* 8: 353–367.
119. Ellett, F., and G. J. Lieschke. 2010. Zebrafish as a model for vertebrate hematopoiesis. *Current Opinion in Pharmacology* 10: 563–570.
120. Chen, J. N., F. J. van Eeden, K. S. Warren, A. Chin, C. Nüsslein-Volhard, P. Haffter, and M. C. Fishman. 1997. Left-right pattern of cardiac BMP4 may drive asymmetry of the heart in zebrafish. *Development* 124: 4373–4382.
121. Henry, K. M., L. Pase, C. F. Ramos-Lopez, G. J. Lieschke, S. A. Renshaw, and C. C. Reyes-Aldasoro. 2013. PhagoSight: an open-source MATLAB® package for the analysis of fluorescent neutrophil and macrophage migration in a zebrafish model. *PLoS ONE* 8: e72636.
122. Robertson, A. L., G. R. Holmes, A. N. Bojarczuk, J. Burgon, C. A. Loynes, M. Chimen, A. K. Sawtell, B. Hamza, J. Willson, S. R. Walmsley, S. R. Anderson, M. C. Coles, S. N. Farrow, R. Solari, S. Jones, L. R. Prince, D. Irimia, G. E. Rainger, V. Kadirkamanathan, M. K. B. Whyte, and S. A. Renshaw. 2014. A zebrafish compound screen reveals modulation of neutrophil reverse migration as an anti-inflammatory mechanism. *Sci Transl Med* 6: 225ra29.
123. de Jong, J. L. O., and L. I. Zon. 2005. Use of the zebrafish system to study primitive and definitive hematopoiesis. *Annu. Rev. Genet.* 39: 481–501.
124. Herbomel, P., B. Thisse, and C. Thisse. 1999. Ontogeny and behaviour of early macrophages in the zebrafish embryo. *Development* 126: 3735–3745.
125. Lieschke, G. J., A. C. Oates, M. O. Crowhurst, A. C. Ward, and J. E. Layton. 2001. Morphologic and functional characterization of granulocytes and macrophages in embryonic and adult zebrafish. *Blood* 98: 3087–3096.
126. Renshaw, S. A., C. A. Loynes, D. M. I. Trushell, S. Elworthy, P. W. Ingham, and M. K.

B. Whyte. 2006. A transgenic zebrafish model of neutrophilic inflammation. *Blood* 108: 3976–3978.
127. Gray, C., C. A. Loynes, M. K. B. Whyte, D. C. Crossman, S. A. Renshaw, and T. J. A. Chico. 2011. Simultaneous intravital imaging of macrophage and neutrophil behaviour during inflammation using a novel transgenic zebrafish. *Thromb. Haemost.* 105: 811–819.
128. Ellett, F., L. Pase, J. W. Hayman, A. Andrianopoulos, and G. J. Lieschke. 2011. mpeg1 promoter transgenes direct macrophage-lineage expression in zebrafish. *Blood* 117: e49–56.
129. Brothers, K. M., Z. R. Newman, and R. T. Wheeler. 2011. Live imaging of disseminated candidiasis in zebrafish reveals role of phagocyte oxidase in limiting filamentous growth. *Eukaryotic Cell* 10: 932–944.
130. Colucci-Guyon, E., J.-Y. Tinevez, S. A. Renshaw, and P. Herbomel. 2011. Strategies of professional phagocytes in vivo: unlike macrophages, neutrophils engulf only surface-associated microbes. *J. Cell. Sci.* 124: 3053–3059.
131. Palić, D., C. B. Andreasen, J. Ostojić, R. M. Tell, and J. A. Roth. 2007. Zebrafish (*Danio rerio*) whole kidney assays to measure neutrophil extracellular trap release and degranulation of primary granules. *J. Immunol. Methods* 319: 87–97.
132. Deng, Q., M. Sarris, D. A. Bennin, J. M. Green, P. Herbomel, and A. Huttenlocher. 2013. Localized bacterial infection induces systemic activation of neutrophils through Cxcr2 signaling in zebrafish. *J. Leukoc. Biol.* 93: 761–769.
133. Ogryzko, N. V., E. E. Hoggett, S. Solaymani-Kohal, S. Tazzyman, T. J. A. Chico, S. A. Renshaw, and H. L. Wilson. 2014. Zebrafish tissue injury causes upregulation of interleukin-1 and caspase-dependent amplification of the inflammatory response. *Dis Model Mech* 7: 259–264.
134. Stadtmann, A., and A. Zarbock. 2012. CXCR2: From Bench to Bedside. *Front Immunol* 3: 263.
135. Trede, N. S., D. M. Langenau, D. Traver, A. T. Look, and L. I. Zon. 2004. The use of zebrafish to understand immunity. *Immunity* 20: 367–379.
136. Kanwal, Z., G. F. Wiegertjes, W. J. Veneman, A. H. Meijer, and H. P. Spaink. 2014. Comparative studies of Toll-like receptor signalling using zebrafish. *Dev. Comp. Immunol.* 46: 35–52.
137. Davis, J. M., H. Clay, J. L. Lewis, N. Ghori, P. Herbomel, and L. Ramakrishnan. 2002. Real-time visualization of mycobacterium-macrophage interactions leading to initiation of granuloma formation in zebrafish embryos. *Immunity* 17: 693–702.
138. Petrie, T. A., N. S. Strand, C. T. Yang, J. S. Rabinowitz, and R. T. Moon. 2015. Macrophages modulate adult zebrafish tail fin regeneration. *Development* 142: 406–406.
139. Keightley, M.-C., C.-H. Wang, V. Pazhakh, and G. J. Lieschke. 2014. Delineating the roles of neutrophils and macrophages in zebrafish regeneration models. *Int. J. Biochem. Cell Biol.* 56: 92–106.
140. Chen, M. C., H. Y. Gong, C. Y. Cheng, J. P. Wang, J. R. Hong, and J. L. Wu. 2000. Cloning and characterization of a novel nuclear Bcl-2 family protein, zfMcl-1a, in zebrafish embryo. *Biochem. Biophys. Res. Commun.* 279: 725–731.
141. Brown, S. B., C. S. Tucker, C. Ford, Y. Lee, D. R. Dunbar, and J. J. Mullins. 2007. Class III antiarrhythmic methanesulfonanilides inhibit leukocyte recruitment in zebrafish. *J. Leukoc. Biol.* 82: 79–84.
142. Cvejic, A., C. Hall, M. Bak-Maier, M. V. Flores, P. Crosier, M. J. Redd, and P. Martin. 2008. Analysis of WASp function during the wound inflammatory response--live-imaging studies in zebrafish larvae. *J. Cell. Sci.* 121: 3196–3206.
143. Matrone, G., J. M. Taylor, K. S. Wilson, J. Baily, G. D. Love, J. M. Girkin, J. J. Mullins, C. S. Tucker, and M. A. Denvir. 2013. Laser-targeted ablation of the zebrafish embryonic ventricle: a novel model of cardiac injury and repair. *Int. J. Cardiol.* 168: 3913–3919.
144. Evans, M. A., N. Smart, K. N. Dubé, S. Bollini, J. E. Clark, H. G. Evans, L. S. Taams, R. Richardson, M. Lévesque, P. Martin, K. Mills, J. Riegler, A. N. Price, M. F. Lythgoe, and P. R. Riley. 2013. Thymosin β4-sulfoxide attenuates inflammatory cell infiltration and promotes

cardiac wound healing. *Nat Commun* 4: 2081.
145. Gray, C., I. M. Packham, F. Wurmser, N. C. Eastley, P. G. Hellewell, P. W. Ingham, D. C. Crossman, and T. J. A. Chico. 2007. Ischemia is not required for arteriogenesis in zebrafish embryos. *Arterioscler. Thromb. Vasc. Biol.* 27: 2135–2141.
146. Sieger, D., C. Moritz, T. Ziegenhals, S. Prykhozhij, and F. Peri. 2012. Long-range Ca2+ waves transmit brain-damage signals to microglia. *Developmental Cell* 22: 1138–1148.
147. Niethammer, P., C. Grabher, A. T. Look, and T. J. Mitchison. 2009. A tissue-scale gradient of hydrogen peroxide mediates rapid wound detection in zebrafish. *Nature* 459: 996–999.
148. Mathias, J. R., B. J. Perrin, T.-X. Liu, J. Kanki, A. T. Look, and A. Huttenlocher. 2006. Resolution of inflammation by retrograde chemotaxis of neutrophils in transgenic zebrafish. *J. Leukoc. Biol.* 80: 1281–1288.
149. Starnes, T. W., and A. Huttenlocher. 2012. Neutrophil reverse migration becomes transparent with zebrafish. *Adv Hematol* 2012: 398640–11.
150. Elks, P. M., F. J. van Eeden, G. Dixon, X. Wang, C. C. Reyes-Aldasoro, P. W. Ingham, M. K. B. Whyte, S. R. Walmsley, and S. A. Renshaw. 2011. Activation of hypoxia-inducible factor-1α (Hif-1α) delays inflammation resolution by reducing neutrophil apoptosis and reverse migration in a zebrafish inflammation model. *Blood* 118: 712–722.
151. d'Alençon, C. A., O. A. Peña, C. Wittmann, V. E. Gallardo, R. A. Jones, F. Loosli, U. Liebel, C. Grabher, and M. L. Allende. 2010. A high-throughput chemically induced inflammation assay in zebrafish. *BMC Biol.* 8: 151.
152. de Oliveira, S., A. Lopez-Muñoz, F. J. Martínez-Navarro, J. Galindo-Villegas, V. Mulero, and A. Calado. 2015. Cxcl8-l1 and Cxcl8-l2 are required in the zebrafish defense against *Salmonella Typhimurium*. *Dev. Comp. Immunol.* 49: 44–48.
153. Elks, P. M., S. Brizee, M. van der Vaart, S. R. Walmsley, F. J. van Eeden, S. A. Renshaw, and A. H. Meijer. 2013. Hypoxia inducible factor signaling modulates susceptibility to mycobacterial infection via a nitric oxide dependent mechanism. *PLoS Pathog* 9: e1003789.
154. Gaj, T., C. A. Gersbach, and C. F. Barbas III. 2013. ZFN, TALEN, and CRISPR/Cas-based methods for genome engineering. *Trends in Biotechnology* 31: 397–405.
155. Fan, L., J. Crodian, X. Liu, A. Aleström, P. Aleström, and P. Collodi. 2004. Zebrafish embryo cells remain pluripotent and germ-line competent for multiple passages in culture. *Zebrafish* 1: 21–26.
156. Grunwald, D. J., and G. Streisinger. 1992. Induction of recessive lethal and specific locus mutations in the zebrafish with ethyl nitrosourea. *Genet. Res.* 59: 103–116.
157. Bolli, N., E. M. Payne, J. Rhodes, E. Gjini, A. B. Johnston, F. Guo, J.-S. Lee, R. A. Stewart, J. P. Kanki, A. T. Chen, Y. Zhou, L. I. Zon, and A. T. Look. 2011. cpsf1 is required for definitive HSC survival in zebrafish. *Blood* 117: 3996–4007.
158. Sander, J. D., and J. K. Joung. 2014. CRISPR-Cas systems for editing, regulating and targeting genomes. *Nature Biotechnology* 32: 347–355.
159. Hruscha, A., P. Krawitz, A. Rechenberg, V. Heinrich, J. Hecht, C. Haass, and B. Schmid. 2013. Efficient CRISPR/Cas9 genome editing with low off-target effects in zebrafish. *Development* 140: 4982–4987.
160. Hwang, W. Y., Y. Fu, D. Reyon, M. L. Maeder, S. Q. Tsai, J. D. Sander, R. T. Peterson, J.-R. J. Yeh, and J. K. Joung. 2013. Efficient genome editing in zebrafish using a CRISPR-Cas system. *Nature Biotechnology* 31: 227–229.
161. Ablain, J., E. M. Durand, S. Yang, Y. Zhou, and L. I. Zon. 2015. A CRISPR/Cas9 vector system for tissue-specific gene disruption in zebrafish. *Developmental Cell* 32: 756–764.
162. Hwang, W. Y., R. T. Peterson, and J.-R. J. Yeh. 2014. Methods for targeted mutagenesis in zebrafish using TALENs. *Methods* 69: 76–84.
163. Moulton, J. D. 2007. Using morpholinos to control gene expression. *Curr Protoc Nucleic Acid Chem* Chapter 4: Unit 4.30–4.30.24.
164. Kawakami, K., A. Shima, and N. Kawakami. 2000. Identification of a functional transposase of the Tol2 element, an Ac-like element from the Japanese medaka fish, and its

transposition in the zebrafish germ lineage. *Proc. Natl. Acad. Sci. U.S.A.* 97: 11403–11408.
165. Pletnev, S., N. G. Gurskaya, N. V. Pletneva, K. A. Lukyanov, D. M. Chudakov, V. I. Martynov, V. O. Popov, M. V. Kovalchuk, A. Wlodawer, Z. Dauter, and V. Pletnev. 2009. Structural basis for phototoxicity of the genetically encoded photosensitizer KillerRed. *J. Biol. Chem.* 284: 32028–32039.
166. Curado, S., D. Y. R. Stainier, and R. M. Anderson. 2008. Nitroreductase-mediated cell/tissue ablation in zebrafish: a spatially and temporally controlled ablation method with applications in developmental and regeneration studies. *Nat Protoc* 3: 948–954.
167. Langheinrich, U. 2003. Zebrafish: a new model on the pharmaceutical catwalk. *Bioessays* 25: 904–912.
168. Loynes, C. A., J. S. Martin, A. Robertson, D. M. I. Trushell, P. W. Ingham, M. K. B. Whyte, and S. A. Renshaw. 2010. Pivotal Advance: Pharmacological manipulation of inflammation resolution during spontaneously resolving tissue neutrophilia in the zebrafish. *J. Leukoc. Biol.* 87: 203–212.
169. Suster, M. L., H. Kikuta, A. Urasaki, K. Asakawa, and K. Kawakami. 2009. Transgenesis in zebrafish with the tol2 transposon system. *Methods Mol. Biol.* 561: 41–63.
170. Westerfield, M. 2000. *The zebrafish book. A guide for the laboratory use of zebrafish (Danio rerio)*, 5 ed. Univ. of Oregon Press, Eugene.
171. Kimmel, C. B., W. W. Ballard, S. R. Kimmel, B. Ullmann, and T. F. Schilling. 1995. Stages of embryonic development of the zebrafish. *Dev. Dyn.* 203: 253–310.
172. Denvir, M. A., C. S. Tucker, and J. J. Mullins. 2008. Systolic and diastolic ventricular function in zebrafish embryos: influence of norepenephrine, MS-222 and temperature. *BMC Biotechnol.* 8: 21.
173. Collymore, C., A. Tolwani, C. Lieggi, and S. Rasmussen. 2014. Efficacy and safety of 5 anesthetics in adult zebrafish (Danio rerio). *J. Am. Assoc. Lab. Anim. Sci.* 53: 198–203.
174. Gerlach, G. F., L. N. Schrader, and R. A. Wingert. 2011. Dissection of the Adult Zebrafish Kidney. *J Vis Exp* 1–5.
175. Dorward, D. A., C. D. Lucas, A. L. Alessandri, J. A. Marwick, F. Rossi, I. Dransfield, C. Haslett, K. Dhaliwal, and A. G. Rossi. 2013. Technical advance: autofluorescence-based sorting: rapid and nonperturbing isolation of ultrapure neutrophils to determine cytokine production. *J. Leukoc. Biol.* 94: 193–202.
176. Mathias, J. R., M. E. Dodd, K. B. Walters, S. K. Yoo, E. A. Ranheim, and A. Huttenlocher. 2009. Characterization of zebrafish larval inflammatory macrophages. *Dev. Comp. Immunol.* 33: 1212–1217.
177. Zakrzewska, A., C. Cui, O. W. Stockhammer, E. L. Benard, H. P. Spaink, and A. H. Meijer. 2010. Macrophage-specific gene functions in Spi1-directed innate immunity. *Blood* 116: e1–11.
178. Yoo, S. K., and A. Huttenlocher. 2011. Spatiotemporal photolabeling of neutrophil trafficking during inflammation in live zebrafish. *J. Leukoc. Biol.* 89: 661–667.
179. Dorward, D. A., C. D. Lucas, G. B. Chapman, C. Haslett, K. Dhaliwal, and A. G. Rossi. 2015. The role of formylated peptides and formyl peptide receptor 1 in governing neutrophil function during acute inflammation. *Am. J. Pathol.* 185: 1172–1184.
180. Wang, X., A. L. Robertson, J. Li, R. J. Chai, W. Haishan, P. Sadiku, N. V. Ogryzko, M. Everett, K. Yoganathan, H. R. Luo, S. A. Renshaw, and P. W. Ingham. 2014. Inhibitors of neutrophil recruitment identified using transgenic zebrafish to screen a natural product library. *Dis Model Mech* 7: 163–169.
181. Li, Z., A. R. Burns, and C. W. Smith. 2006. Two Waves of Neutrophil Emigration in Response to Corneal Epithelial Abrasion: Distinct Adhesion Molecule Requirements. *Invest. Ophthalmol. Vis. Sci.* 47: 1947–9.
182. Das, A., M. Sinha, S. Datta, M. Abas, S. Chaffee, C. K. Sen, and S. Roy. 2015. Monocyte and Macrophage Plasticity in Tissue Repair and Regeneration. *Am. J. Pathol.*
183. Iles, K. E., and H. J. Forman. 2002. Macrophage signaling and respiratory burst. *Immunol. Res.* 26: 95–105.

184. Ray, A., K. Redhead, S. Selkirk, and S. Poole. 1991. Variability in LPS composition, antigenicity and reactogenicity of phase variants of Bordetella pertussis. *FEMS Microbiol. Lett.* 63: 211–217.
185. Zon, L. I., and R. T. Peterson. 2005. In vivo drug discovery in the zebrafish. *Nat Rev Drug Discov* 4: 35–44.
186. Wittmann, C., M. Reischl, A. H. Shah, R. Mikut, U. Liebel, and C. Grabher. 2012. Facilitating drug discovery: an automated high-content inflammation assay in zebrafish. *J Vis Exp* e4203–e4203.
187. Hagedorn, E. J., E. M. Durand, E. M. Fast, and L. I. Zon. 2014. Getting more for your marrow: boosting hematopoietic stem cell numbers with PGE2. *Exp. Cell Res.* 329: 220–226.
188. Chen, E. X., S. Hotte, H. Hirte, L. L. Siu, J. Lyons, M. Squires, S. Lovell, S. Turner, L. McIntosh, and L. Seymour. 2014. A Phase I study of cyclin-dependent kinase inhibitor, AT7519, in patients with advanced cancer: NCIC Clinical Trials Group IND 177. *Br. J. Cancer* 111: 2262–2267.
189. Singh, M., M. Kaur, and O. Silakari. 2014. Flavones: an important scaffold for medicinal chemistry. *Eur J Med Chem* 84: 206–239.
190. Ohtsuka, M., K. Fukuda, H. Yano, and M. Kojiro. 1995. Effects of nine active ingredients in Chinese herbal medicine sho-saiko-to on 2-(2-furyl)-3-(5-nitro-2-furyl)acrylamide mutagenicity. *Jpn. J. Cancer Res.* 86: 1131–1135.
191. Polier, G., J. Ding, B. V. Konkimalla, D. Eick, N. Ribeiro, R. Köhler, M. Giaisi, T. Efferth, L. Desaubry, P. H. Krammer, and M. Li-Weber. 2011. Wogonin and related natural flavones are inhibitors of CDK9 that induce apoptosis in cancer cells by transcriptional suppression of Mcl-1. *Cell Death Dis* 2: e182.
192. Polier, G., M. Giaisi, R. Köhler, W. W. Müller, C. Lutz, E. C. Buss, P. H. Krammer, and M. Li-Weber. 2015. Targeting CDK9 by wogonin and related natural flavones potentiates the anti-cancer efficacy of the Bcl-2 family inhibitor ABT-263. *Int. J. Cancer* 136: 688–698.
193. Milan, D. J., T. A. Peterson, J. N. Ruskin, R. T. Peterson, and C. A. MacRae. 2003. Drugs that induce repolarization abnormalities cause bradycardia in zebrafish. *Circulation* 107: 1355–1358.
194. Hoodless, L. J., C. T. Robb, J. M. Felton, C. S. Tucker, and A. G. Rossi. 2016. Models for the Study of the Cross Talk Between Inflammation and Cell Cycle. In *Cyclin-Dependent Kinase (CDK) Inhibitors*. Methods in Molecular Biology vol. 1336. Springer New York, New York, NY. 179–209.
195. Silva, M. T. 2010. Secondary necrosis: the natural outcome of the complete apoptotic program. *FEBS Lett.* 584: 4491–4499.
196. Rossi, A. G., C. Ward, and I. Dransfield. 2004. Getting to grips with the granulocyte: manipulation of granulocyte behaviour and apoptosis by protein transduction methods. *Biochem. Soc. Trans.* 32: 452–455.
197. Dransfield, I., and A. G. Rossi. 2004. Granulocyte apoptosis: who would work with a "real" inflammatory cell? *Biochem. Soc. Trans.* 32: 447–451.
198. Heasman, J. 2002. Morpholino oligos: making sense of antisense? *Dev. Biol.* 243: 209–214.
199. Collas, P., M. R. Liang, M. Vincent, and P. Aleström. 1999. Active transgenes in zebrafish are enriched in acetylated histone H4 and dynamically associate with RNA Pol II and splicing complexes. *J. Cell. Sci.* 112 (Pt 7): 1045–1054.
200. Hanisch, A., M. V. Holder, S. Choorapoikayil, M. Gajewski, E. M. Özbudak, and J. Lewis. 2013. The elongation rate of RNA polymerase II in zebrafish and its significance in the somite segmentation clock. *Development* 140: 444–453.
201. Oqani, R. K., H. R. Kim, Y. F. Diao, C. S. Park, and D. I. Jin. 2011. The CDK9/cyclin T1 subunits of P-TEFb in mouse oocytes and preimplantation embryos: a possible role in embryonic genome activation. *BMC Dev. Biol.* 11: 33.
202. Meier, N., S. Krpic, P. Rodriguez, J. Strouboulis, M. Monti, J. Krijgsveld, M. Gering, R. Patient, A. Hostert, and F. Grosveld. 2006. Novel binding partners of Ldb1 are required for

haematopoietic development. *Development* 133: 4913–4923.
203. Wada, T., M. Hara, T. Taneda, C. Qingfu, R. Takata, K. Moro, K. Takeda, T. Kishimoto, and H. Handa. 2012. Antisense morpholino targeting just upstream from a poly(A) tail junction of maternal mRNA removes the tail and inhibits translation. *Nucleic Acids Res.* 40: e173–e173.
204. Ganuza, M., C. Sáiz-Ladera, M. Cañamero, G. Gómez, R. Schneider, M. A. Blasco, D. Pisano, J. M. Paramio, D. Santamaría, and M. Barbacid. 2012. Genetic inactivation of Cdk7 leads to cell cycle arrest and induces premature aging due to adult stem cell exhaustion. *EMBO J.* 31: 2498–2510.
205. Liu, Q. Y., Z. L. Wu, W. J. Lv, Y. C. Yan, and Y. P. Li. 2007. Developmental expression of Cyclin H and Cdk7 in zebrafish: the essential role of Cyclin H during early embryo development. *Cell Res* 17: 163–173.
206. Weber, F. C., T. Németh, J. Z. Csepregi, A. Dudeck, A. Roers, B. Ozsvári, E. Oswald, L. G. Puskás, T. Jakob, A. Mócsai, and S. F. Martin. 2015. Neutrophils are required for both the sensitization and elicitation phase of contact hypersensitivity. *J. Exp. Med.* 212: 15–22.
207. Rinkenberger, J. L., S. Horning, B. Klocke, K. Roth, and S. J. Korsmeyer. 2000. Mcl-1 deficiency results in peri-implantation embryonic lethality. *Genes Dev.* 14: 23–27.
208. Krueger, B. J., C. Jeronimo, B. B. Roy, A. Bouchard, C. Barrandon, S. A. Byers, C. E. Searcey, J. J. Cooper, O. Bensaude, E. A. Cohen, B. Coulombe, and D. H. Price. 2008. LARP7 is a stable component of the 7SK snRNP while P-TEFb, HEXIM1 and hnRNP A1 are reversibly associated. *Nucleic Acids Res.* 36: 2219–2229.
209. Uchikawa, E., K. S. Natchiar, X. Han, F. Proux, P. Roblin, E. Zhang, A. Durand, B. P. Klaholz, and A.-C. Dock-Bregeon. 2015. Structural insight into the mechanism of stabilization of the 7SK small nuclear RNA by LARP7. *Nucleic Acids Res.* 43: 3373–3388.
210. Markert, A., M. Grimm, J. Martinez, J. Wiesner, A. Meyerhans, O. Meyuhas, A. Sickmann, and U. Fischer. 2008. The La-related protein LARP7 is a component of the 7SK ribonucleoprotein and affects transcription of cellular and viral polymerase II genes. *EMBO Rep.* 9: 569–575.
211. Okamura, D., I. Maeda, H. Taniguchi, Y. Tokitake, M. Ikeda, K. Ozato, N. Mise, K. Abe, T. Noce, J. C. Izpisua Belmonte, and Y. Matsui. 2012. Cell cycle gene-specific control of transcription has a critical role in proliferation of primordial germ cells. *Genes Dev.* 26: 2477–2482.
212. Smallie, T., G. Ricchetti, N. J. Horwood, M. Feldmann, A. R. Clark, and L. M. Williams. 2010. IL-10 inhibits transcription elongation of the human TNF gene in primary macrophages. *J. Exp. Med.* 207: 2081–2088.
213. Bedell, V. M., S. E. Westcot, and S. C. Ekker. 2011. Lessons from morpholino-based screening in zebrafish. *Brief Funct Genomics* 10: 181–188.
214. Rossi, A., Z. Kontarakis, C. Gerri, H. Nolte, S. Hölper, M. Krüger, and D. Y. R. Stainier. 2015. Genetic compensation induced by deleterious mutations but not gene knockdowns. *Nature*.
215. Garriga, J., and X. Graña. 2014. CDK9 inhibition strategy defines distinct sets of target genes. *BMC Res Notes* 7: 301.
216. Dahlberg, O., O. Shilkova, M. Tang, P.-H. Holmqvist, and M. Mannervik. 2015. P-TEFb, the super elongation complex and mediator regulate a subset of non-paused genes during early Drosophila embryo development. *PLoS Genet.* 11: e1004971.
217. Oehlers, S. H. B., M. V. Flores, C. J. Hall, R. O'Toole, S. Swift, K. E. Crosier, and P. S. Crosier. 2010. Expression of zebrafish cxcl8 (interleukin-8) and its receptors during development and in response to immune stimulation. *Dev. Comp. Immunol.* 34: 352–359.
218. Roca, F. J., I. Mulero, A. Lopez-Muñoz, M. P. Sepulcre, S. A. Renshaw, J. Meseguer, and V. Mulero. 2008. Evolution of the inflammatory response in vertebrates: fish TNF-alpha is a powerful activator of endothelial cells but hardly activates phagocytes. *J. Immunol.* 181: 5071–5081.
219. Nguyen-Chi, M., B. Laplace-Builhe, J. Travnickova, P. Luz-Crawford, G. Tejedor, Q. T.

Phan, I. Duroux-Richard, J.-P. Levraud, K. Kissa, G. Lutfalla, C. Jorgensen, and F. Djouad. 2015. Identification of polarized macrophage subsets in zebrafish. *Elife* 4: e07288.
220. Kanther, M., X. Sun, M. Mühlbauer, L. C. Mackey, E. J. Flynn, M. Bagnat, C. Jobin, and J. F. Rawls. 2011. Microbial colonization induces dynamic temporal and spatial patterns of NF-κB activation in the zebrafish digestive tract. *Gastroenterology* 141: 197–207.
221. Gregory, C. D., and A. Devitt. 2004. The macrophage and the apoptotic cell: an innate immune interaction viewed simplistically? *Immunology* 113: 1–14.
222. Li, L., H. Jin, J. Xu, Y. Shi, and Z. Wen. 2011. Irf8 regulates macrophage versus neutrophil fate during zebrafish primitive myelopoiesis. *Blood* 117: 1359–1369.
223. Canduri, F., P. C. Perez, R. A. Caceres, and W. F. de Azevedo. 2008. CDK9 a potential target for drug development. *Med Chem* 4: 210–218.
224. Grosveld, F., P. Rodriguez, N. Meier, S. Krpic, F. Pourfarzad, P. Papadopoulos, K. Kolodziej, G. P. Patrinos, A. Hostert, and J. Strouboulis. 2005. Isolation and characterization of hematopoietic transcription factor complexes by in vivo biotinylation tagging and mass spectrometry. *Ann. N. Y. Acad. Sci.* 1054: 55–67.
225. Bettencourt-Dias, M., R. Giet, R. Sinka, A. Mazumdar, W. G. Lock, F. Balloux, P. J. Zafiropoulos, S. Yamaguchi, S. Winter, R. W. Carthew, M. Cooper, D. Jones, L. Frenz, and D. M. Glover. 2004. Genome-wide survey of protein kinases required for cell cycle progression. *Nature* 432: 980–987.
226. Glover-Cutter, K., S. Larochelle, B. Erickson, C. Zhang, K. Shokat, R. P. Fisher, and D. L. Bentley. 2009. TFIIH-associated Cdk7 kinase functions in phosphorylation of C-terminal domain Ser7 residues, promoter-proximal pausing, and termination by RNA polymerase II. *Mol. Cell. Biol.* 29: 5455–5464.
227. Ekker, S. C., and J. D. Larson. 2001. Morphant technology in model developmental systems. *Genesis* 30: 89–93.
228. Remillieux-Leschelle, N., P. Santamaria, and N. B. Randsholt. 2002. Regulation of larval hematopoiesis in Drosophila melanogaster: a role for the multi sex combs gene. *Genetics* 162: 1259–1274.
229. Barboric, M., T. Lenasi, H. Chen, E. B. Johansen, S. Guo, and B. M. Peterlin. 2009. 7SK snRNP/P-TEFb couples transcription elongation with alternative splicing and is essential for vertebrate development. *Proc. Natl. Acad. Sci. U.S.A.* 106: 7798–7803.
230. Moulding, D. A., C. Akgul, M. Derouet, M. R. White, and S. W. Edwards. 2001. BCL-2 family expression in human neutrophils during delayed and accelerated apoptosis. *J. Leukoc. Biol.* 70: 783–792.
231. Kettleborough, R. N. W., E. M. Busch-Nentwich, S. A. Harvey, C. M. Dooley, E. de Bruijn, F. van Eeden, I. Sealy, R. J. White, C. Herd, I. J. Nijman, F. Fényes, S. Mehroke, C. Scahill, R. Gibbons, N. Wali, S. Carruthers, A. Hall, J. Yen, E. Cuppen, and D. L. Stemple. 2013. A systematic genome-wide analysis of zebrafish protein-coding gene function. *Nature* 496: 494–497.
232. Hall, C., M. V. Flores, T. Storm, K. Crosier, and P. Crosier. 2007. The zebrafish lysozyme C promoter drives myeloid-specific expression in transgenic fish. *BMC Dev. Biol.* 7: 42.
233. Wang, S., and P. M. Fischer. 2008. Cyclin-dependent kinase 9: a key transcriptional regulator and potential drug target in oncology, virology and cardiology. *Trends Pharmacol. Sci.* 29: 302–313.
234. Renshaw, S. A., C. A. Loynes, S. Elworthy, P. W. Ingham, and M. K. B. Whyte. 2007. Modeling inflammation in the zebrafish: how a fish can help us understand lung disease. *Exp. Lung Res.* 33: 549–554.
235. Drummond, I. A., and A. J. Davidson. 2010. Zebrafish kidney development. *Methods Cell Biol.* 100: 233–260.
236. Sugiyama, S., Y. Okada, G. K. Sukhova, R. Virmani, J. W. Heinecke, and P. Libby. 2001. Macrophage myeloperoxidase regulation by granulocyte macrophage colony-stimulating factor in human atherosclerosis and implications in acute coronary syndromes. *Am. J. Pathol.* 158: 879–891.

237. McCormack, R., and E. R. Podack. 2015. Perforin-2/Mpeg1 and other pore-forming proteins throughout evolution. *J. Leukoc. Biol.* jlb.4MR1114–523RR.
238. McCormack, R., L. R. de Armas, M. Shiratsuchi, J. E. Ramos, and E. R. Podack. 2013. Inhibition of intracellular bacterial replication in fibroblasts is dependent on the perforin-like protein (perforin-2) encoded by macrophage-expressed gene 1. *J Innate Immun* 5: 185–194.
239. Mosimann, C., and L. I. Zon. 2011. Advanced zebrafish transgenesis with Tol2 and application for Cre/lox recombination experiments. *Methods Cell Biol.* 104: 173–194.
240. Leverson, J. D., H. Zhang, J. Chen, S. K. Tahir, D. C. Phillips, J. Xue, P. Nimmer, S. Jin, M. Smith, Y. Xiao, P. Kovar, A. Tanaka, M. Bruncko, G. S. Sheppard, L. Wang, S. Gierke, L. Kategaya, D. J. Anderson, C. Wong, J. Eastham-Anderson, M. J. C. Ludlam, D. Sampath, W. J. Fairbrother, I. Wertz, S. H. Rosenberg, C. Tse, S. W. Elmore, and A. J. Souers. 2015. Potent and selective small-molecule MCL-1 inhibitors demonstrate on-target cancer cell killing activity as single agents and in combination with ABT-263 (navitoclax). *Cell Death Dis* 6: e1590.
241. Gores, G. J., and S. H. Kaufmann. 2012. Selectively targeting Mcl-1 for the treatment of acute myelogenous leukemia and solid tumors. *Genes Dev.* 26: 305–311.
242. Nguyen-Chi, M., Q. T. Phan, C. Gonzalez, J.-F. Dubremetz, J.-P. Levraud, and G. Lutfalla. 2014. Transient infection of the zebrafish notochord with E. coli induces chronic inflammation. *Dis Model Mech* 7: 871–882.
243. Chablais, F., J. Veit, G. Rainer, and A. Jaźwińska. 2011. The zebrafish heart regenerates after cryoinjury-induced myocardial infarction. *BMC Dev. Biol.* 11: 21.
244. Buckley, C. D., E. A. Ross, H. M. McGettrick, C. E. Osborne, O. Haworth, C. Schmutz, P. C. W. Stone, M. Salmon, N. M. Matharu, R. K. Vohra, G. B. Nash, and G. E. Rainger. 2006. Identification of a phenotypically and functionally distinct population of long-lived neutrophils in a model of reverse endothelial migration. *J. Leukoc. Biol.* 79: 303–311.
245. Ellett, F., P. M. Elks, A. L. Robertson, N. V. Ogryzko, and S. A. Renshaw. 2015. Defining the phenotype of neutrophils following reverse migration in zebrafish. *J. Leukoc. Biol.* jlb.3MA0315–105R.
246. Goessling, W., and T. E. North. 2014. Repairing quite swimmingly: advances in regenerative medicine using zebrafish. *Dis Model Mech* 7: 769–776.
247. Li, L., B. Yan, Y.-Q. Shi, W.-Q. Zhang, and Z.-L. Wen. 2012. Live imaging reveals differing roles of macrophages and neutrophils during zebrafish tail fin regeneration. *J. Biol. Chem.* 287: 25353–25360.
248. Shiau, C. E., Z. Kaufman, A. M. Meireles, and W. S. Talbot. 2015. Differential requirement for irf8 in formation of embryonic and adult macrophages in zebrafish. *PLoS ONE* 10: e0117513.
249. Prajsnar, T. K., R. Hamilton, J. Garcia-Lara, G. McVicker, A. Williams, M. Boots, S. J. Foster, and S. A. Renshaw. 2012. A privileged intraphagocyte niche is responsible for disseminated infection of Staphylococcus aureus in a zebrafish model. *Cell. Microbiol.* 14: 1600–1619.
250. Walters, K. B., J. M. Green, J. C. Surfus, S. K. Yoo, and A. Huttenlocher. 2010. Live imaging of neutrophil motility in a zebrafish model of WHIM syndrome. *Blood* 116: 2803–2811.

8. Appendix A

8.1. General materials

- Petri Dishes – Corning 60mm x 15mm (Corning) or 100mm x 15mm tissue culture treated, polystyrene cell culture dish (Thermo Scientific)
- Plastic Pasteur pastettes (Scientific Labs)
- Tricaine Solution (see Appendix B)
- Methylene Blue Solution (see Appendix B)
- Embryo Medium Solution (see Appendix B)
- System Water (see Appendix B)
- 0.5mL, 1mL, 2mL Microcentrifuge Tubes (Eppendorf)
- Falcon 15mL and 50mL Conical Centrifuge Tubes (Bectin Dickinson)
- 0.2mL 8-strip PCR Tubes and Caps (Starlab Group)
- UltraPure^{TM} Agarose (Life Technologies)
- Ethanol (Molecular Biology Grade, Sigma Aldrich)
- Glycerol solution (Sigma Aldrich)
- Tris-Buffered Saline (TBS, see Appendix B)
- Tris-Buffered Saline-Tween (TBS, see Appendix B)
- Mastercycler PCR machine (Eppendorf)
- Horizontal DNA Gel Apparatus (BioRad)
- Nanodrop machine (to assess DNA concentration)

8.2. Zebrafish lines used

- Tg(mpx:EGFP)^{i114}
- Tg(mpx:mCherry)
- Tg(MPEG1:mCherry)
- Tg(MPEG1:EGFP)
- Tg(fms:mCherry)
- Tg(mpx:GFP)^{i114} + CDK9 knockdown (using CRISPRcas9)
- Tg(LysC:mcl1a:cmlc2:EGFP)
- Tg(LysC:mcl1b:cmlc2:EGFP)

8.3. Zebrafish husbandry and breeding

- Pair-mating boxes
- Sieves
- 28°C Incubator

8.4. Zebrafish tailfin injury

- Sterile Scalpel #23 (Swann Morton)
- 19 G Needle (Bectin Dickinson Microlance)
- 48 well cell culture flat-bottomed plate (Costar)

8.5. Imaging, measuring and analysis of inflammation

- LabTekII 8 chambered #1.5 cover glass slide (Nunc)
- Leica MZ16F dissecting scope with Green Fluorescent Protein (Ex. 488) and Texas Red (Ex. 596) filters
- Leica DFC300 FX Digital Colour Camera
- Leica sp5 Confocal Microscope
- Zeiss LSM 510 Meta Microscope

8.6. Digestion of whole embryos and isolation of neutrophils by FACS

- 40μM Nylon Cell Strainer (Corning)
- Trypsin/EDTA
- Rosewell Park Memorial Institute (RPMI) 1640 Medium (Gibco)
- Foetal Bovine Serum (Sigma Aldrich)
- FACS Aria II Cell Sorter (Bectin Dickinson)

8.7. Stimluation of FACS-isolated EGFP+ cells using N-formyl-Met-Leu-Phe (fMLF)

- N-Formyl-Met-Leu-Phe (fMLF)
- Phosphate-Buffered Saline (PBS) containing Ca^{2+} and Mg^{2+} (Gibco)
- Phosphate-Buffered Saline (PBS) without Ca^{2+} and Mg^{2+} (Gibco)

- LSR Fortessa Flow Cytometer (Bectin Dickinson)

8.8. Drug treatment of zebrafish embryos

Table A.1. Compound Manufacturers

Drug	Manufacturer
AT7519	Astex Therapeutics
Wogonin	Sigma Aldrich
Luteolin	Sigma Aldrich
Apigenin	Sigma Aldrich
FVP	Sigma Aldrich
SNS-032	Selleckchem
zVAD-fmk	Tocris Bioscience
QVD-OPh	R & D

8.9. Incubation of zebrafish embryos with compounds

- 48 well cell culture flat-bottomed plate (Costar)
- Dimethyl Sulfoxide (DMSO, Sigma Aldrich)

8.10. Injection of zebrafish with compounds or morpholinos

- Microloader Pipette Tips 0.5-20µL (Eppendorf)
- Microcapillary needles, pulled on a Flaming Brown Needle Puller. Typical needle settings: Heat 580, Pull 100, Velocity 55, Time 250. (TW100F-4 Borosilicate thin-wall glass capillary, 1mm OD with filament microcapillaries).
- Micromanipulator (Narishige)
- Microinjecter (Narishige)
- 1mm Stage Micrometer (Pyser SGI)
- Morpholinos were dissolved in sterile dH_20 to 1µM stock then diluted to desired concentration in dH_20.

- All morpholinos (Table 2.3, Methods Chapter 2) were ordered from Gene Tools LLC and were designed using the Gene Tools software design tool.

8.11. Fixing embryos for staining

- 1.5mL microcentrifuge tube (Eppendorf)
- Tris Buffered Saline (see Appendix B for recipe)
- Paraformaldehyde Solution (PFA, 4%, Chem Cruz)
- Methanol (Fisher Chemicals)

8.12. TSA/TUNEL staining

- Tyramide Signal Amplication kit (Perkin Elmer), containing Amplification Diluent and Fluorescein dye.
- ApopTag Red *In Situ* Apoptosis Detection Kit (Millipore), containing TdT enzyme, Reaction Buffer, Stop Buffer, anti-Dig Rhodamine, Blocking Solution
- Proteinase K from *Tritirachium album* (Sigma Aldrich)
- Paraformaldehyde Solution (PFA, 4%, Chem Cruz)
- Fluorescent Microscope (EVOS FL Cell Imaging System)
- Acetone

8.13. Western blotting

- Radioimmunoprecipitation Assay (RIPA) buffer (Sigma Aldrich)
- Protease Inhibitor Cocktail (Sigma Aldrich)
- Pestle for 1.5mL/2mL microcentrifuge tubes (Eppendorf)
- SoniPrep 150 Sonicator (MSE)
- BCA Protein Assay Kit, consisting of Reagent A, Regent B and Protein Standards (Thermo Scientific)
- Synergy HT Plate Reader (BioTek)
- Sample Buffer (4x, See Appendix B)
- Bromophenol blue (Sigma Aldrich)

- β-mercaptoethanol (Sigma Aldrich)
- Novex Tris-Glycine gel (4-12%, Life Technologies)
- Gel Running and Transfer Tanks (Biorad)
- Running Buffer (see Appendix B)
- Methanol (Fisher Chemicals)
- Transfer Buffer (See Appendix B)
- Immobilon Polyvinylidene fluoride (PVDF) Transfer Membrane, Pore Size 45um (Millipore)
- Dried milk powder (Marvel)
- Electrochemiluminescence Prime Western Blotting Detection Reagent (GE Healthcare), containing Solution A and Solution B.
- SRX-101A Developer (Konika)
- Biomax Light Film (Kodak)

Table A.2. Western Blotting Antibodies

Antibody	**Company**
CDK9	Santa Cruz Biotechnology
CDK7	Santa Cruz Biotechnology
Mcl-1	Santa Cruz Biotechnology
LaRP7	Sigma Aldrich
Goat Anti-Rabbit	DAKO
Goat Anti Mouse	DAKO

8.14. Heritable gene knockdown using CRISPR/cas9

- Guide Oligonucleotides (Eurofins)
- Primers (Invitrogen)
- Ambion MEGAscript T7 kit (containing 10x Reaction Buffer, Enzyme Mix, dNTPs, and Turbo DNAse)
- MEGAclear kit (containing Elution Solution, Binding Solution Concentrate, Wash Solution, collection tubes and filters)

- Phenol Red solution (Sigma Aldrich)
- Proteinase K from *Tritirachium album* (Sigma Aldrich)
- Tris-Acetate EDTA Buffer (50x, Life Technologies)
- One*Taq* Quick Load Master Mix with Standard Buffer (New England Biolabs)
- Primers (Life Technologies)
- Hpy188I (New England Biolabs)
- Hpy99I (New England Biolabs)
- Cutsmart Buffer (New England Biolabs)
- SYBR® Safe DNA Gel Stain (Life Technologies)
- Gene Ruler 100bp plus DNA ladder (Thermo Scientific)

8.15. Creation of Mcl-1 over-expressing zebrafish using Tol2 gateway cloning

- Primers (Life Technologies)
- OneShot Top10^{TM} chemically competent E. Coli (Life Technologies)
- S.O.C. medium (Life Technologies)
- Kanamycin antibiotic (Sigma Aldrich)
- Lysogeny Broth (LB) medium
- Glycerol (Sigma)
- Qiagen Spin-Miniprep Kit (containing Buffer P1, Buffer P2, Buffer N3, Buffer PB, Buffer PE, QIAprep spin columns and collecting tubes)
- *Pyrococcus furiosus* (PFU) DNA Polymerase (Promega)
- Loading dye 6x (Thermo Scientific)
- QIAquick Gel Extraction Kit, containing buffer QG, isopropanol, spin columns (Qiagen)
- BP Clonase II Enzyme Mix (Life Technologies)
- LR Clonase II Enzyme Mix (Life Technologies)
- SeqSmart Sequencing kit (Eurofins)
- Rhodamine/Dextran (Sigma)

8.16. Isolating neutrophils from peripheral blood and assessing apoptosis after CDKi treatment

- Iscove's Modified Dulbecco's Medium (IMDM)
- Penicillin / Streptomycin (Thermo Scientific)
- 96-well flat bottomed plate (CoStar)
- Dulbecco's Phosphate-Buffered Saline (DPBS)
- Cytocentrifuge chambers, filter cards, glass slides, and coverslips
- Diff-Quik™ stains (Thermo Scientific)
- DPX mounting medium (Sigma Aldrich)
- Annexin-V conjugated to fluorescein isothiocynate (FITC, Abcam)
- AnnV binding buffer, - Hanks balanced salt solution (HBSS) with 5mM Ca^{2+} (Stored at $4^{o}C$)
- Propidium iodide (PI), 1mg/ml in sterile ddH_2O (Sigma Aldrich)

9. Appendix B

9.1. Embryo medium solution

- 1.0 mL Hank's Solution #1
- 0.1 mL Hank's Solution #2
- 1.0 mL Hank's Solution #4
- 1.0 mL Hank's Solution #5
- 1.0 mL fresh Hank's Solution #6
- 95.9 mL ddH_20
- Use about 10 drops 1 M NaOH to pH 7.2

Hank's Solution #1: 8.0 g NaCl, 0.4 g KCl, 100 mL ddH_20

Hank's Solution #2: 0.358 g Na_2HPO_4 anhydrous, 0.6 g KH_2PO_4, 100 mL ddH_20

Hank's Solution #4: 0.72 g $CaCl_2$, 50 mL ddH_20

Hank's Solution #5: 1.23 g $MgSO_4$ x7 H_2O in 50 mL ddH_2O

Hank's Solution #6: made fresh: 0.35 g $NaHCO_3$, 10 mL ddH_20

9.2. Methylene blue solution

Make Conditioned H_20: 0.8 g sodium bicarbonate, 4.5 mL Marine Salts (Tropic Marin®), 750 L H_20**.** Then add 0.6 mL methylthioninium chloride (methylene blue) per 10 L of conditioned water (equivalent to 0.5 mg/mL)

9.3. System water solution

0.03% salt (Tropic Marin®) in dH_20

9.4. Danieau's solution

58 mM NaCl

0.7 mM KCl

0.4 mM MgSO4

0.6 mM Ca(NO3)2

5.0 mM HEPES

9.5. Tricaine solution

400 mg Tricaine powder in 97.9 mL embryo medium

0.26 g Tris in 2.1 mL embryo medium

Adjust pH to pH 7.

9.6. Western Blotting Reagents

All chemicals below obtained from Sigma Aldrich

9.6.1. Running buffer

121 g Tris Base

238 g HEPES

10 g SDS

9.6.2. Transfer buffer (Western blotting)

- (x10 stock)

  30.3 g Tris Base

  144.12 g Glycine

  Make up to 1l with dH_2O (no need to pH)

- (x1)

  100ml of 10x transfer buffer stock

  200ml methanol

  700ml dH_2O

9.6.3. Tris-buffered saline (pH 7.4)

- (x10 stock)

  24.22g Tris Base

  87.66g NaCl

  Dissolve in ~800ml dH_2O, pH with HCl (~15.61ml of 11.4M HCl)

  Make up to final volume of 1 L

- (x1)

  100ml of 10x TBS stock

  899ml dH_2O

  1ml Tween-20

9.6.4. Sample buffer

4ml 20% SDS

4ml Glycerol

2.5ml 1M Tris-HCl pH6.8

Bromophenol blue

400ul B-mercaptoethanol

10.Appendix C

10.1. Publications

Hoodless LJ, Robb CT, Felton JM, Tucker CS, Rossi AG. Models for the study of the crosstalk between inflammation and cell cycle (2015). *Methods Mol Biol 1336:179-209*

Dalton JE, Glover AC, **Hoodless L**, Lim E, Beattie L, Kirby A, Kaye PM. The Neurotrophic Receptor Ntrk2 Directs Lymphoid Tissue Neovascularization during Leishmania donovani Infection (2015) *PLoS Pathogens 11(2): e1004681*.

Lucas CD, **Hoodless LJ,** Rossi AG (2014). Swimming against the tide: drugs drive neutrophil reverse migration. *Sci Transl Med. 6 (225):225fs9*.

Canham M, Charsou C, Stewart J, Moncur S, **Hoodless L**, Bhatia R, Cong D, Cubie H, Busby-Earle C, Williams A, McLoughlin V, Campbell JD, Cuschieri K, Howie SEM. (2014). Increased Cycling Cell Numbers and Stem Cell Associated Proteins as Potential Biomarkers for High Grade Human Papillomavirus+ve Pre-Neoplastic Cervical Disease. *PLoS One 9(12): e115379*.

Lucas CD, Allen KC, Dorward DA, **Hoodless LJ**, Melrose LA, Marwick JA, Tucker CS, Haslett C, Duffin R, Rossi AG (2013). Flavones induce neutrophil apoptosis by downregulation of Mcl-1 via a proteasomal-dependent pathway. *FASEB J. 27(3):1084-94*.

10.2. Conference Contributions

10.2.1. Oral Presentations

- *25th UK Adhesion Society meeting, University of Birmingham, 25th November 2013*: Investigating the Role and Function of Cyclin-Dependent Kinases in the Resolution of Innate Inflammation *in vivo* using the Zebrafish Tailfin Transection Model. **Hoodless LJ,** Lucas CD, Duffin R, Haslett C, Tucker CS, Rossi AG.

10.2.2. Poster Presentations

- *Banff Inflammation Workshop, Calgary, Canada. 30th January – 1st February 2015:* The Role of Cyclin-Dependent Kinase 9 in the Resolution of Innate Inflammation in a Zebrafish Model. **Hoodless LJ,** Lucas CD, Duffin R, Haslett C, Tucker CS, Rossi AG.
- *British Society for Immunology Inflammation & Disease Meeting, University of Manchester, 9-10th September 2014*: Investigating cyclin-dependent kinases in the resolution of innate inflammation using zebrafish tailfin injury. **Hoodless LJ,** Lucas CD, Duffin R, Haslett C, Tucker CS, Rossi AG.
- *8th European ZebraFish Meeting 9-13th July 2013, Barcelona*: Investigating cyclin-dependent kinases in the resolution of innate inflammation using zebrafish tailfin injury. **Hoodless LJ,** Lucas CD, Duffin R, Haslett C, Tucker CS, Rossi AG.

10.2.3. Courses/Training

- UK Home Office License for rodent and zebrafish handling.
- Various Institute for Academic Development training courses, including writing and science communication workshops.

- Attended the 13th College of Medicine & Veterinary Medicine Microscopy Course (2014).

10.2.4. Mentoring

- Running workshops for children aged 6-11 at the annual Edinburgh International Science Festival
- Demonstrator at the 2014 Zebrafish Transgenesis Workshop in Edinburgh.
- Assisting with mentoring two Masters degree students